JAEA-Research
2009-011

CET Performance at ROSA/LSTF Tests

- Twelve Tests with Core Heat-up -

Mitsuhiro SUZUKI and Hideo NAKAMURA

Reactor Safety Research Unit
Nuclear Safety Research Center

July 2009

Japan Atomic Energy Agency

日本原子力研究開発機構

JAEA-Research

CET Performance at ROSA/LSTF Tests
- Twelve Tests with Core Heat-up -

Mitsuhiro SUZUKI and Hideo NAKAMURA

Reactor Safety Research Unit
Nuclear Safety Research Center
Japan Atomic Energy Agency
Tokai-mura, Naka-gun, Ibaraki-ken

(Received April 22, 2009)

This report summarizes performance of core exit thermocouple (CET) observed in twelve ROSA/LSTF tests which include ten small-break loss-of-coolant accident (SBLOCA) tests and two abnormal transient tests. The report was prepared to a task group in the Working Group of Analysis and Management of Accident (WGAMA) at OECD/NEA, which had been set up to review and consolidate background knowledge of CET application to PWR accident management (AM) measures. The LSTF is the largest PWR simulator in the world with full-height, full-pressure and 1/48 volumetric scaling design. General CET performance to detect core heat-up in the LSTF tests is clarified as follows. (1) A time delay to detect core heat-up and a significant temperature difference from the hottest core are observed in most tests, (2) no CET heat-up was observed in two tests in which fall-back water from hot legs significantly influenced not only the CETs but also the local core cooling, (3) steam flow concentration into the control rod guide tube (CRGT) in case of a PV top SBLOCA test delayed heat-up of CETs installed outside of the CRGT, (4) two abnormal transient tests showed needs of CET superheat indication above saturation temperature during significantly high and low pressure boil-off transients, and (5) applicability of LSTF CET performance to PWR conditions should be carefully analyzed with respect to the fall-back water effects on atypical upper plenum configuration.

Keywords : OECD/NEA/WGAMA, ROSA/LSTF Test, PWR, SBLOCA, Abnormal Transient, Core Heat-up, Performance of Core Exit Thermocouple (CET), Accident Management (AM)

ROSA/LSTF 実験における炉心出口温度計(CET)の特性
- 炉心過熱に至った 12 実験の事例 -

日本原子力研究開発機構安全研究センター原子炉施設安全評価研究ユニット
鈴木　光弘・中村　秀夫

(2009 年 4 月 22 日受理)

本報は 12 件の ROSA/LSTF 実験における炉心出口温度計(CET)特性をまとめたものであり、これには 10 件の小破断冷却材喪失事故(SBLOCA)模擬実験と 2 件の異常過渡模擬実験が含まれる。本報は、PWR アクシデントマネジメント策に CET を利用する上で必要な知識基盤を再検討し統合するために設置された、OECD/NEA/WGAMA のタスクグループに対して準備したものである。LSTF は高さ実寸、実規模圧力及び容積比 1/48 で模擬する世界最大規模の PWR 模擬試験装置である。炉心過熱を検出する LSTF の一般的 CET 特性は以下の通りである。(1)大部分の実験で、炉心過熱からの検出遅れと炉心最高温度からの乖離が見られた、(2)２つの実験で CET は過熱温度を検出しなかったが、これらはホットレグからの流下水が CET に著しい影響を及ぼしただけでなく、炉心の部分的冷却にも影響を与えたためである、(3)原子炉頂部破断実験では、制御棒案内管(CRGT)内に集中する蒸気流により、その外側に設置した CET の過熱検出を遅らせた、(4)２つの異常過渡実験では、著しい高圧又は低圧下のボイルオフにおいて CET の飽和温度以上の過熱度を指標にする必要性を示した、(5)LSTF における CET 特性を PWR 条件に適用するには、形状の相違する上部プレナムにおける流下水影響について慎重な検討が必要である。

原子力科学研究所（駐在）: 〒319-1195　茨城県那珂郡東海村白方白根２－４

CONTENTS

目　　次

List of Tables

List of Figures

Acronyms and Abbreviations

AM	Accident Management
AFW	Auxiliary Feedwater
AIS	Accumulator Injection System
CET	Core Exit Thermocouple
CRGT	Control Rod Guide Tube
CSNI	Committee on the Safety of Nuclear Installations
DP	Differential Pressure
ECCS	Emergency Core Cooling System
EL	Elevation Level above Core Bottom
HL	Hot Leg
HPI	High Pressure Injection
ID	Inner Diameter
JAEA	Japan Atomic Energy Agency
LPI	Low Pressure Injection
LSTF	Large Scale Test Facility
NEA	Nuclear Energy Agency
OECD	Organization for Economic Cooperation and Development
PCT	Peak Cladding Temperature
PORV	Power-Operated Relief Valve
PV	Pressure Vessel
PWR	Pressurized Water Reactor
PZR	Pressurizer
RHR	Residual Heat Removal (System)
RPF	Radial Peaking Factor
RV	Relief Valve
SBLOCA	Small Break Loss-of-coolant Accident
SG	Steam Generator
SI	Safety Injection
SV	Safety Valve
UCP	Upper Core Plate
UP	Upper Plenum
UH	Upper Head
WGAMA	Working Group of Analysis and Management of Accident

1. Introduction

The OECD/NEA ROSA Project Test 6-1[1] (SB-PV-09 in JAEA) clarified the limited performance of core exit thermocouples (CETs) to detect the core heat-up phenomena during the vessel top SBLOCA simulation test indicating a time delay of 230s from the start of core heat-up to initiate accident management (AM) action by the CET set-point temperature of 623 K and resulting significant temperature discrepancy between the CET and the hottest core. It also pointed out influence of the CET installation locations at the outside of control rod guide tubes (CRGTs) in the case of the PV top break LOCA test. The CET performance was observed under uprising steam flow conditions in the heated core and no reflux water fall-back from steam generators (SGs). This point was discussed in the Working Group of Analysis and Management of Accident (WGAMA) in September 2007 and a task group was set up in WGAMA in April 2008 to review and consolidate background knowledge of CET application to PWR AM measures. The task group requested JAEA to summarize some other relevant LSTF tests useful for comprehensive understanding of the CET performance during various LOCA or transient simulation.

The LSTF/CET performance during SBLOCA simulation tests had been studied[2] in the early phase of ROSA-IV Program with respect to the detection time delay from the core heat-up start. The present report indicates the additional results on the LSTF/CET performance during twelve tests which recorded core uncovery followed by a pronounced temperature increase in the core and core exit, under influences of primary pressure, water inventory in the pressure vessel especially in the core and core power. **Table 1-1** shows a list of these tests with respect to their break location (see **Fig.1-1**), break size, kinds of transients, usage of CETs or other indicators for AM action including hot leg temperature (HL T) superheat, with or without water fall-back conditions, and test date (month/year). Ten SBLOCA tests consist of three pressure vessel (PV) top break tests (SB-PV-07, SB-PV-02[3] and SB-PV-08) with break sizes ranging from 1.0 to 0.1% equivalent to cold leg break, three cold leg break tests (SB-CL-09[4], SB-CL-01 and SB-CL-24[5]) with break sizes from 10 to 0.5%, two vessel bottom break tests (SB-PV-01[3] and SB-PV-03[6]) with 0.5 and 0.2% break sizes, one 0.5% hot leg break test (SB-HL-05) and a TMI-type LOCA test (AT-SB-03[3]) (see test conditions in Chapter 3). Two abnormal transient tests are a station blackout (TMLB’; refer Section 4.11) simulation test and a mid-loop operation test with loss-of-RHR. In most of SBLOCA tests, total failure or manual actuation of the high pressure injection (HPI) system was assumed.

The superheating was detected by CETs after the core heat-up in many tests except for two tests (SB-CL-09 and SB-PV-03) affected by fall-back water. Individual test results are briefly described in Chapter 4. Chapter 5 gives general CET performance in the LSTF experiments and Chapter 6 presents conclusions.

2. Facility Description

(1) Brief Description on LSTF Design Bases

Figure 2-1 shows schematic view of LSTF with two primary loops, pressure vessel (PV) with simulated core assembly and a pressurizer in one loop. Each primary loop includes a SG with 141 U-tubes, a primary coolant pump and emergency core cooling system (ECCS) such as the accumulator injection system (AIS). Figure 2-2 shows a flow diagram of LSTF which typically shows blowdown system with break locations. Figure 2-3 compares the PV dimensions between LSTF and the reference PWR (Westinghouse-type four-loop PWR with 3423 MWt output). It should be noted that the LSTF upper plenum (UP) configuration is atypical to that in the reference PWR with respect to the diameter and the hot leg bottom elevation. This point should be taken into account in the discussion of fall-back water influences on the CET temperature responses. These design bases are common to all the LSTF experiments. Table 2-1 shows summary of design change in the 1st, 2nd and 4th core assemblies at LSTF.

Figure 2-4 shows location of twenty CETs, twenty four flow holes at the upper core plate (UCP), eight CRGT-basements and ten support columns. Four CETs shown in Fig.2-4 (a) are installed outside of the CRGT-basements above the rod bundles of B10, B12, B22 and B24 while other CETs shown in Fig.2-4 (b) are installed at the fringe of UCP flow path holes above the other rod bundles except for four high-power bundles of B13, B16, B17 and B20 which have CRGT at their exit regions. Similar thermocouple arrangement is prepared at the UCP inlet side (below the UCP lower surface). These fluid temperature measurements at inlet and outlet regions of UCP are common for all LSTF experiments.

(2) History of Core Assembly Changes

Since the shake-down of LSTF, the core assembly (simulated fuel bundles) has been replaced three times[7-10] with several facility changes onto the LSTF. Major characteristics associated with each fuel assembly and their changes are summarized in the followings.

a) The 1st Core Assembly (March 1985 - Aug. 1988)

Instrumentations in the 1st simulated core assembly[7,8] are heavily installed onto 53 heater rods for surface temperature measurement out of 1064 heater rods. Figure 2-5 (1) shows horizontal cross-section of the 1st simulated core assembly consisting of 16 rod bundles with 7x7 rod array and 8 peripheral bundles. The rod bundles of B13 through B20 are high-power bundles with radial peaking factor (RPF) of 1.51, those of B21 through B24 in the center region are middle-power bundles with RPF=1.0 and those of B01 through B12 in the peripheral region are low-power bundles with RPF=0.66, respectively. Tie rods in each bundle simulate control rod guide thimble in the reference PWR. The LSTF peripheral bundles are surrounded by dummy rods and core barrel. The 1st core assembly was used for six tests of AT-SB-03 (SB3), SB-CL-01 (SC1), SB-CL-09 (SC9), SB-PV-01 (SP1), SB-PV-02 (SP2) and TR-LF-03 (LF3). **Figure 2-6** shows nine vertical locations of heater rod thermocouple for the 4th core assembly, which is similar to other core assemblies except for their horizontal arrangement and number of thermocouples.

b) The 2nd Core Assembly (Dec. 1988 - July 1993)

Table 2-1 shows major LSTF facility remodeling for the 2nd core assembly[9]. **Figure 2-5 (2)** shows horizontal cross-section of the 2nd simulated core assembly with 1008 heater rods including 54 instrumented rods. Differential pressure (DP) measurement devices are installed in the core peripheral region. This simulated core assembly was used for three tests of SB-CL-24 (SC0), SB-HL-05 (SH5) and TR-RH-06 (RH6). Temperature measurements in the core and core exit are similar to those in the 1st core assembly.

c) The 4th Core Assembly (Dec. 1997 - 2008)

Table 2-1 shows major LSTF facility remodeling with the 4th core assembly[10]. **Figure 2-5 (3)** shows horizontal cross-section of the 4th simulated core assembly with 1008 heater rods including only six instrumented rods. It should be noted that the number of instrumented heater rods is significantly lowered from those with the 1st and 2nd core assemblies at LSTF. Differential pressure (DP) measurement devices installed in the core peripheral region, however, are not used. This simulated core assembly was used for three SBLOCA tests of SB-PV-03 (SP3), SB-PV-07 (SP7) and SB-PV-08 (SP8).

3. Major Test Conditions

Major test conditions for ten SBLOCA tests are similar to those for the OECD/NEA ROSA Project Test 6-1 except for the break conditions, core power decay curves, operator actions, and selected indicator for operator or AM actions during core heat-up. Initial test conditions and control logics for the scram, primary pump coast-down, SG isolation, SG pressure control are common for ten SBLOCA tests in addition to the ECCS conditions with total failure of HPI system. Test conditions for two abnormal transient tests are different from the SBLOCA tests as shown below.

(1) Break Conditions

Ten SBLOCA tests are selected with different break conditions as shown in Table 1-1. Five break locations are PV top head, PV bottom head, cold leg, hot leg and pressurizer top (stuck-open power-operated relief valve (PORV)). The break size ranges from 10% (31.9 mm inner diameter (ID)) to 0.1% (3.2 mm ID) of the cold leg flow area. Thin-edged break orifice (Fig.3-1 (1)) is used for most of SBLOCA tests except for SB-HL-05 and SB-CL-24 with flush-type break orifice (Fig.3-1 (2)) mounted flush with the inner leg surface.

On the other hand, the TR-LF-03 test simulated the primary coolant discharge through the pressurizer safety valve (SV) under high pressure conditions and the TR-RH-06 test simulated open manhole by 58.4 mm ID orifice at the pressurizer during mid-loop operation under the atmospheric pressure condition.

(2) Common ECCS Conditions

In all tests, total failure of HPI system was commonly assumed as shown in Table 3-1. In five tests of SB-PV-07, SB-PV-02, SB-CL-01, SB-PV-01 and AT-SB-03, an operator action of the HPI recovery was made based on such indications as the CET superheat, hot leg temperature (HL T) superheat or timings. The accumulator injection system (AIS) and low pressure injection (LPI) system are available for ten SBLOCA tests but not for the mid-loop operation test (TR-RH-06).

(3) Primary Pump Coast-down and Core Power Decay Curves

In the initial steady state of ten SBLOCA tests and TR-LF-03 test, the primary pump speed was limited to simulate primary fluid temperature distribution in the reference PWR rated conditions under the limited core electric power of 10 MW (14% of the 1/48 scaled PWR power). It was increased to PWR pump speed immediately after the test start to simulate PWR pump coast-down characteristics after the scram. The pump speed control after the scram is shown in Table 3-2. In TR-RH-06 test, the primary pumps were not operated.

Tables 3-3 (1) and 3-3 (2) show two types of core power decay curves applied for eleven tests after the scram signal generation. The JAERI power curve (noted by J in **Table 3-1**) shown in **Table 3-3 (2)** was used for seven earlier tests conducted in and before 1990 and the new power curve (noted by N in **Table 3-1**) shown in **Table 3-3 (1)** was used for four tests conducted in and after 2002. **Figure 3-2** shows these core power curves[11] related to the PWR core power.

(4) Starting Conditions for Operator or AM Action

Table 3-1 shows operator or AM actions and indicators to start actions for all the tests. The CET superheat of 623 K was adopted in SB-PV-07 and SB-PV-08 tests as in the OECD/NEA ROSA Project Test 6-1 while the hot leg fluid superheat was adopted in SB-PV-02, SB-HL-05 and SB-PV-01 tests. For three tests of SB-CL-01, SB-CL-24 and SB-PV-03, grace time of 10-20 minutes from the break or SI signal was applied for the logic of operator actions. In the 10% cold leg break test of SB-CL-09, operator action was not conducted because fast primary depressurization resulted in early actuation of AIS. In the TMI-type test of AT-SB-03, an operator action to start HPI was initiated at 6600 s after the break by detecting core heat-up. In two tests of SB-CL-24 and SB-PV-03, the second AM action was conducted to promote primary system cooling by opening the PORVs when the primary pressure turned to increase under loss of SG secondary water levels (SB-CL-24) or the primary depressurization was significantly degraded by non-condensable gas inflow from the AIS tanks (SB-PV-03). In the TR-RH-06 test, an operator action to start the auxiliary feedwater (AFW) system was performed in case of core heat-up after the RHR system failed.

4. Overview of Twelve ROSA/LSTF Tests Focused on CET Performance

Major results in twelve LSTF tests are described in this Chapter with a focus on each CET performance to detect core heat-up conditions in addition to brief descriptions on major system responses and primary coolant mass or water level transients in each test. Chronology of events and test procedures in each test are shown in **Tables 4-1** through **4-12**.

4.1 1.0% PV Top Break Test (SB-PV-07) with HPI Actuation by CET Superheat

(1) Primary and Secondary Pressures Related to Major Events

The primary pressure became lower than the SG secondary pressures at about 1800s as shown in **Fig.4.1-1** by the progress of core boil-off after about 1600s in addition to the steam discharge at the break. Thereafter, the SG secondary sides became heat sources to the primary fluid and no steam condensation occurred in the SG U-tubes. The manual actuation of HPI system was initiated at 1926s by detecting the CET temperature increase up to 623 K. The HPI actuation promoted the primary depressurization and contributed to rapid core cooling under the continuous core power supply (**Fig.4.1-2**). The core heat-up was observed between 1610 and 2296s (**Fig.4.1-5**). After completion of core quench, the SG secondary depressurization action associated with auxiliary feedwater (AFW) supply was initiated to promote further primary depressurization at about 4200s. This test was terminated at 7266s by closing the break valve.

(2) Coolant Mass Decrease in PV and Hot Legs

The collapsed water levels in PV showed decreases as shown in **Fig.4.1-3** and recovered by the HPI actuation. The upper plenum (UP) water level started to decrease below the hot leg elevation just after the hot leg became almost empty of water (**Fig.4.1-4**). The core water level decrease started just after the UP was emptied. The hot leg mass recovery was observed after UP was fulfilled with water up to hot leg level.

(3) Core Heat-up Transients

The core heat-up behavior is shown in **Figs.4.1-6 (1)** through **4.1-6 (3)** by heater rod surface temperatures at the top (Pos.9), Pos.7 with peak cladding temperature (PCT) and Pos.5 at the middle height. Each rod temperature rise above saturation temperature (RC 200) derived from the system pressure at UP is dependent on each local power density. The overall core dryout progressed as shown in **Fig.4.1-7** from the top to middle core height suggesting a mixture level transient which is higher than the collapsed water level by less than 1m. The PCT was detected as 880.5 K at 2080s at Pos.7 of high-power rod B17(4,4).

(4) CET Performance to Detect Core Heat-up in SB-PV-07 Test

The CET temperatures were analyzed and related to core top rod temperatures (**Fig.4.1-8**) as shown below. An apparent superheat of CET started at 1722s at the core exit of central bundle (B23) and reached the AM set-point temperature (623 K) at 1836s (Figs. 4.1-9 (1) and 4.1-9 (2)). The CET temperatures monitoring, however, caused an arrival timing as 1926s by confirming more than two CET data above 623 K. Thus, a time delay of core heat-up detection by CETs from the core heat-up start is 316s for this test. The CET superheat distribution during the core heat-up period is shown in Fig. 4.1-10. A relation of superheats between the average CET temperature (DTave (UCP Outlet=CET)) during 1600 and 2200s and average core top elevation temperature (DTave (P9)) during the same period is shown in Fig. 4.1-11. When the average CET superheat started to increase, the average Pos. 9 rod surface temperature was 28.1 K. Thereafter, DTave (CET) increased almost linearly according to increase of DTave(P9) in a relation of

$$DTave(P9) = 1.98 \times DTave(CET) + 28.1 \text{ [K]}. \quad (1)$$

On the other hand, the maximum core rod temperature at 1926s was 789 K at Pos. 7 of high-power rod B17(4,4) indicating a temperature discrepancy of 166 K above the monitored CET temperature of 623 K.

The CET performance to detect the core heat-up in SB-PV-07 was similar to that in Test 6-1 under no fall-back water effects during most of the core boil-off period. Steam temperature difference was observed clearly between the high-power bundle B20 with CRGT at the core exit and the high-power bundle B15 without CRGT at the exit as shown in Figs. 4.1-12 (1) and 4.1-12 (2). The three-dimensional steam flows suggested in the OECD/NEA ROSA Project Test 6-1 due to the hot steam concentrating into the CRGT inlets may have occurred in this test too.

4.2 0.5% PV Top Break Test (SB-PV-02) with HPI Actuation by Hot Leg Superheat

(1) Primary and Secondary Pressures Related to Major Events

The primary pressure in SB-PV-02 test[3] was maintained slightly higher than the SG secondary pressures for a long time after the break as shown in Fig. 4.2-1. In the core heat-up period (3532-3980s), the primary pressure was controlled by the SG-A pressure regulation in intact loop while the SG-B pressure was close to the primary pressure (Fig. 4.2-3) until the HPI start at 3930s when hot leg superheat was detected by 10 K (refer Fig. 4.2-12). This indicates that steam condensation continued during the core heat-up process at least in the SG-A U-tubes. The HPI actuation contributed to immediate core cooling with no core power limitation (Fig. 4.2-2).

(2) Coolant Mass Decrease in PV and Hot Legs

Differential pressure (DP) data measured in the core, UP and downcomer indicate gradual water level decreases both in core and downcomer during the heat-up period and rapid recovery after the HPI actuation at 3930s (Fig. 4.2-4). It is shown here that the core water level temporarily decreased just after the HPI actuation due to a manometer effect caused by steam condensation in the cold legs and downcomer region. The Beam C fluid density data in HL-A (Fig.4.2-5) shows that water mass in HL-A bottom intermittently increased when the SG-A RV opened and the HL-A water level remained in the bottom during the all core heat-up period indicating continuous reflux water fall-back onto the CETs.

(3) Core Heat-up Transients

The core heat-up was observed before the HPI actuation at 3930s in the upper core region (Pos.9 to Pos.7) as shown in Fig.4.2-6 and Figs.4.2-8 (1) through 4.2-8 (4) and temporary core heat-up occurred after 3930s at Pos.6 through Pos.4. A part of upper core region, especially in peripheral bundle B07 under the HL-A, did not heat up before 3930s irrespective of the low core water level. This local core cooling can be attributed to effects of fall-back water from the HL-A. It should be noted that the CETs installed on the UCP were more affected by the fall-back water than a part of core top region as shown below. The peak cladding temperature (PCT) of 658 K was detected at 3973s at Pos.8 of high-power rod B14 (4,4) as shown in Fig.4.2-8 (2).

(4) CET Performance to Detect Core Heat-up in SB-PV-02 Test

As already stated, the core heat-up was not monitored by CETs but by the hot leg superheat in SB-PV-02 test. The CET temperatures showed limited heat-up at the exits of four central bundles (B21 through B24) and a few bundles (B14, B18, B11 & B05) at 3704s while the other CETs were maintained at saturation temperature (Figs.4.2-7 (1) and 4.2-7 (2)) because of fall-back water. The earliest CET superheat at 3704s was 172s later than the core heat-up start at 3532s. An average CET superheat (DTave (CET), Fig.4.2-9) during 3500 and 3950s is related to the limited average rod superheat at the core top (DTave (P9), Fig.4.2-10) during the same period in Fig.4.2-11. This shows a linear relation between them under the fall-back water conditions as,

$$DTave(P9) = 1.47 \times DTave(CET) + 16.9 \text{ [K]}. \quad (2)$$

The maximum CET temperature at 3973s was 600 K and it was 58 K lower than the PCT shown above. It should be noted that an extrapolation of the maximum CET temperature rise (TE 155 in Fig.4.2-7 (1)) between 3850 and 3950s may reach 623 K at about 4180s.

4.3 0.1% PV Top Break Test (SB-PV-08) with AM Action by CET Superheat

(1) Primary and Secondary Pressures Related to Major Events

The significantly small break at the PV top head resulted in very long transients and slightly higher primary pressure than those of two SGs which were regulated by the RV cycle opening (Fig.4.3-1). The core heat-up started at 38140s under low core power condition (Fig.4.3-2) and the AM action was initiated by detecting CET temperature at 623 K in this test. The core quench started just after the AM action start at 40760s and completed at 41040s by the core water level recovery. The AIS started water injection at 41188s. The lower SG pressures than the primary pressure suggest continued steam condensation at the SG U-tubes and fall-back water effects on the CET temperatures.

(2) Coolant Mass Decrease in PV and Hot Legs

The collapsed water level in UP (Fig.4.3-3) started to decrease below the hot leg level after the hot leg water level almost diminished at about 32000s (Fig.4.3-4). It is shown in Fig.4.3-3 that the downcomer water level almost balanced with the core water level during the boil-off process.

(3) Core Heat-up Transients

The core heat-up was observed in the upper region between Pos.9 and Pos.6 as shown in Fig.4.3-5 and Figs.4.3-6 (1) through 4.3-6 (4). The intermittent cooling at the core top was observed three times as a result of increased fall-back water caused by the intermittent SG-A relief valve (RV) opening. It should be noted that a part of core, especially in the peripheral bundles (B03 & B08) below the hot legs, was kept cooled for a long time suggesting the fall-back water effects and some intermediate rod temperature responses were also observed between the hot and cold rods. Thus, the fall-back water contributed to the local core cooling and also to the CET responses as shown below. The PCT was 700 K at 40790s at Pos.7 of high-power rod B17 (4,4). The detected core heat-up period is shown in Fig.4.3-7 between the earliest core heat-up time and the latest quench time at each thermocouple elevation.

(4) CET Performance to Detect Core Heat-up in SB-PV-08 Test

Figures 4.3-8 (1) and 4.3-8 (2) show the measured data of twenty CET temperatures during the core boil-off period. The CET superheat started to occur at 39125s and the monitored CET temperature increased to 623 K at 40760s. The CET temperature at 623 K is 2620s later than the core heat-up start of 38140s. The higher CET temperatures were detected at the exit of central bundles (B21 through B23) but most of the CETs showed low temperatures due to fall-back water. An average CET superheat (DTave (CET), Fig.4.3-9) between 39400 and 40800s related to the average rod superheat at the core top (DTave (P9), Fig.4.3-10) indicates a limited linear relation between them (see Fig.4.3-11) when the DTave (CET) is higher than 10 K, as,

$$\mathrm{DTave(P9)} = 1.96 \times \mathrm{DTave(CET)} + 28.9\ [\mathrm{K}]. \qquad (3)$$

A temperature discrepancy between the maximum core rod temperature (694 K) at 40760s and the monitored CET temperature (623 K) was 71 K.

4.4 10% Cold Leg Break Test (SB-CL-09)

(1) Primary and Secondary Pressures Related to Major Events

The larger break size of SB-CL-09 test[4] caused faster primary depressurization (Fig.4.4-1) than other SBLOCA tests. The primary pressure became lower than the SG secondary pressures at about 100s after the loop-seal clearing (LSC) that occurred at 74s. Thereafter, the SG secondary sides became heat sources to the primary fluid and no steam condensation could occur in the SG U-tubes. The core heat-up started at 67s at the middle height (Pos.5) during the LSC process and the increased rod temperature up to 923 K (**Fig.4.4-5**) caused trip-off of the core power at 111s (**Fig.4.4-2**). The AIS water injection started at 195s and the low pressure injection (LPI) started at 303s.

(2) Coolant Mass Decrease in PV and Hot Legs

After the start of break at the broken loop cold leg (CL-B), the downcomer collapsed water level was kept higher than 7.2m (equal to EL 5.4m at the cold leg bottom) until the LSC at 74s while the core collapsed water level decreased between 16 and 55s suggesting an increase of the void fraction in the core (**Fig.4.4-3**). The collapsed water level was especially lowered during the LSC process resulting in core heat-up in most of the core region except for the bottom (Pos.1) as will be shown in **Fig.4.4-5**. It was confirmed in the data report[4] that more water remained in the hot legs (**Fig.4.4-4**) and in SG U-tube inlet sides than in the cold legs and U-tube outlet sides respectively, and contributed to significant core water level depression. The core water level recovered after the LSC completion at 80s but only to the middle height. This resulted in further rod temperature excursion in the upper core region until the core power trip. A large pressure difference between UP and downcomer (**Fig.4.4-9**) is resulted from the specific primary coolant mass distribution. The PV collapsed water levels increased after the AIS actuation at 195s.

(3) Core Heat-up Transients and No CET Temperature Rise

The core heat-up started at 67s at the core middle height (Pos.5 with maximum linear heat rate), progressed until the core power trip time at 111s and finally quenched at 153s as shown in **Figs.4.4-7 (1)** through **4.4-7 (5)**. It appeared that heater rod temperature increases distributed widely suggesting effects of two-dimensional water fall-back. The PCT of 930 K was recorded at Pos.6 of high-power rod B16 (4,4) at the time of power trip (111s) with saturation temperature of 566.1 K. Variety of rod heat-up and quench behavior in this test is shown in **Fig.4.4-8**. The later heat-up was observed in the high-power bundle B20 in the loop-A hot leg side than those in bundles B15 and B16 in the loop-B hot leg side. In the peripheral bundles (B07 and B10) with low power density, similar tendency was observed.

All the CET temperatures showed no heat-up during the core heat-up process as shown in **Figs.4.4-6 (1)** and **4.4-6 (2)**. It should be noted that the measurement of twenty CETs were more largely influenced by the fall-back water on the UCP.

4.5 2.5% Cold Leg Break Test (SB-CL-01) with HPI Actuation after 20 Minutes

(1) Primary and Secondary Pressures Related to Major Events

The primary pressure turned to decrease after the LSC at 360s by steam discharge at the break and became lower than the SG secondary pressures at about 440s (**Fig.4.5-1**). Thereafter, the SG secondary sides became heat source to the primary fluid and no steam condensation occurred in the SG U-tubes. The SG-A secondary pressure decreased faster than that of SG-B because the AFW was unexpectedly supplied only to the SG-A side while there was no AFW flow to the SG-B side. The core heat-up started at 575s at the top part (Pos.9) and finally reached the maximum limiting temperature (923 K) resulting in core power trip at 887s (**Fig.4.5-2**). The AIS injection started at 850s and the core was finally quenched at 1086s. The HPI started at 1200s.

(2) Coolant Mass Decrease in PV and Hot Legs

The DP data in PV (**Fig.4.5-3**) show that the core water level temporarily decreased a little at the time of LSC and continuously decreased in the boil-off process after 550s. The PV water mass recovery started after the AIS actuation. The hot leg remaining water almost diminished until 650s suggesting very little fall-back water effects on CETs except for early core heat-up period.

(3) Core Heat-up Transients

There was no core heat-up observed in the LSC process but the core heat-up during boil-off extended to Pos.4 below the core middle height (**Figs.4.5-5** and **4.5-7 (1)** through **4.5-7 (7)**). The core was finally quenched at 1086s. The heater rods showed that the temperature excursion started at almost the same time in the horizontal domain. The PCT of 929 K was recorded at Pos.7 of high-power bundle B20 (4,4) at the time of core power trip.

(4) CET Performance in SB-CL-01 Test

In this test, the CETs were not used for core heat-up monitoring and showed the earliest heat-up at 629s (54s later than the core heat-up start) and the latest heat-up at 769s (**Figs. 4.5-6 (1)** and **4.5-6 (2)**). The maximum CET temperature increased to 623K at 790s at the exit of central bundle (B21), which was 182 K lower than the hottest rod and 215s later than the core heat-up start (575s). Wide variety was observed among the CET temperature increases especially between the central region and the peripheral region. When the PCT was recorded at 887s, the maximum CET temperature was 669 K which was 260 K lower than the PCT.

An average CET superheat (DTave (CET), **Fig.4.5-9**) during 560 and 880s is related to the average heater rod superheat at the core top (DTave (P9), **Fig.4.5-8**) during the same period as shown in **Fig.4.5-10**. Therefore, this relation does not include the time period after the core power trip. This shows a good linear relation between them as,

$$DTave(P9) = 2.15 \times DTave(CET) + 26.0 \text{ [K]}. \qquad (4)$$

4.6 0.5% Cold Leg Break Test (SB-CL-24) with Three AM Actions

(1) Primary and Secondary Pressures Related to Major Events

The primary pressure in SB-CL-24 test[5] was kept slightly higher than the SG secondary pressures for most of the test period. Meanwhile, the SG depressurization action was started as the 1st AM action at 600s, being followed by the AIS actuation at 2110s and final AIS termination at 4086s (**Fig.4.6-1**). The primary pressurization started at about 4160s due to complete loss of SG secondary coolant mass under continued core power supply (**Fig.4.6-4**). The PORV was manually opened as the 2nd AM action at 6568s by detecting CET heat-up and then the pressurizer safety valve was opened as the 3rd AM action at 6610s (**Fig.4.6-9**). The further core heat-up caused the core power limitation to 75% at 7109s, 50% at 7156s and 10% at 7166s, respectively. As the SG secondary pressures were lower than the primary pressure, SG reflux water effects may have remained even in the core boil-off and heat-up period (5929 - 7675s). The test period was divided into four phases[5] as noted in **Fig.4.6-1**.

(2) Coolant Mass Decrease and Observed Three LSC Processes

The collapsed water levels in the core and UP (**Fig.4.6-2**) show three temporary water level decreases corresponding to three LSC processes and later core boil-off process. The fluid density data in both HL-A and CL-B also show water level changes corresponding to three LSC processes (**Figs.4.6-5** and **4.6-6**). The lowest mixture level was detected at Pos.5 in the core (core middle height) just before the primary depressurization action. A temporary recovery of core mixture level was caused by the PORV and safety valve opening (see **Fig.4.6-2** and **Fig.4.6-14**). The core water level recovered by the LPI that started at 7371s.

(3) Core Heat-up Transients

Temporary core heat-up was observed at the upper part of core (between Pos.9 and Pos.7) during the three LSC processes (**Fig.4.6-8**).

Significant core heat-up occurred in the boil-off process with different rod heat-up timing in the horizontal domain depending on rod location relative to the hot legs from which SG reflux water flowed down (**Figs.4.6-12 (1)** through **4.6-12 (3)**, **4.6-13** and **4.6-14**). Then, SG reflux water fall-back partly cooled the core especially in the peripheral core region under the hot legs. The core heat-up was limited after the core power limitation. The PCT of 921K was detected at Pos.8 of the high-power rod B18 (4,4) at 7166s.

(4) CET Performance in SB-CL-24 Test

No CET superheat was observed during three LSC processes (**Fig.4.6-7**) while a temporary core heat-up was observed at the upper core region in each LSC process (**Fig.4.6-8**) .

The CET heat-up started at 6280s; 351s after the core heat-up start, and the earliest heat-up reached 623 K at 6536s which was 158 K lower than the hottest rod temperature of 781 K and 607s later than the core heat-up start (**Figs.4.6-10 (1)**, **4.6-10 (2)** and **4.6-11**). All the CETs detected superheat within 360s from the detection start.

An average CET superheat (DTave (CET), **Fig.4.6-11**) during 5900 and 7500s is related to the average heater rod superheat at the core top (DTave (P9T), **Fig.4.6-15**) during the same period as shown in **Fig.4.6-16**. This relation at lower DTave (P9T) than 280 K shows almost linear relationship in the heat-up process until 7000s under no core power limitation as,

$$DTave(P9) = 1.88 \times DTave(CET) + 40 \text{ [K]}. \quad (5)$$

4.7 0.5% Hot Leg Break Test (SB-HL-05) with AM Action by Hot Leg Superheat

(1) Primary and Secondary Pressures Related to Major Events

The break location at the bottom of HL-B caused earlier coolant mass loss and later steam discharge through the break comparing with the hot leg side and top break cases. The primary pressure was kept slightly higher than the SG secondary pressures until the AM action at 2162s (**Fig.4.7-1**) which was the PORV opening when the hot leg fluid temperature showed slight superheat by 5 K (**Fig.4.7-10**). Thereafter, two SG secondary sides became heat sources to the primary fluid and no reflux water affected the core heat-up behavior. The AIS injection started at 2750s. The core power was temporarily limited after 2812s to limit the core heat-up and finally terminated at 2870s (**Fig.4.7-2**).

(2) Coolant Mass Decrease in PV and Hot Legs

The hot leg-B became steam-filled at about 1500s (**Fig.4.7-4**) prior to the start of water level decrease in UP. The water level decrease in core started at about 1920s. The PORV opening temporarily maintained the core water level while the downcomer water level rapidly decreased suggesting coolant mass transport from the downcomer to core region (**Fig.4.7-3**). Rapid mass recovery was observed after the AIS actuation in the PV, then in the hot legs.

(3) Core Heat-up Transients

The core heat-up started at the core top (Pos.9) at 2000s and the PORV opening temporarily cooled once a part of the heated core (Pos.9 and Pos.8). The core heat-up started again at about 2300s and extended to Pos.4 below the core middle height (**Figs.4.7-6 (1)** through **4.7-6 (6)**) with no variation in the heat-up timing at the same elevation. The core power limitation stopped the core heat-up excursion at 2812s.

(4) CET Performance in SB-HL-05 Test

Although the earliest CET heat-up was observed at 2110s at the exit of high power bundle (B14), slow increase in the CET temperatures followed (**Figs.4.7-5 (1)** and **4.7-5 (2)**) because of the decrease in the saturation temperature after the PORV opening at 2162s. Thus, the effective overall CET heat-up started after about 2300s. The highest CET temperature reached 623 K at 2606s at the exit of central bundle (B21).

An average CET superheat (DTave (CET), **Fig.4.7-7**) between 1900 and 2800s under no core power limitation is related to the average heater rod superheat at the core top (DTave (P9), **Fig.4.7-8**) during the same period as shown in **Fig.4.7-9**. This relation consists of two steps; the early one with small CET superheat before 2300s (DTave (CET)$\leqq$5K) and the later one with significant CET heat-up (DTave (CET)$\leqq$100 K). The latter relation can be expressed by almost linear relation as,

$$DTave(P9) = 2.08 \times DTave(CET) \quad \text{[K]}. \quad (6)$$

A time delay of the earliest CET temperature increase up to 623K (2606s) was 606s later than the core heat-up start at 2000s. A temperature discrepancy between the hottest CET and the hottest core at 2606s was 126 K.

4.8 0.5% PV Bottom Break Test (SB-PV-01) with HPI Actuation by Hot Leg Superheat

(1) Primary and Secondary Pressures Related to Major Events

The break location at the PV bottom in SB-PV-01 test[3] caused water discharge and no steam discharge until about 2000s. The primary pressure response in SB-PV-01 test (**Fig.4.8-1**) was similar to that in SB-HL-05 test and started to gradually decrease after core heat-up initiation at 1498s. It should be noted that the core became completely empty of liquid at 1638s. The HPI was actuated at 1676s. All the HPI liquid, however, was discharged from the break, not reaching the core. The core power was finally terminated at 1775s (**Fig.4.8-2**). The HPI actuation caused rapid depressurization and resulted in AIS actuation at 2057s. In the rapid primary depressurization process, two SG secondary sides became heat sources to the primary fluid and no reflux water affected the core heat-up behavior.

(2) Coolant Mass Decrease in PV and Hot Legs

The PV collapsed water level and DP data in UP, lower plenum and downcomer regions show significant mass decrease after about 1400s and mass recovery after the AIS actuation (**Fig.4.8-3**). The hot leg-A became almost steam-filled after about 1400s (**Fig.4.8-5**) and fluid temperature showed superheat of 10 K (**Fig.4.8-6**) at 1676s for HPI actuation. The PV coolant mass did not well recover after the HPI actuation but recovered rapidly after the AIS actuation (**Fig.4.8-12**).

(3) Core Heat-up Transients

The core heat-up started at Pos.8 of high-power rod (B18) at 1498s and the whole core started heat-up within a very short time by 1638s (**Fig.4.8-4**, **Figs.4.8-8 (1)** through **4.8-8 (8)** and **Fig.4.8-12**). In the upper core part, variation in the heat-up timing was slightly observed, especially in the peripheral bundle. The PCT of 923 K was recorded at Pos.5 (core middle height, **Fig.4.8-8 (5)**) of high-power rod B16 (1,7) at 1775s. The core power termination limited further core heat-up.

(4) CET Performance in SB-PV-01 Test

The CET heat-up started at 1586s at the exit of central bundle (B22) and the highest CET temperature reached 623 K at 1612s at the exit of central bundle (B21) (**Figs.4.8-7 (1)** and **4.8-7 (2)**). Apparent time difference appeared when the CET temperature reached 623 K between the higher CET temperatures in the central region and lower CET temperatures in the peripheral region.

An average CET superheat (DTave (CET), **Fig.4.8-9**) between 1450 and 1770s is related to the average heater rod superheat at the core top (DTave (P9), **Fig.4.8-10**) in the same period as shown in Fig.4.8-11. This relation can be roughly expressed by a linear relation as,

$$DTave(P9) = 2.05 \times DTave(CET) \quad [K]. \qquad (7)$$

The attenuation in the CET temperature became significant at high temperature region, being resulted from the decrease in upward steam flow after the complete loss of coolant from the PV at about 1700s.

A time delay of the earliest CET temperature increase up to 623K at 1612s was 114s later than the core heat-up start (1498s) and a temperature discrepancy between the hottest CET (623 K) and the maximum temperature at Pos.6 of B17(4,4) rod was 109 K.

4.9 0.2% PV Bottom Break Test (SB-PV-03) with Three AM Actions

(1) Primary and Secondary Pressures Related to Major Events

The smaller break area in SB-PV-03 test[6] resulted in slower primary depressurization than in SB-PV-01 test until the AM action which was initiated at 945s by opening SG relief valves (RVs) that were controlled to cause the primary loop cooling rate at -55 K/h (Fig.4.9-1). The AIS started at 3241s. After the end of AIS coolant injection, non-condensable gas inflow occurred from the AIS tanks, which caused degradation of primary depressurization (Fig.4.9-6). The 2nd and 3rd AM actions were initiated by fully opening the SGRVs at 8970s and by opening PORV of pressurizer at 9060s, respectively. The LPI started at 9280s. The HPI was injected after the test to estimate remained gas volume under pressurization.

The boil-off core heat-up was observed between 8573 and 9680s (Fig.4.9-2). The core power was degraded to 50% at 9198s and to 10% at 9200s, respectively to limit further core heat-up (Figs.4.9-3 (1) and 4.9-3 (2)). As the secondary pressures were kept lower than the primary pressure for all test period, steam condensation in the SG U-tubes continued resulting in fall-back water effects on the CETs and local core cooling.

(2) Coolant Mass Decrease in PV and Hot Legs

The UP and core collapsed water levels temporarily decreased during the AIS injection period (Fig.4.9-4) and caused a limited heat-up at the top part of core. The core boil-off started after the completion of coolant injection by AIS and was diminished by the LPI actuation. During the core boil-off process, the hot leg beam-C density data (Fig.4.9-5) detected water level at the bottom suggesting reflux water from SG.

(3) Core Heat-up Transients

The core heat-up due to boil-off started at Pos.8 at 8573s and extended to Pos.2 in the lower part by about 9300s (Fig.4.9-7, Figs.4.9-9 (1) through 4.9-9 (7) and Fig.4.9-10). It is shown that the fall-back water largely contributed to local cooling above the mixture water level, which caused large time delay for local dryout from the earliest core heat-up front (Fig.4.9-10). The PCT was detected at Pos.6 of the high-power rod B13 (4,4) as 925

K at 9200s.

(4) CET Performance in SB-PV-03 Test

All the CET temperatures showed no heat-up during the boil-off core heat-up process (**Fig.4.9-8**) until the PORV opening because of the fall-back water from two SGs.

After the PORV opening at 9060s, the CET started heat-up at 9182s (**Fig.4.9-8**) under the uprising steam flow conditions in the core. This CET heat-up time is 609s later than the core heat-up start. The maximum CET temperature at 9200s was 488 K which was 437 K lower than the PCT in the core.

An average CET superheat (DTave (CET), **Fig.4.9-13**) between 9100 and 9600s is related to the average heater rod superheat at the core top (DTave (P9), **Fig.4.9-11**) as shown in **Fig.4.9-14**. This relation includes a time period of significantly limited core power between 9200 and 9600s. It is clear that the DTave (CET) showed no superheat in a time period before the core power limitation at 9200s irrespective of the superheat of DTave (P9) above 50 K.

4.10 TMI-type LOCA Test (AT-SB-03) with HPI Actuation by Core Heat-up Monitoring

(1) Primary and Secondary Pressures Related to Major Events

The PORV stuck-open is the origin of coolant mass loss, and the resulted primary and SG secondary pressure transients (**Fig.4.10-1**) are similar to those in 0.5% PV top break test (SB-PV-02). The core heat-up started at 5517s and the core power was significantly degraded after 6050s to limit the core heat-up (**Fig.4.10-2**). Thereafter, the primary pressure decreased faster than the SG secondary pressures resulting in decrease of fall-back water effects on core cooling. The early core heat-up period was under influences of reflux fall-back water from SGs. The HPI was manually actuated at 6600s. The core quench was completed until 6830s.

(2) Coolant Mass Decrease in PV and Hot Legs

The collapsed water levels in PV (**Fig.4.10-3**) started to decrease after the water levels in two hot legs almost diminished at 4800s (**Figs.4.10-4** and **4.10-5**). The primary coolant mass recovered after the HPI actuation.

(3) Core Heat-up Transients

The core heat-up by boil-off started at Pos.9 of high-power rods at 5517s and extended to Pos.4 below the middle height by about 6390s (**Figs.4.10-6 (1)** through **4.10-6 (7)**). It is shown that the fall-back water caused wide distribution of heat-up timing from 5517 to 6120s at Pos.9 (**Fig.4.10-6 (1)**). Similar but narrower time range of heat-up timing appeared down to Pos.8 (**Fig.4.10-6 (2)**). The fall-back water effects on local core cooling continued until 6200s (see Pos.7 in **Fig.4.10-6 (3)**). The maximum core temperature was 698 K at Pos.7 of the high-power rod B13 (4,4) when the CET temperature reached 623 K (5996s).

(4) CET Performance in AT-SB-03 Test

The earliest CET heat-up started at 5850s at the exit of peripheral bundle (B05) which is located far from two hot leg nozzles. As the last CET heat-up was detected at about 6130s, it took about 280s to complete all CETs heat-up. When the hottest CET reached 623 K at 5996s, a temperature discrepancy to the coldest CET was 75 K.

An average CET superheat (DTave (CET), Fig.4.10-8) between 5500 and 6700s is related to the average heater rod superheat at the core top (DTave (P9), Fig.4.10-9) as shown in Fig.4.10-10. A time range of no core power limitation corresponds to DTave (P9) lower than 89 K. Although this time period includes a period of fall-back water effects (before 6200s) and the limited core power period (6050 - 6700s), almost linear relation is reduced as,

$$DTave(P9) = 1.42 \times DTave(CET) + 23.6 \ [K]. \qquad (8)$$

4.11 Transient TMLB' Simulation Test (TR-LF-03)

(1) Primary and Secondary Pressures Related to Major Events

Loss of off-site power (T), loss of main feedwater (M), loss of AFW (L) and loss of on-site power (B') resulted in safety valve operation at two SGs until 4552s (Fig.4.11-1). When the SG secondary coolant was almost lost, the primary pressure turned to increase at about 3600s through the pressurizer water level increase (Fig.4.11-4). The pressurizer PORV started cycle opening at 4400s. The core heat-up started at 9657s due to coolant discharge through the pressurizer. As the primary side was kept at higher pressure than the SG secondary sides, steam condensation in U-tubes could be possible (but not evident).

(2) Coolant Mass Decrease in PV and Hot Legs

The PV mass inventory started to decrease after 4400s (Fig.4.11-3). The hot leg was filled with water until about 7000s (Fig.4.11-6) and thereafter steam phase was detected in the upper region of hot leg. Coolant mass depletion in the SG U-tubes started at about 7500s and the primary loop natural circulation almost stopped after 7700s (Fig.4.11-5). The core DP data (DP 50 in Fig.4.11-3) showed fast decrease at 9600s indicating start of core boil-off. Thereafter, less fall-back water came from hot legs on to the UCP and core.

(3) Core Heat-up Transients

The radial power profile was assumed to be flat in this test. The core heat-up started at the top part (Pos.9) at 9657s and extended to Pos.3 in the lower part by 10520s (Fig.4.11-8 & Figs.4.11-9 (1) through 4.11-9 (5)). The core power was stepwise decreased after the test end at 11000s (Fig.4.11-2).

(4) CET Performance in TR-LF-03 Test

As the primary pressure was kept higher than 17 MPa during the core boil-off process, all the CET temperatures were always higher than 626 K (Fig.4.11-7 (1) and 4.11-7 (2)). This means that an usual criterion of 623 K is not applicable to this kind of abnormal transient. The criterion should then be replaced with an alternative indicator such as a CET superheat above the saturation temperature. The earliest CET superheat was detected at 9780s in the central region and the last one was observed at 10050s in the peripheral region below the HL-B (exit of B03 and B04 bundles). The earliest CET superheat time was 123s later than the core heat-up initiation.

At 11000s just before the core power limitation, the highest rod temperature of 902.4 K was detected at Pos.7 of B20 (1,1) rod. As the highest CET temperature at 11000s was 842.7 K, a temperature discrepancy between them was about 60 K.

An average CET superheat (DTave (CET), Fig.4.11-10) between 9600 and 11000s is related to the average heater rod superheat at the core top (DTave (P9), Fig.4.11-11) as shown in Fig.4.11-12. It is shown here that a good linear relation is found between them as,

$$DTave(P9) = 1.58 \times DTave(CET) \quad [K]. \tag{9}$$

4.12 Loss-of-RHR Test during Mid-loop Operation (TR-RH-06)

(1) Primary and Secondary Pressures Related to Major Events

This test was initiated with the primary pressure at 0.11 MPa (Fig.4.12-1), SG secondary pressures at about 0.13 MPa, no SG secondary side water level, hot leg water level at middle height, constant core power at 0.38 MW (Fig.4.12-2), break orifice with 58.4 mm ID at the pressurizer top in addition to the LPI coolant injection (about 40 K) into cold leg ECCS nozzle under RHR mode with circulation flow rate at about 5 kg/s (Fig.4.12-7) toward outlet at hot leg bottom (about 60 K).

The Loss-of-RHR which was initiated at 683s caused coolant boiling in the core and the primary pressurization at about 1250s. The pressurizer water level started to increase at 1930s (Fig.4.12-4). The core heat-up started at the top part at 9045s by boil-off. The AFW supply to SG-B was initiated at 9830s by detecting the core heat-up at 523 K in order to pull down the pressurizer coolant mass back to the core due to steam condensation in SG U-tubes. HPI was injected to cold legs at 10340s because the steam condensation in the SG U-tubes did not occur. The core power was temporarily terminated at 10870s to limit the core heat-up. The heated core was quenched until 11130s.

(2) Coolant Mass Decrease in PV and Hot Legs

The hot legs became almost empty until about 6500s except for the bottom of HL-B in which subcooled reflux water from the SG-B was detected in a thin layer (Fig.4.12-6). This reflux water remained until 10700s in the HL-B. The PV water levels started to monotonically decrease after about 5500s (Fig.4.12-3). The downcomer and core water levels turned to rise after the HPI actuation.

(3) Core Heat-up Transients

The core superheat above saturation temperature (384 K) started at the top part (Pos.9) at 9045s and extended to Pos. 6 above the middle height by 10130s (Fig. 4.12-8 and Figs. 4.12-10 (1) through 4.12-10 (5)). The core was finally cooled by the HPI actuation until 11130s. Each heater rod temperature rise mainly depended on transient core water level and the radial peaking factors among the high, middle and low-power bundles. The PCT was 926 K at Pos. 8 of B14(4,4) rod when the core power was decreased to zero at 10870s.

(4) CET Performance in TR-RH-06 Test

The earliest CET heat-up started at about 9800s in the central region and this time was later than the core heat-up start by 755s. The last CET heat-up was about 10190s with a delay time of 390s from the earliest one. The hottest CET at 10870s was 477.2 K which is 449 K lower than the PCT.

An average CET superheat (DTave (CET), Fig. 4.12-11) is related to the average heater rod superheat at the core top (DTave (P9), Fig. 4.12-12) between 9000 and 11400s as shown in Fig. 4.12-13. This time period includes the temporary core power limitation period. An almost linear relation between them is reduced for a time period with no core power limitation before 10870s (DTave(P9) less than 290 K) as,

$$DTave(P9) = 3.85 \times DTave(CET) + 120 \text{ [K]}. \quad (10)$$

This result may suggest significant influences of cold reflux water from the SG-B and larger steam velocity at the core exit (estimated as 2.0 m/s in average at the UCP flow paths during the core heat-up period, which was significantly larger than those in other tests) in addition to the cold structural materials including the UCP on the CET performance to detect core heat-up.

5. General CET Performance in LSTF Experiments

The followings are derived with respect to CET performance to detect core heat-up through additional twelve LSTF experiments.

(1) No CET Heat-up in Two Tests

As the most significant effects of fall-back water, all the CETs showed no heat-up during the core heat-up period in two tests. One is the 10% cold leg break LOCA test (SB-CL-09) with core heat-up period followed by the loop-seal clearing process in which much coolant in the hot legs and SG inlet sides fell down to CETs and core peripheral region. Another one is the 0.2% PV bottom break LOCA test (SB-PV-03) with core heat-up period under the SG depressurization action until the start of further AM action to open PORV. The former case may not be significant as to an AM action because the transient is faster before the operator intervention is required.

(2) General Time Delay of CET from Core Heat-up in Ten Tests

In other ten tests, the CETs detected core heat-up with each time delay including limited fall-back water effects (see **Table 5-1**). The time of CET heat-up start (t_{CET}) can be related to core heat-up (inadequate core cooling; ICC) start time (t_{ICC}) as, t_{CET} / t_{ICC} varies from 1.01 to 1.09. On the other hand, a relation[2] obtained in the earlier LSTF tests, 0.7603 x $(t_{CET})^{1.027}$ / t_{ICC} gives a good agreement within ±6%.

A relatively large delay time was observed in TR-RH-06 test in which both cooling effects of cold reflux water from SG-B and larger steam velocity at core exit were observed under significantly low pressure conditions of mid-loop operation.

(3) CET Location with Maximum Heat-up in Ten Tests

The CETs in central region detected maximum superheat in most of tests (see **Table 5-2**). The maximum core heat-up was, however, observed in the high-power bundles which are located between the central region with middle-power bundles and the peripheral region with low-power bundles. Each CET heat-up behavior showed a variety depending on several factors such as the SG reflux water fall-back, radial core power profile, effects of colder structural materials and three-dimensional steam flows in the core and core exit. Best arrangement of CETs and locations of monitored CETs for early detection in AM actions can be investigated by considering influences of such factors onto CET performance.

(4) Temperature Discrepancy from the Hottest Core Region in Ten Tests

In general, a temperature discrepancy between the core and CETs increases as the core heat-up increases due to the following reasons; (a) when structural materials are colder than the superheated steam temperature at the core exit, (b) when core water level decreases to the middle height at higher axial power, (c) when cold reflux water falls back to UCP and (d) when hotter steam flow concentrates to CRGTs in case of PV top break, CET at outside of CRGT detects lower steam temperatures. The temperature discrepancy from the hottest core region at the time of CET at 623 K was less than 200 K in most tests (see Table 5-3) except for three tests; two tests (SB-CL-09 and SB-PV-03) with no CET heat-up and a mid-loop operation test (TR-RH-06). In these three tests, the PCT exceeded the CET by 360-450 K.

(5) Effects of Elevated Pressure Conditions above 17 MPa

The TMLB' transient test (TR-LF-03) showed that all the CET temperatures rose up above 623 K prior to the core heat-up initiation because of high saturation temperature. This indicates that an alternative indicator such as a CET superheat above the saturation temperature is necessary as an AM indicator instead of the absolute CET temperatures.

(6) No CET Heat-up during Loop-seal Clearing Process

In the 2.5% (SB-CL-01) and 0.5% (SB-CL-24) cold leg break LOCA tests, no CET superheat was observed during the temporary time period of loop-seal clearing in which early but limited core heat-up occurred in upper core region comparing with the general CET heat-up during boil-off transient.

(7) Average CET Heat-up Behavior Related to Average Core Top Heat-up in Ten Tests

The average CET heat-up was almost linearly related to the average rod heat-up at the core top (Pos.9) in ten tests (see Table 5-4 and Fig.5-1) in a form of,

$$DTave(P9) = C1 \times DTave(CET) + C2 \text{ [K]}. \qquad (11)$$

C1 varies from 1.4 to 2.2 (1.84 in average) for nine tests including limited fall-back conditions except for extremely low pressure test (TR-RH-06) in which C1=3.85. C2 varies from 0 to 40 K for nine tests while C2 was extremely high as 120 K for TR-RH-06 test. These relations are useful to estimate core top heat-up by using CET temperature responses.

(8) Influences of Break Locations

The linear relationships similarly appeared in the average CET temperature superheating against the Pos.9 average temperature superheating in the core when steam in the core was led to the break at such locations as hot leg, cold leg, upper head and pressurizer irrespective of their different break locations. When the core liquid level decreased to the lower parts in PV bottom break test, the steam upflow at the core exit was not well attained, causing inadequate heat-up of CETs. Since the liquid level decrease rate in the core is greater in the PV bottom break LOCA than in the other LOCA cases, this condition may lead to a large delay in the operator action.

6. Conclusions

This report summarizes performances of core exit thermocouples (CETs) observed in twelve ROSA/LSTF tests that include ten SBLOCA tests and two abnormal transient tests, as a supplement to the results of OECD/NEA ROSA Project Test 6-1[1].

Ten SBLOCA tests consist of three pressure vessel (PV) top break tests with break sizes ranging from 1.0 to 0.1% equivalent to cold leg break, three cold leg break tests with break sizes from 10 to 0.5%, two PV bottom break tests with 0.5 and 0.2% break, one 0.5% hot leg break test and a TMI-type PORV stuck-open LOCA test. Two abnormal transient tests respectively simulate a TMLB' (station blackout) and a loss-of-RHR during mid-loop operation.

General CET performances observed in these LSTF tests are summarized in Chapter 5 on eight points such as (1) No CET heat-up, (2) General time delay from core heat-up, (3) CET location with maximum heat-up, (4) Temperature discrepancy from hottest core, (5) Effect of high saturation temperature, (6) CET response during loop-seal clearing, (7) Average CET heat-up behavior against average core top-elevation heat-up and (8) Influences of break location.

Major findings and notices are summarized as follows;

(1) CET performance in the 1.0% PV top break test (SB-PV-07) was confirmed similar to that in the OECD/NEA ROSA Test 6-1 including a time delay to detect core heat-up and resulting temperature discrepancy between the CETs and hottest core. Influences of 3D steam flow in the core and core exit was observed too around high-power bundles with or without control rod guide tubes (CRGTs) due to uprising steam flow toward the break at PV top through the CRGTs.

(2) No CET superheat was detected in two tests; 10% cold leg break test (SB-CL-09) and 0.2% PV bottom break test (SB-PV-03). There was a significant core heat-up during loop-seal clearing (LSC) process and two-phase downward flow in the core in the former test. In the latter test, there was SG reflux water fell down to the upper plenum and core resulting in local core cooling even above the lowered collapsed water level. The CETs then detected core heat-up only after the PORV opening.

(3) In ten LSTF tests except for two tests (SB-CL-09 & SB-PV-03), the CETs contributed to detect core heat-up with each time delay from the core heat-up start and each temperature discrepancy between the CETs and the hottest core. Test conditions of these tests include

five break locations at the PV top, PV bottom, cold leg, hot leg and PORV stuck-open at the pressurizer. In these tests, the average CET superheat was almost linearly related to average rod superheat at the core top measurement location (Position 9 in LSTF core). Followings are two exceptional cases that may raise an important notice that the CET superheat above saturation temperature should be used as an AM indicator instead of the absolute CET temperatures.

a) The delay time and temperature discrepancy in the loss-of-RHR test (TR-RH-06) were significantly larger than those in the other tests probably due to cooling effects of reflux water fall-back from empty SG and larger steam velocity under low-pressure transient.

b) CET temperatures in the TMLB’ test (TR-LF-03) were elevated above 623 K prior to core heat-up initiation as a result of primary pressure higher than 17 MPa.

(4) Applicability of the LSTF CET performance to PWR LOCA/transients conditions should be carefully analyzed with respect to the effects of scaled configuration of the LSTF upper plenum and core from those in the PWRs on the fall-back water behavior, the CET locations and monitoring methods of CETs as one of the AM indicators. An optimized CET monitoring method for early detection of core heat-up may then be possible considering such CET superheat behavior.

Acknowledgement

The authors are grateful to Dr. Yoshiaki SUZUKI of Nuclear Safety Research Center for his review of this report, all ROSA members for their contribution to conduct twelve LSTF tests during a long period between April 1985 and October 2005 and Ms. K.TOYODA of IT-TEC Inc. for her contribution to experimental data processing.

References

[1] M.SUZUKI, et al., "Performance of Core Exit Thermocouple for PWR Accident Management Action in Vessel Top Break LOCA Simulation Experiment at OECD/NEA ROSA Project," Proceedings of ICONE16-48754, 11p, (2008) in CD-ROM.

[2] M.SUZUKI, "Characteristic Responses of Core Exit Thermocouples during Inadequate Core Cooling in Small Break LOCA Experiments Conducted at Large-Scale Test Facility (LSTF) of ROSA-IV Program", Proceedings of ICONE2, pp.63-68, Vol.1 (1993).

[3] M.SUZUKI, "Break Location Effects on PWR Small Break LOCA Phenomena - Inadequate Core Cooling in Lower Plenum Break Test at LSTF", JAERI-M 88-271, January 1989.

[4] M.SUZUKI, et al., "A Study on ROSA/LSTF SB-CL-09 Test Simulating PWR 10% Cold Leg Break LOCA - Loop-seal Clearing and 3D Core Heat-up Phenomena", JAEA-Research 2008-087, October 2008.

[5] M.SUZUKI, et al., "ROSA/LSTF Experiment Report for RUN SB-CL-24, Repeated Core Heatup Phenomena during 0.5% Cold Leg Break LOCA", JAERI-Tech 2000-016, March 2000.

[6] M.SUZUKI, et al., "Experimental Study on Secondary Depressurization Action for PWR Vessel Bottom Small Break LOCA with HPI Failure and Gas Inflow (ROSA-V/LSTF Test SB-PV-03)", JAERI-Research 2005-014, June 2005.

[7] The ROSA IV Group, "ROSA-IV Large Scale Test Facility (LSTF) System Description", JAERI-M 84-237, January 1985.

[8] The ROSA IV Group, "Supplemental Description of ROSA-IV/LSTF with No.1 Simulated Fuel-Rod Assembly", JAERI-M 89-113, September 1989.

[9] The ROSA IV Group, "ROSA-IV Large Scale Test Facility (LSTF) System Description for Second Simulated Fuel Assembly", JAERI-M 90-176, October 1990.

[10] The ROSA-V Group, "ROSA-V Large Scale Test Facility (LSTF) System Description for the Third and Fourth Simulated Fuel Assemblies", JAERI-Tech 2003-037, March 2003.

[11] H.KUMAMARU, et al., "Recalculation of Simulated Post-Scram Core Power Decay Curve for Use in ROSA-IV/LSTF Experiments on PWR Small-Break LOCAs and Transients", JAERI-M 90-142, August 1990.

Table 1-1 Summary of twelve LSTF tests for CET performance study

Test No. (Run ID)	Break Location	Break Size %CLB Equi. (mm)	Core Heat-up	Detec-tion by CET	Start of Action	Water Fall-Back*	Month/ Year	Data Report
Test 6-1 (SP9)	**PV top**	**1.9 (13.8)**	○	○	**CETs**	×	**Nov./05**	**[1]**
1. SB-PV-07(SP7)	PV top	1.0 (10.1)	○	○	CETs	×	June/05	---
2. SB-PV-02(SP2)	PV top	0.5 (7.2)	○	○	HL T.	○	May/87	[3]
3. SB-PV-08(SP8)	PV top	0.1 (3.2)	○	○	CETs	○	Oct./05	---
4. SB-CL-09(SC9)	Cold leg	10.0 (31.9)	○	×	---	○	Aug./86	[4]
5. SB-CL-01(SC1)	Cold leg	2.5 (16.0)	○	○	Time	△	May/85	---
6. SB-CL-24(SC0)	Cold leg	0.5 (7.2)	○	○	Time	△	Feb./90	[5]
7. SB-HL-05(SH5)	Hot leg	0.5 (7.2)	○	○	HL T.	△	Feb./89	---
8. SB-PV-01(SP1)	PV bottom	0.5 (7.2)	○	○	HL T.	△	Dec./86	[3]
9. SB-PV-03(SP3)	PV bottom	0.2 (4.6)	○	×	SI+10min	○	Nov./02	[6]
10. AT-SB-03(SB3)	TMI-type	0.45 (6.8)	○	○	Time	△	Apr./85	[3]
11. TR-LF-03(LF3)	TMLB' transient		○	○	---	×	Aug./88	---
12. TR-RH-06(RH6)	Mid-loop/Loss-of-RHR**		○	○	Core T.	△	July/93	---

* Note on effects of water fall-back during core heat-up period; ○:Effects in all period, △:Effects in earlier period and ×:No effects or negligibly small.

** Open manhole at pressurizer is simulated by break orifice with 58.4 mm ID (33.5% CLB equivalent).

Table 2-1 Summary of design change in LSTF core

Items	1st Core Assembly	2nd Core Assembly	4th Core Assembly
Tests	AT-SB-03, SB-CL-01, SB-CL-09, SB-PV-01, SB-PV-02 & TR-LF-03	SB-HL-05, SB-CL-24 & TR-RH-06	SB-PV-03, SB-PV-07 & SB-PV-08
No. of Heater Rods	1064	1008	1008
No. of Non-heaters	152	136	136
No. of Inst. Heaters	53	54	6
Others in Core	---	8 DP cells	8 DP cells (unused)

Table 3-1 Summary of major test conditions for twelve LSTF tests

Tests	Scram at 12.97MPa	HPI Failure	SG Pres. Control	Operator/ AM Action	Set-point of 1st Action	2nd Action	Core Power	Power Limited
Test 6-1*	○	○	○	**SGRV open**	**CET≧623K**	---	**N**	○
SB-PV-07	○	○	○	HPI start	CET≧623K	---	N	---
SB-PV-02	○	○	○	HPI start	HL $T \geqq T_S$+10K	---	J	---
SB-PV-08	○	○	○	SGRV open	CET≧623K	---	N	---
SB-CL-09	○	○	○	---	---	---	J	○
SB-CL-01	○	○	○	HPI start	t=1200s	---	J	○
SB-CL-24	○	○	○	SGRV open	t=600s	PORV	J	○
SB-HL-05	○	○	○	PORV open	HL $T \geqq T_S$+5K	---	J	○
SB-PV-01	○	○	○	HPI start	HL $T \geqq T_S$+10K	---	J	○
SB-PV-03	○	○	○	SGRV open	SI+600s	PORV	N	○
AT-SB-03	○	○	○	HPI start	t=6600s	---	J	○
TR-LF-03	t=0s	○	○	---	---	---	N	○
TR-RH-06	---	○	---	AFW start	Core heat-up	---	0.4 MW	○

* Test conditions of OECD Test 6-1 are shown for reference.

Table 3-2 Controlled rotation speed of primary coolant pump after scram

Time (s)	Rotation Speed Ratio	Time (s)	Rotation Speed Ratio	Time (s)	Rotation Speed Ratio
0	1.000	30	0.280	80	0.125
2	0.850	40	0.220	90	0.110
5	0.730	50	0.185	100	0.100
10	0.540	60	0.160	250	0.000
20	0.370	70	0.140		

Table 3-3 Two types of core power decay curve after scram

(1) New power curve

Time (s)	Power (MW)	Time (s)	Power (MW)	Time (s)	Power (MW)	Time (s)	Power (MW)
0	10.0	80	3.042	600	1.832	5000	0.936
18	10.0	100	2.763	800	1.577	6000	0.886
20	8.150	150	2.423	1000	1.487	8000	0.814
30	5.366	200	2.263	1500	1.342	10000	0.763
40	4.504	300	2.079	2000	1.238	20000	0.629
50	3.906	400	2.000	3000	1.096	50000	0.491
60	3.538	500	1.913	4000	1.003	100000	0.405

(2) JAERI power curve

Time (s)	Power (MW)	Time (s)	Power (MW)	Time (s)	Power (MW)	Time (s)	Power (MW)
0	10.0	150	3.632	1500	1.280	19980	0.592
29	10.0	200	2.848	2000	1.200	60000	0.464
40	8.912	400	1.776	4000	0.992	100020	0.368
60	7.344	600	1.568	6000	0.848		
80	6.128	800	1.488	7980	0.784		
100	5.200	1000	1.424	10020	0.784		

Table 4-1 Chronology of major events and procedures in LSTF test SB-PV-07

Time (s)	Events and Procedures
0	Break valve open (PV top)
50	Scram signal (primary pressure = 12.97 MPa)
76	SI signal (primary pressure = 12.27 MPa)
98	Break flow from single-phase liquid to two-phase flow
301	Primary coolant pumps stopped
1360	Break flow to single-phase vapor
1610	Start of core heat-up at top part (Pos.9)
1722	Start of CET superheat
about 1800	Primary pressure lower than SG secondary-side pressure
1836	Highest CET temperature reached 623 K
1926	Start of manual HPI actuation by monitored CET temperature (623K)
3180	Initiation of AIS injection
4200	SG secondary depressurization and auxiliary feedwater started
7266	Break valve closed

Table 4-2 Chronology of major events and procedures in LSTF test SB-PV-02

Time (s)	Events and Procedures
0	Break valve open (PV top)
85	Scram signal (primary pressure = 12.97 MPa)
About 160	Break flow from single-phase liquid to two-phase flow
336	Primary coolant pumps stopped
About 2200	Break flow to single-phase steam
3532	Start of core heat-up at top part (Pos.9)
3704	Start of CET superheat (not monitored)
3930	Start of manual HPI actuation by HL super-heat = 10K
3950	Primary pressure became lower than SG secondary pressure
(4180)	Highest CET temperature may reach 623 K in case of extrapolation
6330	Initiation of AIS injection
10982	Initiation of LPI injection
11350	Break valve closed

Table 4-3 Chronology of major events and procedures in LSTF test SB-PV-08

Time (s)	Events and Procedures
0	Break valve open (PV top)
627	Scram signal (primary pressure = 12.97 MPa)
880	Primary coolant pumps stopped
About 1000	Break flow from single-phase liquid to two-phase flow
1006	SI signal (primary pressure = 12.27 MPa)
About 1600	Break flow to single-phase vapor
38140	Start of core heat-up at top part (Pos.9)
39125	Start of CET superheat
40760	Start of AM action by monitored CET temperature (623K)
41188	Initiation of AIS injection
43583	Break valve closed

Table 4-4 Chronology of major events and procedures in LSTF test SB-CL-09

Time (s)	Events and Procedures
0	Break valve open (CL-B/side)
8	Scram signal (primary pressure = 12.97 MPa)
11	SI signal (primary pressure = 12.27 MPa)
42	Core power started to decrease along decay power curve
67	Start of core heat-up at middle height core (Pos.5)
74	Loop-seal clearing
78	Steam discharge at break unit
97	Primary pressure became lower than SG secondary pressures
111	Core power supply was terminated
153	Core finally quenched
195	Initiation of AIS injection until 315s (ACC) and 334s(ACH)
263	Primary coolant pumps stopped
303	Initiation of LPI system
1042	Break valve closed

Table 4-5 Chronology of major events and procedures in LSTF test SB-CL-01

Time (s)	Events and Procedures
0	Break valve open (CL-B/side)
15	Scram signal (primary pressure = 12.97 MPa)
19	SI signal (primary pressure = 12.27 MPa)
272	Primary coolant pumps stopped
360	Loop-seal clearing
About 440	Primary pressure became lower than SG secondary pressures
575	Start of core heat-up at top part (Pos.9)
629	Start of CET superheat (not monitored)
790	Highest CET temperature reached 623 K
850	Initiation of AIS injection
887	Core power supply was terminated
1086	Core finally quenched
1200	Initiation of HPI system
2429	Break valve closed

Table 4-6 Chronology of major events and procedures in LSTF test SB-CL-24

Time (s)	Events and Procedures
0	Break valve open (CL-B/side, Flush-type orifice)
75	Scram signal (primary pressure = 12.97 MPa)
332	Primary coolant pump-A stopped, pump-B stopped at 513s
600	Start of SG depressurization action
2110	ACC and ACH started injection
2831	1st loop-seal clearing occurred
4009	2nd loop-seal clearing occurred
About 4160	Start of primary pressurization due to loss of SG secondary water level
5122	3rd loop-seal clearing occurred
5929	Start of core heat-up at top part (Pos.9)
6280	Start of CET superheat (not monitored)
6536	Highest CET temperature reached 623 K
6568 - 6610	PORV and PR safety valve were opened as the 2^{nd} and 3^{rd} AM actions
7156	Core power was limited to 50%
7844	Break valve closed

Table 4-7 Chronology of major events and procedures in LSTF test SB-HL-05

Time (s)	Events and Procedures
0	Break valve open (HL-B/bottom, Flush-type orifice)
84	Scram signal (primary pressure = 12.97 MPa)
113	Core power started to decrease along decay curve
339	Primary coolant pumps stopped
2000	Start of core heat-up at top part (Pos.9)
2110	Start of CET superheat (not monitored)
2162	Start of AM action (PORV open) by HL super-heat = 5K
2606	Highest CET temperature reached 623 K
2750	Initiation of AIS injection
2812	Core power was temporarily terminated by highest rod temp. (>900 K)
2870	Core power was finally terminated
3064	Core finally quenched
3488	Break valve closed

Table 4-8 Chronology of major events and procedures in LSTF test SB-PV-01

Time (s)	Events and Procedures
0	Break valve open (PV bottom)
79	Scram signal (primary pressure = 12.97 MPa)
313	Primary coolant pump-A stopped (Pump-B stopped at 514s)
1420	Upper plenum level decrease below hot leg elevation
1498	Start of core heat-up at upper core (Pos.8)
1586	Start of CET superheat (not monitored)
1612	Highest CET temperature reached 623 K
1638	Start of heat-up at core bottom (Pos.1)
1676	Operator action to start HPI by HL temperature super-heat = 10K
1775	Core power supply was terminated
About 2000	Steam discharge at break unit
2057	Initiation of AIS injection
2248	Core finally quenched
3095	Break valve closed

Table 4-9 Chronology of major events and procedures in LSTF test SB-PV-03

Time (s)	Events and Procedures
0	Break valve open (PV bottom)
250	Scram signal (primary pressure = 12.97 MPa)
340	SI signal (primary pressure = 12.27 MPa)
500	Primary coolant pumps stopped
945	Start of 1st AM action to depressurize SG secondary sides
3241	Initiation of AIS injection
7190	Start of gas inflow from accumulator tanks to cold legs
8573	Start of core heat-up at top core (Pos.8)
8970	SGRVs were fully opened as the 2nd AM action
9060	PORV was fully opened as the 3rd AM action
9182	Start of CET superheat
9198	Core power was limited to 50%
9280	Initiation of LPI system
9680	Core finally quenched
9935	Break valve closed

Table 4-10 Chronology of major events and procedures in LSTF TMI-type test AT-SB-03

Time (s)	Events and Procedures
0	Break valve open (Stuck-open PORV)
64	Scram signal (primary pressure = 12.97 MPa)
314	Primary coolant pumps stopped
4870	UP water level started to decease below hot leg elevation
5517	Start of core heat-up at top part (Pos.9)
5850	Start of CET superheat (not monitored)
5996	Highest CET temperature reached 623 K
6050	Core power was lowered to limit core overheat
About 6070	Primary pressure became lower than SG secondary pressures
6600	Initiation of HPI system
6830	Core was finally quenched

Table 4-11 Chronology of major events and procedures in LSTF test TR-LF-03

Time (s)	Events and Procedures
0	TMLB’ scenario started (Loss of off-site power [T], main feedwater [M], auxiliary feedwater [L] and on-site power [B’])
18	Core power decay started
119	SG-A safety valve operated until 4552 s
141	SG-B safety valve operated until 4048 s
About 3600	Primary pressure started to increase
4400	Start of relief valve on-off operation at pressurizer (about 17 MPa)
About 5000	Loss of SG secondary water levels
About 7700	Primary loop natural circulation stopped
About 9300	Water level in hot legs diminished
9657	Start of core heat-up at top part
9780	Start of CET superheat above 626 K
10520	Lower core (Pos.3) started to heat-up
11000	Test end

Table 4-12 Chronology of major events and procedures in LSTF test TR-RH-06

Time (s)	Events and Procedures
0	Start of mid-loop operation test at 0.11 MPa under RHR-mode with open manhole at pressurizer
683	Loss of RHR-mode (LPI flow stopped)
About 1250	Primary pressure increased
1930	Pressurizer water level was detected
9045	Start of core heat-up at top part (Pos.9)
9800	Start of CET superheat above 384 K at 0.15 MPa
9830	Start of auxiliary feedwater system by detecting core heat-up (523 K)
10340	Initiation of HPI system
10870	Core power was stopped by detecting maximum rod temp. (923 K)
11130	Core was finally quenched
11840	Test end

Table 5-1 LSTF CET performance in time delay to detect core heat-up

Tests	Start of ICC:A(s)	Start of CET:B(s)	CET 623K C(s)	B - A (s)	C - A (s)	B/A (-)	C/A (-)	axB^b/A* (-)
SB-PV-07	1610	1722	1926	112	316	1.07	1.20	0.99
SB-PV-02	3532	3704	(4180)**	172	(648)	1.05	(1.18)	1.00
SB-PV-08	38140	39125	40760	985	2620	1.03	1.07	1.04
SB-CL-09	67	---	---	---	---	---	---	---
SB-CL-01	575	629	790	54	215	1.09	1.37	0.99
SB-CL-24	5929	6280	6536	351	607	1.06	1.10	1.02
SB-HL-05	2000	2110	2606	110	606	1.06	1.30	0.99
SB-PV-01	1498	1586	1612	88	114	1.06	1.08	0.98
SB-PV-03	8573	9182	---	609	---	1.07	---	1.04
AT-SB-03	5517	5850	5996	333	479	1.06	1.09	1.02
TR-LF-03	9657	9780	---	123	---	1.01	---	0.99
TR-RH-06	9045	9800	---	755	---	1.08	---	1.06

* a=0.7603 and b=1.027 in reference [2].

** Maximum CET temperature trend is extrapolated to 623 K.

Table 5-2 CET location with maximum heat-up detection in ten tests

Tests	Location of Earlier CET Heat-up	Location of Faster CET Reached 623 K	Location of Low Temp. CETs at Arrival to 623 K	Location of Hot Rod in Core
SB-PV-07	B21, B18, B24, B06	B21, B18, B24, B23	B15, B12, B07, B10	B17, Pos.7
SB-PV-02	B21, B23, B22, B24	B21, B23, B22, B24	B01, B07, B02, B03	B14, Pos.8
SB-PV-08	B11, B05, B23, B06	B23, B22, B21, B11	B19, B15, B12, B07	B17, Pos.7
SB-CL-09	---	---	---	---
SB-CL-01	B23, B19, B18, B08	B21, B18, B14, B24	B12, B01, B03, B11	B20, Pos.7
SB-CL-24	B21, B23, B22, B24	B21, B23, B22, B24	B07, B08, B12, B19	B18, Pos.8
SB-HL-05	B14, B15, B10, B04	B21, B23, B22, B18	B12, B05, B06, B09	B20, Pos.7
SB-PV-01	B21, B22, B04, B18	B21, B23, B22, B04	B07, B01, B03, B19	B17, Pos.6
SB-PV-03	---	---	---	---
AT-SB-03	B22, B05	B21, B23, B22, B09	B03, B15, B19, B07	B13, Pos.7
TR-LF-03	B21, B23, B22, B24	B21, B19, B24, B18	B10, B14, B02, B03	B20, Pos.7
TR-RH-06	B21, B24, B23, B02	B21, B23, B14, B22	B12, B03, B04, B05	B14, Pos.8

Table 5-3 LSTF CET temperature difference from the hottest core

Tests	Timing of CET 623K (s)	Maximum Rod Temp. (K)	Temp. Diff. From CET T. (K)	Notes
SB-PV-07	1926	789	166	Time at 623 K
SB-PV-02	(4180)*	658	58	Time at PCT
SB-PV-08	40760	694	71	Time at 623 K
SB-CL-09	---	930	(364)	Time at PCT
SB-CL-01	790	805	182	Time at 623 K
SB-CL-24	6536	781	158	Time at 623 K
SB-HL-05	2606	749	126	Time at 623 K
SB-PV-01	1612	732	109	Time at 623 K
SB-PV-03	---	925	(437)	Time at PCT
AT-SB-03	5996	698	75	Time at 623 K
TR-LF-03	---	902	(60)	Time at PCT
TR-RH-06	---	926	(449)	Time at PCT

* Maximum CET temperature trend is extrapolated to 623 K.

Table 5-4 LSTF CET performance in relation to average heat-up at core top

Tests	Relation between Average Core top Superheat and Average CET Superheat (K)	Range of CET Superheat (K)
SB-PV-07	DTave (P9) = 1.98 x DTave (CET) + 28.1	0 ≦ DTave (CET) ≦ 100
SB-PV-02	DTave (P9) = 1.47 x DTave (CET) + 16.9	0 ≦ DTave (CET) ≦ 9
SB-PV-08	DTave (P9) = 1.96 x DTave (CET) + 28.9	10 ≦ DTave (CET) ≦ 26
SB-CL-09	---	---
SB-CL-01	DTave (P9) = 2.15 x DTave (CET) + 26.0	0 ≦ DTave (CET) ≦ 70
SB-CL-24	DTave (P9) = 1.88 x DTave (CET) + 40	0 ≦ DTave (CET) ≦ 130
SB-HL-05	DTave (P9) = 2.08 x DTave (CET)	30 ≦ DTave (CET) ≦ 100
SB-PV-01	DTave (P9) = 2.05 x DTave (CET)	15 ≦ DTave (CET) ≦ 50
SB-PV-03	---	---
AT-SB-03	DTave (P9) = 1.42 x DTave (CET) + 23.6	0 ≦ DTave (CET) ≦ 85
TR-LF-03	DTave (P9) = 1.58 x DTave (CET)	0 ≦ DTave (CET) ≦ 119
TR-RH-06	DTave (P9) = 3.85 x DTave (CET) + 120	0 ≦ DTave (CET) ≦ 48

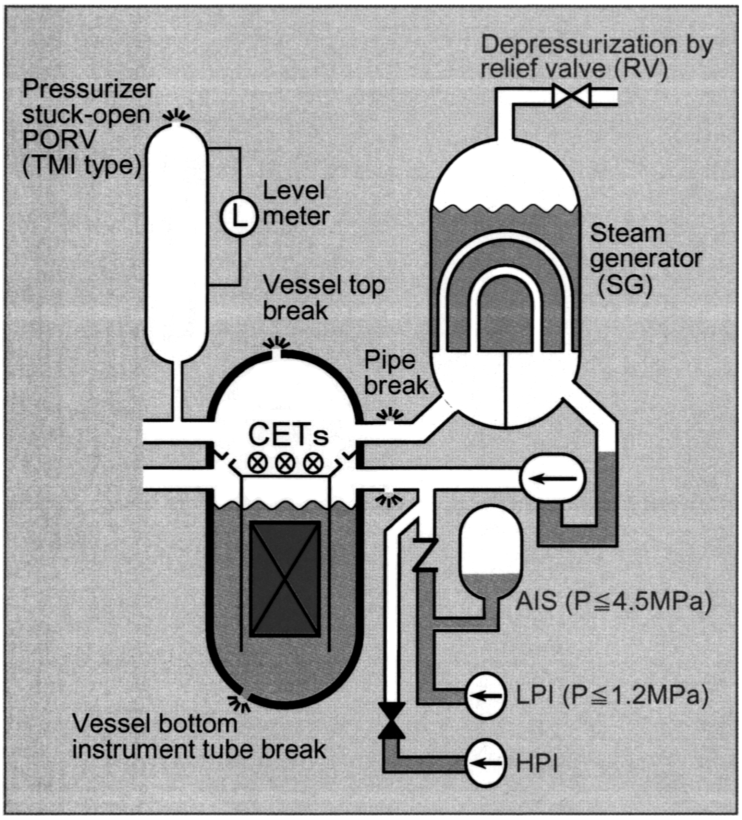

Fig.1-1 Five break locations for PWR SBLOCA simulation tests

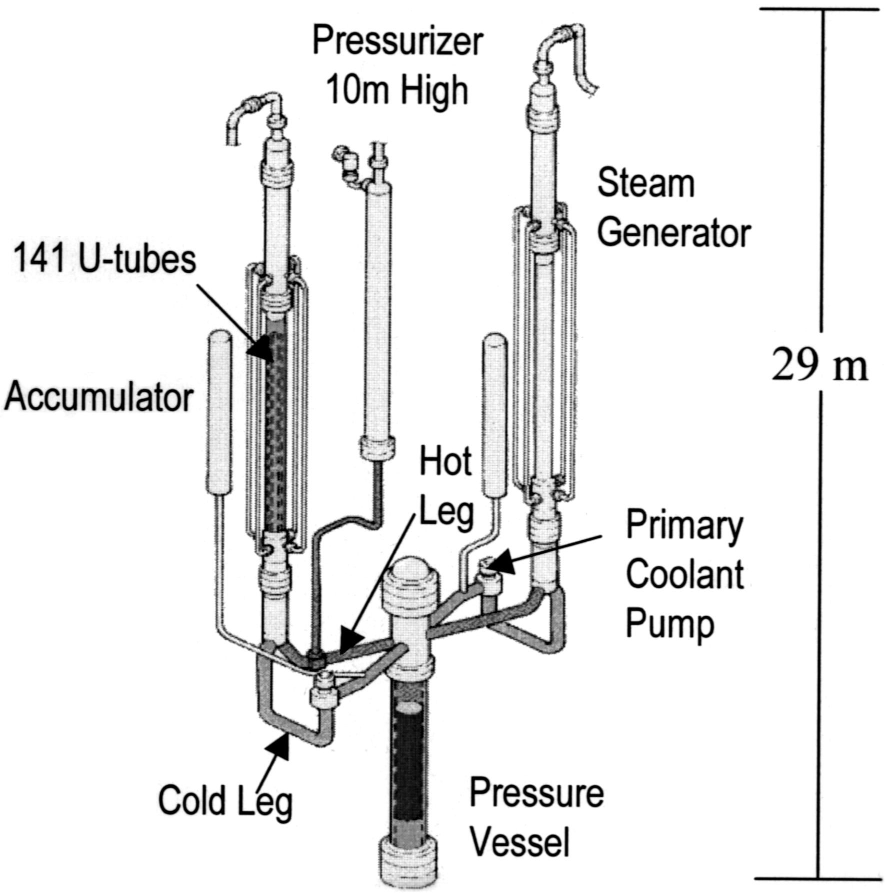

Fig.2-1 Schematic view of the Large Scale Test Facility (LSTF)

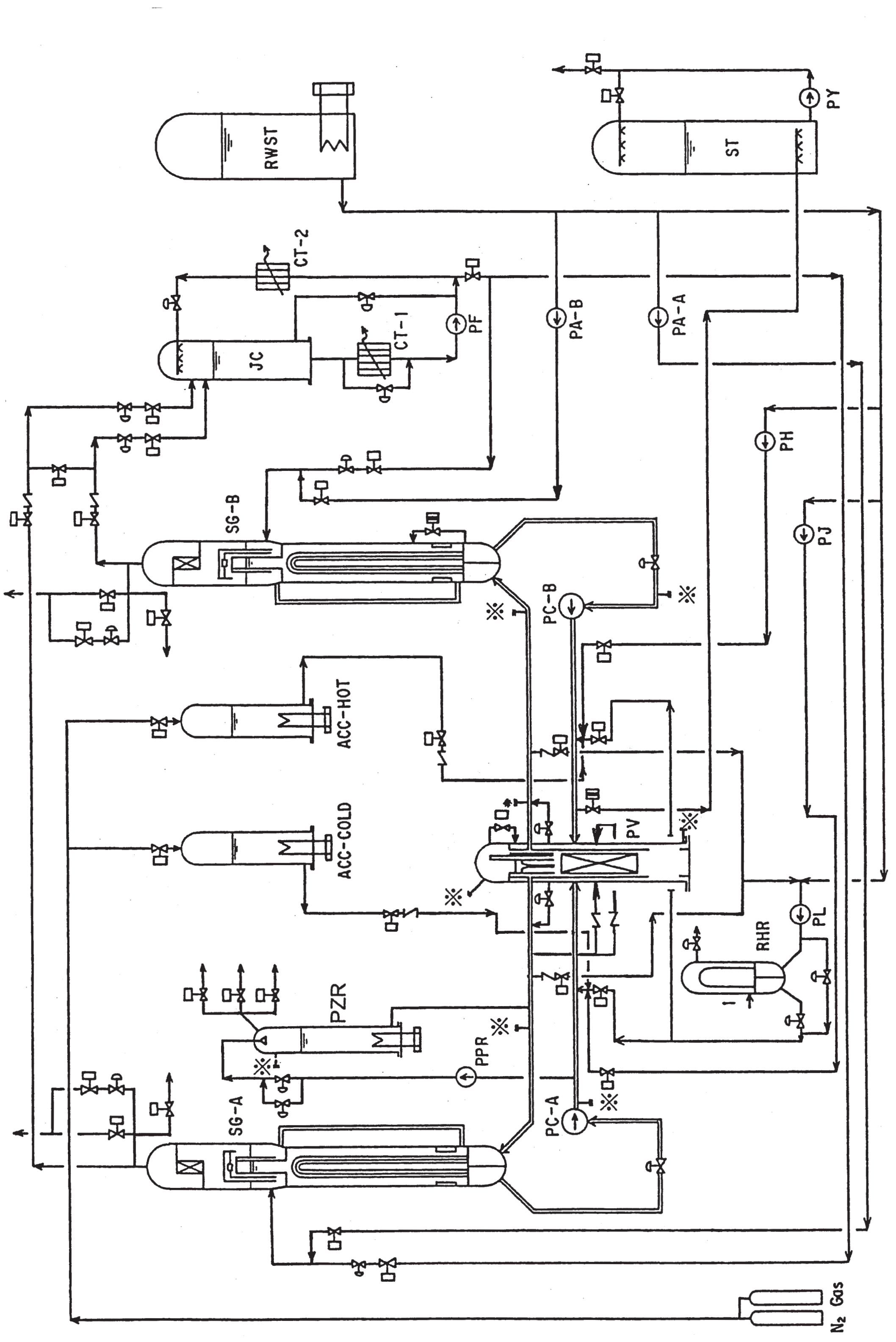

※ Other Break Point

NOTE ECCS can be also connected to hot legs and upper and lower plena of pressure vessel.

Fig.2-2 Flow diagram of LSTF

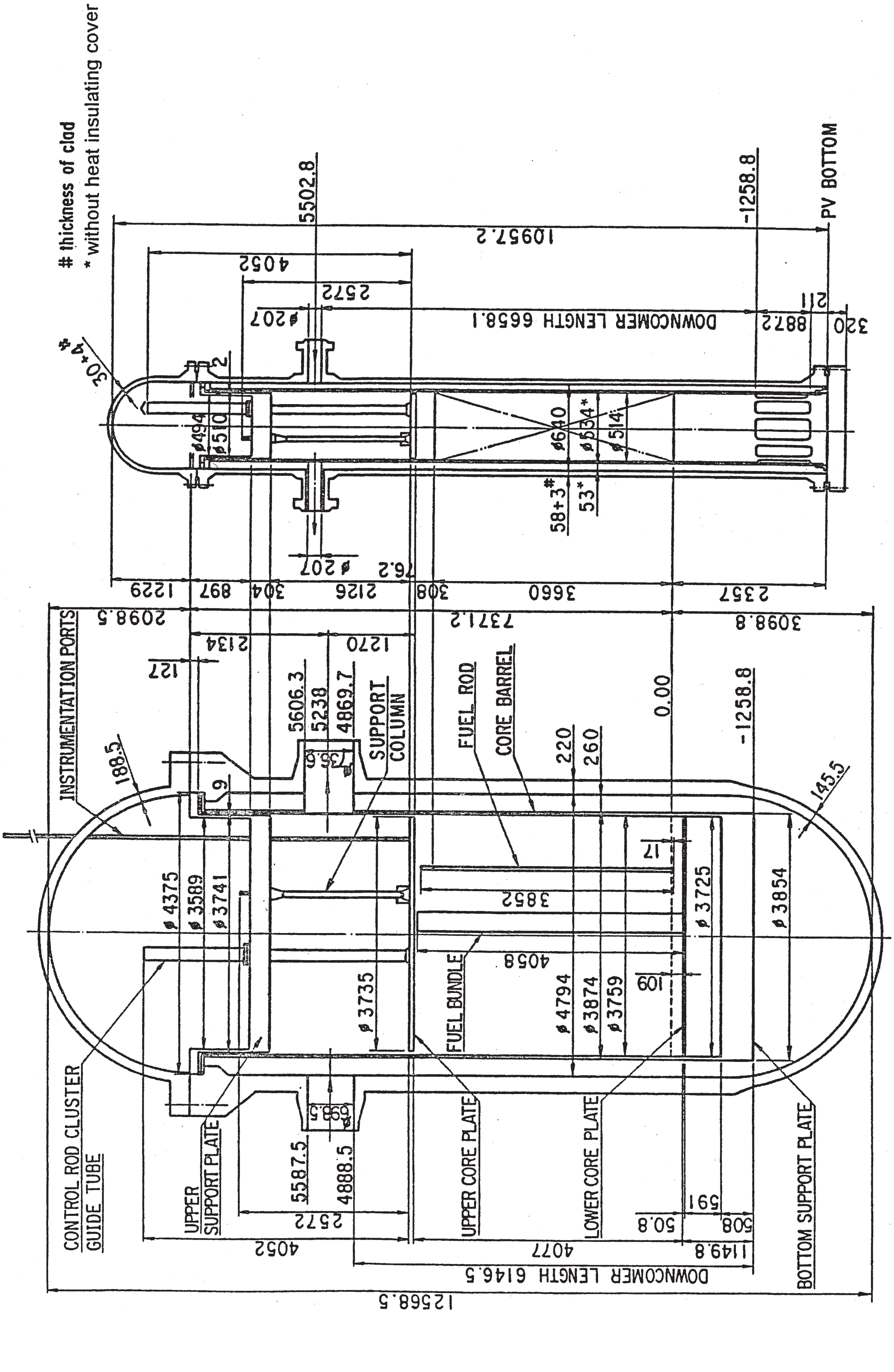

Fig.2-3 Comparison of LSTF and PWR pressure vessel dimensions

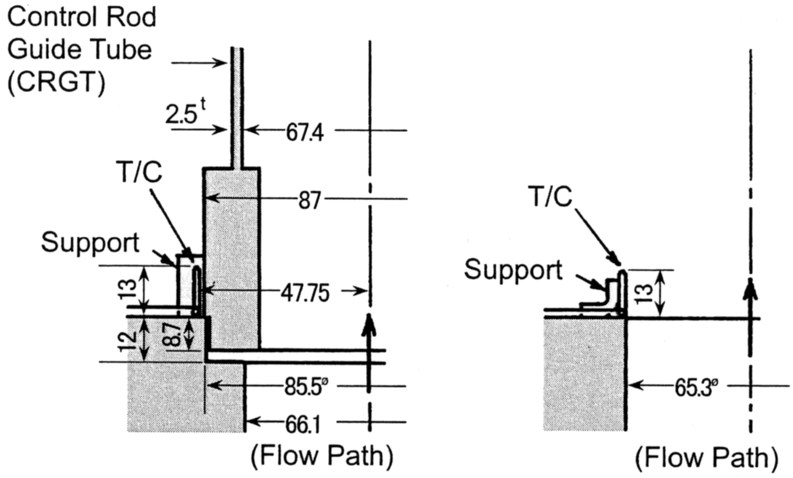

(a) Detail of CET at
CRGT outer surface

(b) Detail of CET at
flow path holes

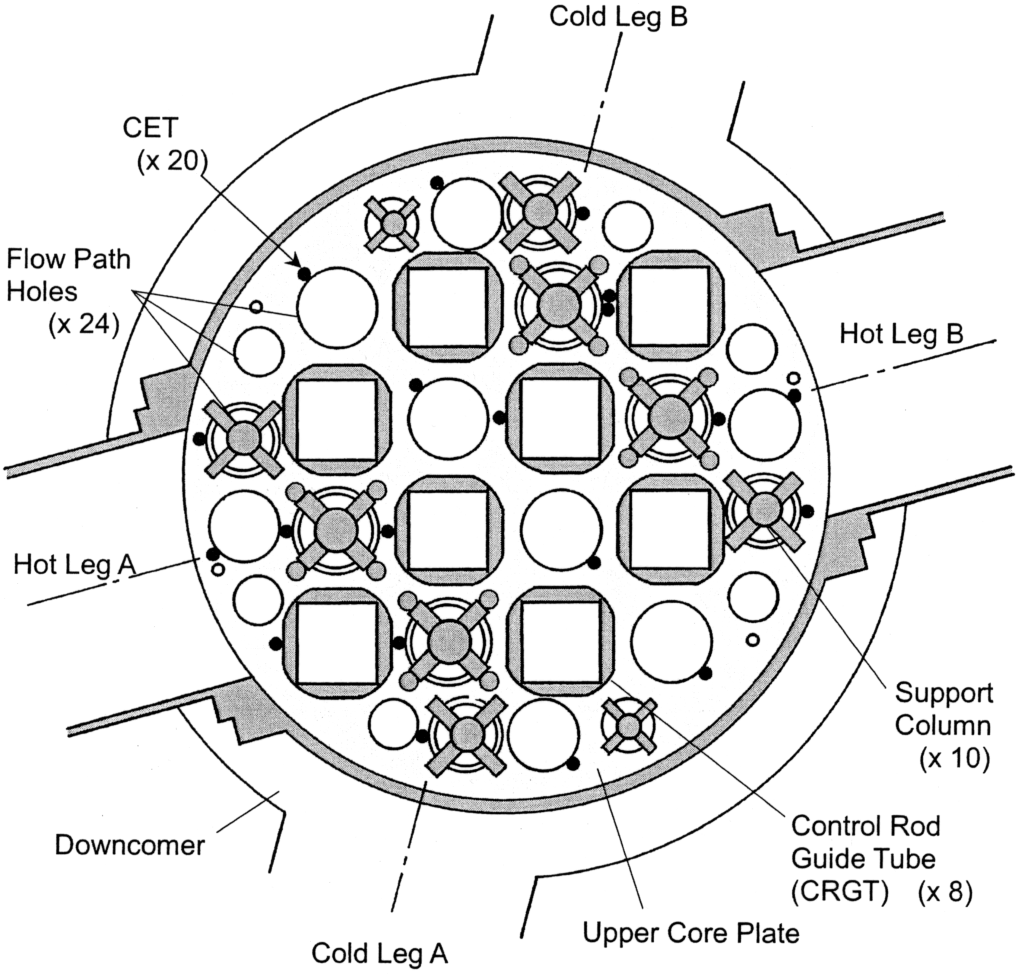

Fig.2-4 Location of core exit thermocouples (CETs) and UP internal structures

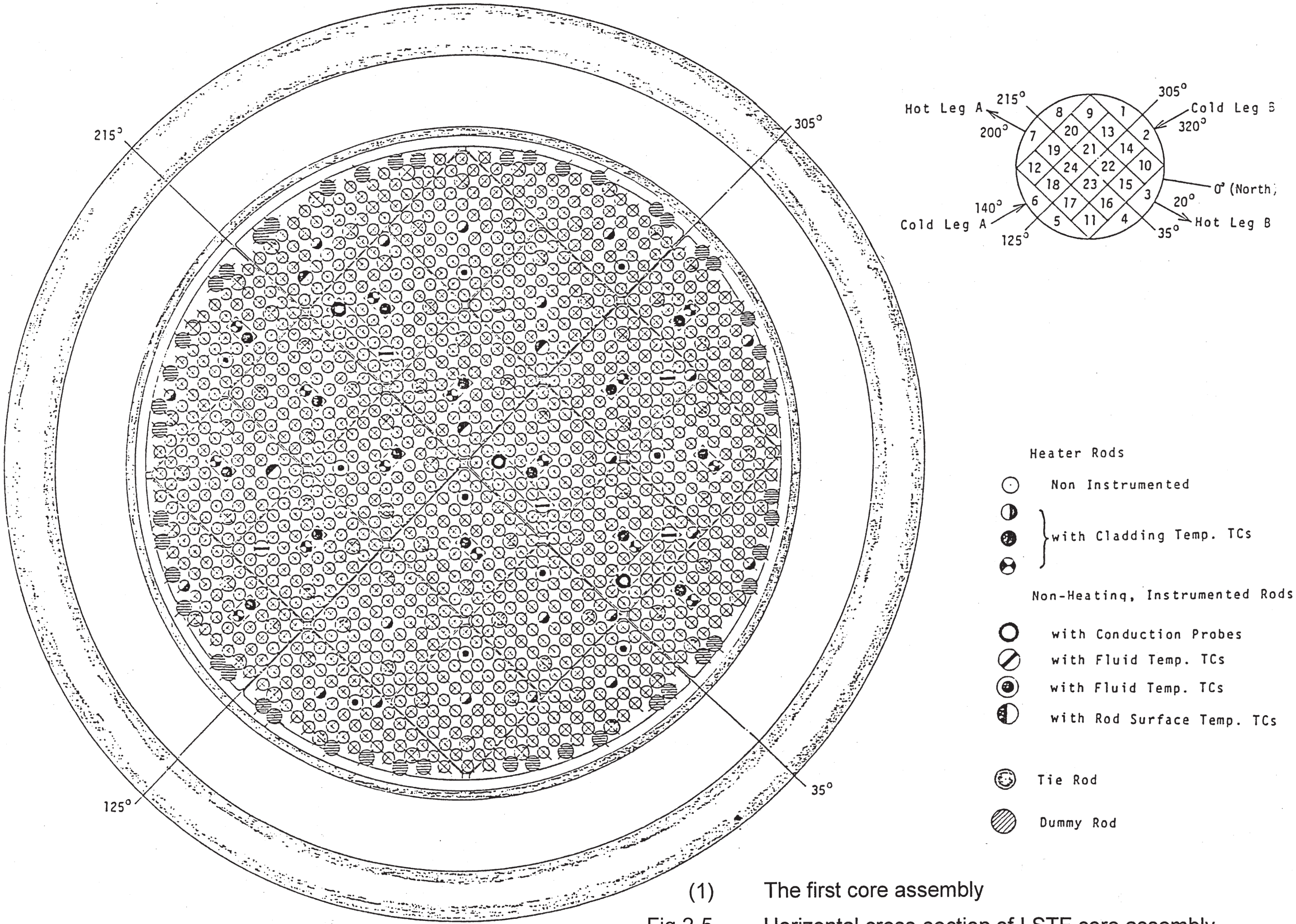

(1) The first core assembly

Fig.2-5 Horizontal cross-section of LSTF core assembly

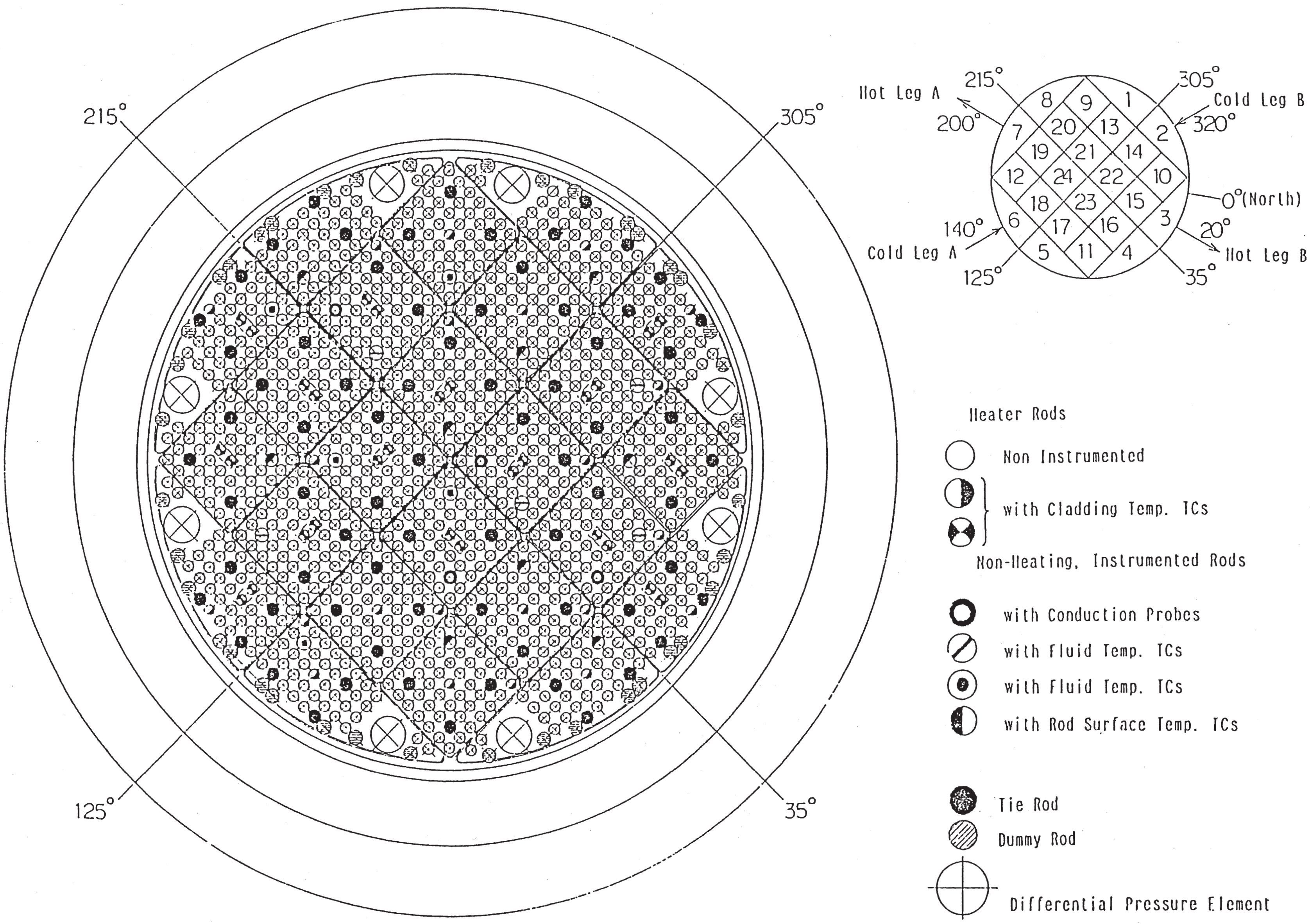

(2) The second core assembly

Fig.2-5 Horizontal cross-section of LSTF core assembly

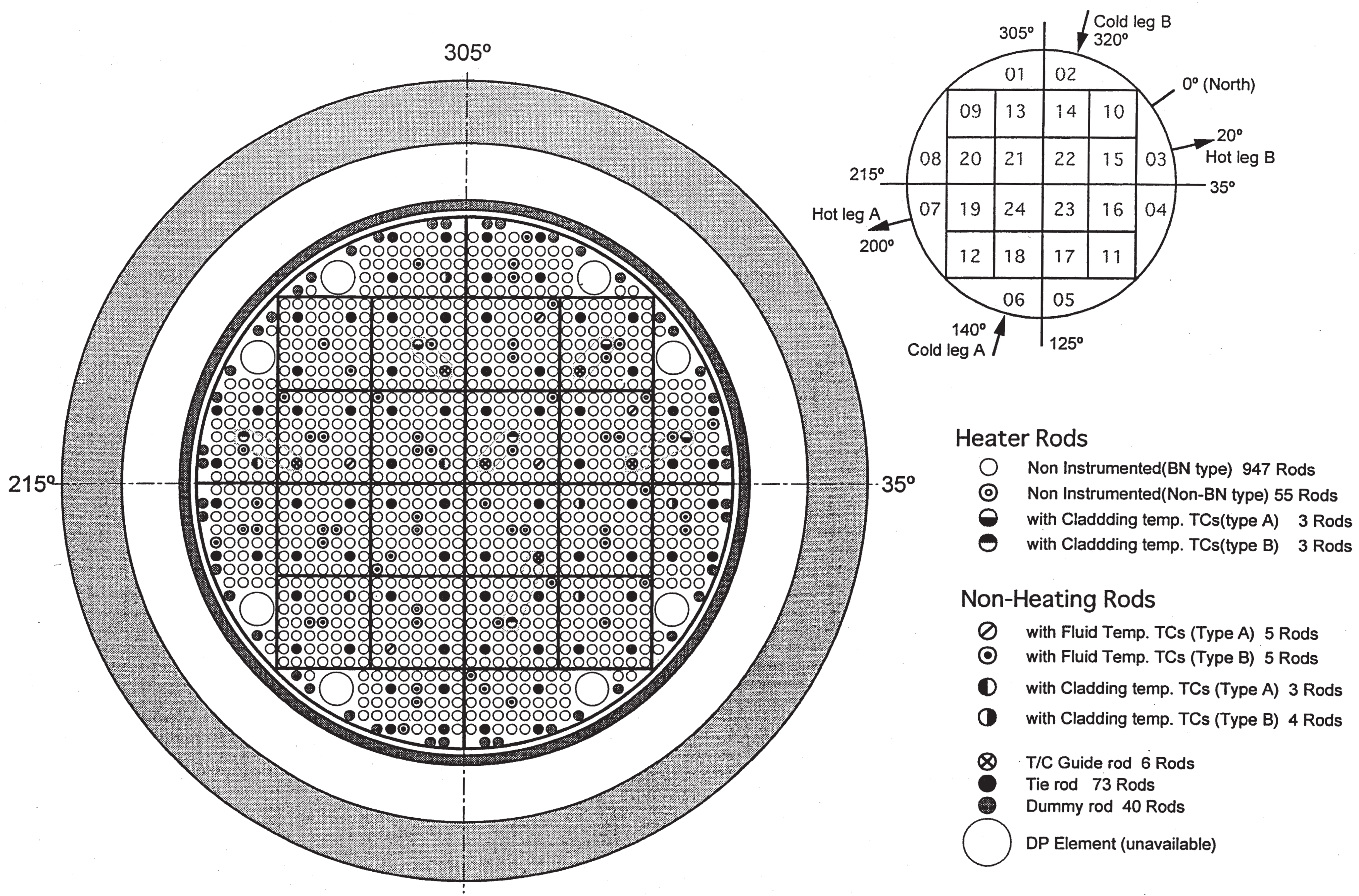

(3) The fourth core assembly

Fig.2-5 Horizontal cross-section of LSTF core assembly

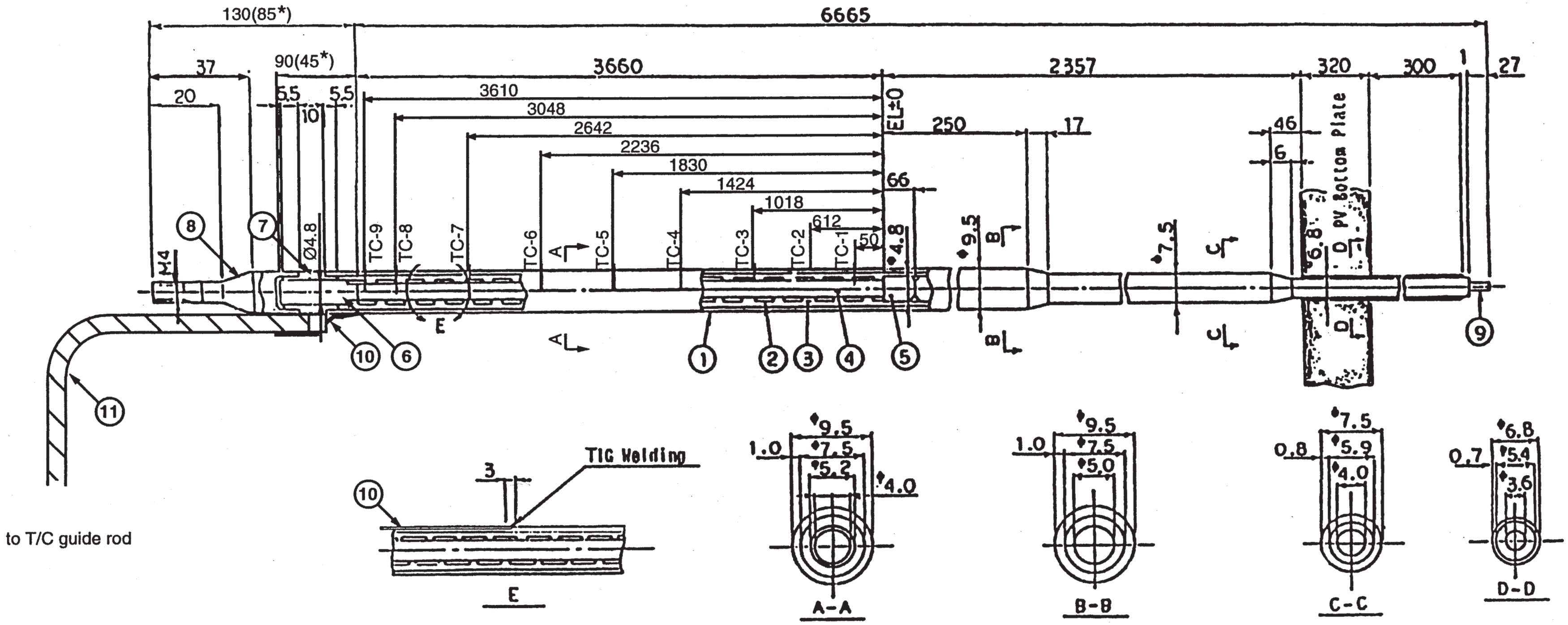

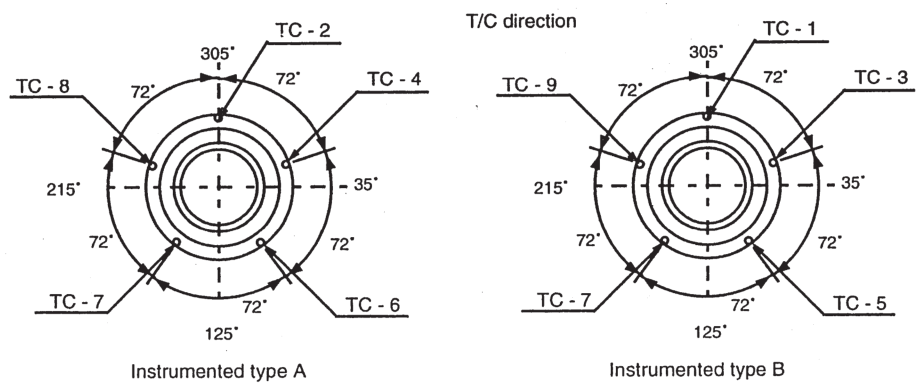

Mark	Description	Material
1	Cladding	Inconel 600
2	Heating Element	Nichrome 5
3	Insulator	MgO, or BN and MgO**
4	Core	Al2O3
5	Lower Conductor	Ni/Cu
6	Upper Conductor	Ni
7	End Gap	SUS316
8	Connector	Ni
9	Plug	Cu
10	Thermocouple	K(C/A)
11	T/C Guide Spring	Inconel 600

* : for non-instrumented heater rods(BN and non-BN type)
** : only for the BN type non-instrumented heater rod

Fig.2-6 Instrumented heater rod

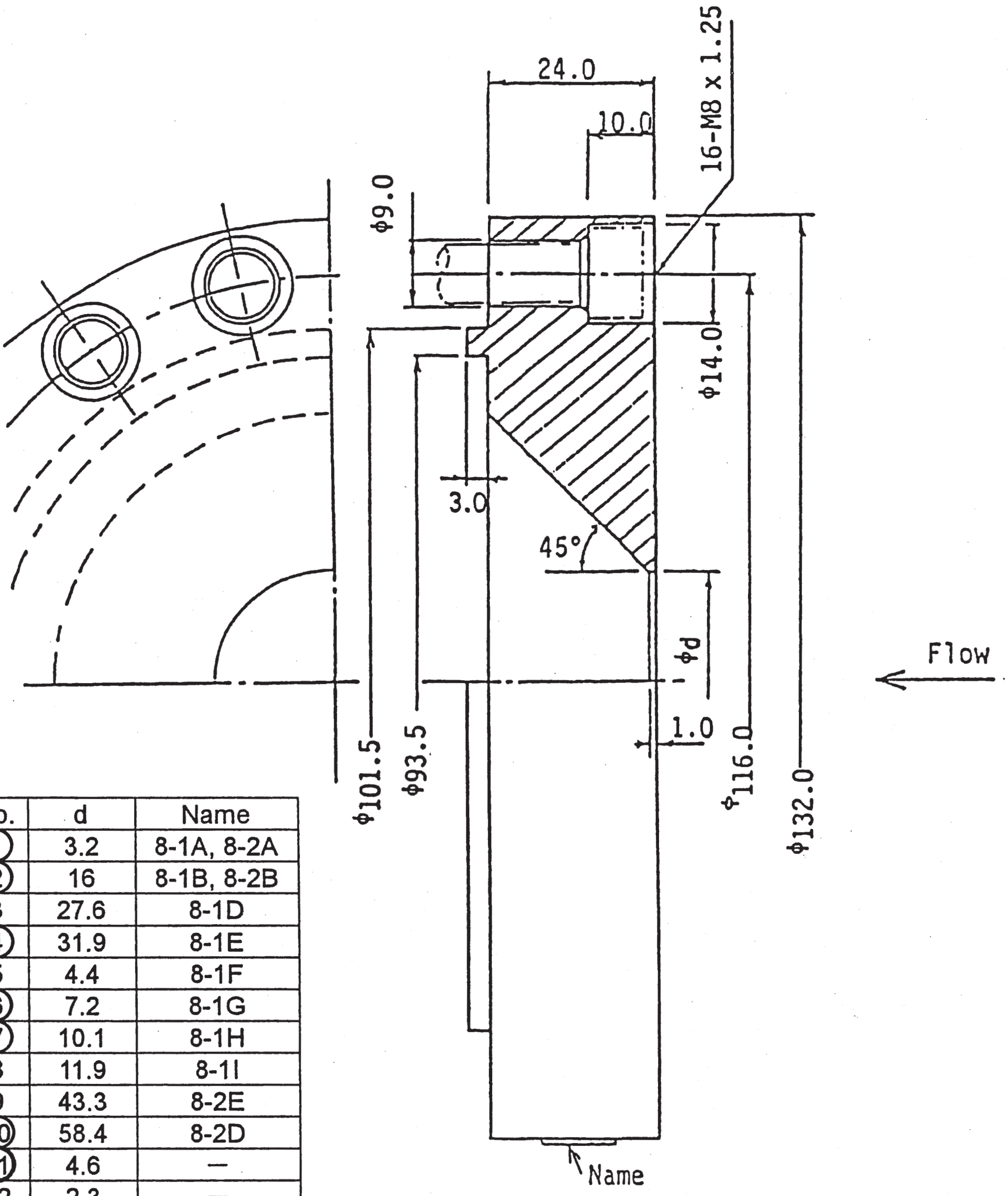

No.	d	Name
1	3.2	8-1A, 8-2A
2	16	8-1B, 8-2B
3	27.6	8-1D
4	31.9	8-1E
5	4.4	8-1F
6	7.2	8-1G
7	10.1	8-1H
8	11.9	8-1I
9	43.3	8-2E
10	58.4	8-2D
11	4.6	—
12	2.3	—
13	9.2	—
14	31.34	—
15	32.2	—
16	6.8	—
17	49.6	8-2C
18	35.82	—
19	13.8	—
20	18.4	—
21	22.5	8-1C

(Unit in mm)

(1) Geometry of break orifice

Fig.3-1 Configuration of two-types break units

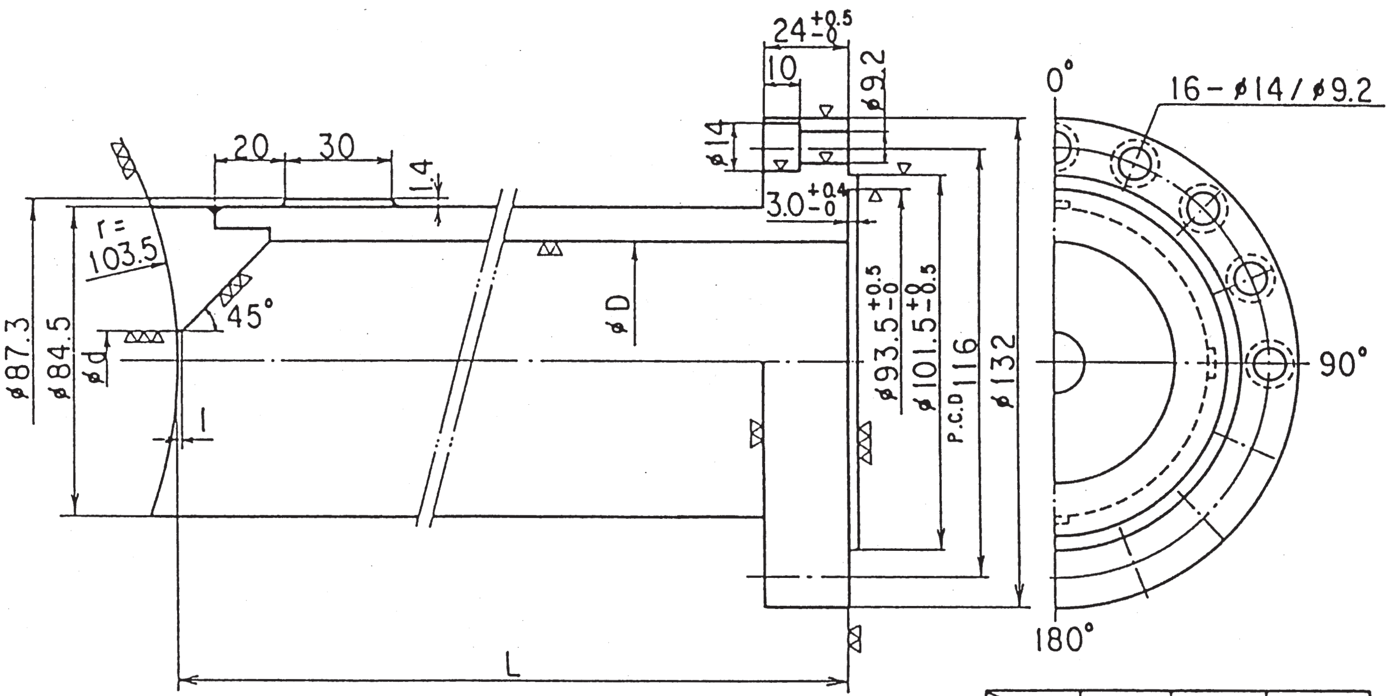

	d	D	L	
No. 1	7.2	60.0	338.3	
No. 2	7.2	60.0	350.8	SB-CL-24
No. 3	7.2	60.0	506.8	SB-HL-05

(2) Geometry of flush-type break orifice (Tests SB-HL-05 and SB-CL-24)

Fig.3-1 Configuration of two-types break units

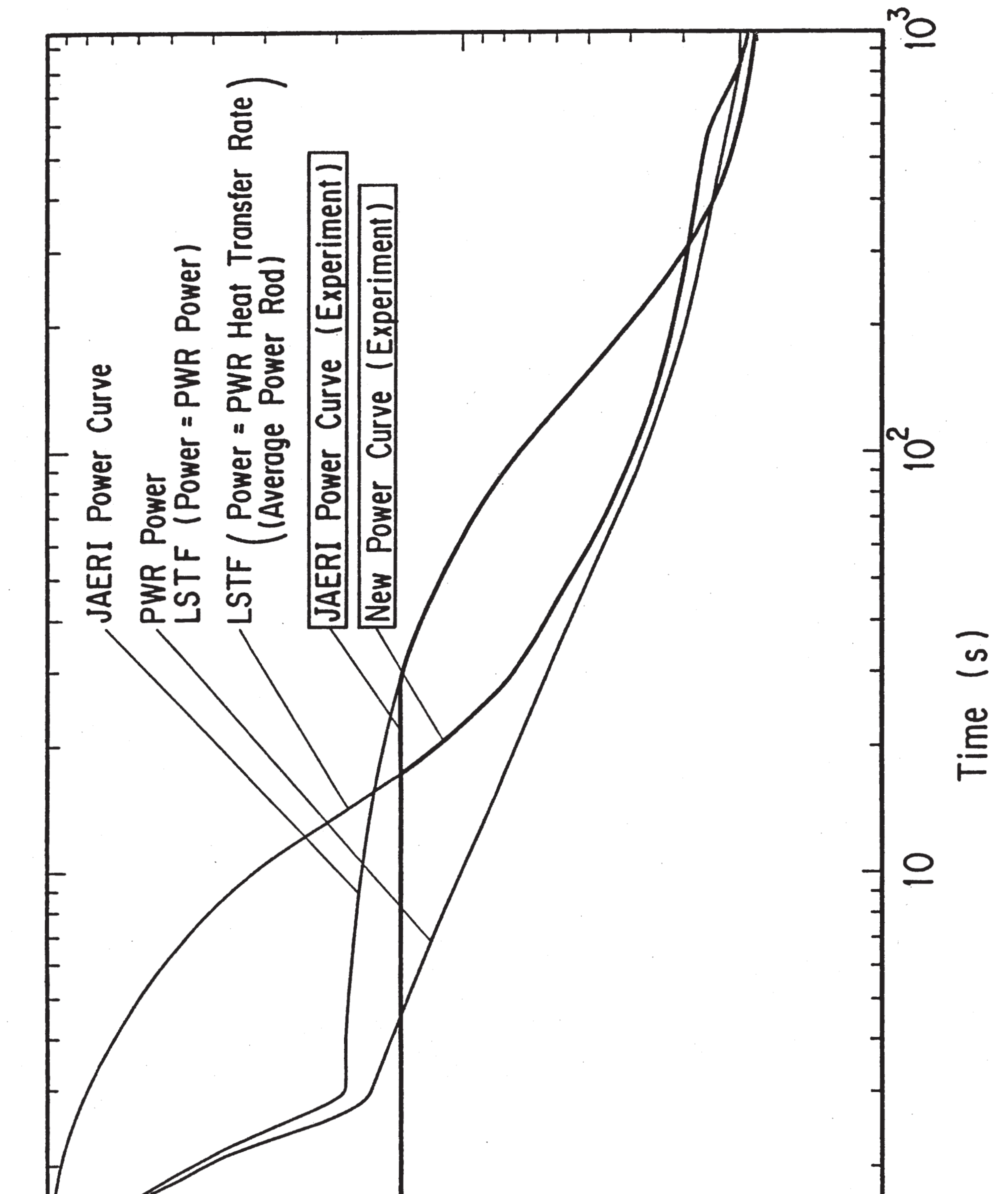

Fig.3-2 Two core power decay curves for LSTF SBLOCA tests

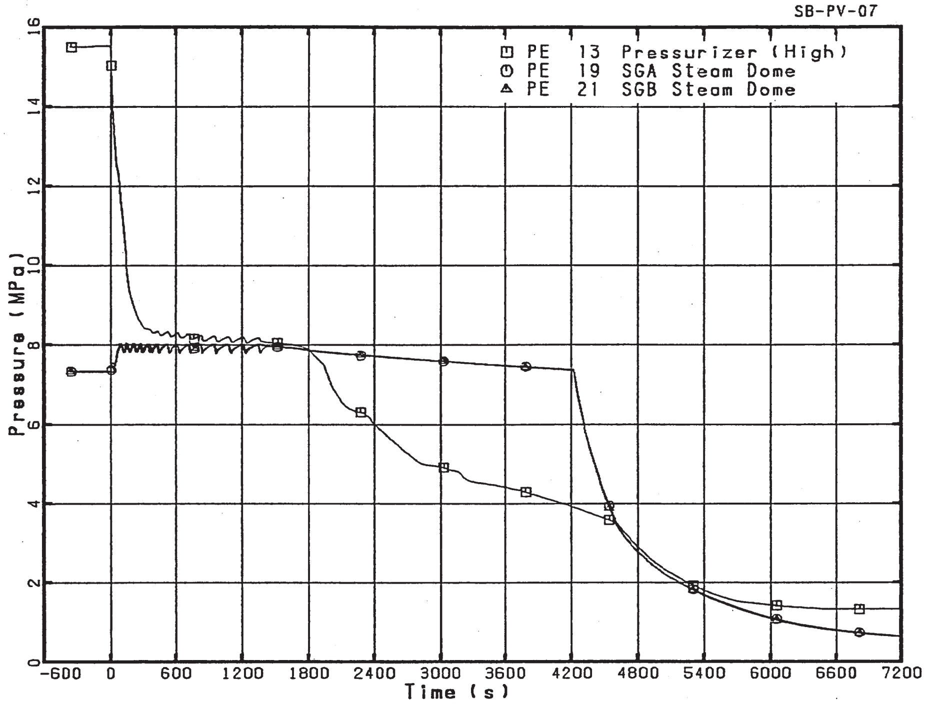

Fig.4.1-1 Primary and secondary pressures in LSTF 1.0% top break test (SB-PV-07)

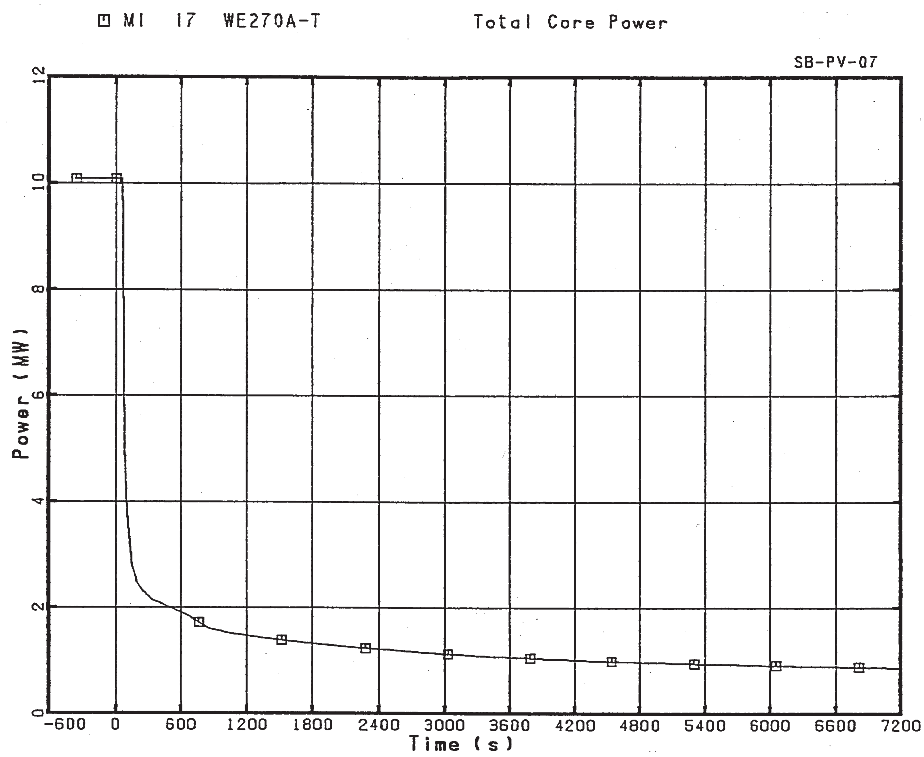

Fig.4.1-2 Core power decay curve in SB-PV-07 test

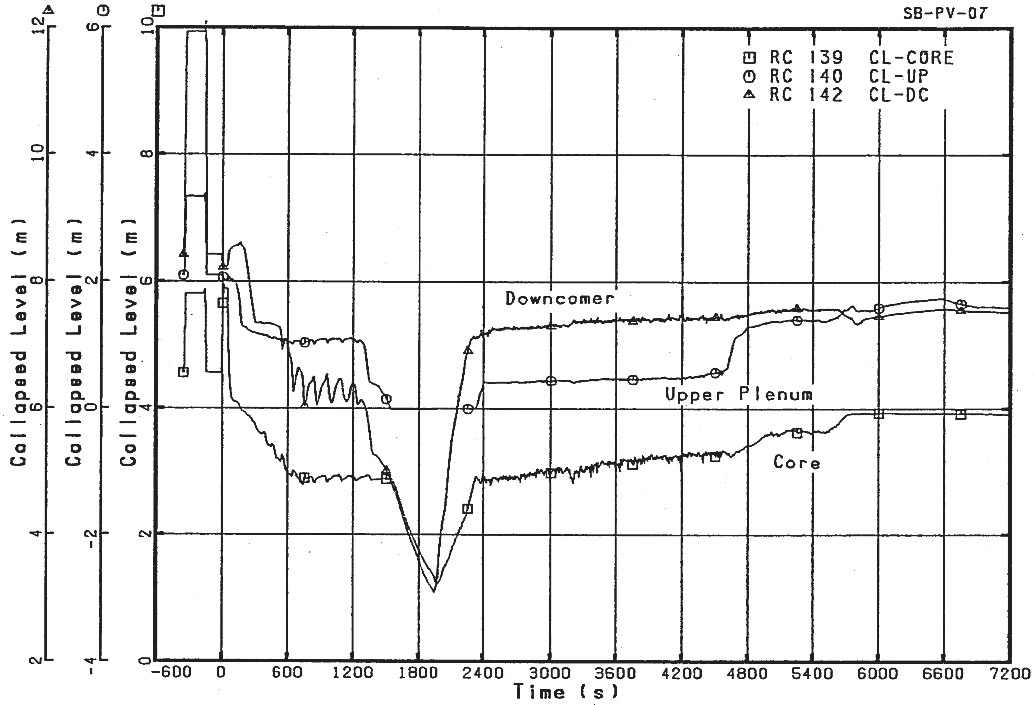

Fig.4.1-3 PV collapsed liquid levels in SB-PV-07 test

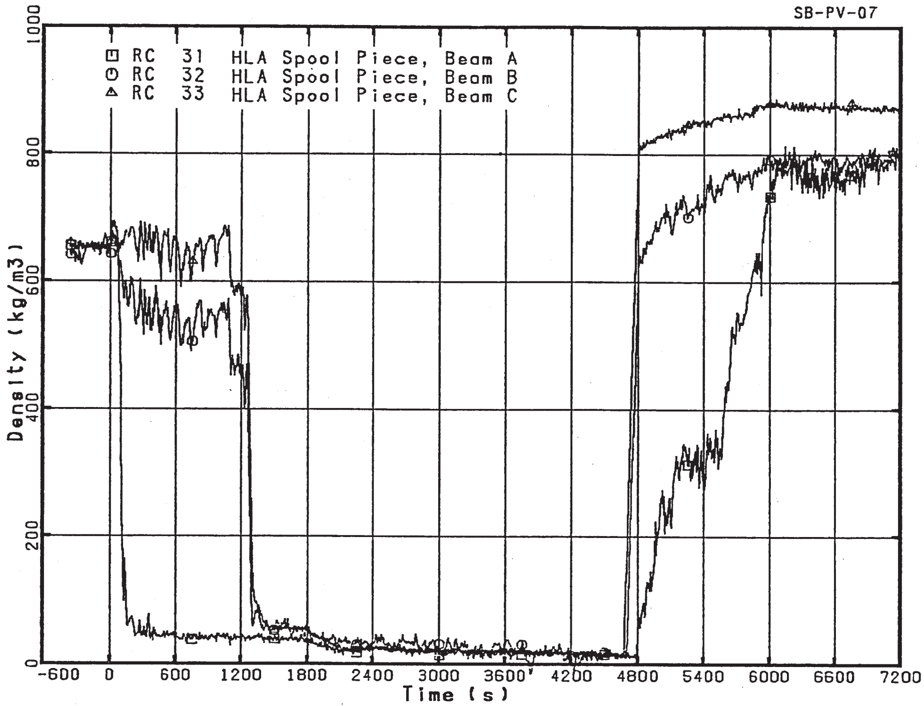

Fig.4.1-4 Fluid density data in intact loop hot leg (HL-A) in SB-PV-07 test

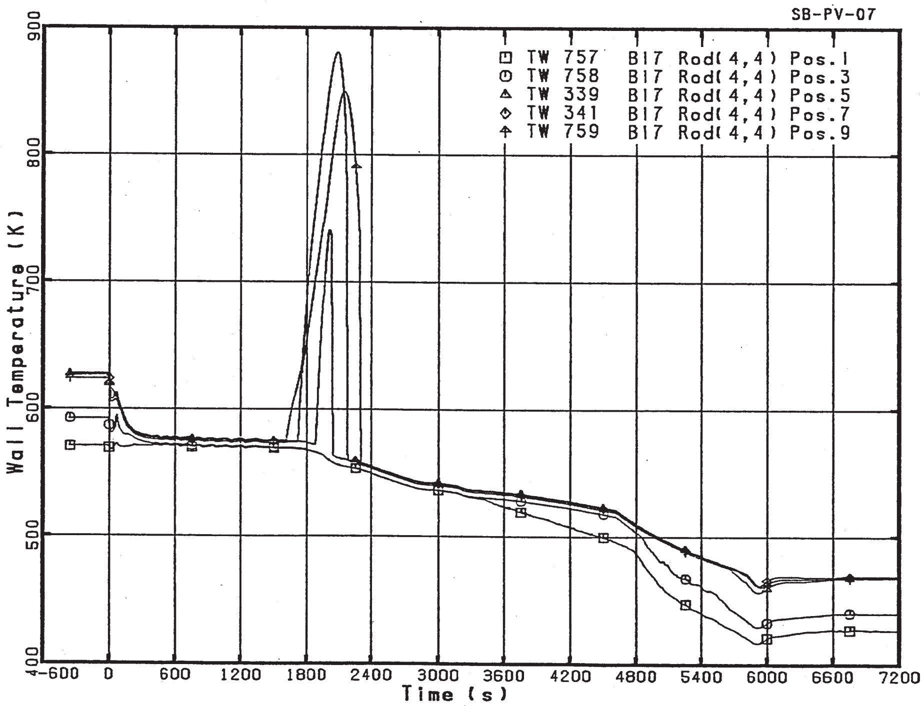

Fig.4.1-5 Representative heater rod surface temperatures in SB-PV-07 test

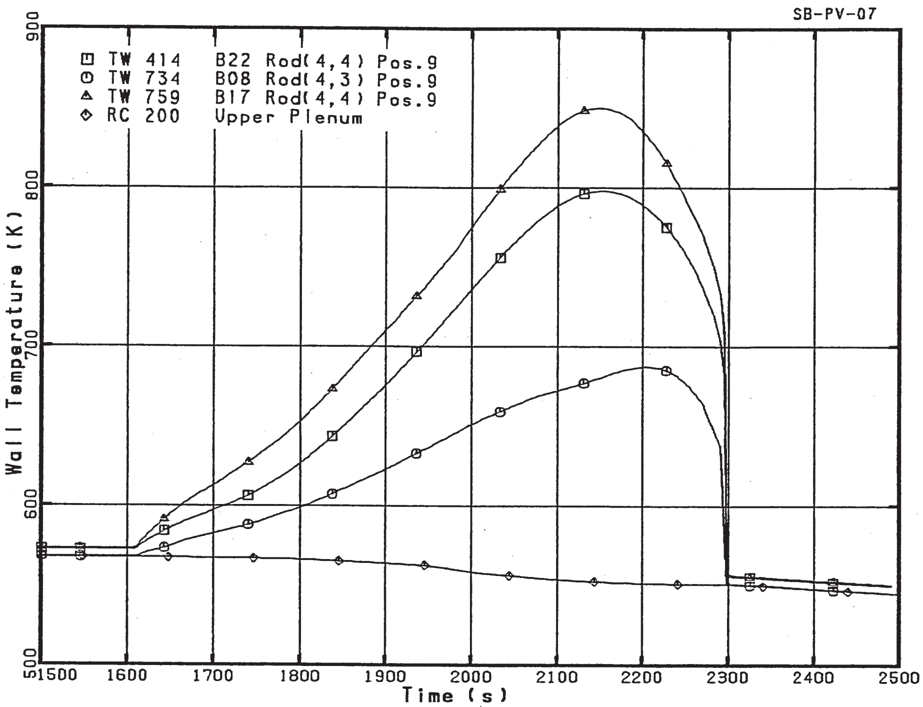

(1) Rod temperatures at Pos.9 (core top) compared with saturation temperature

Fig.4.1-6 Heater rod surface temperatures during boil-off in SB-PV-07 test

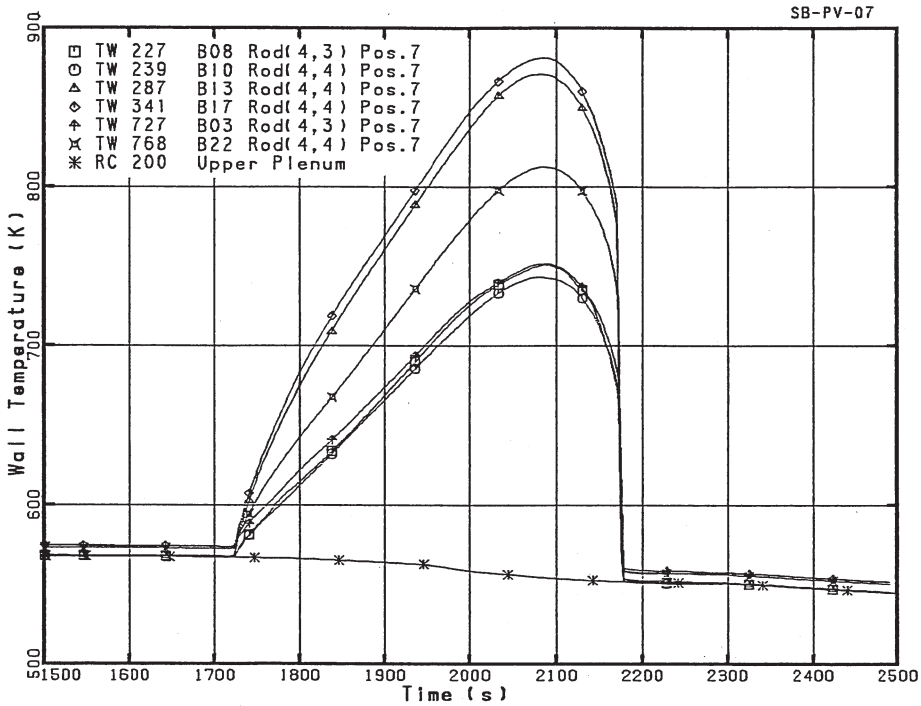

(2) Rod temperatures at Pos.7 with PCT measurement at B17 (4,4) rod

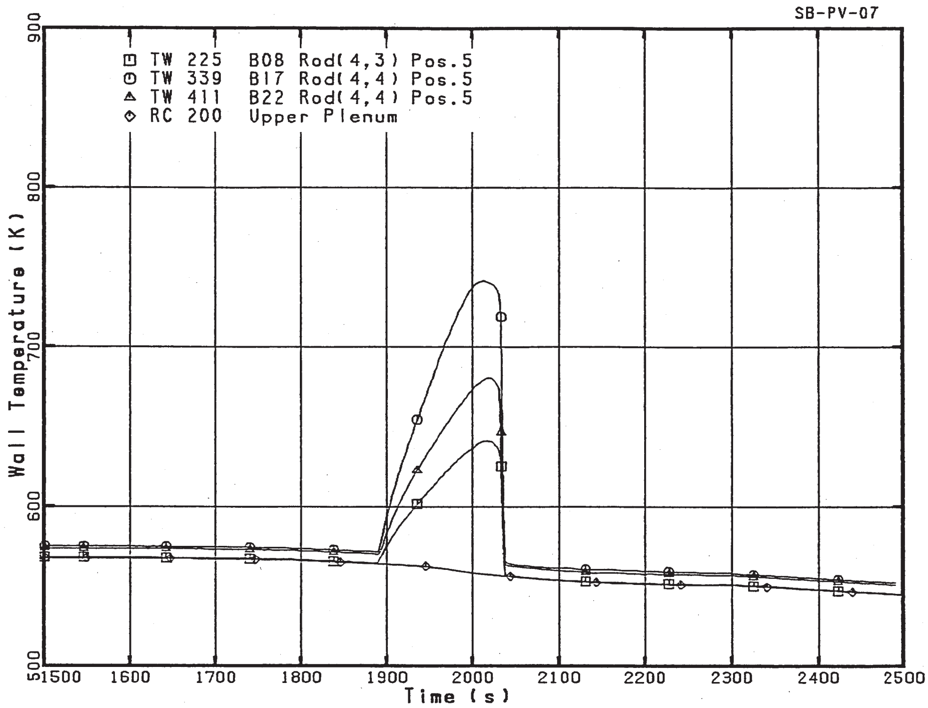

(3) Rod temperatures at Pos.5 (middle) compared with saturation temperature

Fig.4.1-6 Heater rod surface temperatures during boil-off in SB-PV-07 test

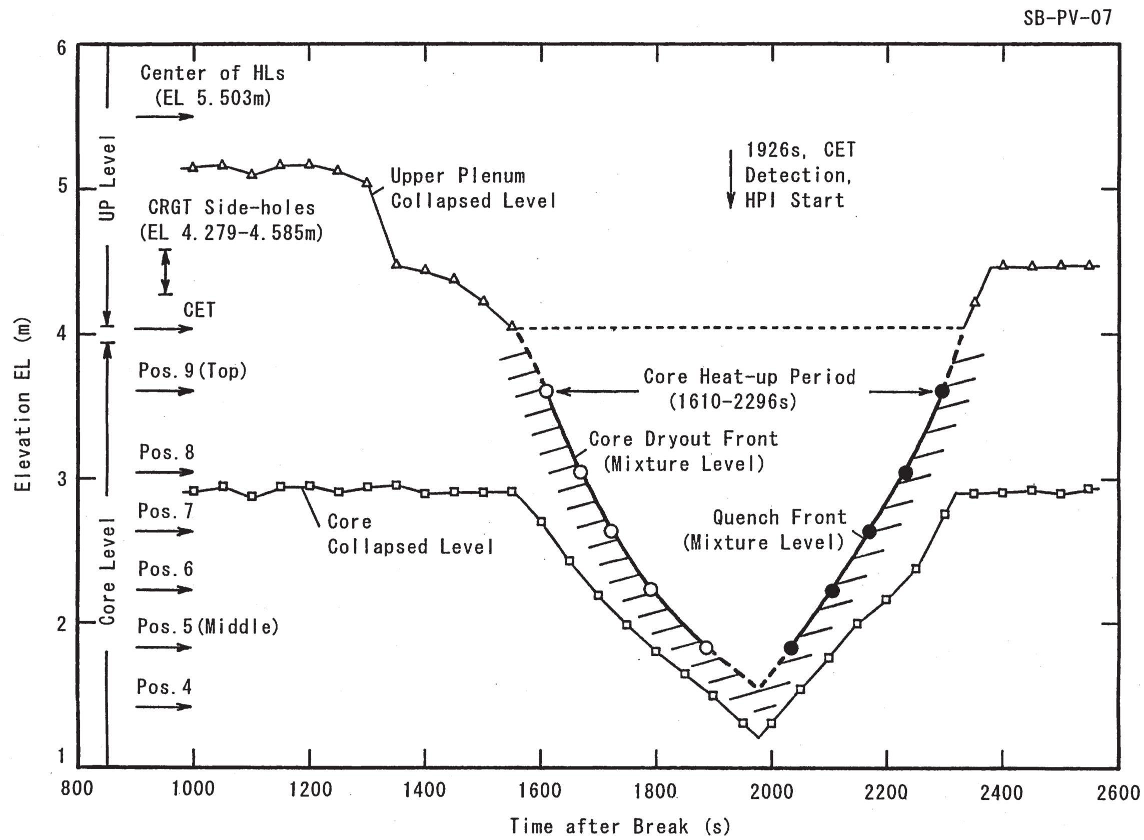

Fig.4.1-7 Core heat-up and quench behavior in SB-PV-07 test

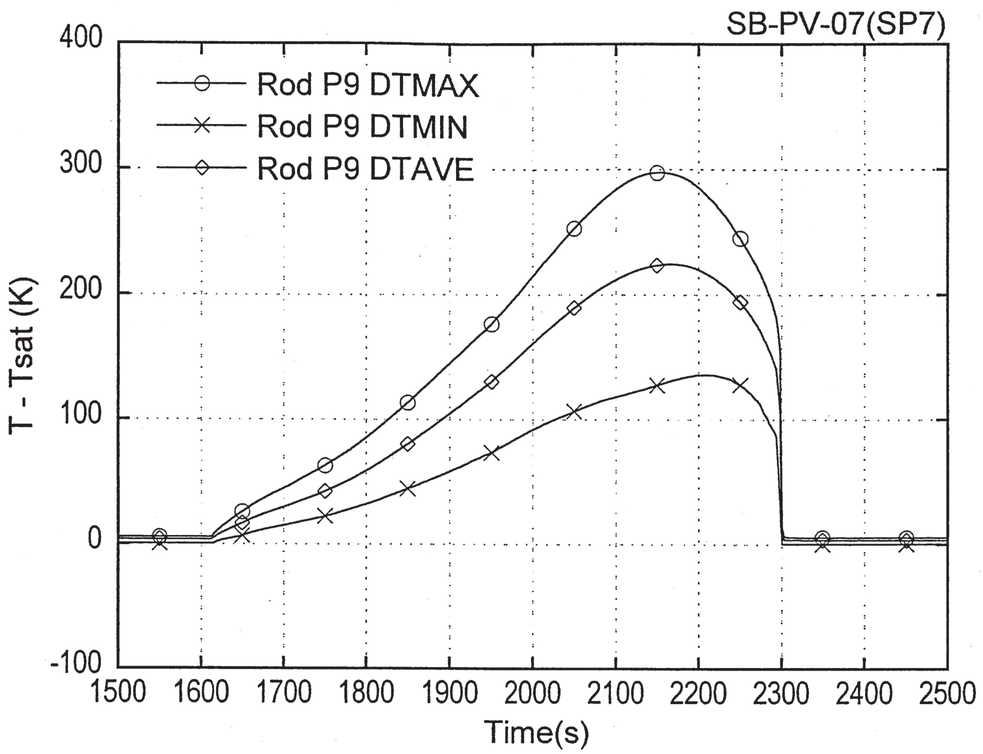

Fig.4.1-8 Distribution of heater rod temperature rises at Pos.9 in SB-PV-07 test (DT_{MAX}, DT_{MIN}, DT_{AVE})

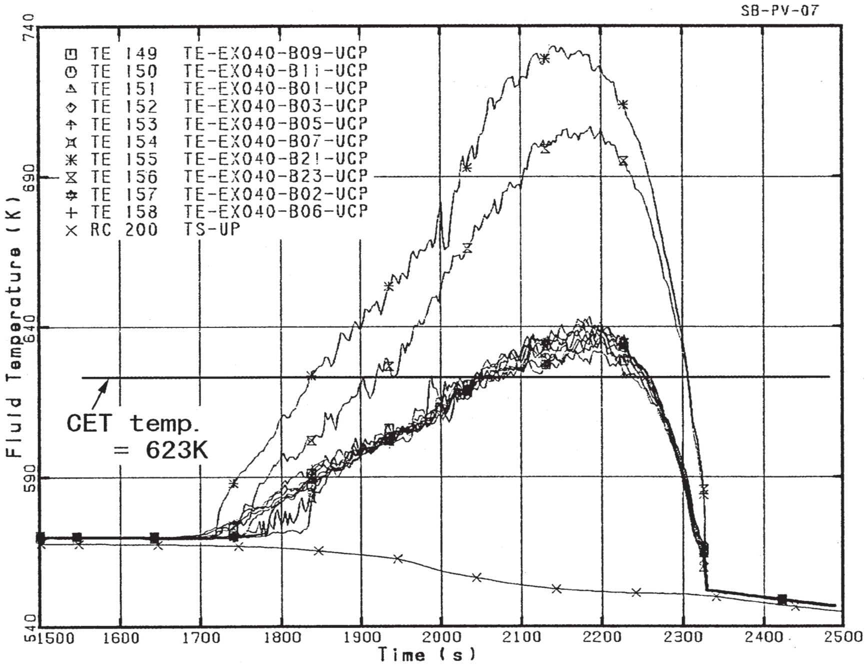

(1) CET temperatures above peripheral and central rod bundles

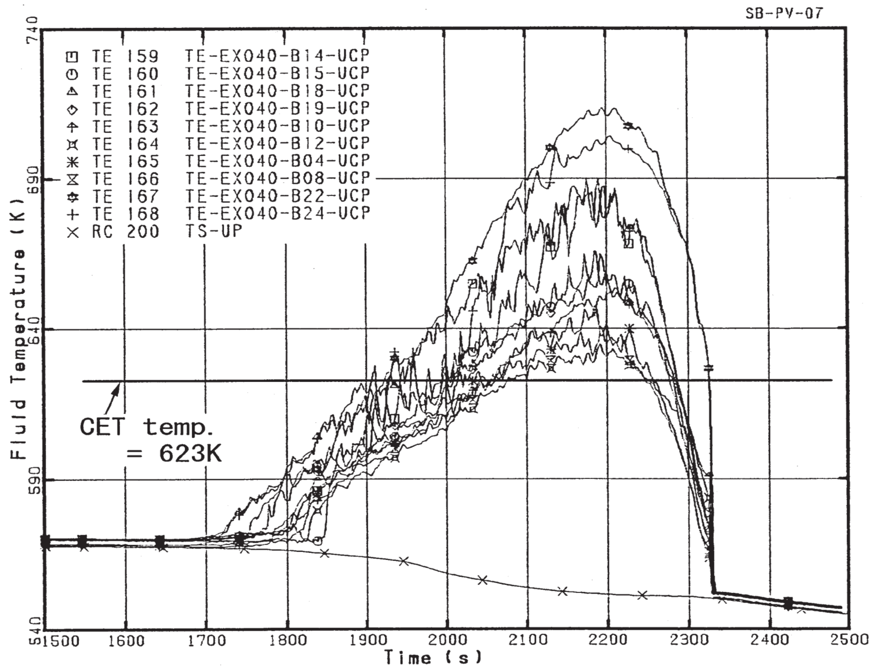

(2) CET temperatures above high-power and other rod bundles

Fig.4.1-9 CET temperatures during boil-off in SB-PV-07 test

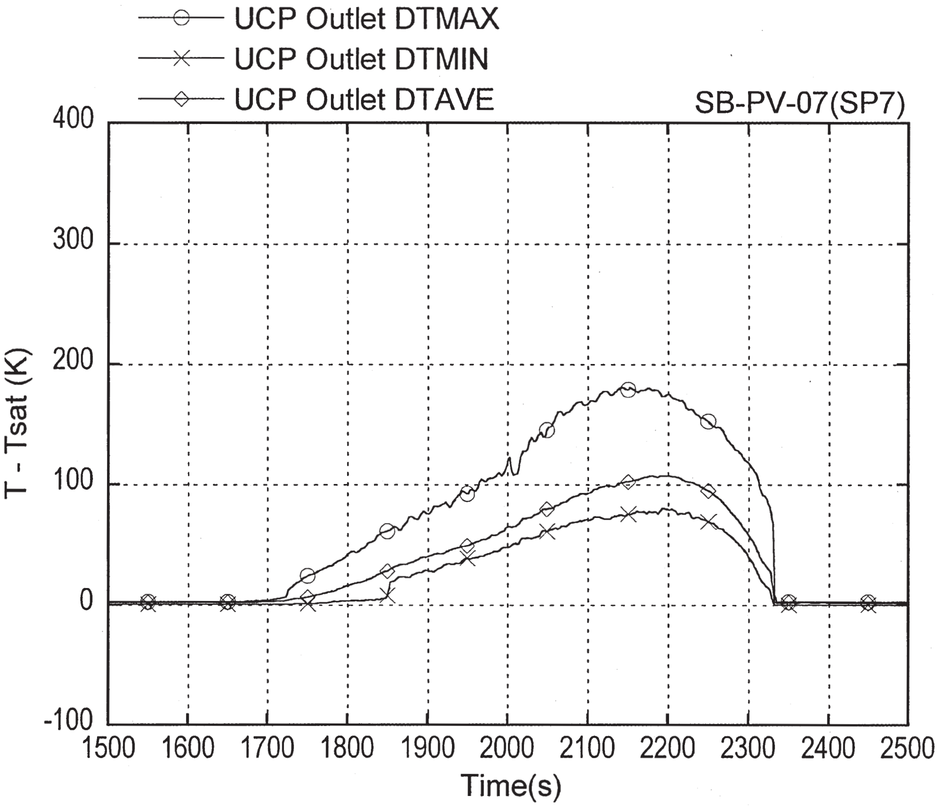

Fig.4.1-10 Distribution of all CET temperature rises above saturation temperature in SB-PV-07 test (DT_{MAX}, DT_{MIN}, DT_{AVE})

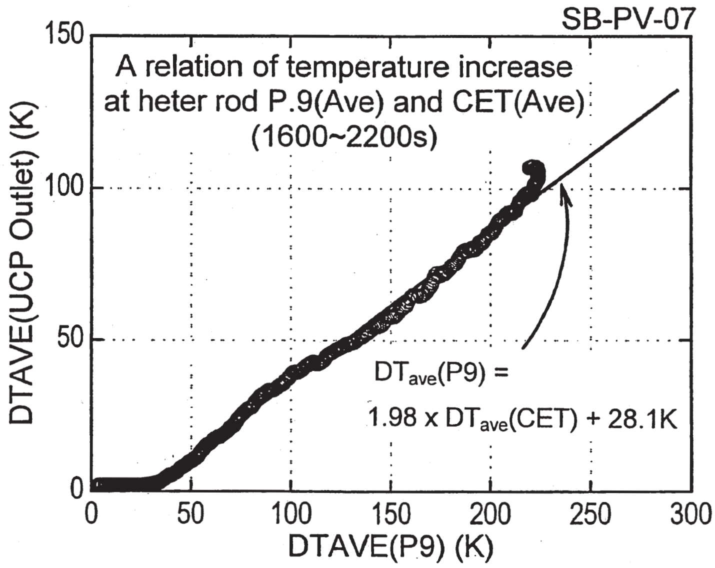

Fig.4.1-11 A relation of temperature rises at heater rod Pos.9, (Ave) and CET (Ave) in SB-PV-07 test

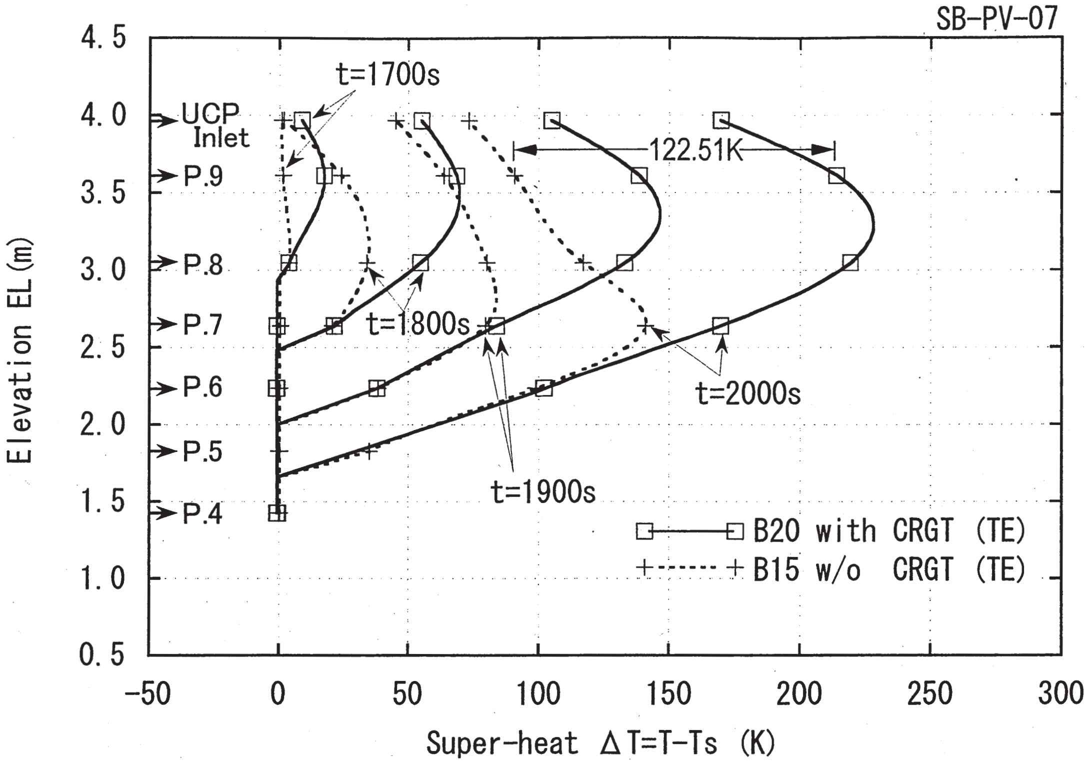

(1) Steam temperatures in two bundles during boil-off process

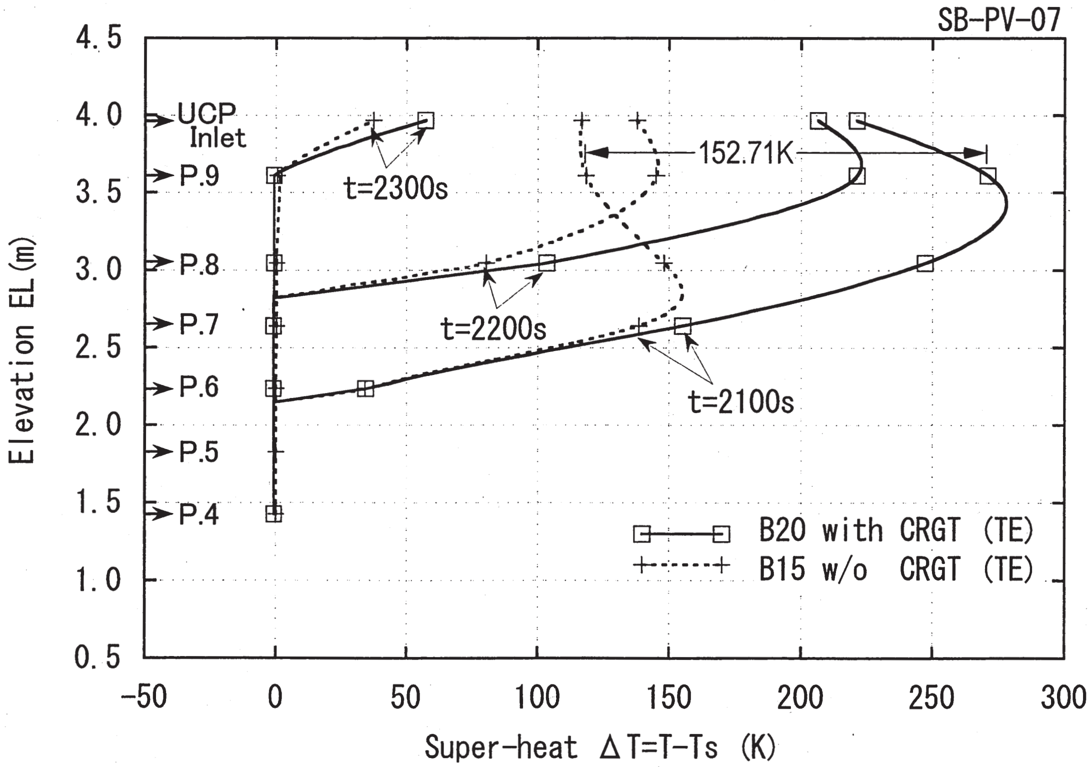

(2) Steam temperatures in two bundles during reflooding process

Fig.4.1-12 Effects of CRGT on steam heat-up behavior in high-power bundles in SB-PV-07 test (Bundle B15 w/o CRGT & bundle B20 with CRGT)

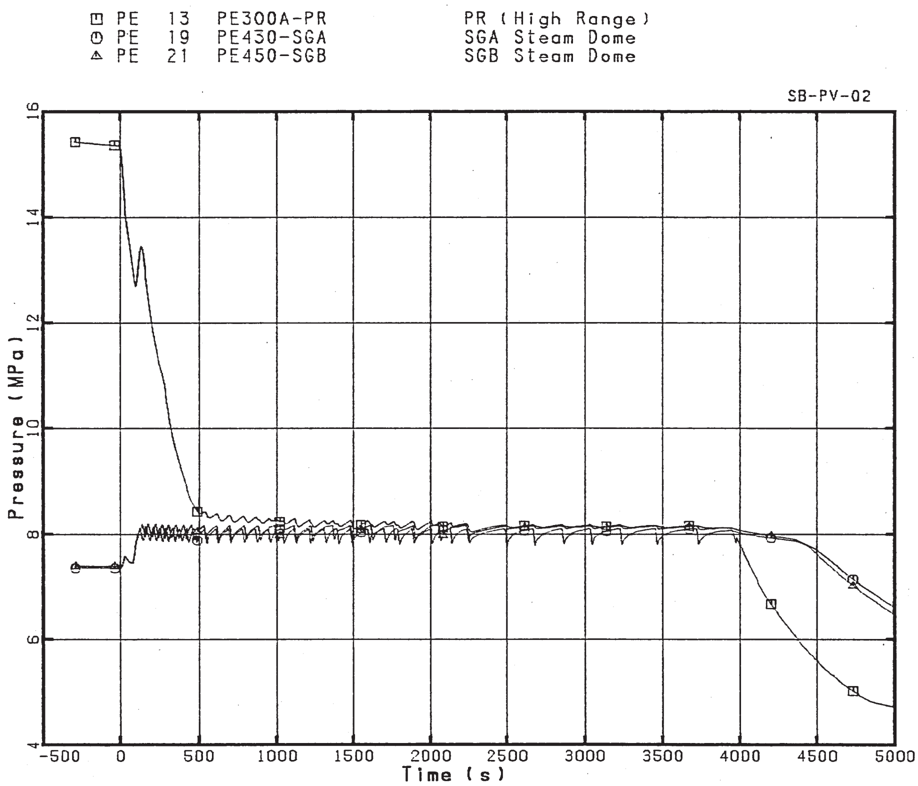

Fig.4.2-1 Primary and secondary pressures in LSTF 0.5% top break test (SB-PV-02)

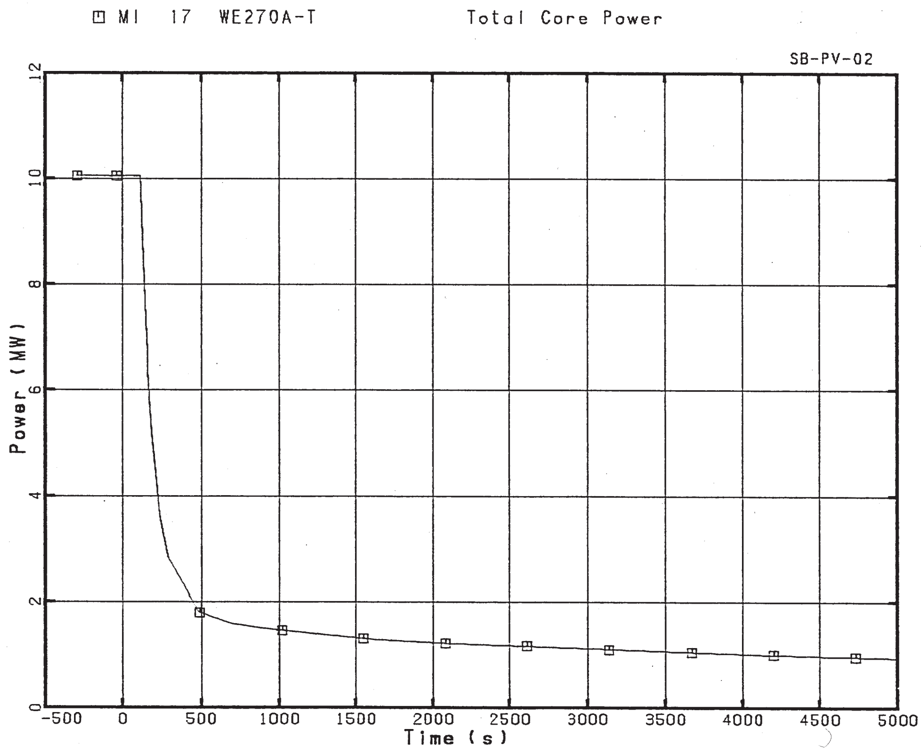

Fig.4.2-2 Core power decay curve in SB-PV-02 test

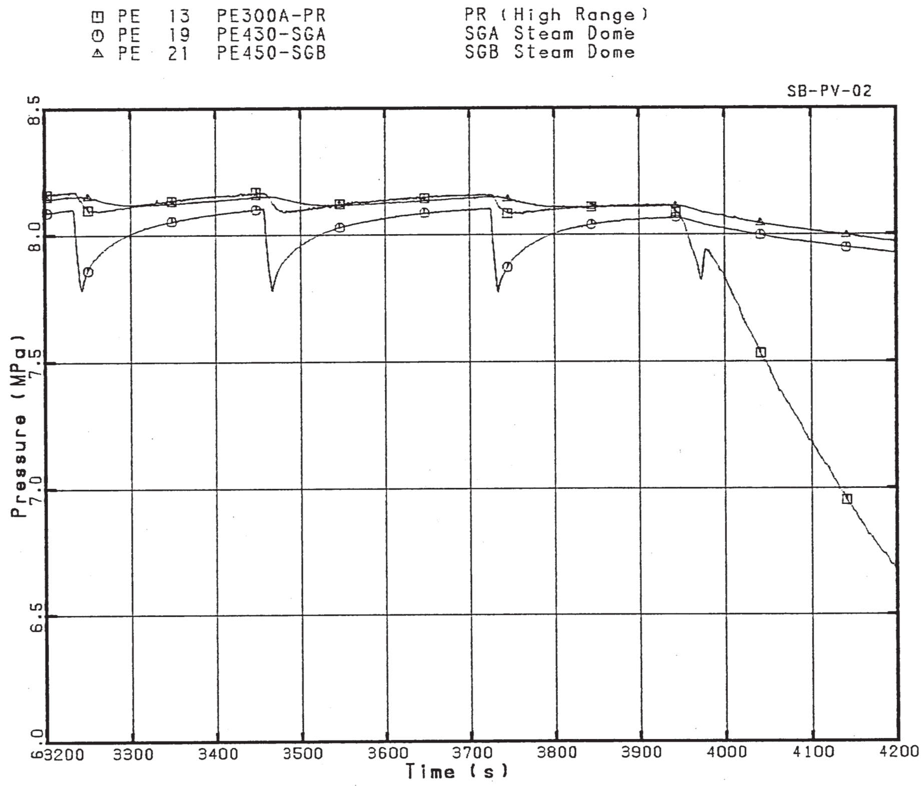

Fig.4.2-3 Pressures in detail during core heat-up in SB-PV-02 test

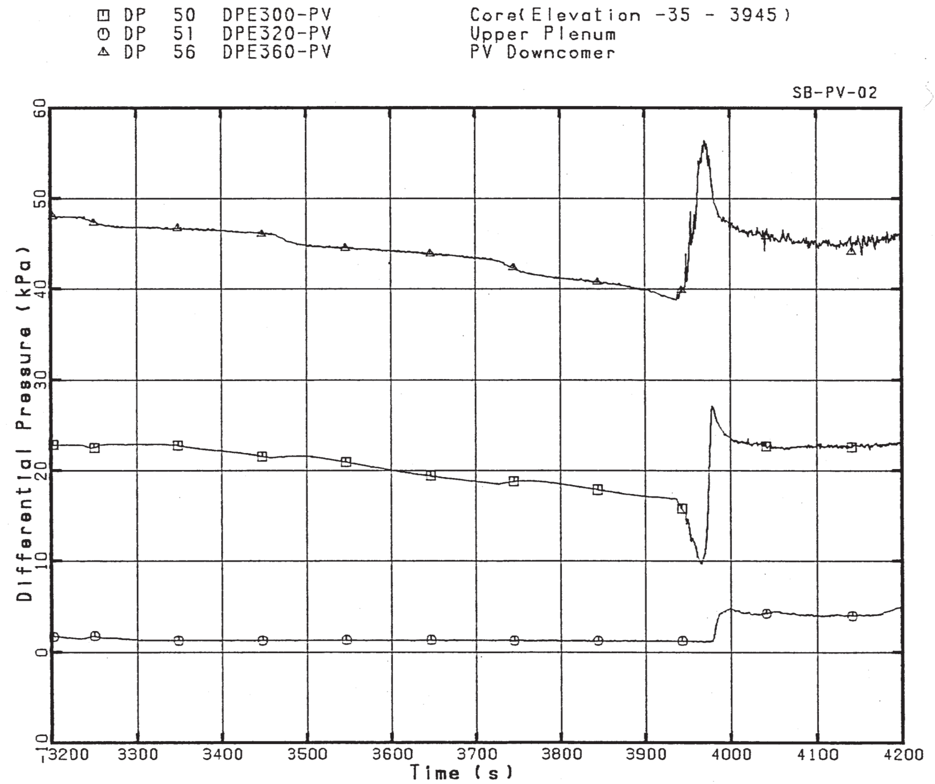

Fig.4.2-4 DP data in core, UP and downcomer during core heat-up in SB-PV-02 test

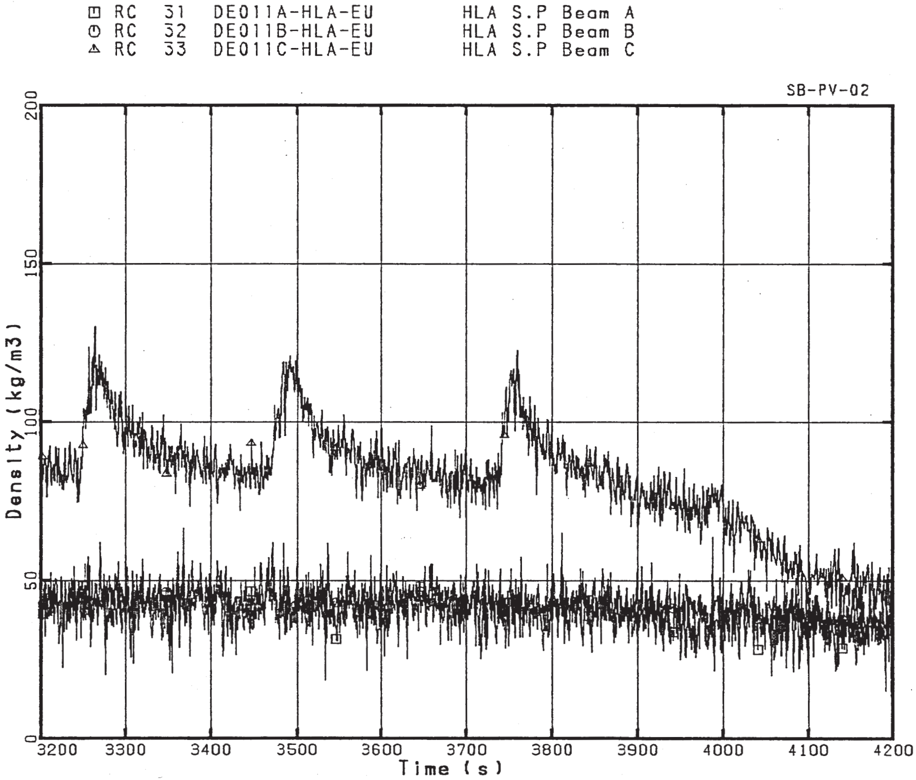

Fig.4.2-5 Fluid density data in HL-A during boil-off process in SB-PV-02 test

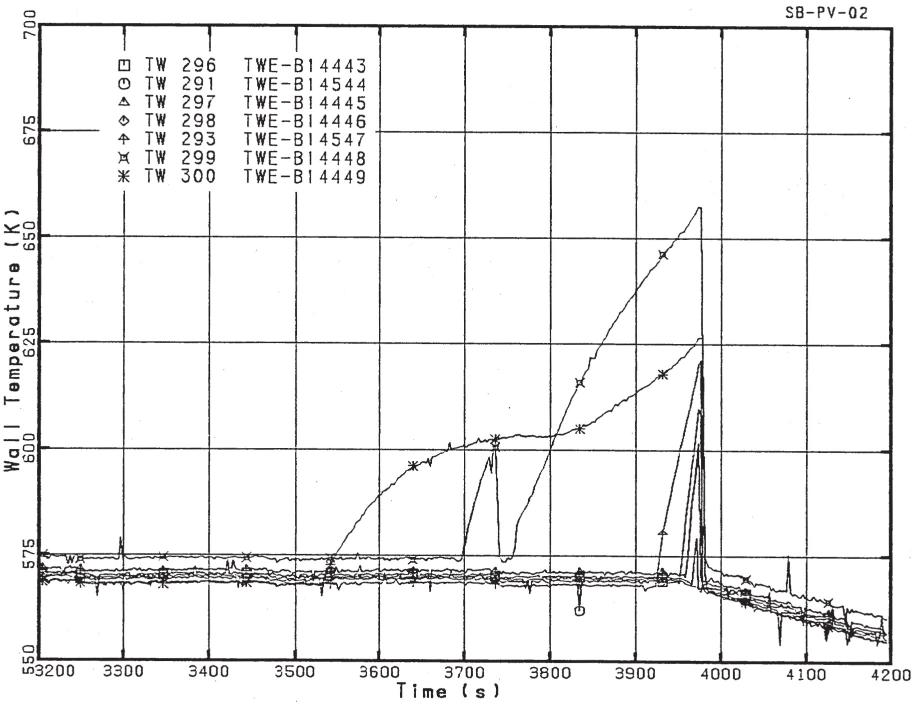

Fig.4.2-6 Representative heater rod surface temperatures in SB-PV-02 test

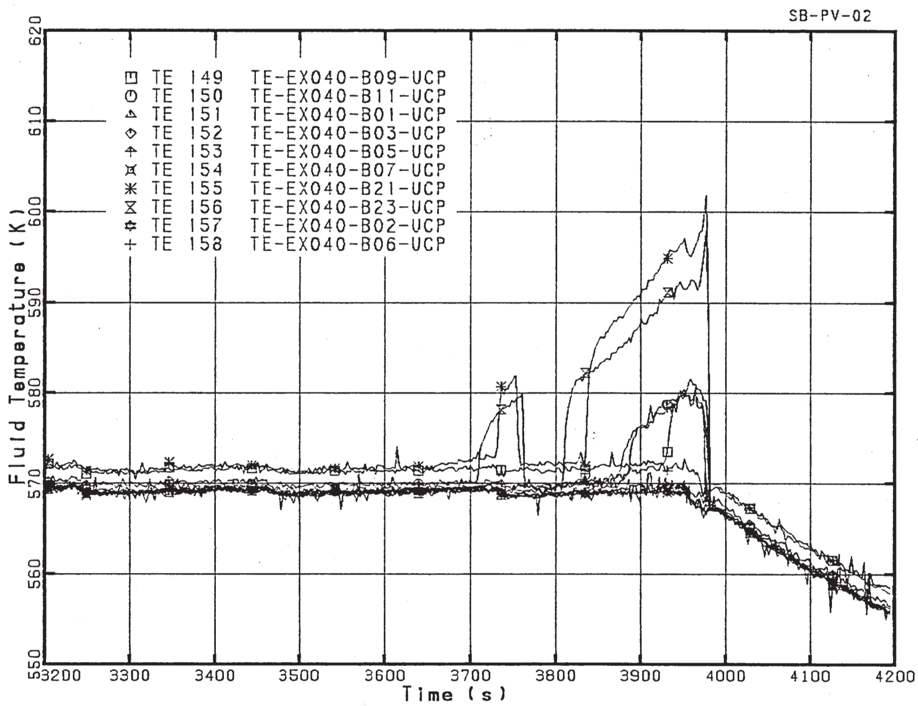

(1) CET temperatures above peripheral and central rod bundles

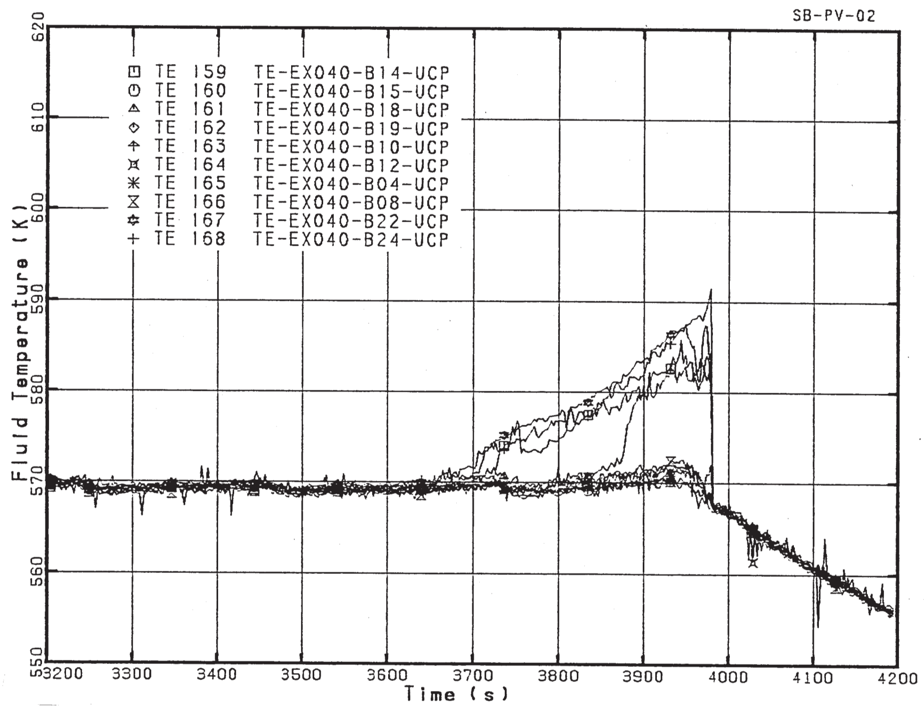

(2) CET temperatures above high-power and other rod bundles

Fig.4.2-7 CET temperatures during boil-off process in SB-PV-02 test

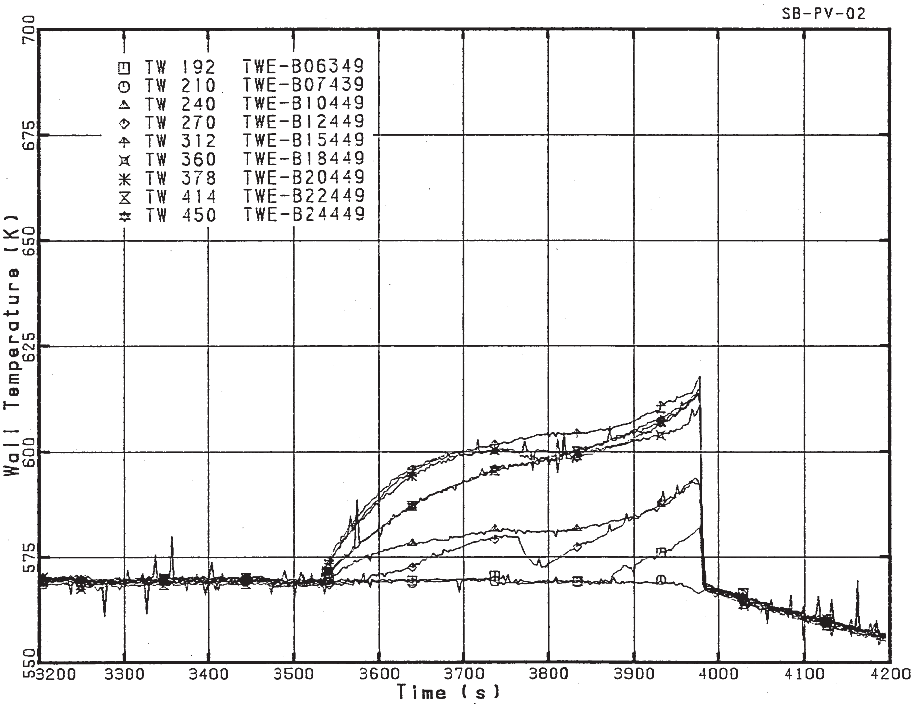

(1) Rod temperatures at Pos.9 (core top)

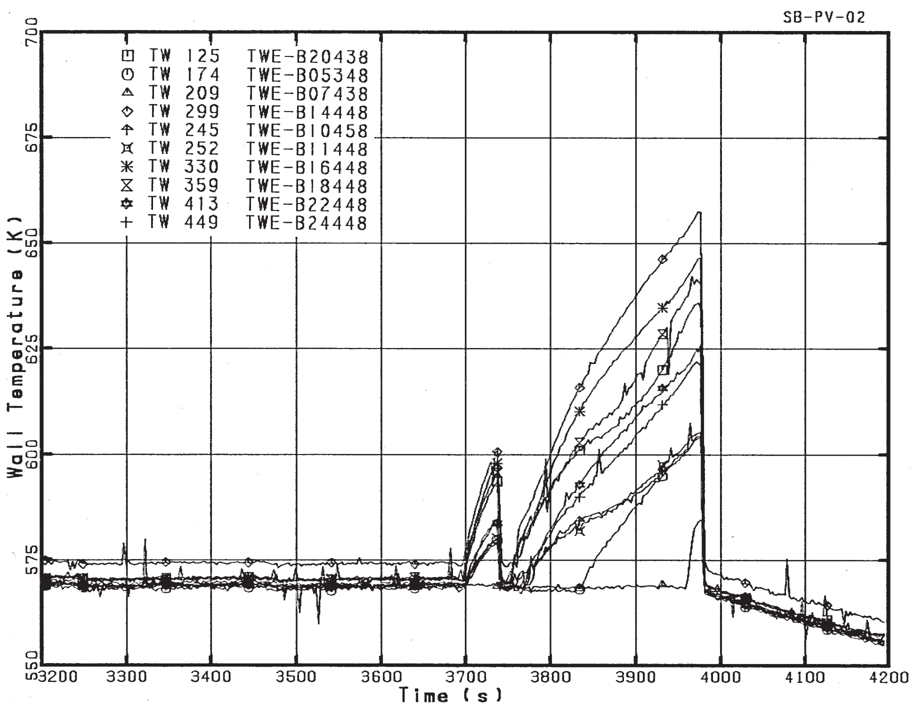

(2) Rod temperatures at Pos.8 with PCT measurement

Fig.4.2-8 Heater rod surface temperatures during boil-off in SB-PV-02 test

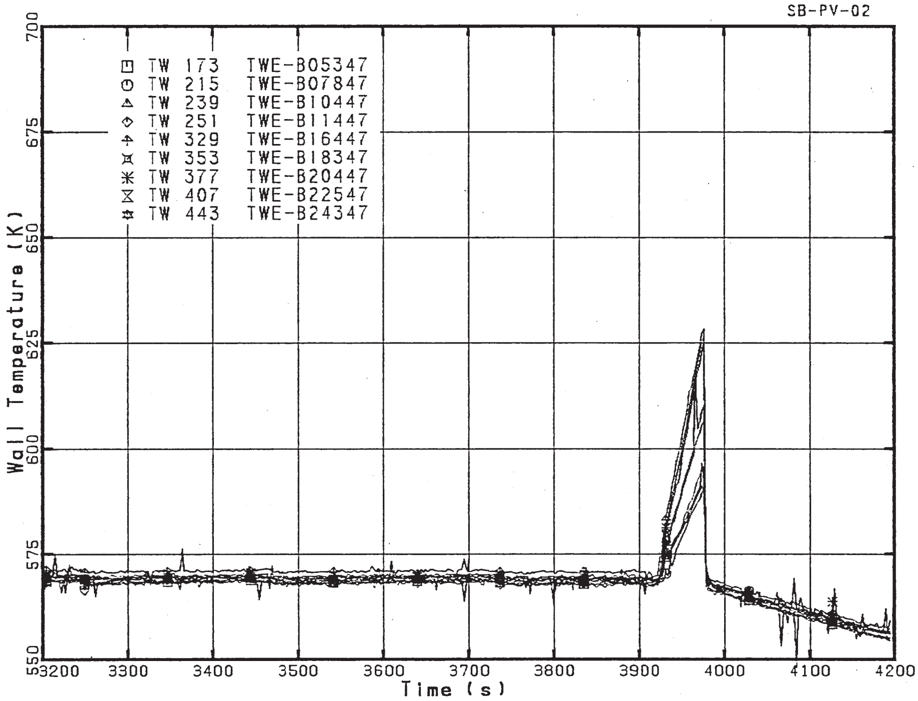

(3) Rod temperatures at Pos.7

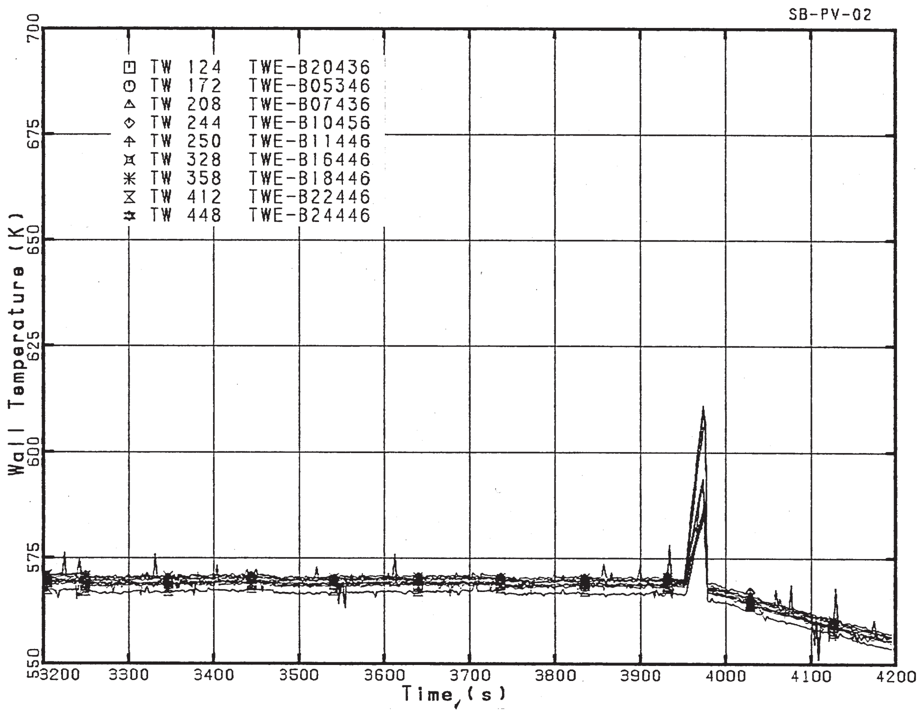

(4) Rod temperatures at Pos.6

Fig.4.2-8 Heater rod surface temperatures during boil-off in SB-PV-02 test

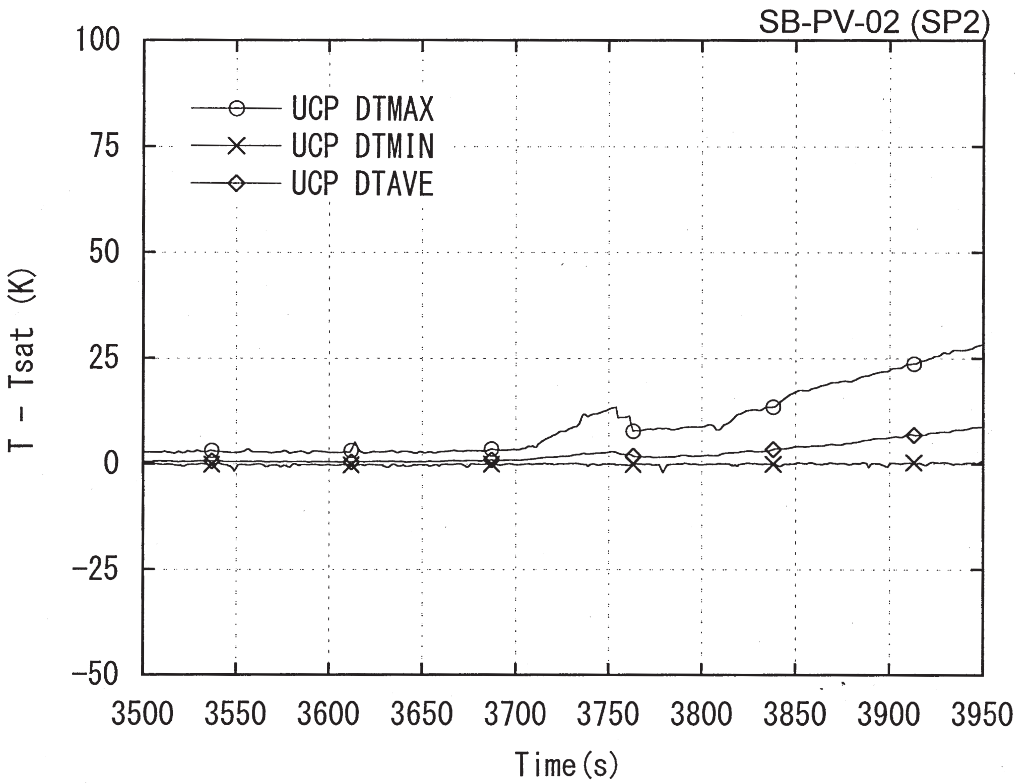

Fig.4.2-9 Distribution of all CET temperature rises above saturation temperature in SB-PV-02 test (DT_{MAX}, DT_{MIN}, DT_{AVE})

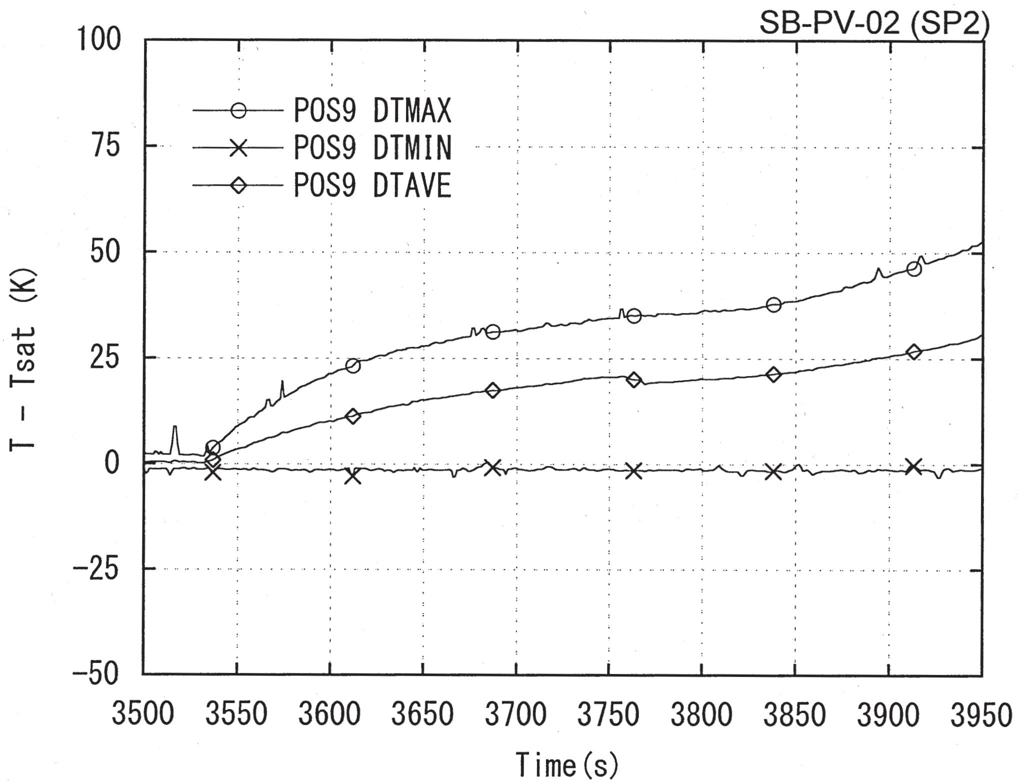

Fig.4.2-10 Distribution of heater rod temperature rises at Pos.9 in SB-PV-02 test (DT_{MAX}, DT_{MIN}, DT_{AVE})

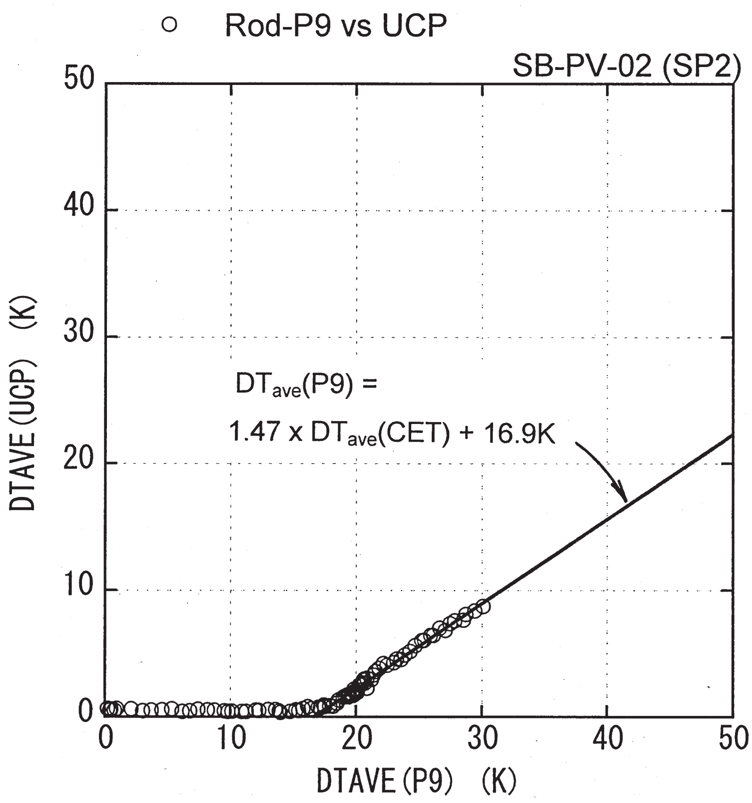

Fig.4.2-11 A relation of temperature rises at heater rod Pos.9, (Ave) and CET (Ave) in SB-PV-02 test (3500 - 3950 s)

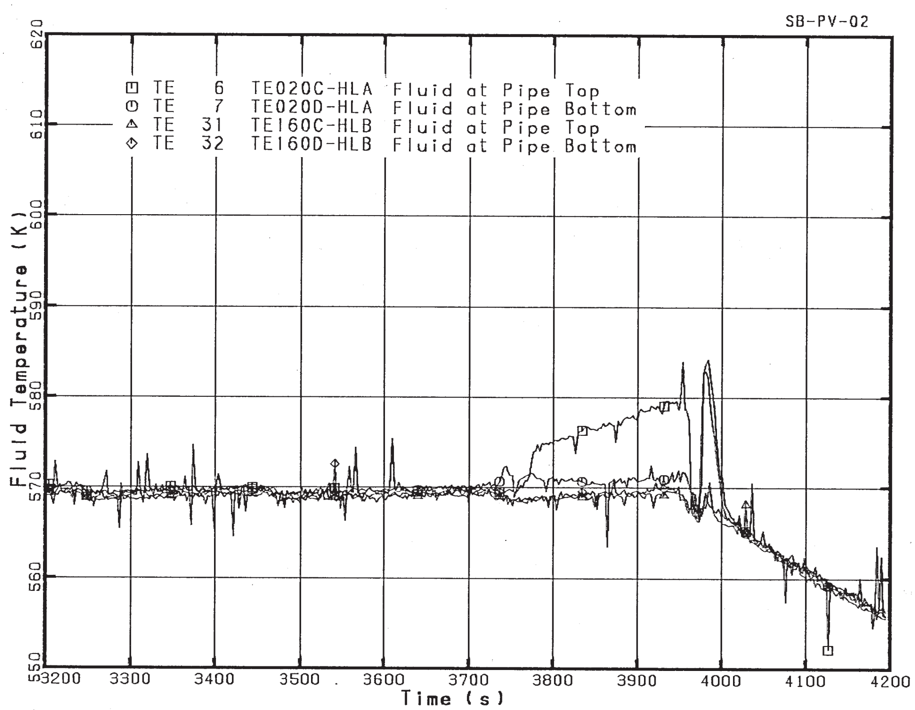

Fig.4.2-12 Fluid temperature data in hot legs during SB-PV-02 test

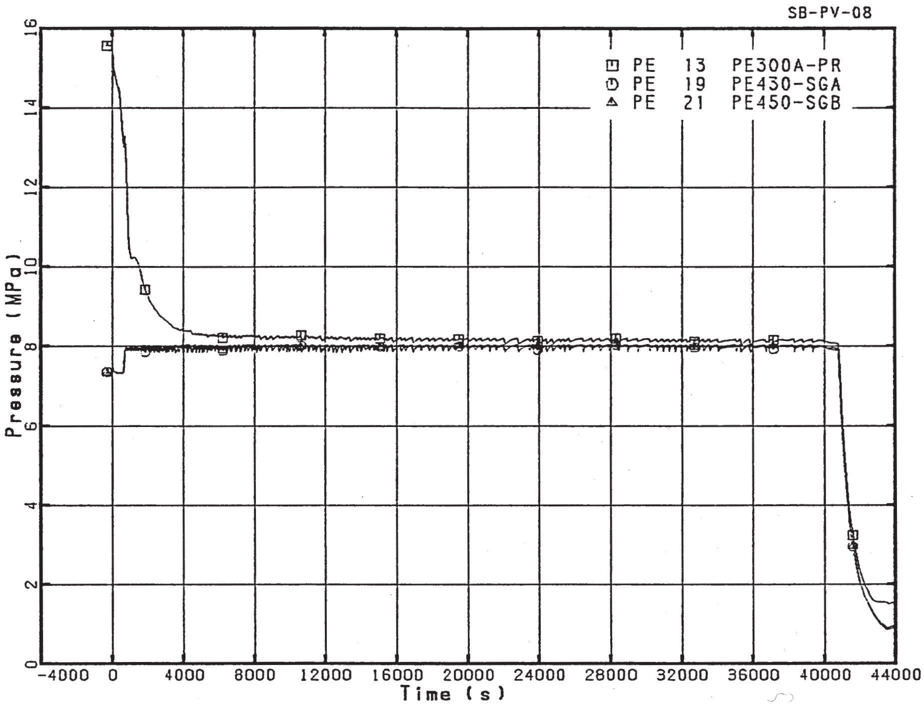

Fig.4.3-1 Primary and secondary pressures in LSTF 0.1% top break test (SB-PV-08)

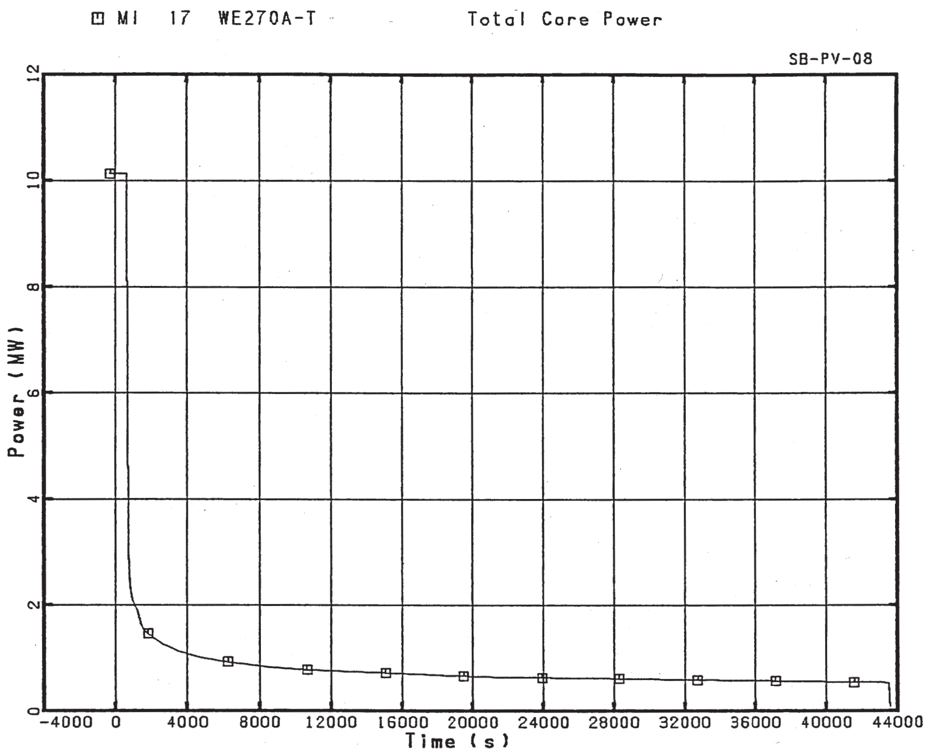

Fig.4.3-2 Core power decay curve in SB-PV-08 test

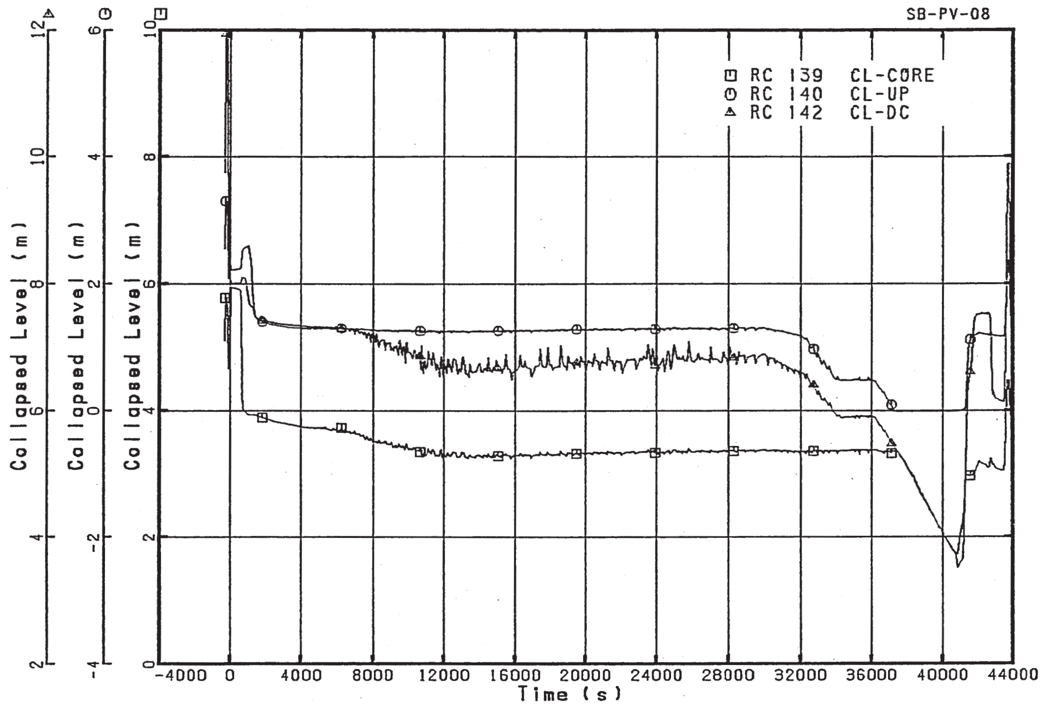

Fig.4.3-3 PV collapsed liquid levels in SB-PV-08 test

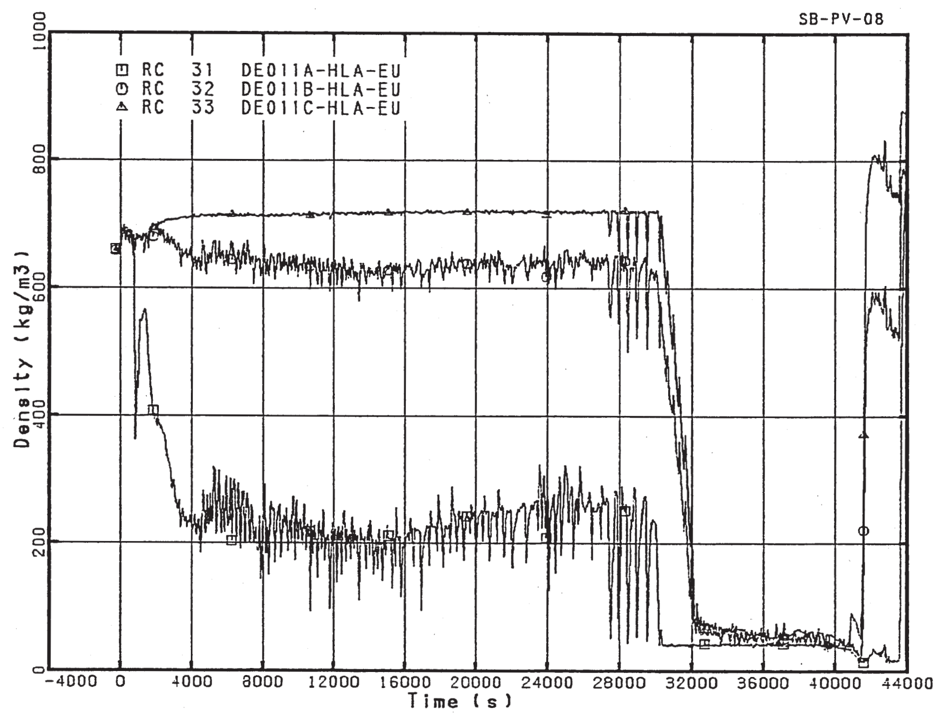

Fig.4.3-4 Fluid density data in intact loop hot leg (HL-A) in SB-PV-08 test

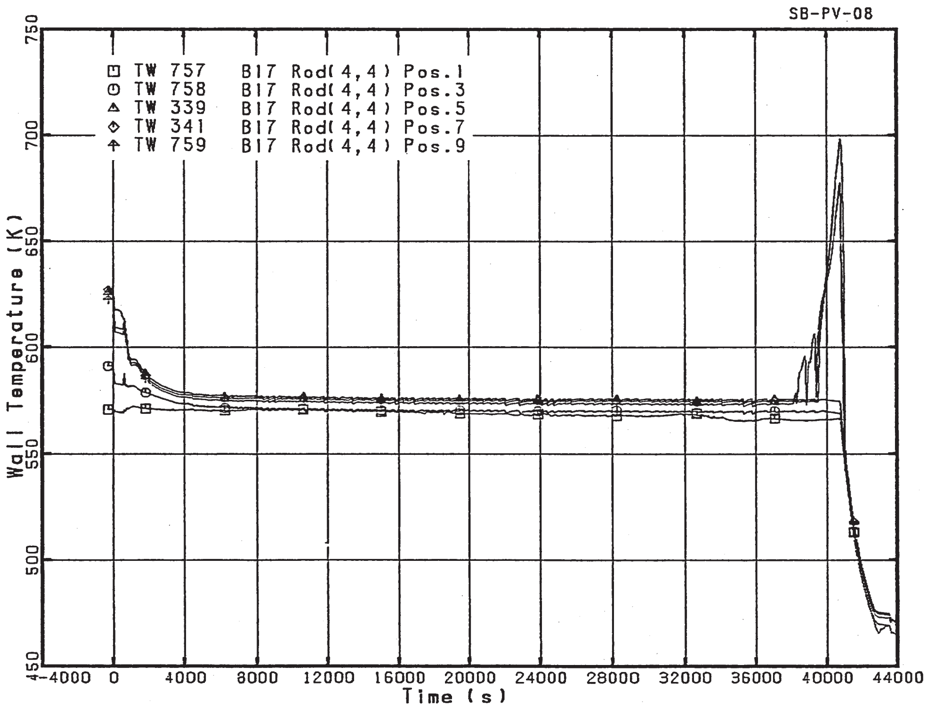

Fig.4.3-5 Representative heater rod surface temperatures in SB-PV-08 test

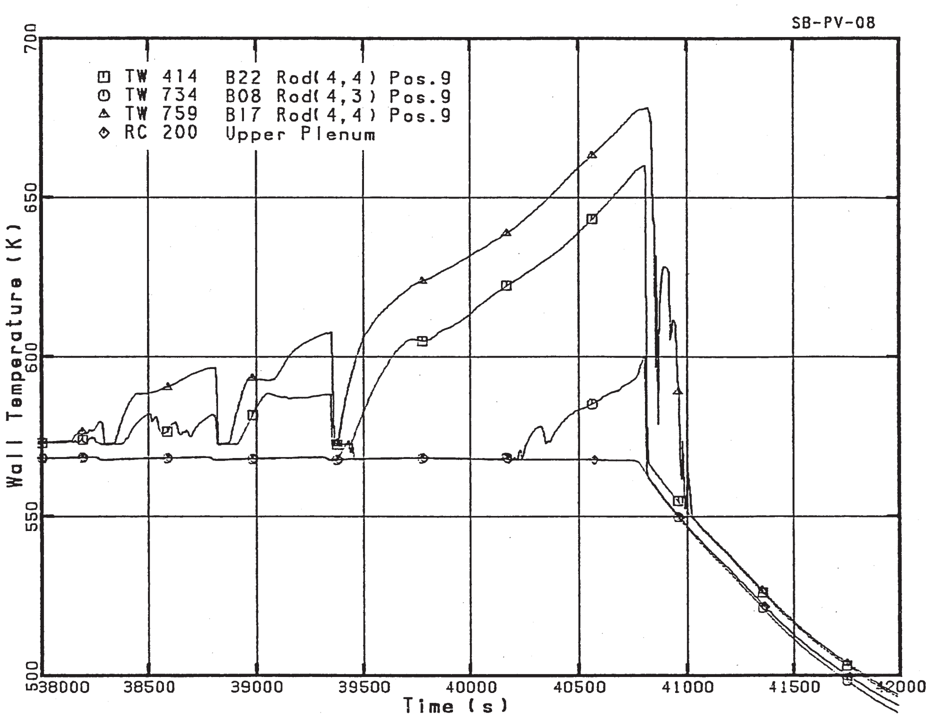

(1) Rod temperatures at Pos.9 (core top) compared with saturation temperature

Fig.4.3-6 Heater rod surface temperatures during boil-off in SB-PV-08 test

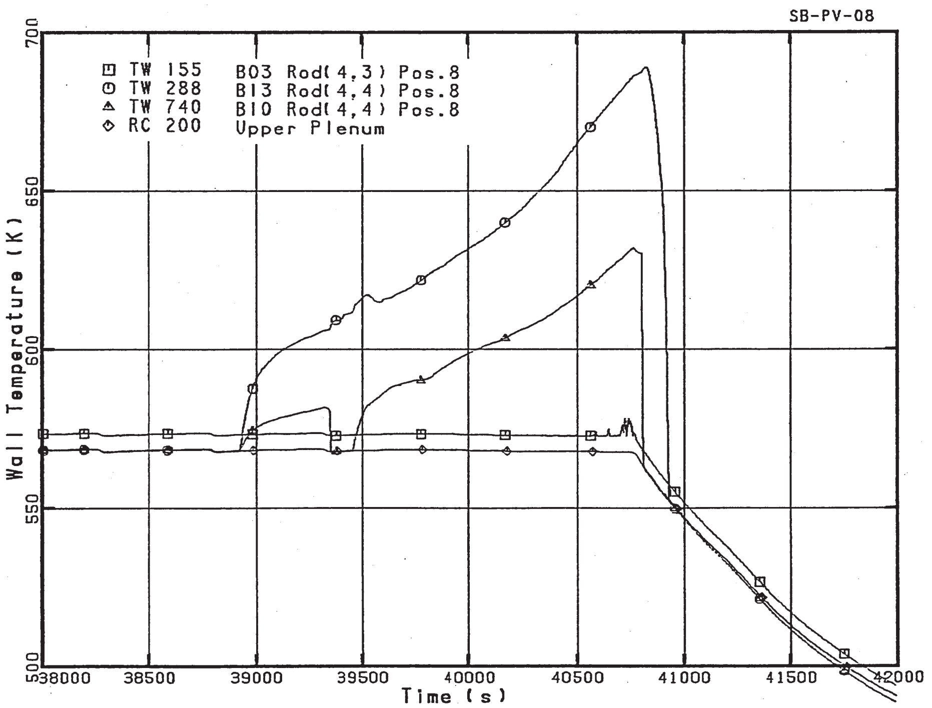

(2) Rod temperatures at Pos.8 compared with saturation temperature

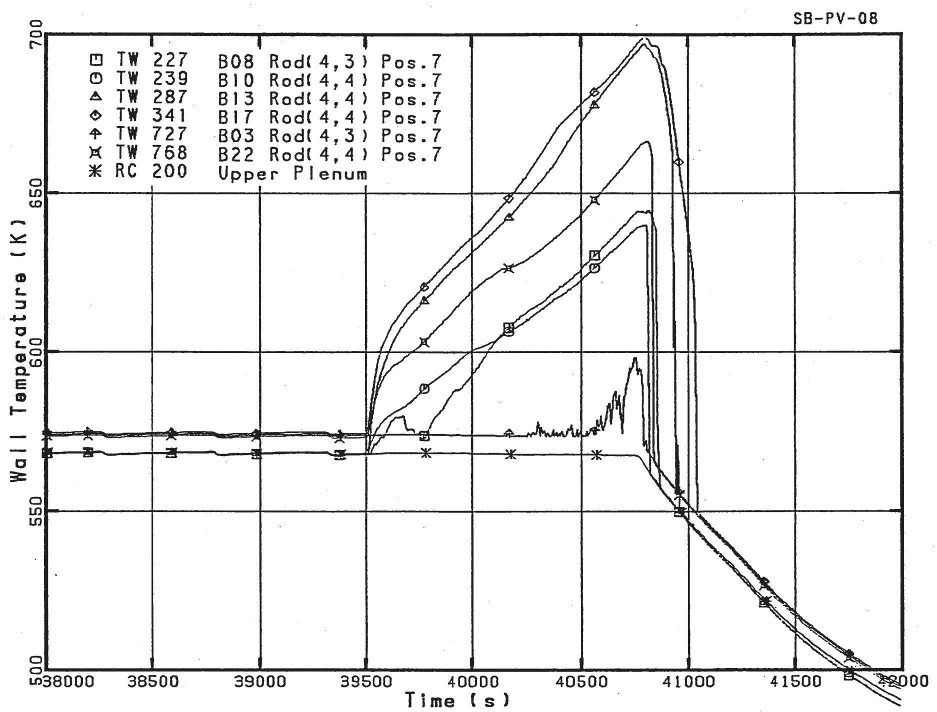

(3) Rod temperatures at Pos.7 with PCT measurement at B17 (4,4) rod

Fig.4.3-6 Heater rod surface temperatures during boil-off in SB-PV-08 test

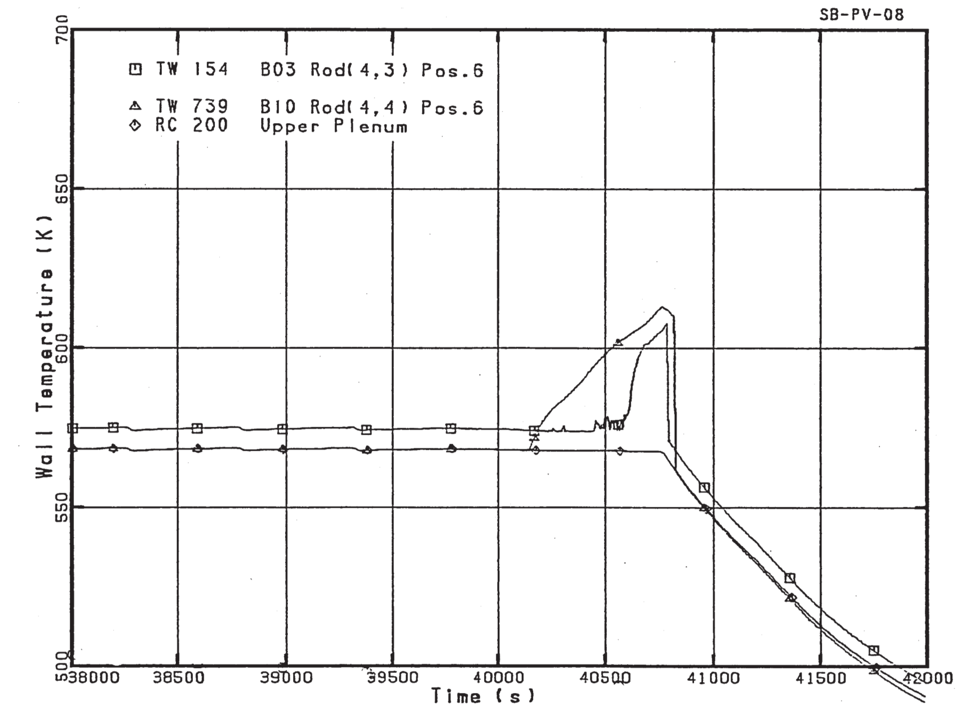

(4) Rod temperatures at Pos.6 compared with saturation temperature

Fig.4.3-6 Heater rod surface temperatures during boil-off in SB-PV-08 test

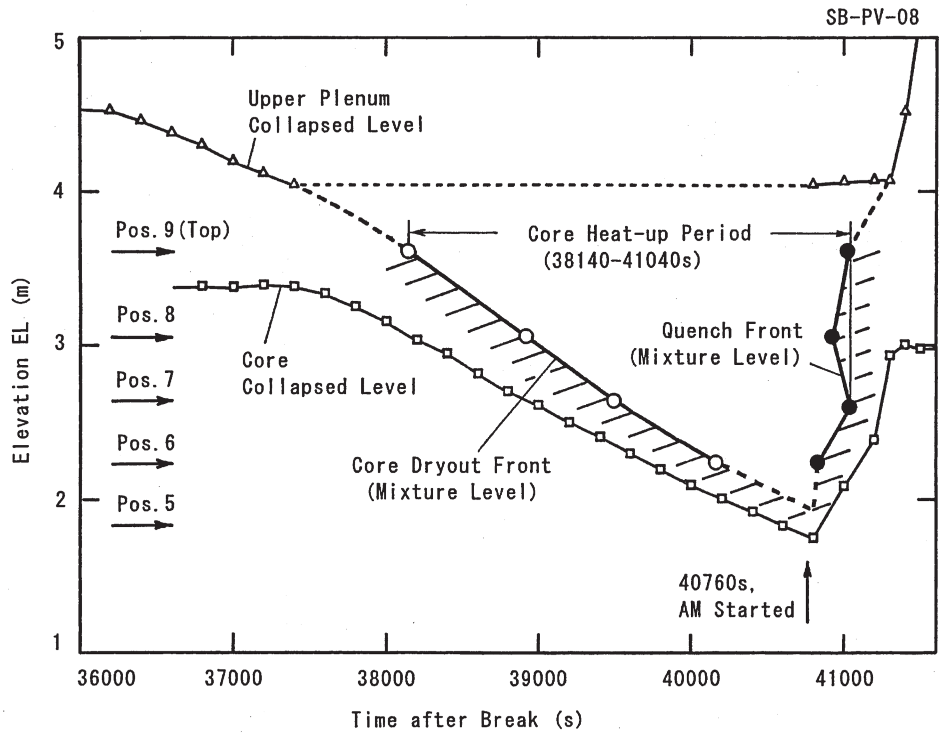

Fig.4.3-7 Core heat-up and quench behavior in SB-PV-08 test

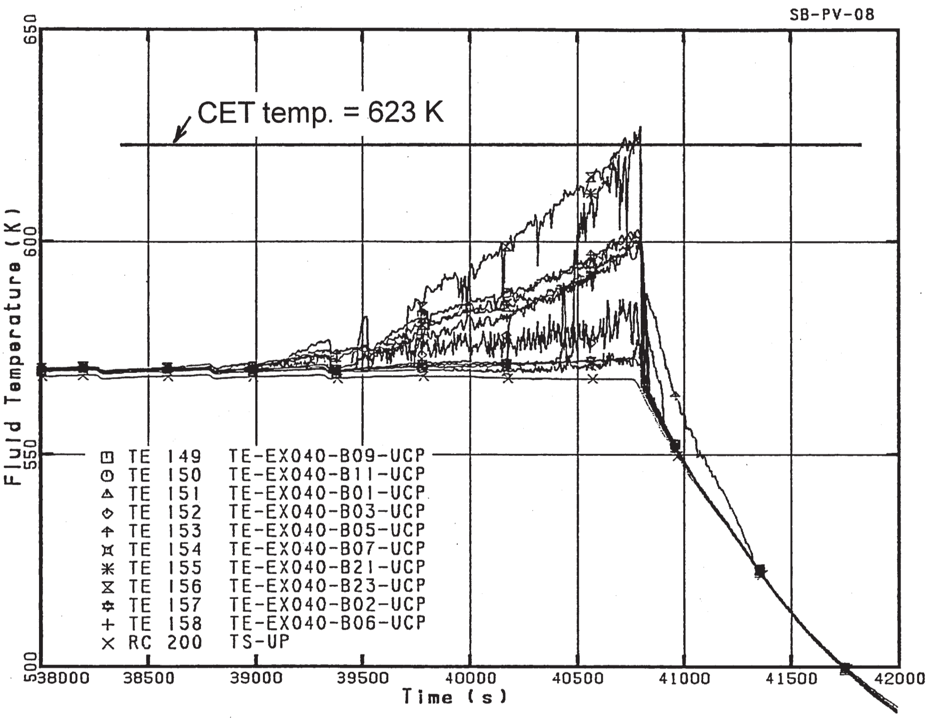

(1) CET temperatures above peripheral and central rod bundles

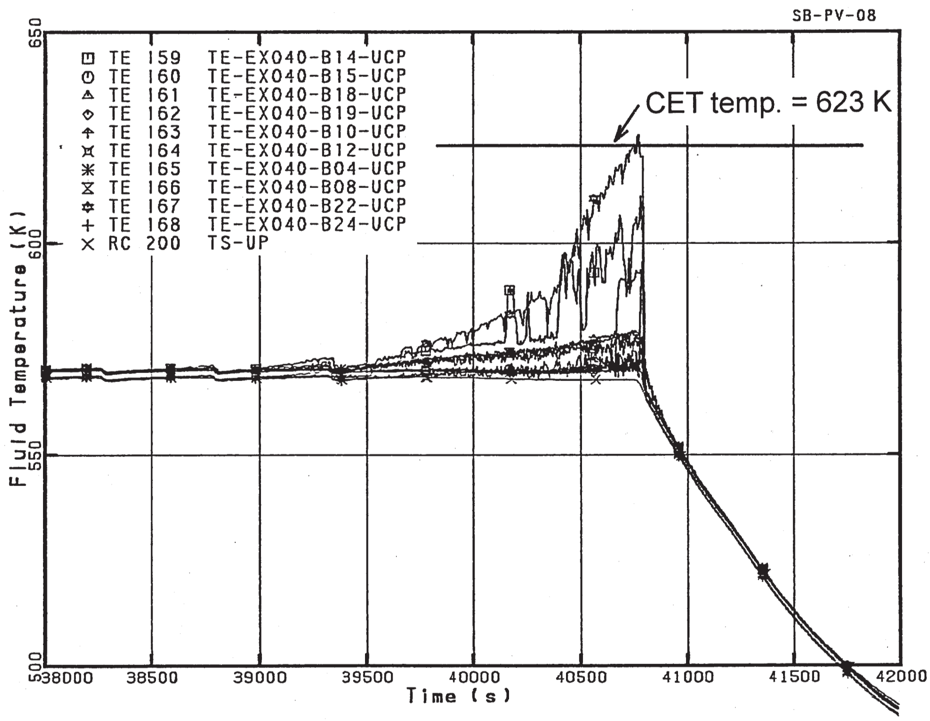

(2) CET temperatures above high-power and other rod bundles

Fig.4.3-8 CET temperatures during core heat-up period in SB-PV-08 test

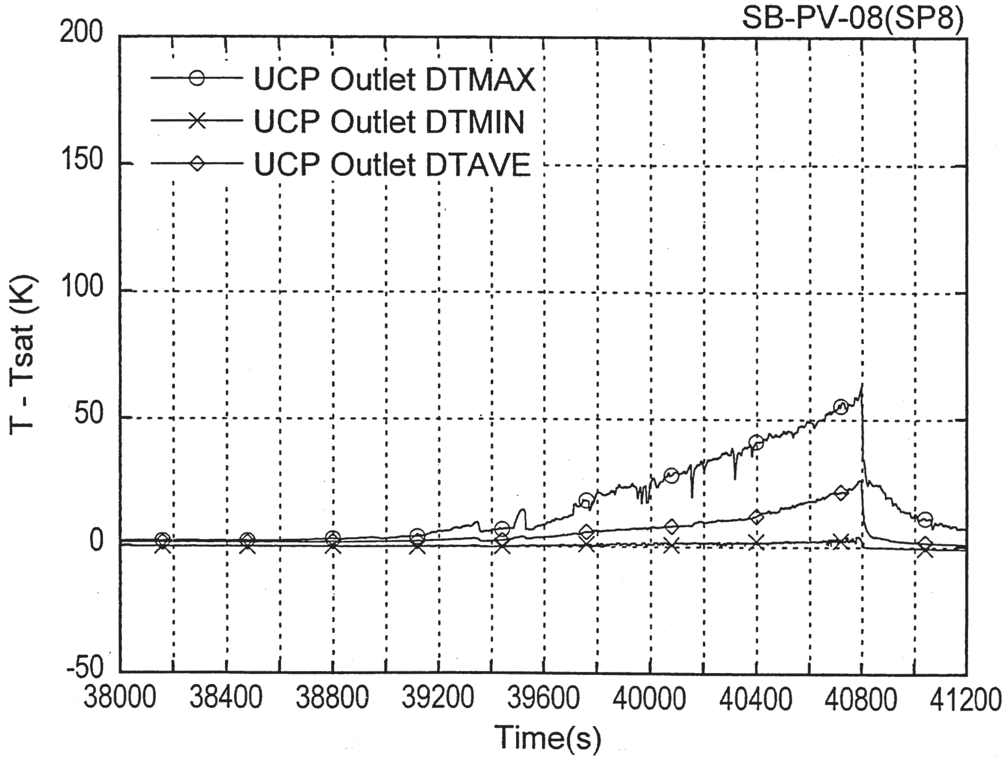

Fig.4.3-9 Distribution of all CET temperature rises above saturation temperature in SB-PV-08 test (DT_{MAX}, DT_{MIN}, DT_{AVE})

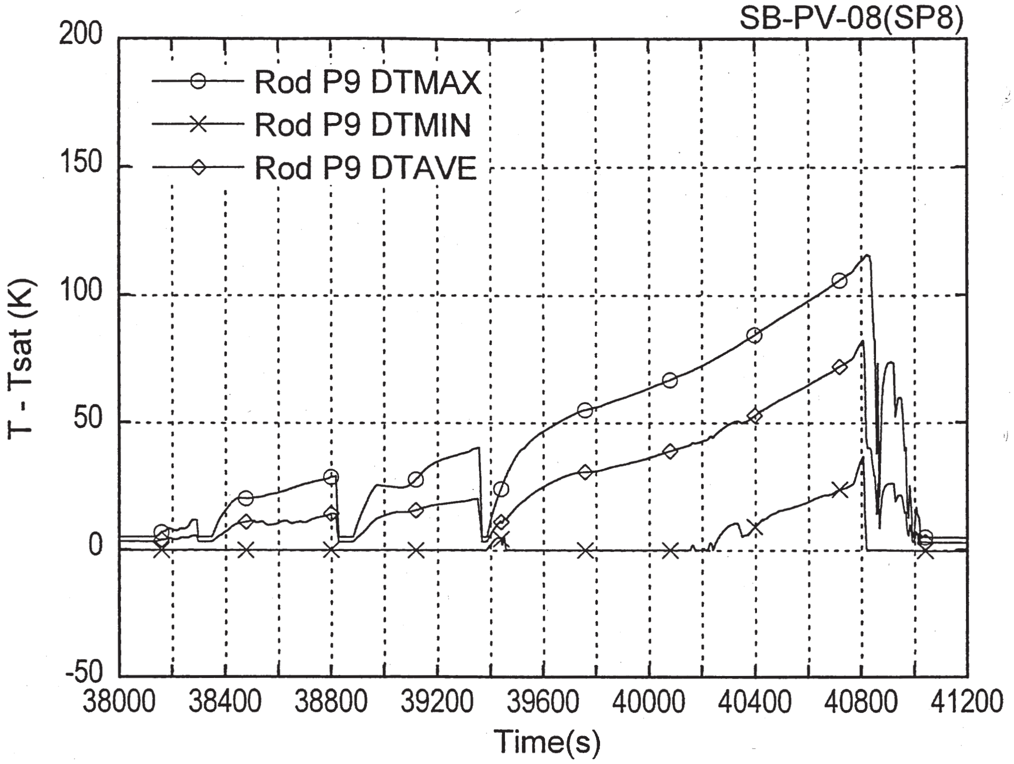

Fig.4.3-10 Distribution of heater rod temperature rises at Pos.9 in SB-PV-08 test (DT_{MAX}, DT_{MIN}, DT_{AVE})

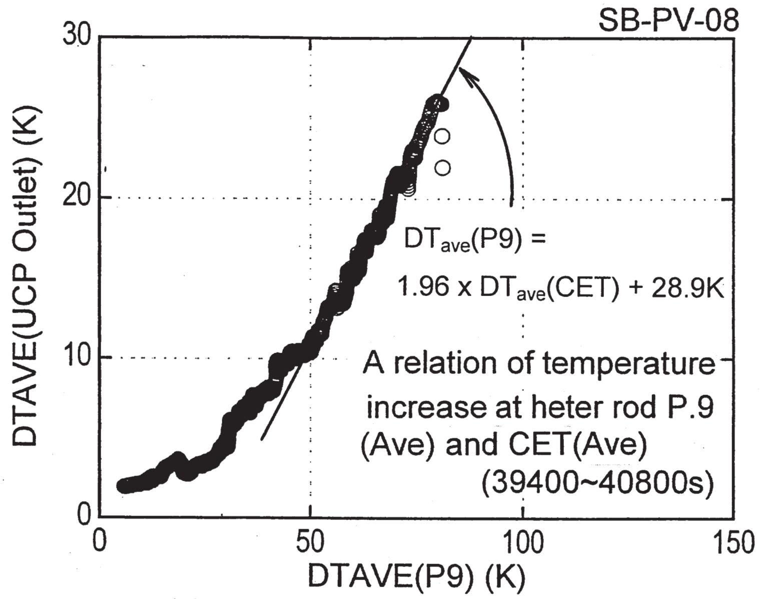

Fig.4.3-11 A relation of temperature rises at heater rod Pos.9, (Ave) and CET (Ave) in SB-PV-08 test

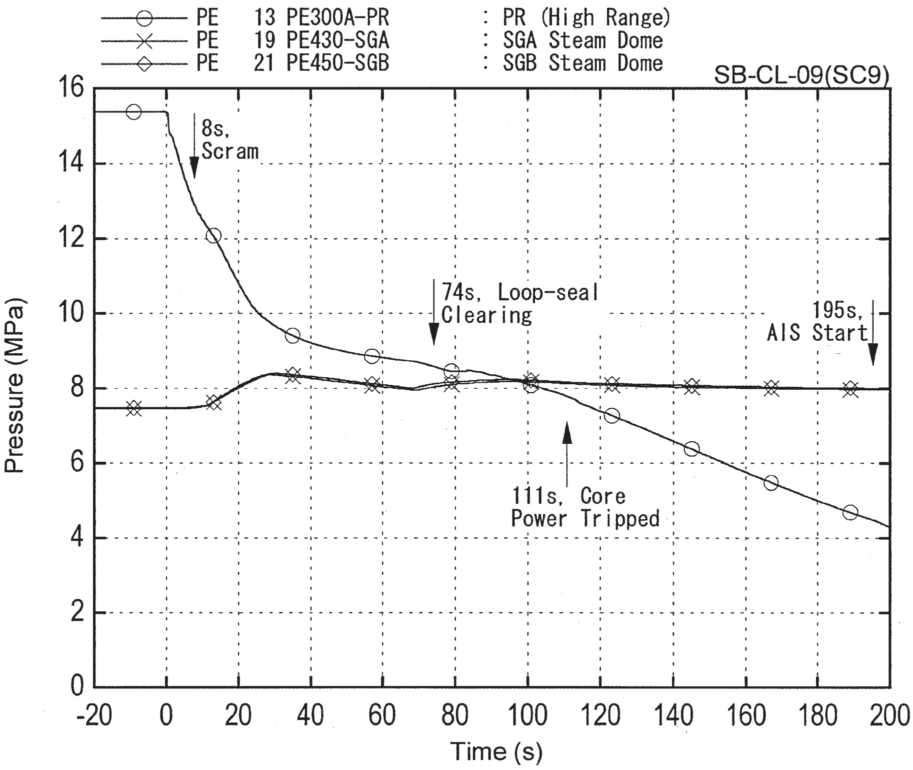

Fig.4.4-1 Primary and secondary pressures in LSTF 10% cold leg break test (SB-CL-09)

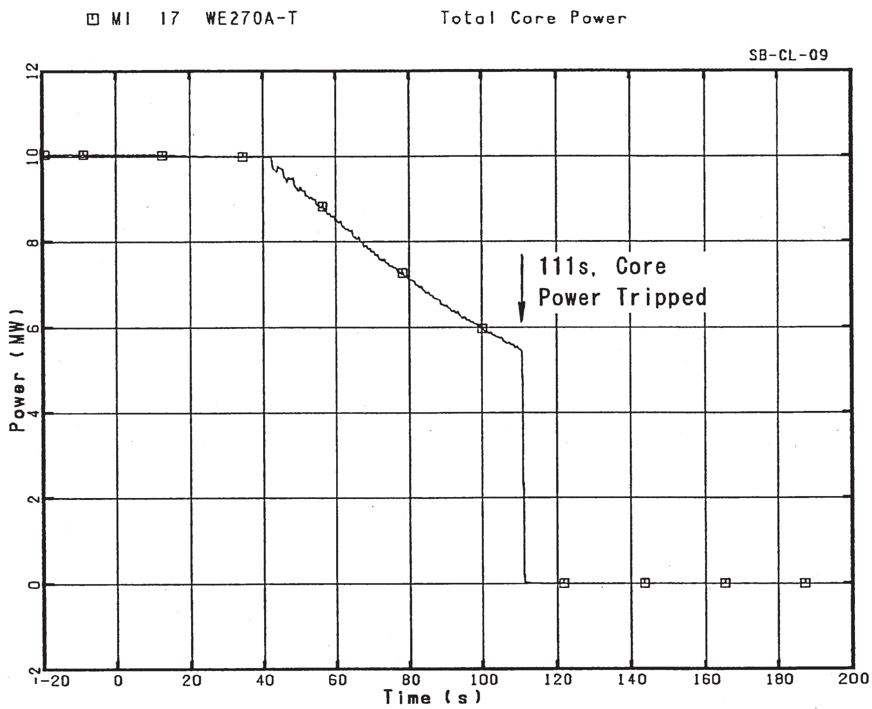

Fig.4.4-2 Core power decay curve in SB-CL-09 test

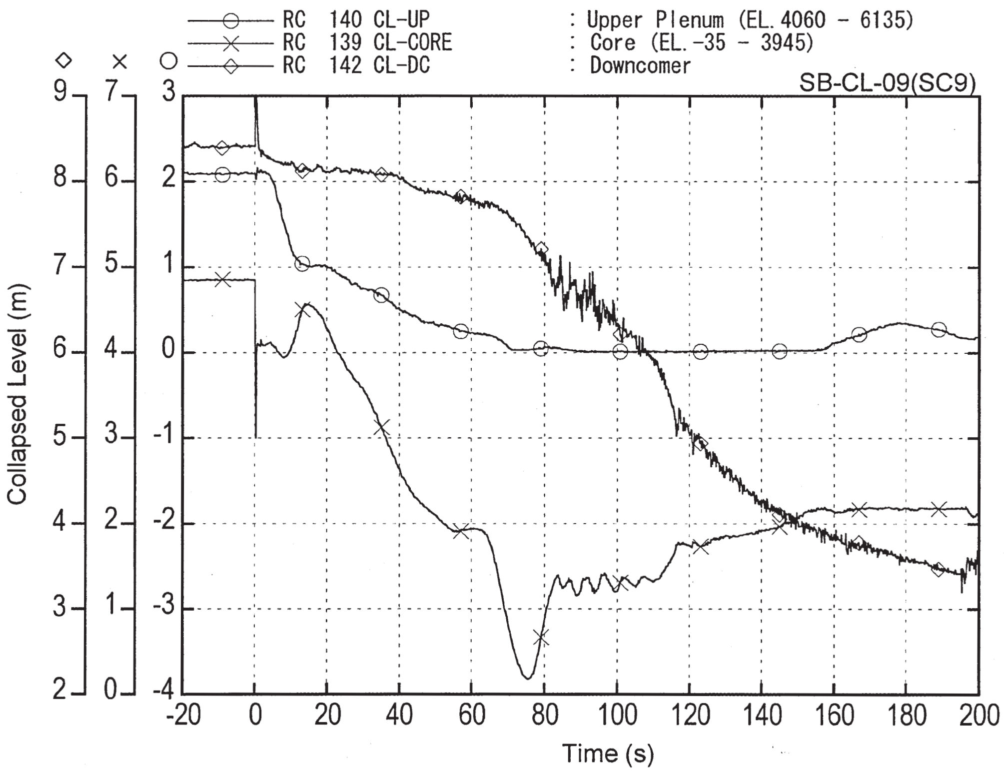

Fig.4.4-3 PV collapsed liquid levels in SB-CL-09 test

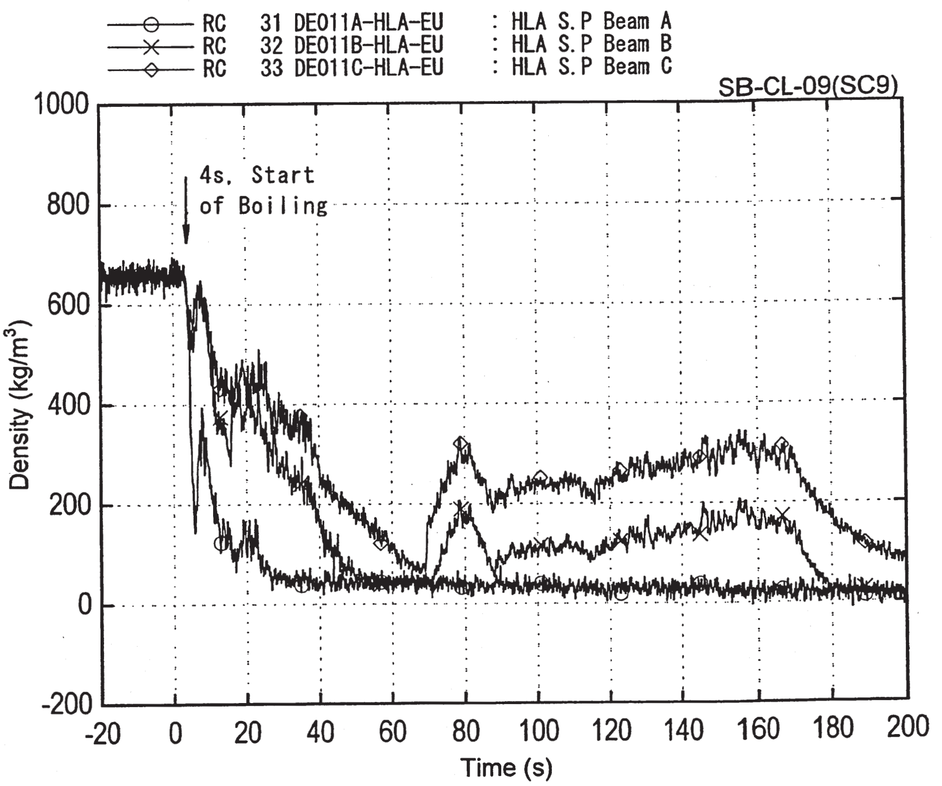

Fig.4.4-4 Fluid density data in intact loop hot leg (HL-A) in SB-CL-09 test

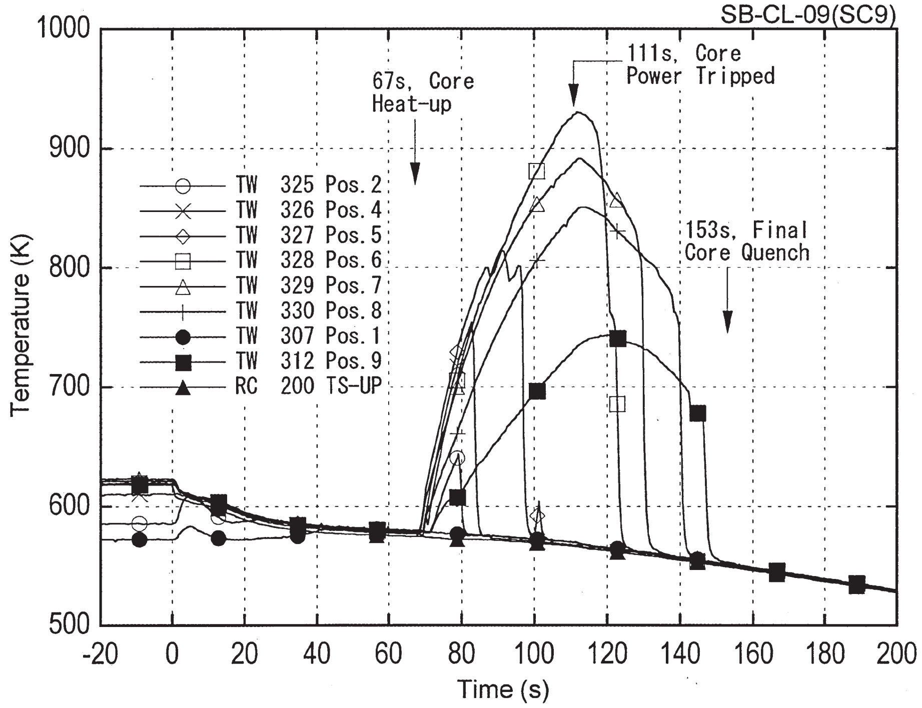

Fig.4.4-5 Representative heater rod surface temperatures in SB-CL-09 test

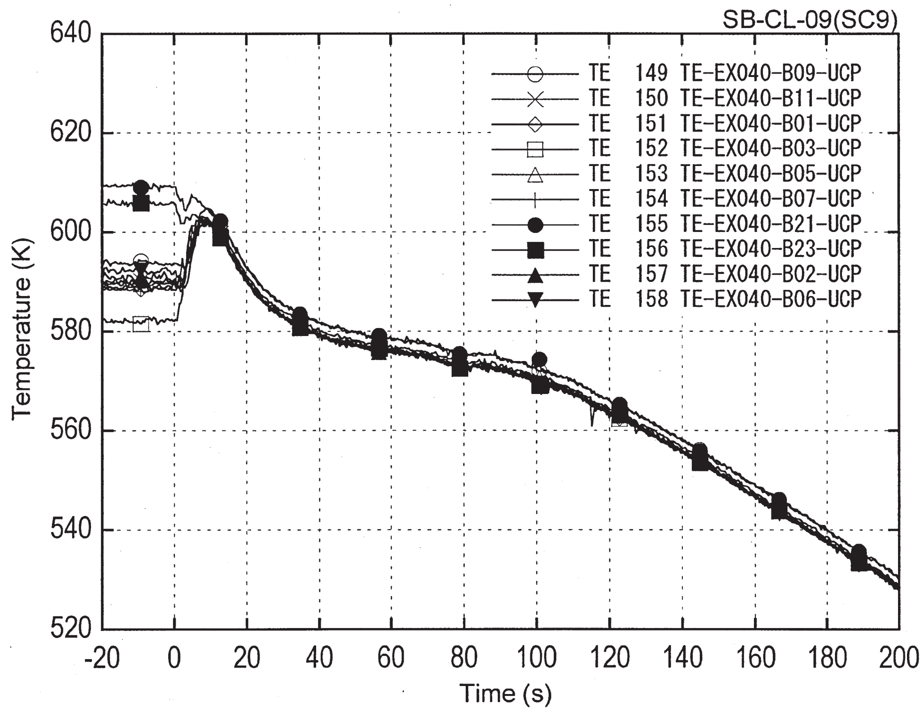

(1) CET temperatures above peripheral and central rod bundles

Fig.4.4-6 CET temperatures during core heat-up period in SB-CL-09 test

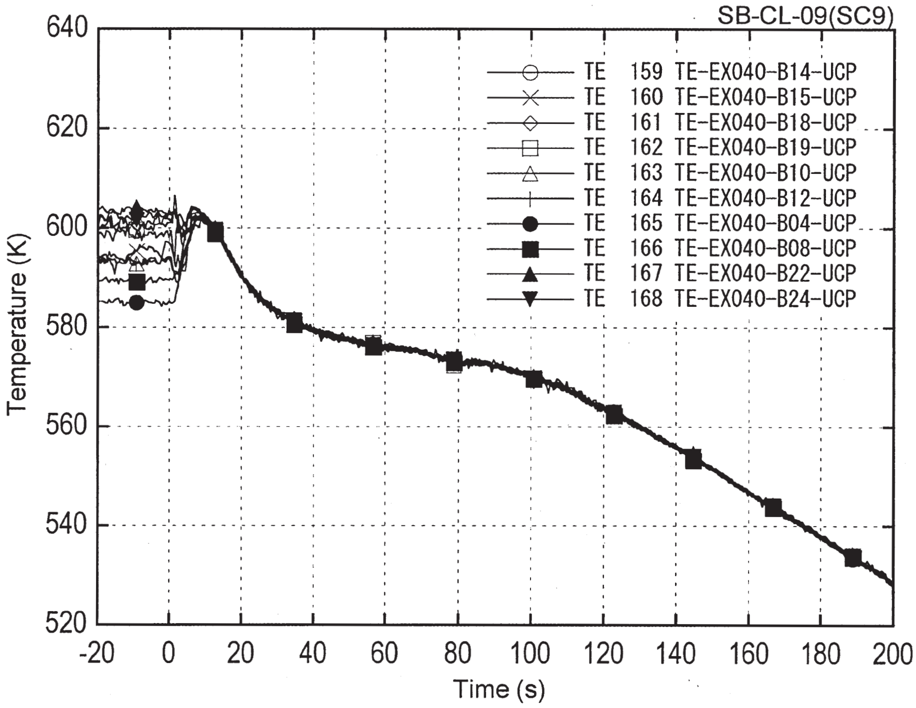

(2) CET temperatures above high-power and other rod bundles

Fig.4.4-6 CET temperatures during core heat-up period in SB-CL-09 test

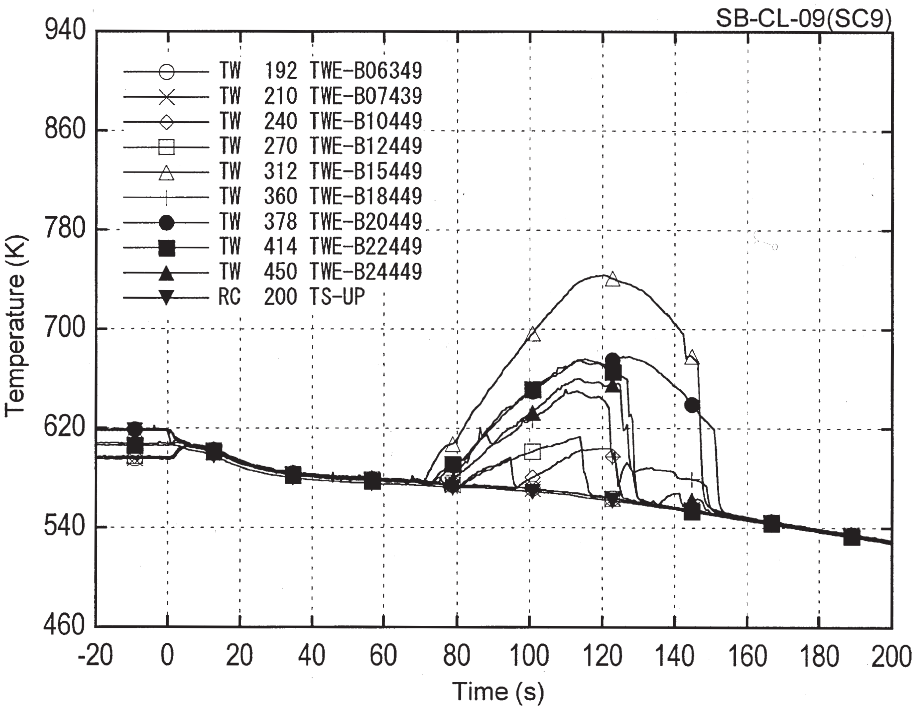

(1) Heater rod temperatures at Pos.9 (core top)

Fig.4.4-7 Heater rod temperatures in SB-CL-09 test

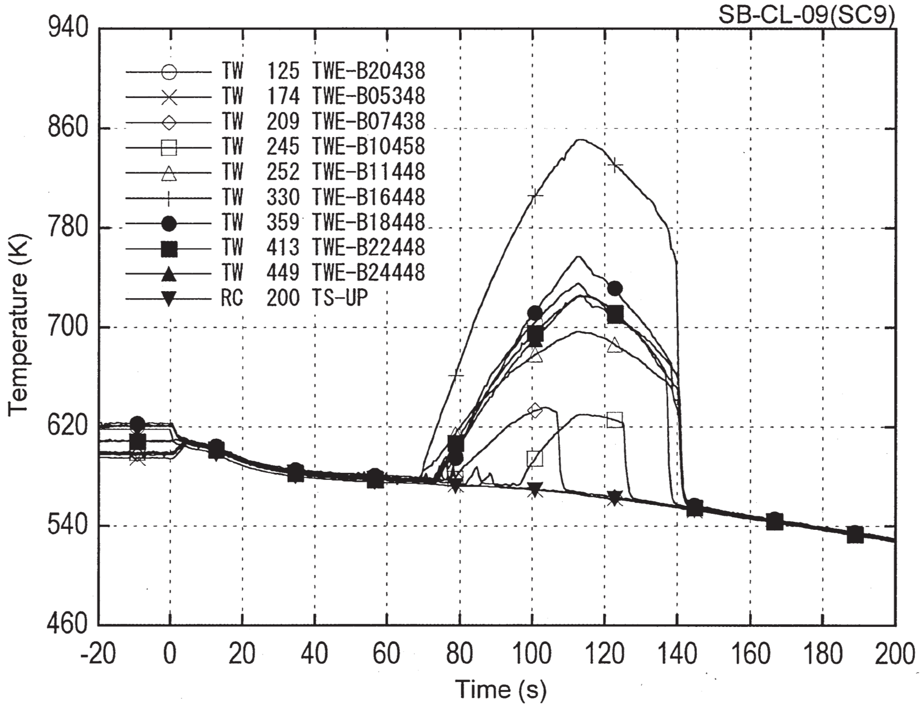

(2) Heater rod temperatures at Pos.8

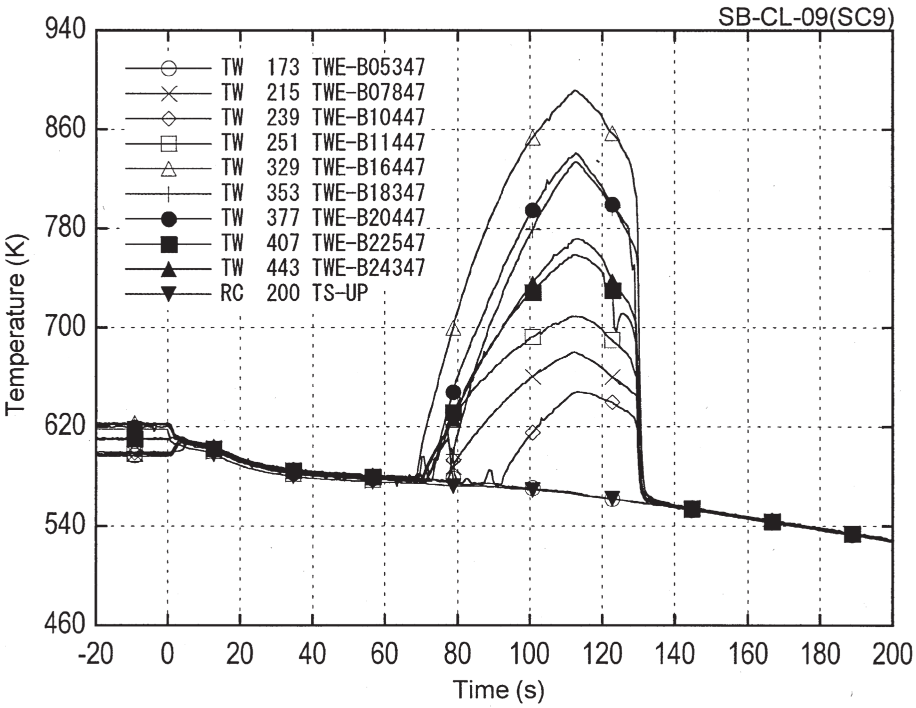

(3) Heater rod temperatures at Pos.7

Fig.4.4-7 Heater rod temperatures in SB-CL-09 test

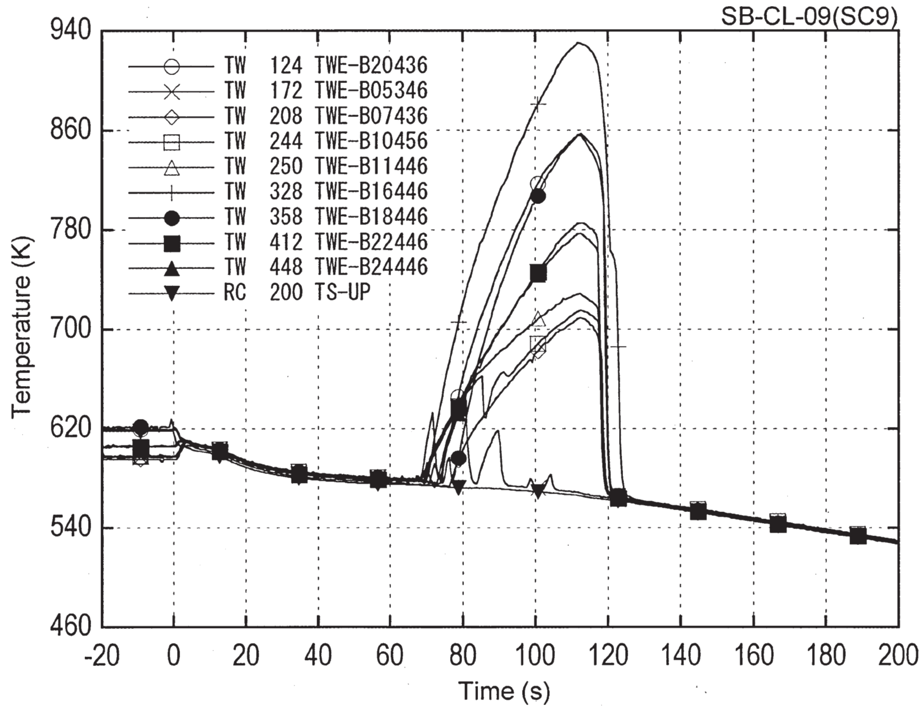

(4) Heater rod temperatures at Pos.6 with PCT measurement

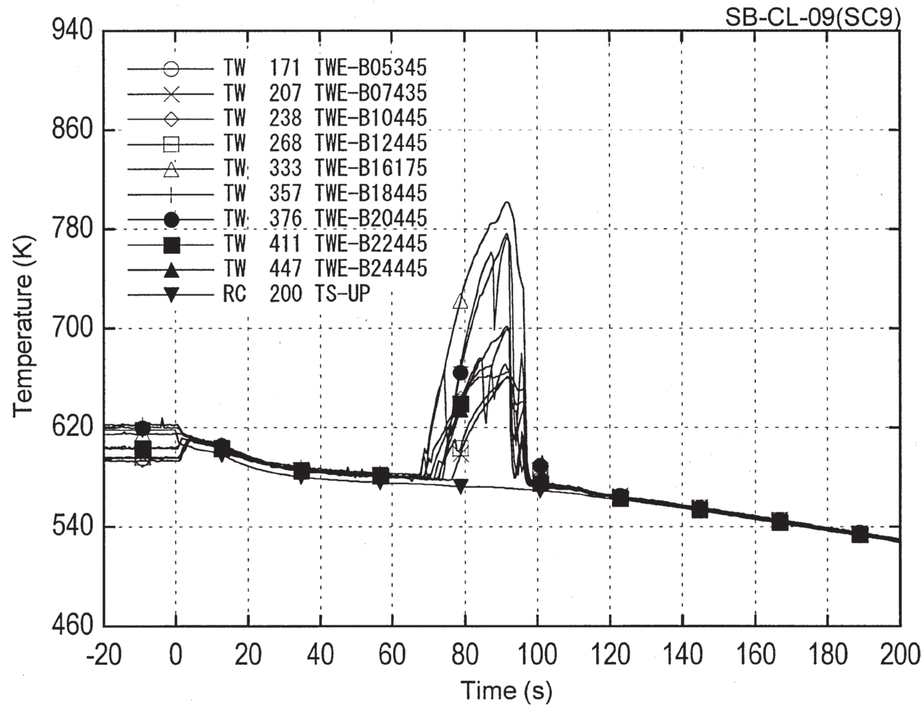

(5) Heater rod temperatures at Pos.5 (core middle height)

Fig.4.4-7 Heater rod temperatures in SB-CL-09 test

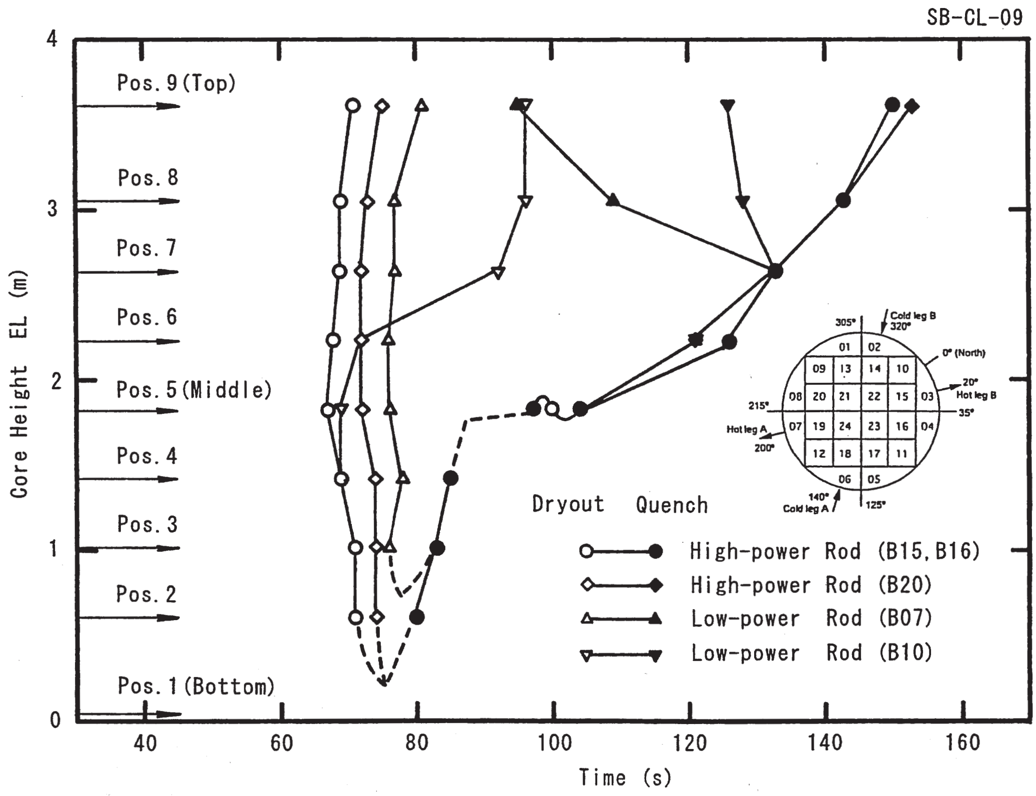

Fig.4.4-8 Variety of rod heat-up and quench behavior in SB-CL-09 test

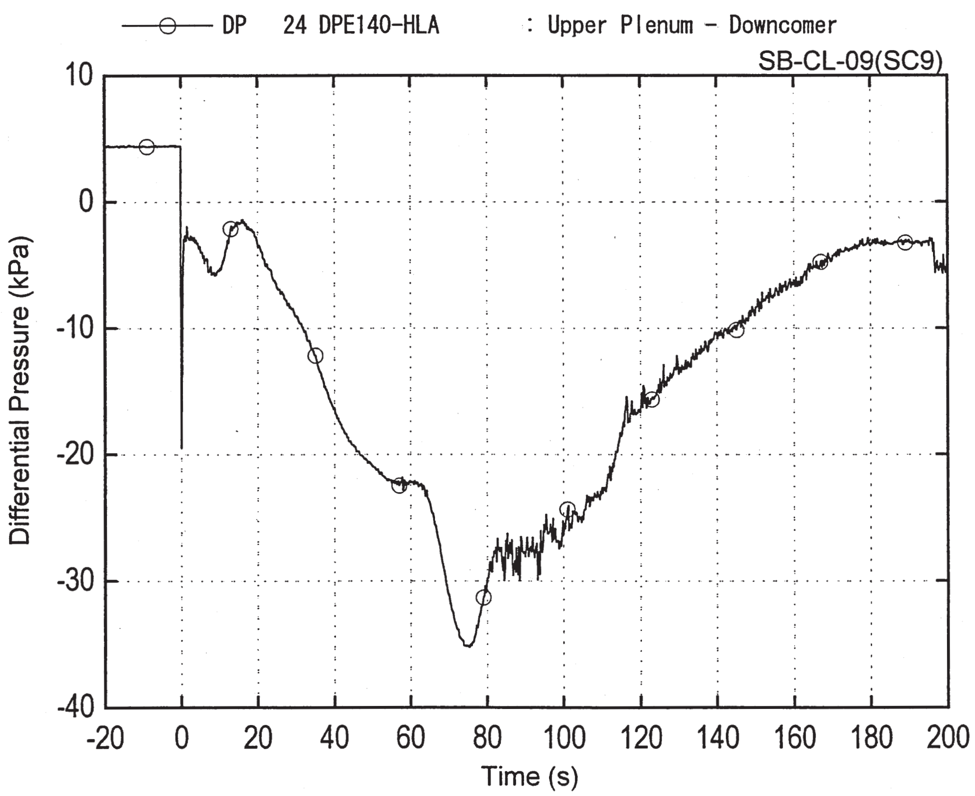

Fig.4.4-9 Differential pressure between upper plenum and downcomer during blowdown in SB-CL-09 test

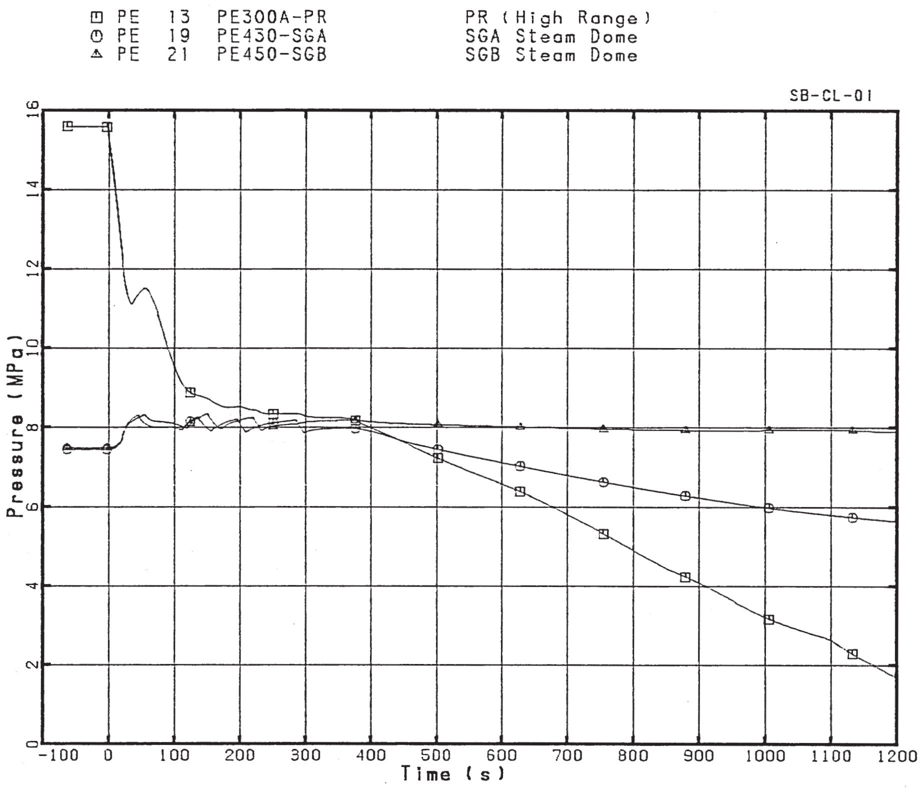

Fig.4.5-1 Primary and secondary pressures in LSTF 2.5% cold leg break test (SB-CL-01)

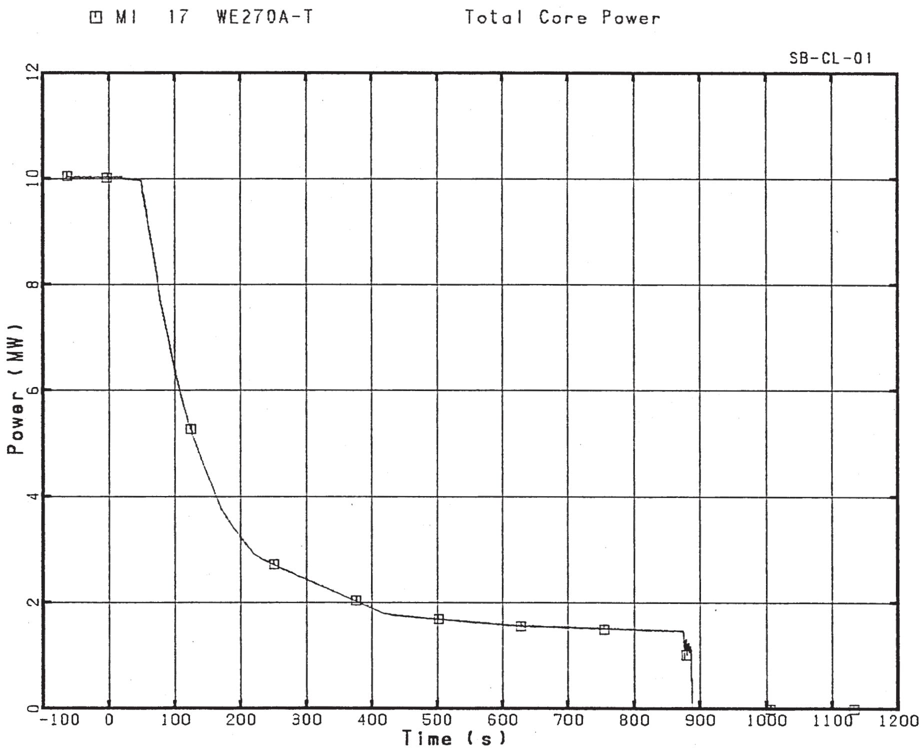

Fig.4.5-2 Core power decay curve in SB-CL-01 test

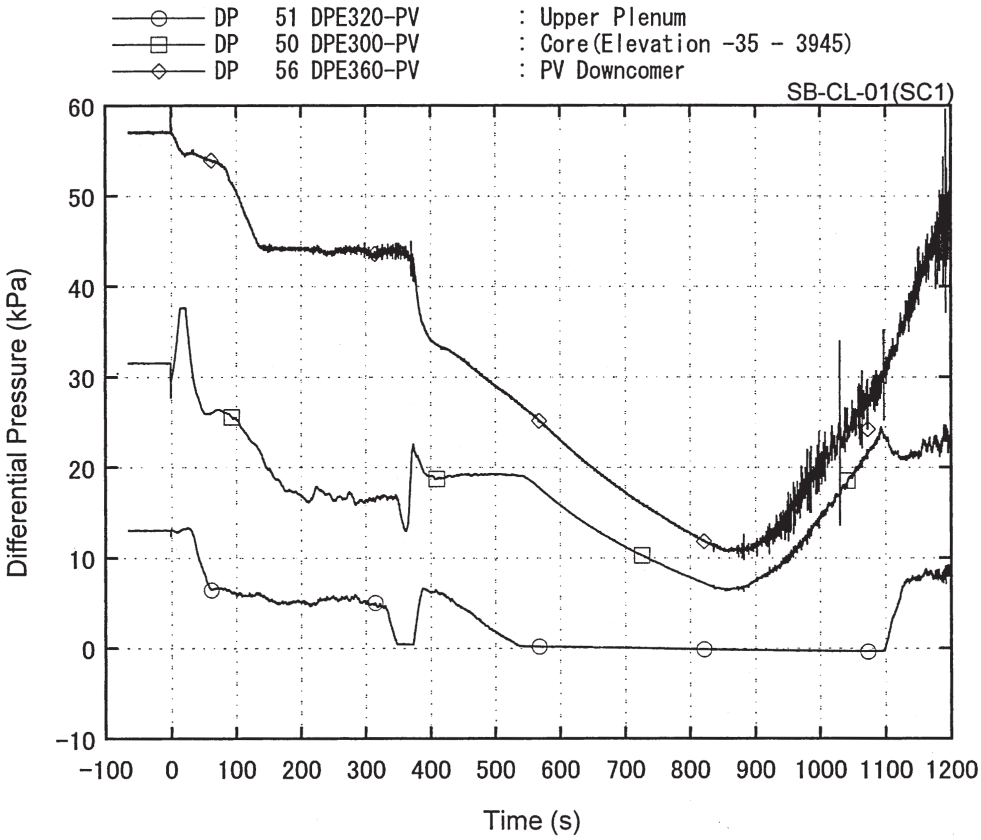

Fig.4.5-3 Differential pressures in core, UP and downcomer in SB-CL-01 test

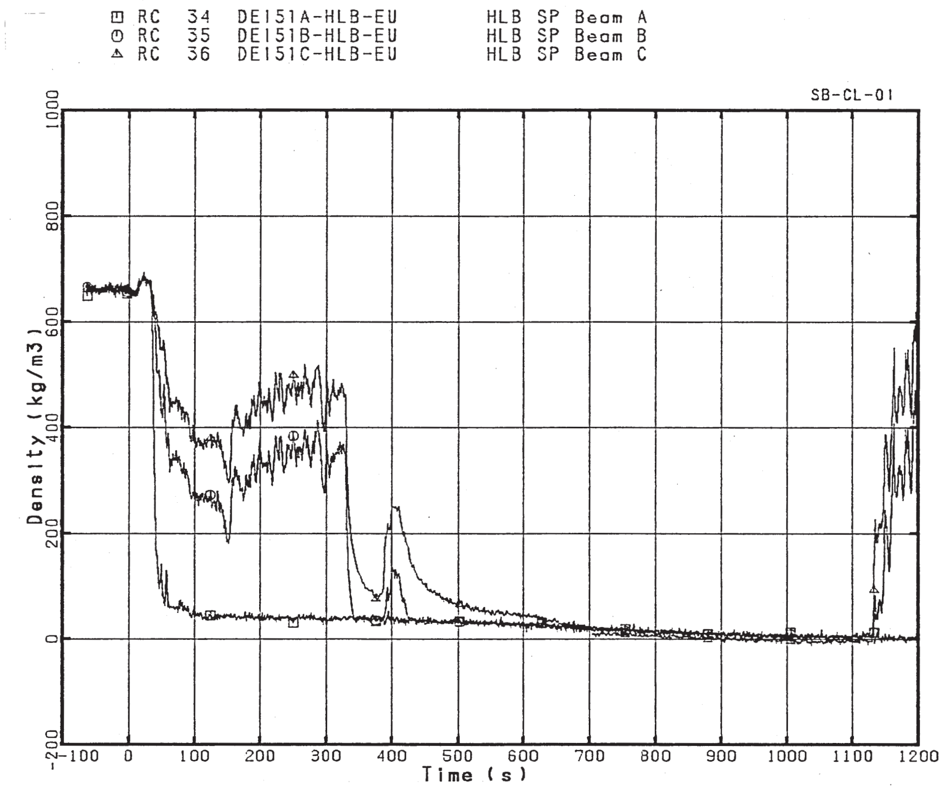

Fig.4.5-4 Fluid density data in broken loop hot leg (HL-B) in SB-CL-01 test

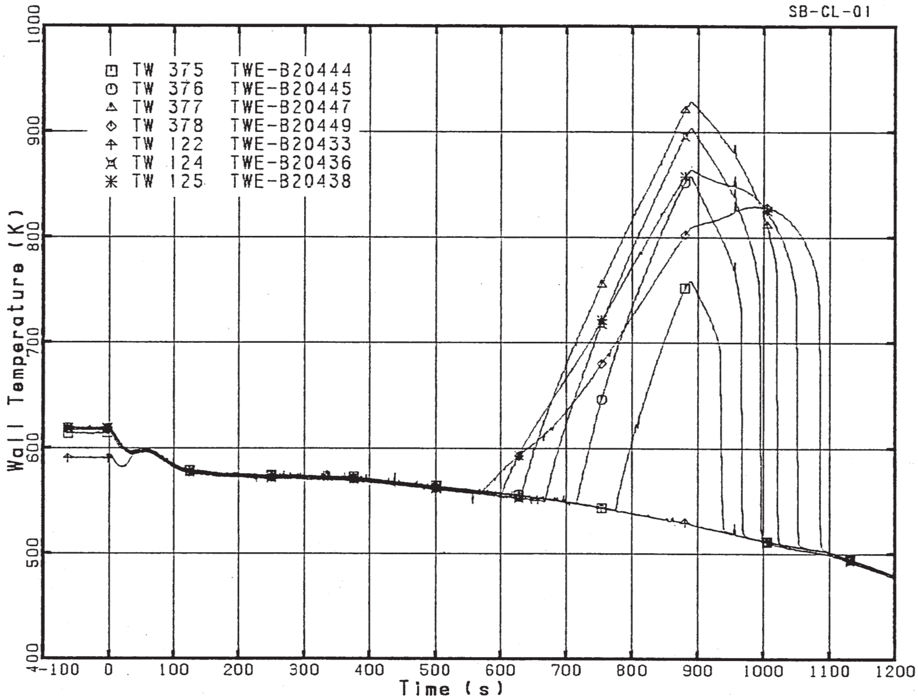

Fig.4.5-5 Representative heater rod surface temperatures in SB-CL-01 test

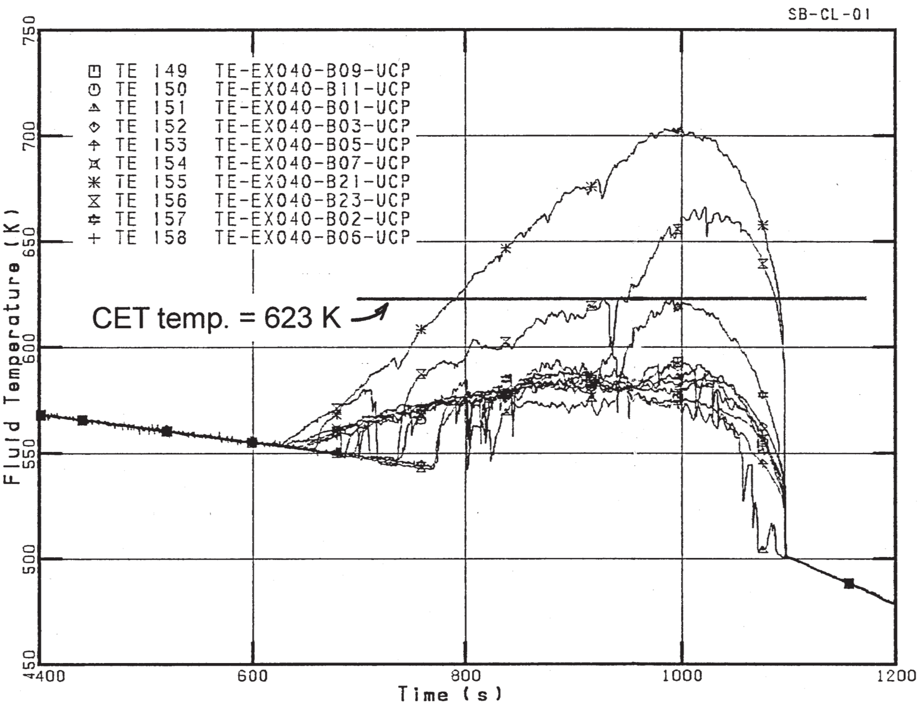

(1) CET temperatures above peripheral and central rod bundles

Fig.4.5-6 CET temperatures during boil-off process in SB-CL-01 test

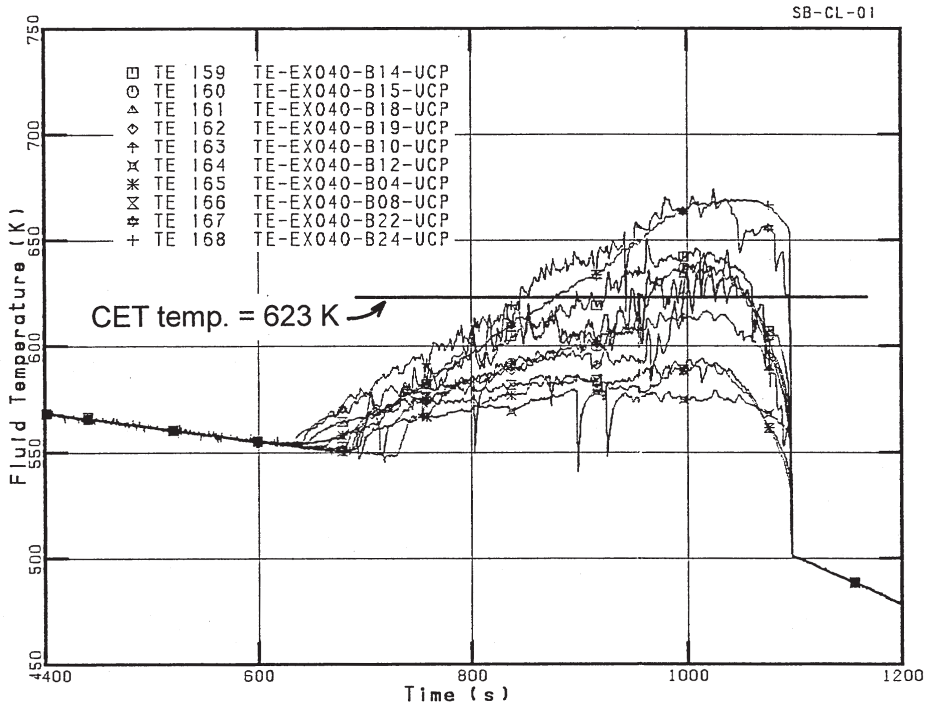

(2) CET temperatures above high-power and other rod bundles

Fig.4.5-6 CET temperatures during boil-off process in SB-CL-01 test

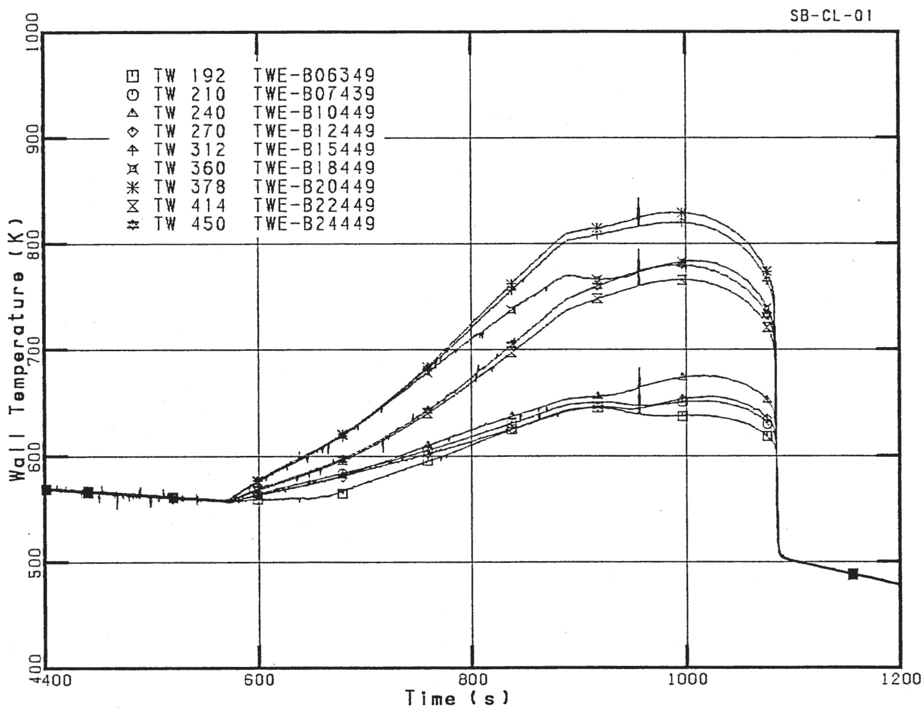

(1) Heater rod temperatures at Pos.9 (core top)

Fig.4.5-7 Heater rod temperatures in SB-CL-01 test

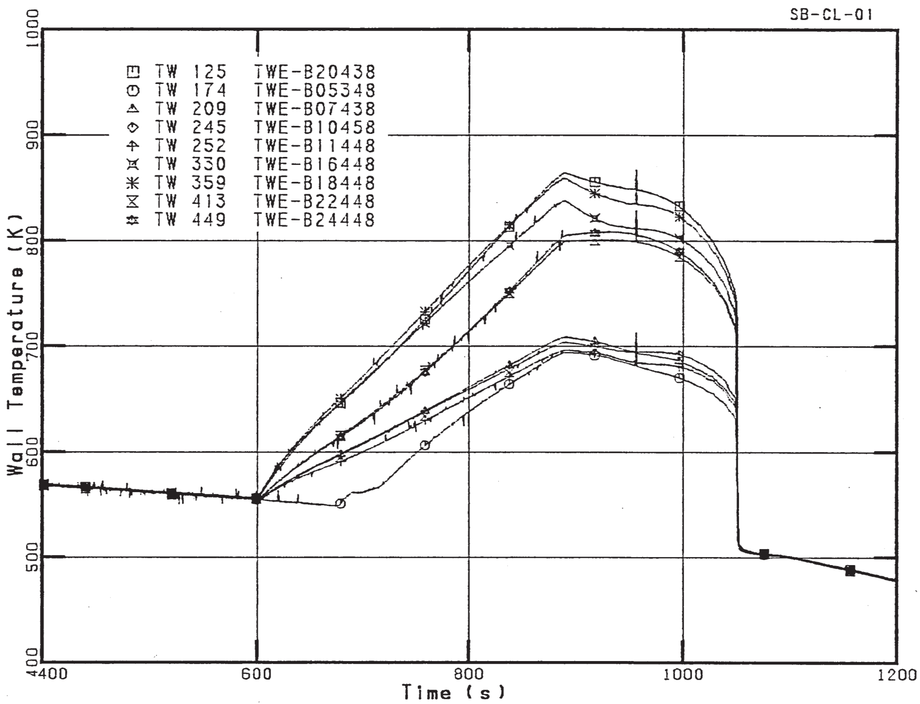

(2) Heater rod temperatures at Pos.8

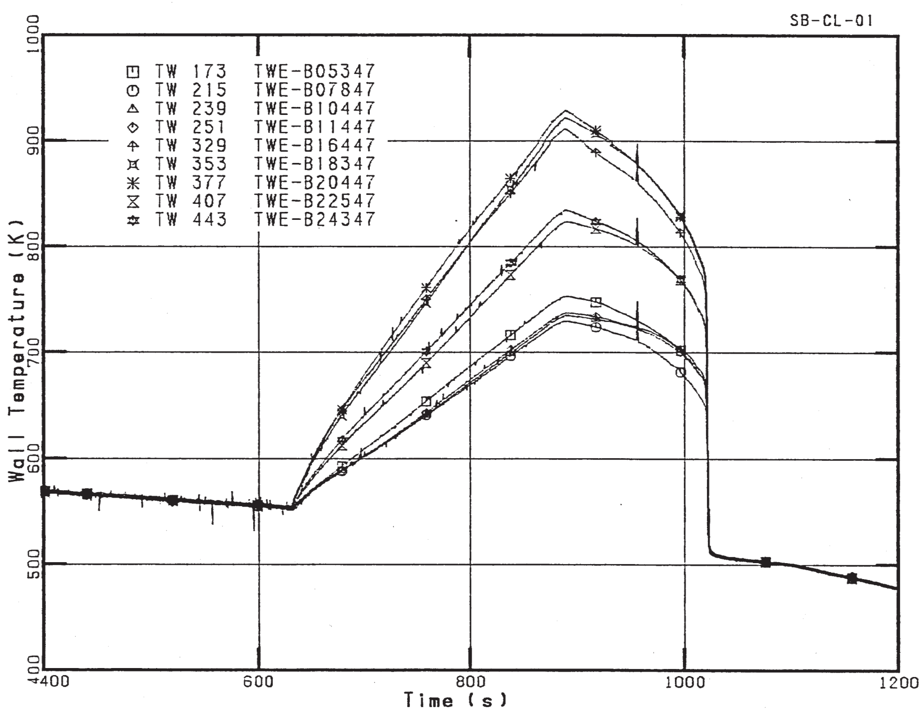

(3) Heater rod temperatures at Pos.7 with PCT measurement

Fig.4.5-7 Heater rod temperatures in SB-CL-01 test

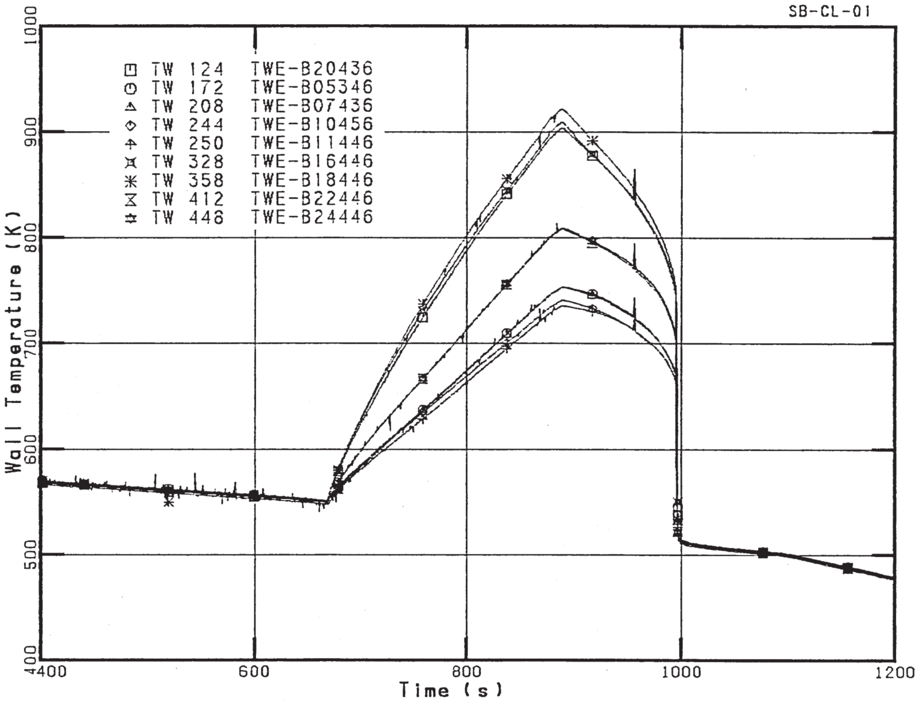

(4) Heater rod temperatures at Pos.6

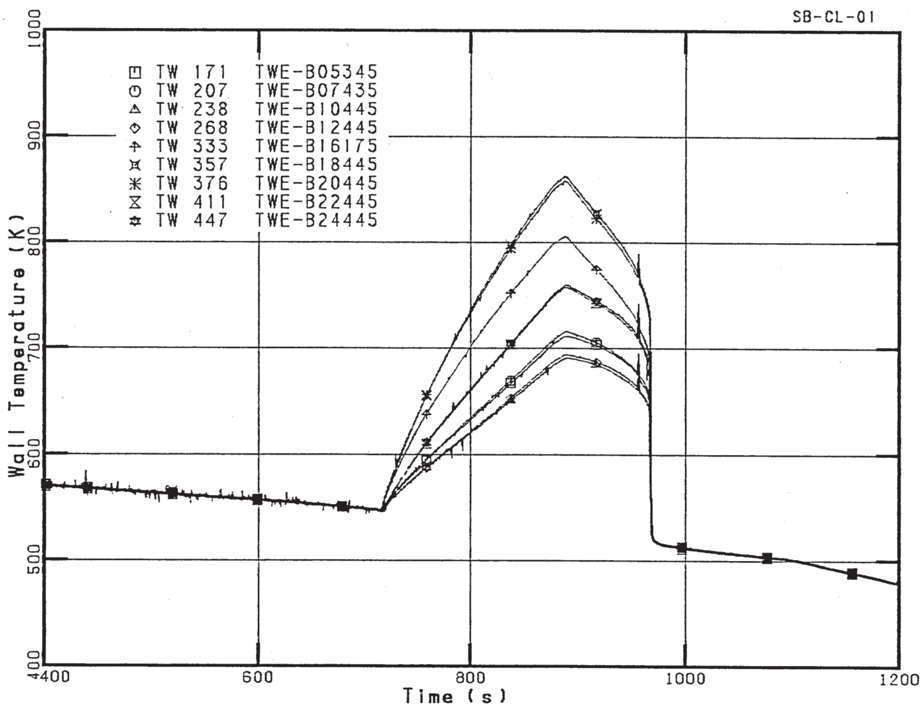

(5) Heater rod temperatures at Pos.5 (core middle height)

Fig.4.5-7 Heater rod temperatures in SB-CL-01 test

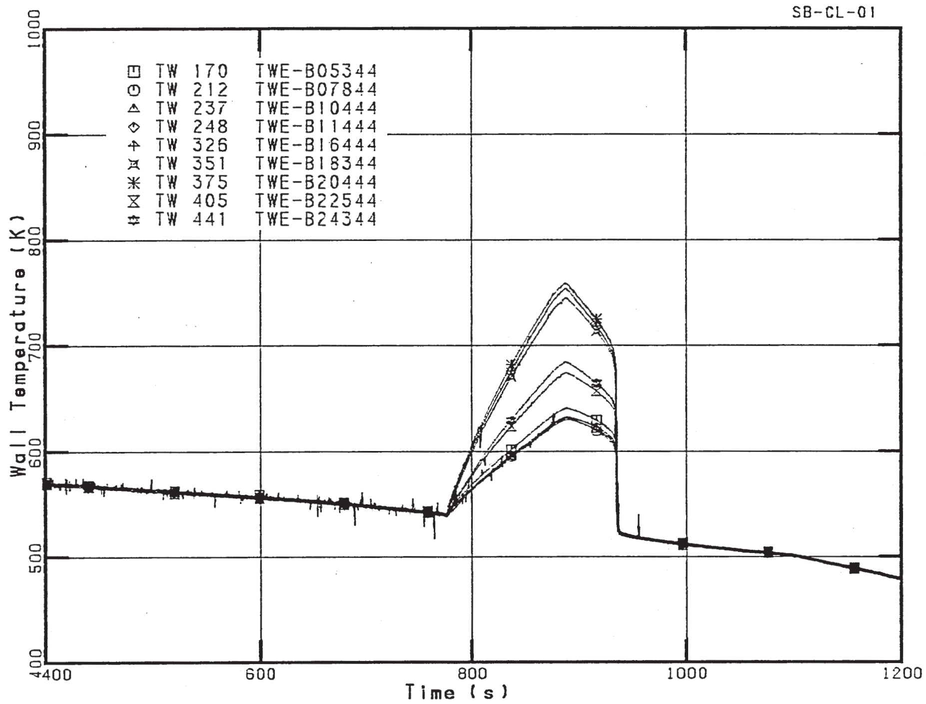

(6) Heater rod temperatures at Pos.4

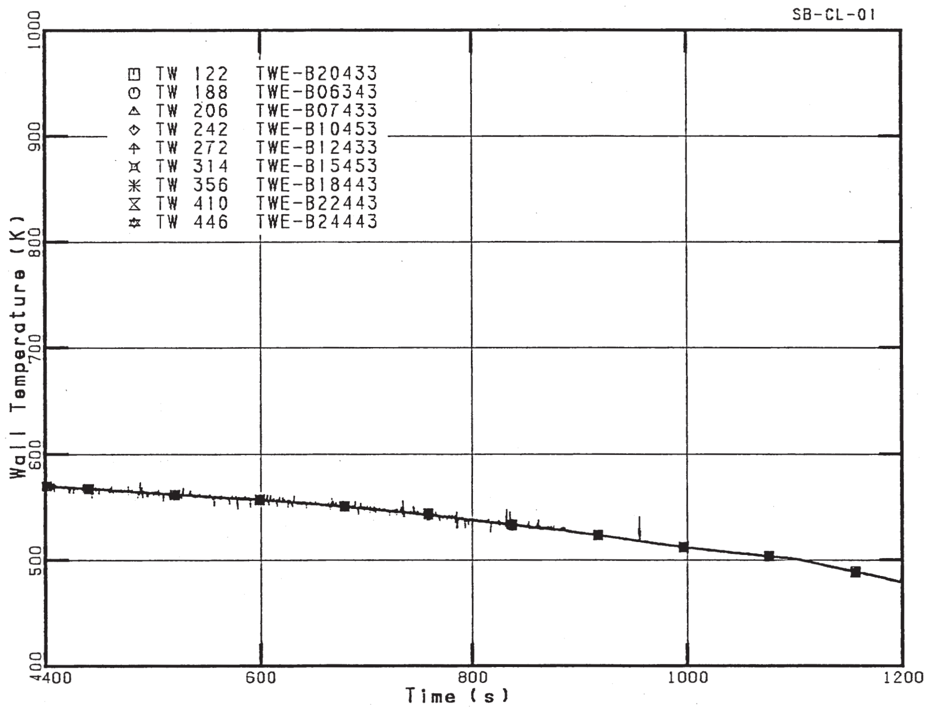

(7) Heater rod temperatures at Pos.3

Fig.4.5-7 Heater rod temperatures in SB-CL-01 test

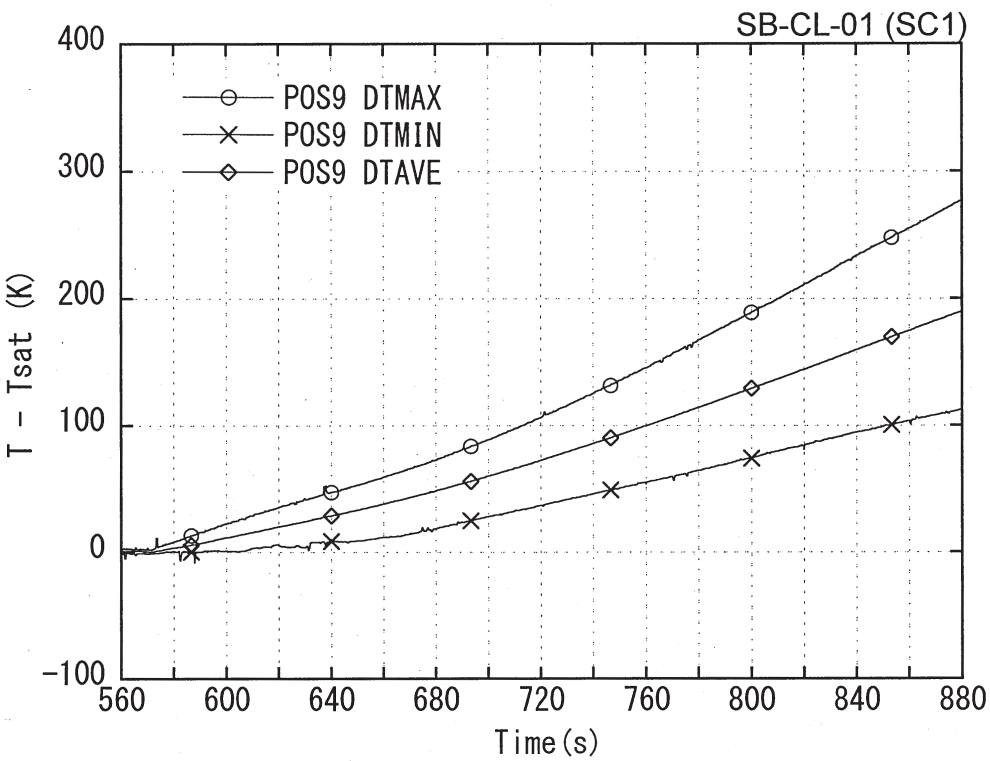

Fig.4.5-8 Distribution of heater rod temperature rises at Pos.9 in SB-CL-01 test (DT_{MAX}, DT_{MIN}, DT_{AVE})

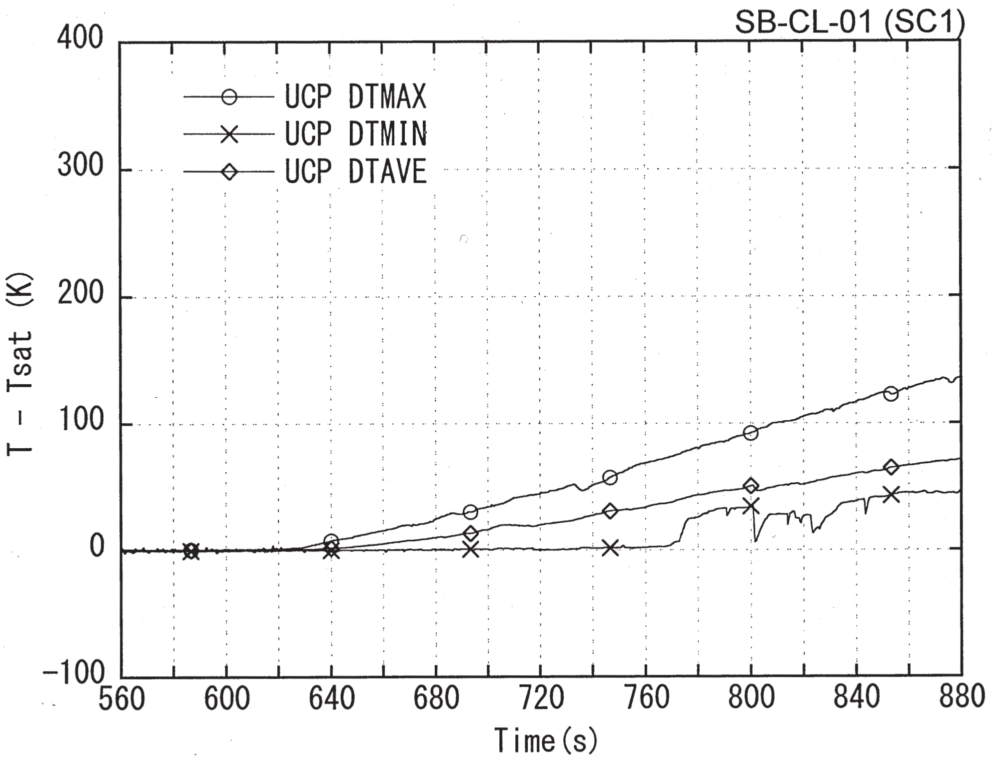

Fig.4.5-9 Distribution of all CET temperature rises above saturation temperature in SB-CL-01 test (DT_{MAX}, DT_{MIN}, DT_{AVE})

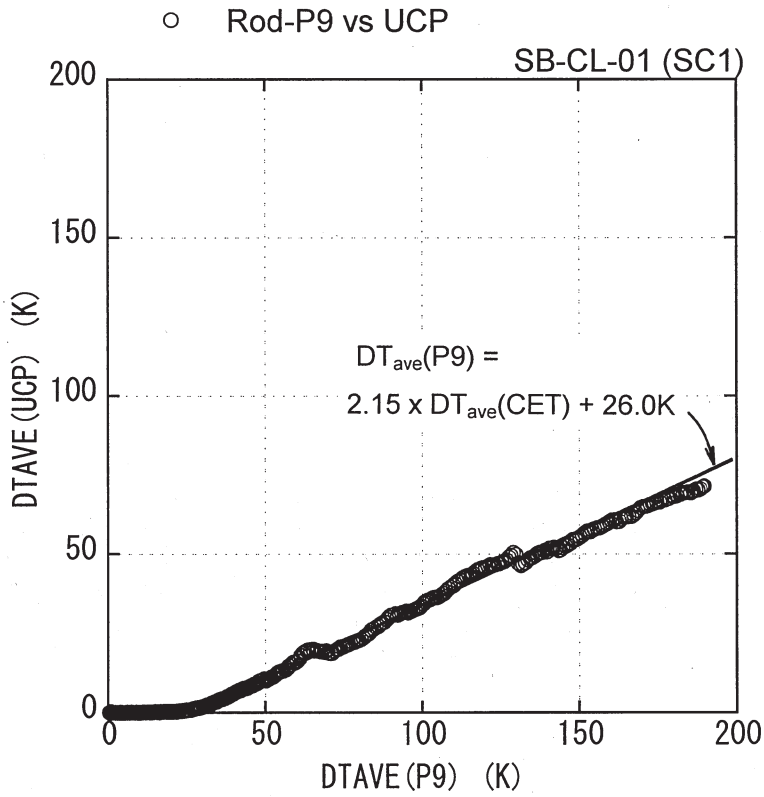

Fig.4.5-10 A relation of temperature rises at heater rod Pos.9, (Ave) and CET (Ave) in SB-CL-01 test (560 - 880 s)

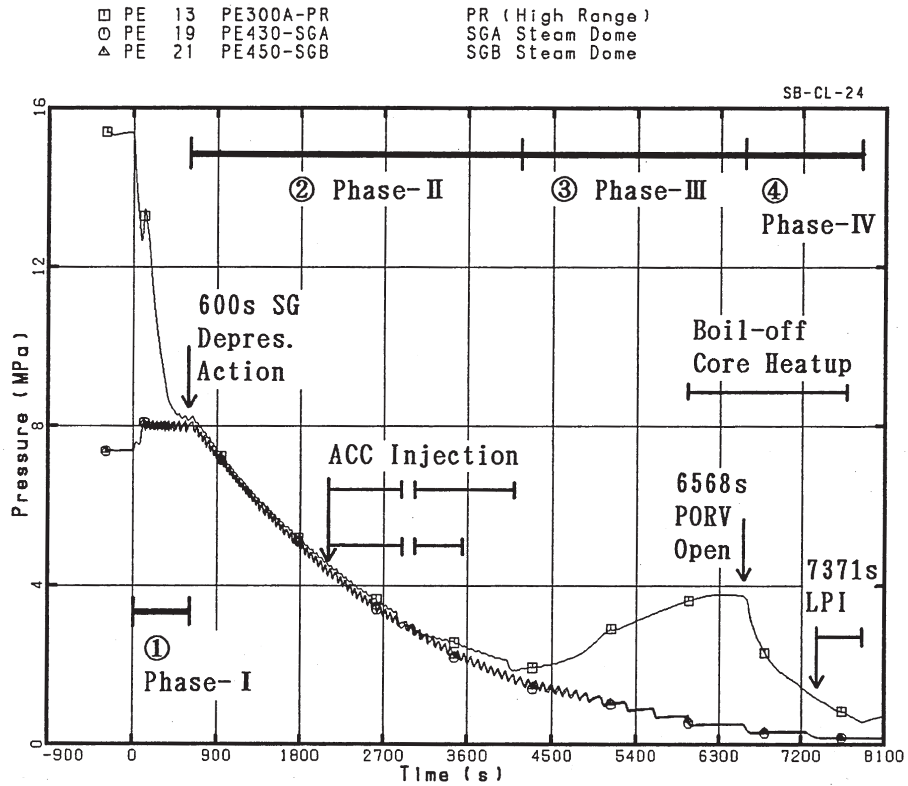

Fig.4.6-1 Primary and secondary pressures in LSTF 0.5% cold leg break test (SB-CL-24)

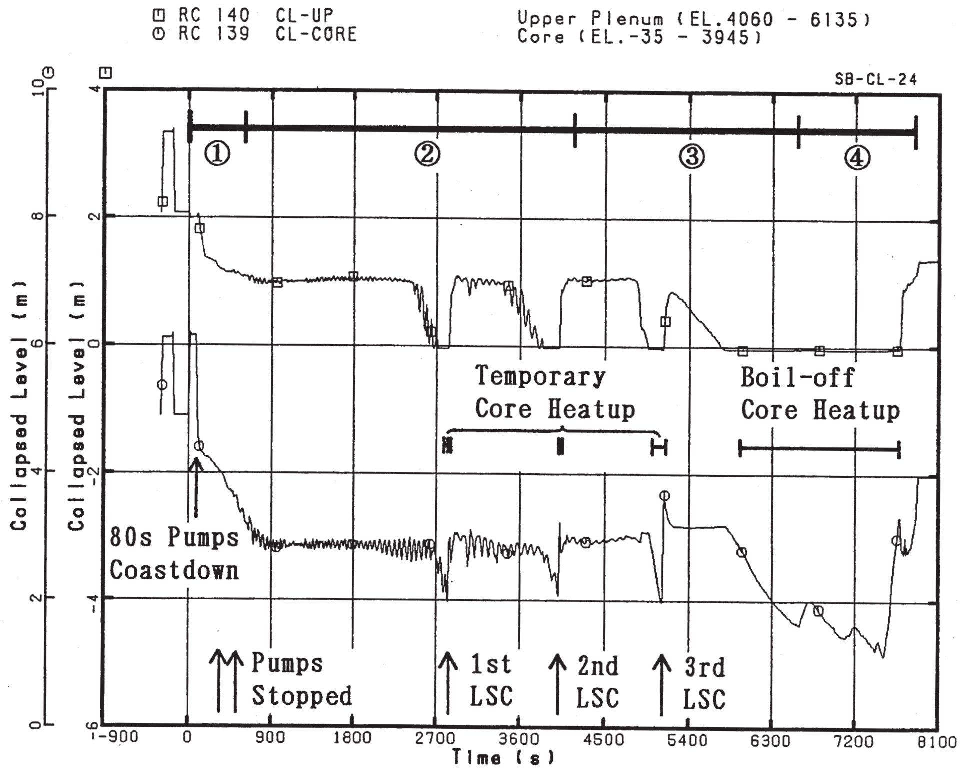

Fig.4.6-2 PV collapsed liquid levels in SB-CL-24 test

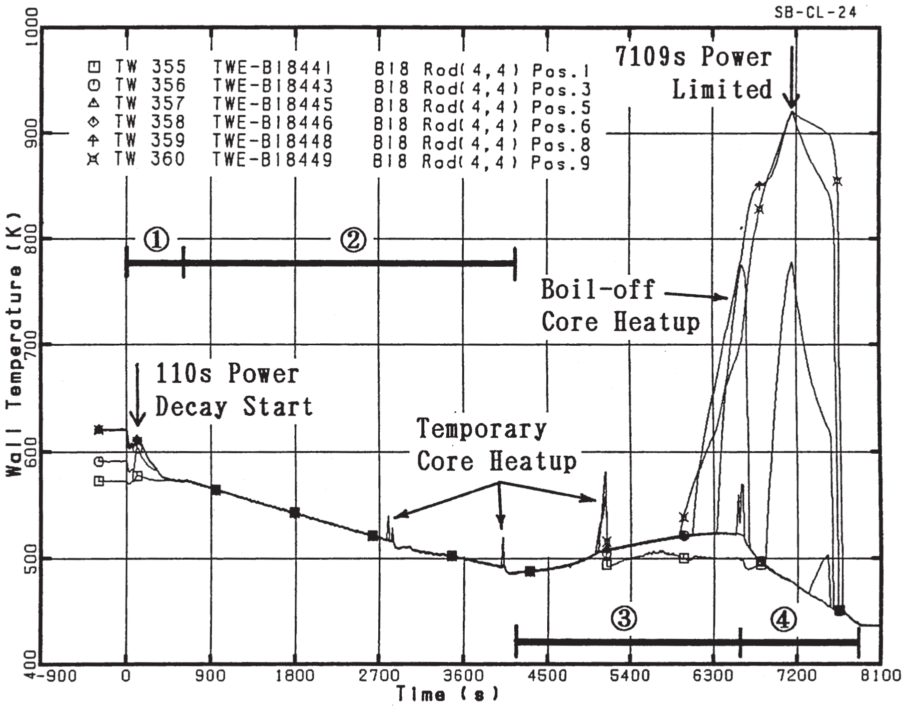

Fig.4.6-3 Representative heater rod surface temperatures in high-power bundle (B18) in SB-CL-24 test

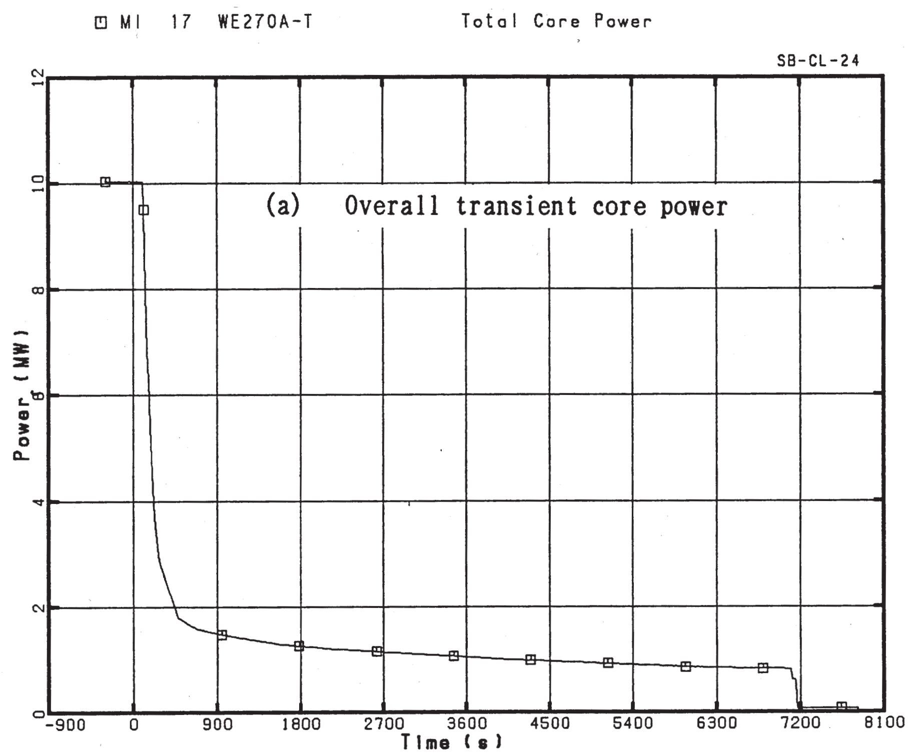

Fig.4.6-4 Core power decay curve in SB-CL-24 test

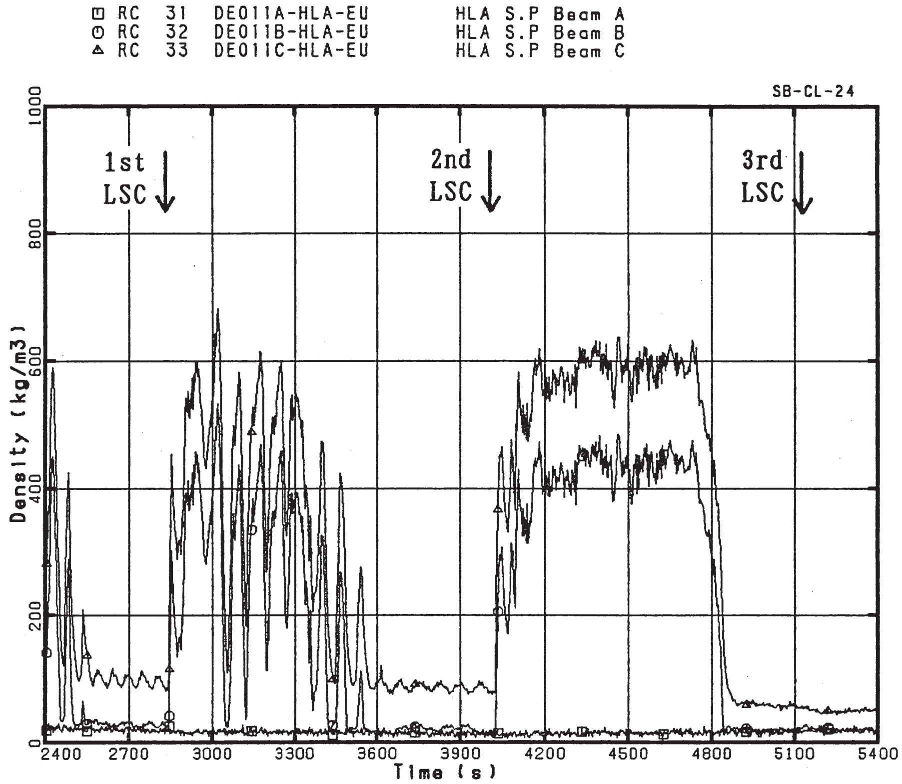

Fig.4.6-5 Fluid density data in HL-A during loop-seal clearing process in SB-CL-24 test

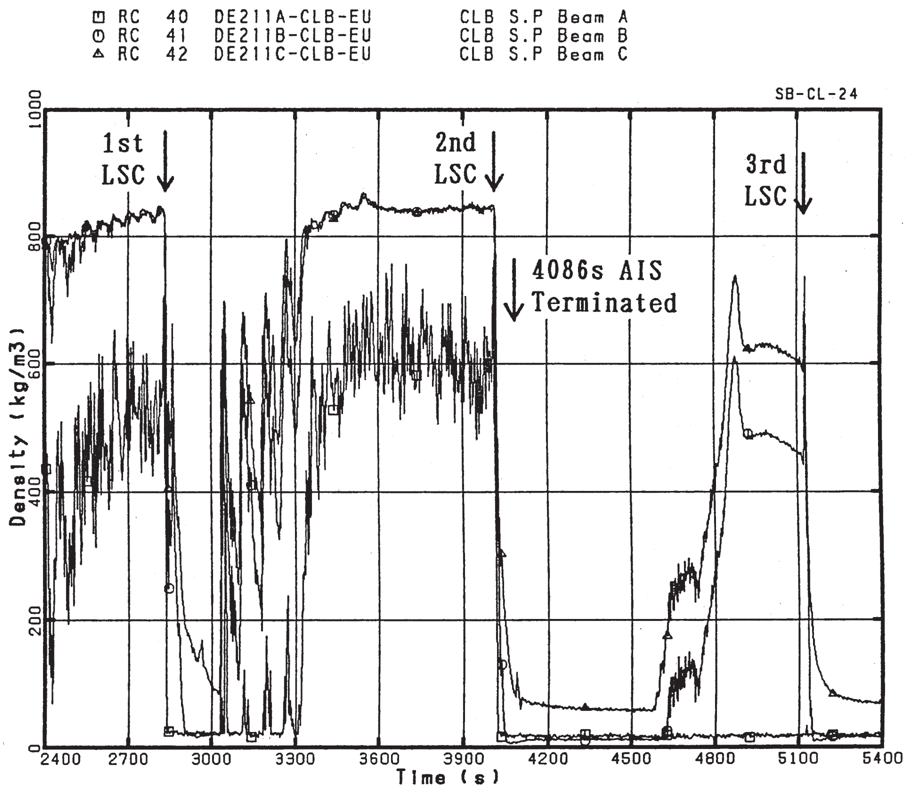

Fig.4.6-6 Fluid density data in CL-A during loop-seal clearing process in SB-CL-24 test

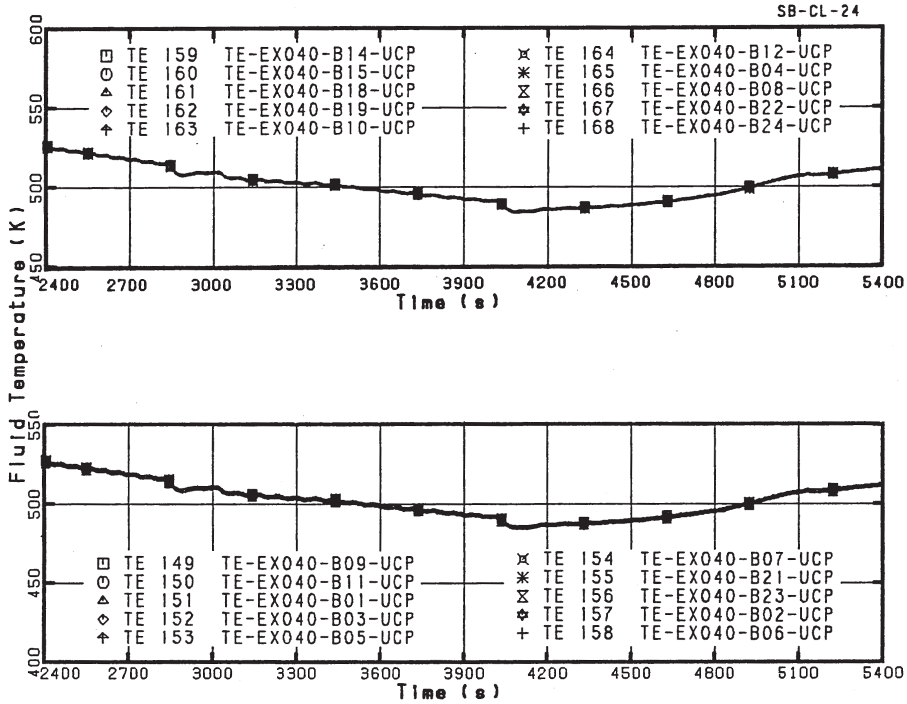

Fig.4.6-7 CET temperatures during loop-seal clearing process in SB-CL-24 test

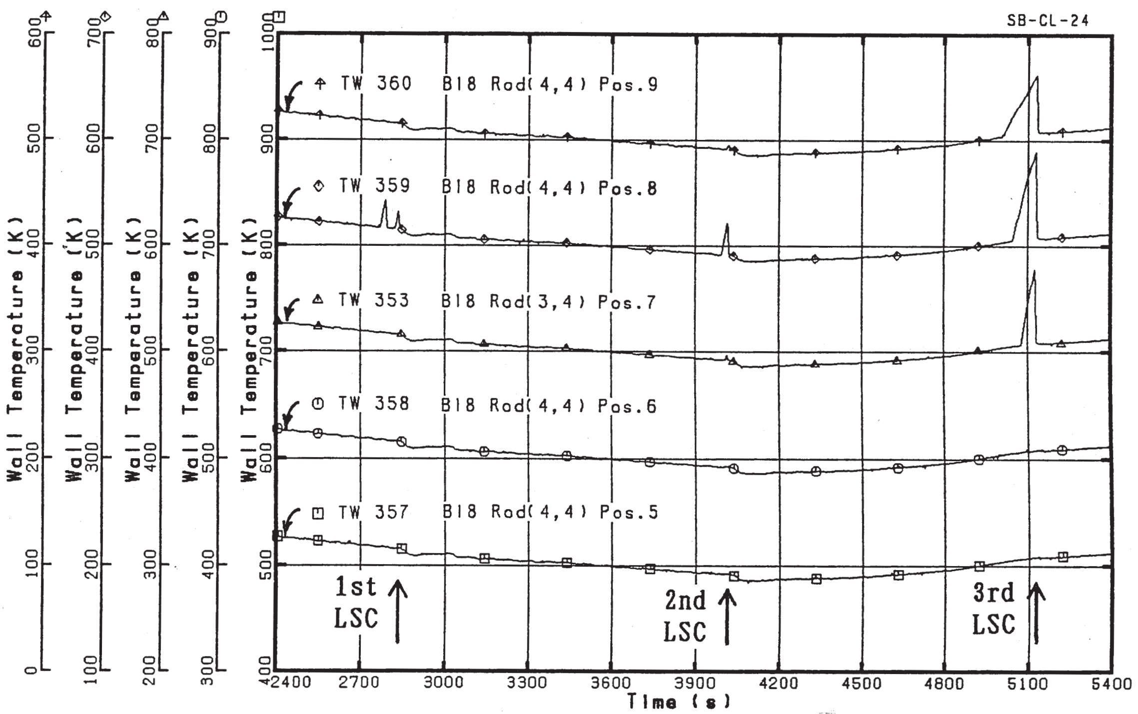

Fig.4.6-8 Heater rod surface temperatures in B18 bundle during loop-seal clearing in SB-CL-24 test

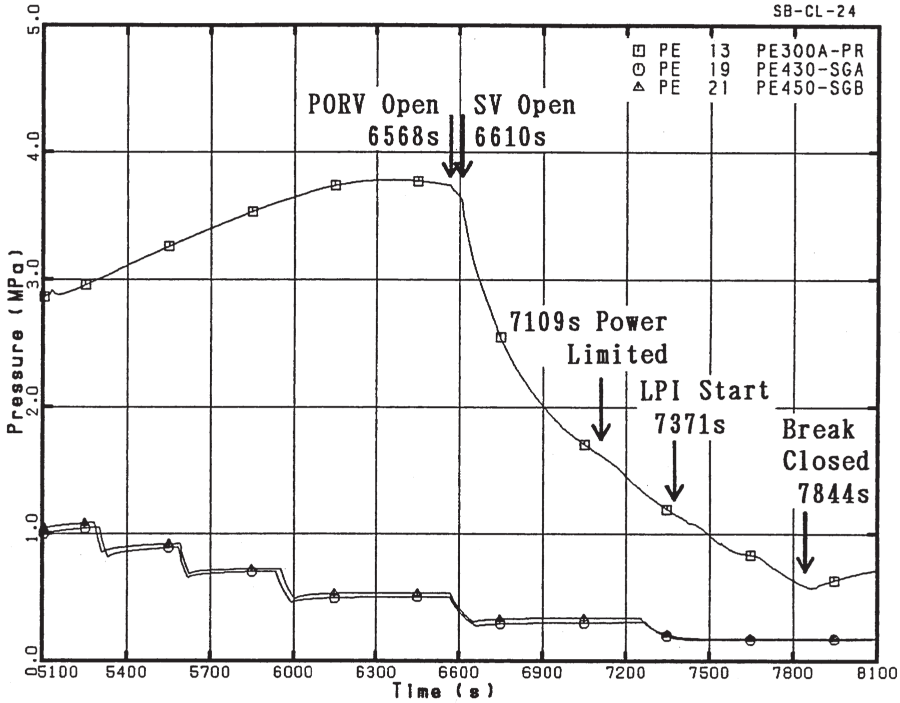

Fig.4.6-9　Pressures in detail during boil-off process in SB-CL-24 test

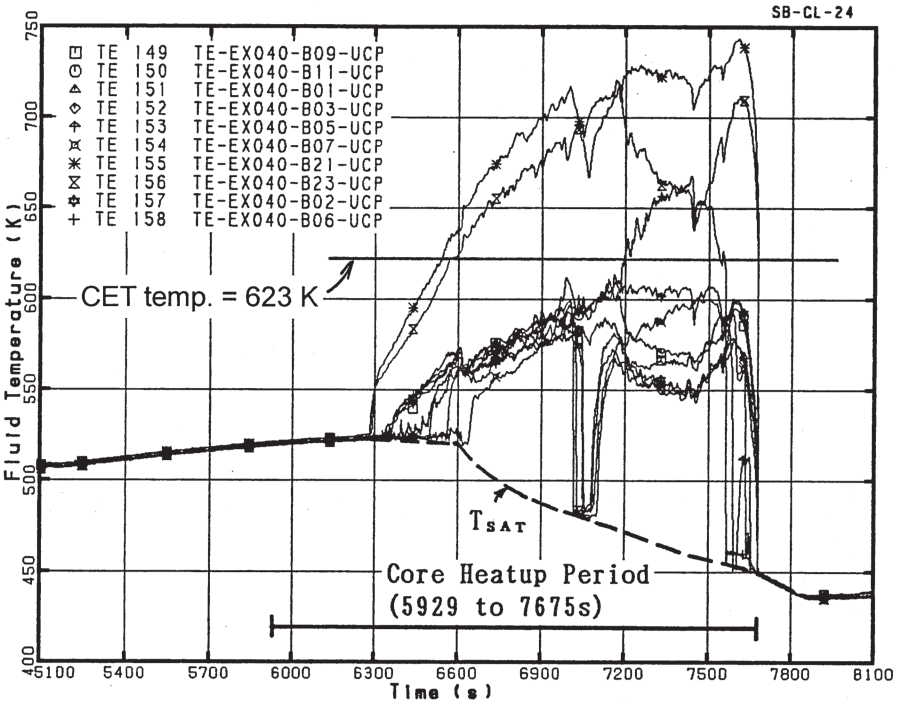

(1)　CET temperatures above peripheral and central rod bundles

Fig.4.6-10　CET temperatures during boil-off process in SB-CL-24 test

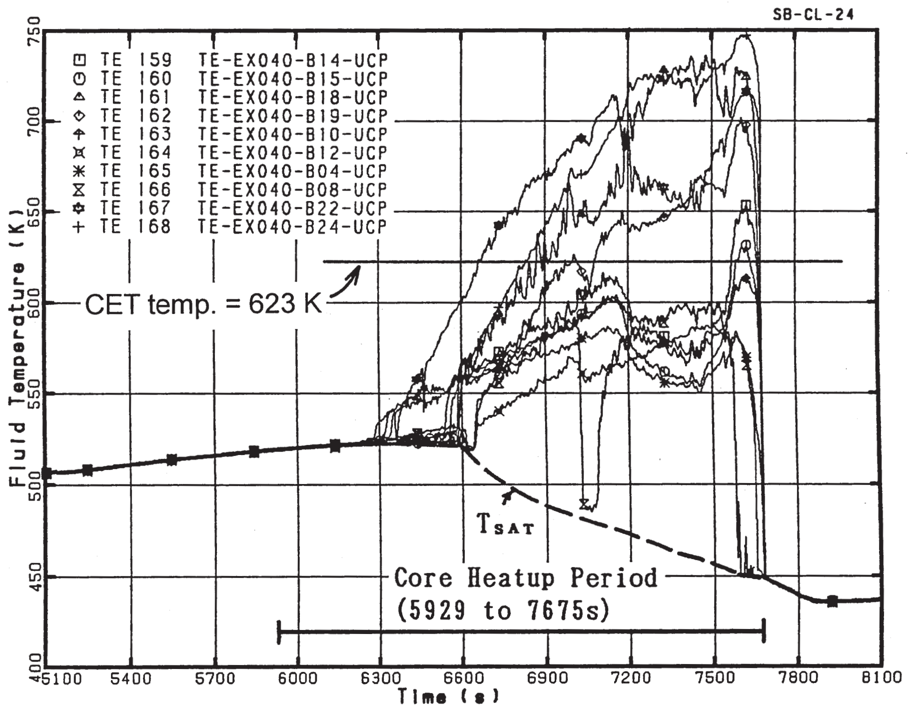

(2) CET temperatures above high-power and other rod bundles

Fig.4.6-10 CET temperatures during boil-off process in SB-CL-24 test

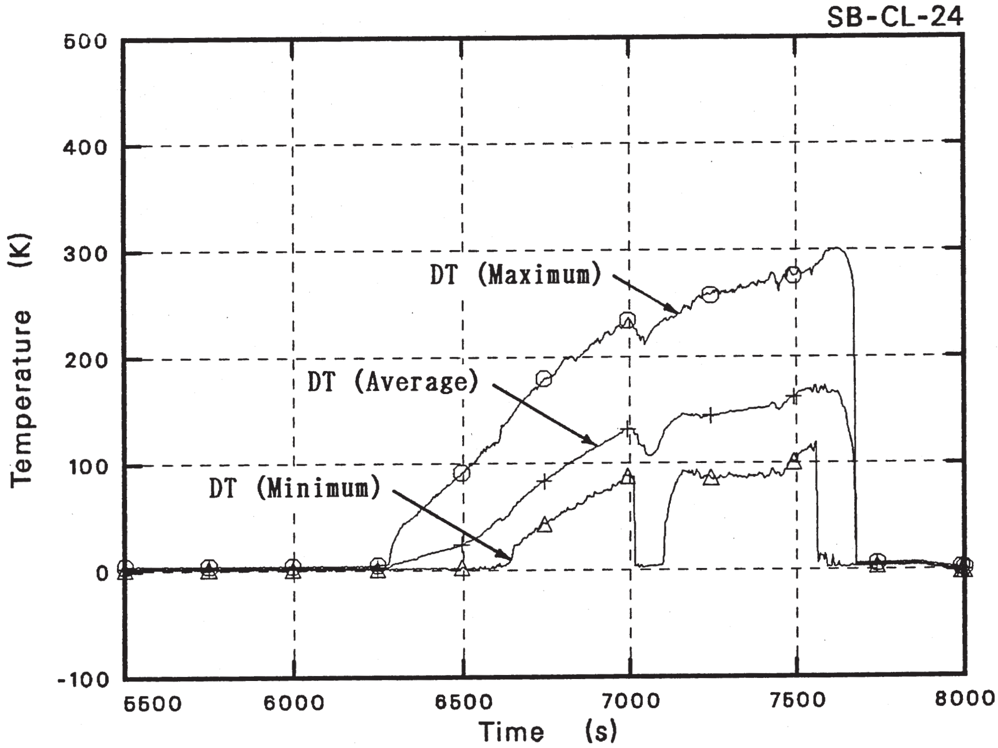

Fig.4.6-11 Distribution of all CET temperature rises above saturation temperature in SB-CL-24 test (DT_{MAX}, DT_{MIN}, DT_{AVE})

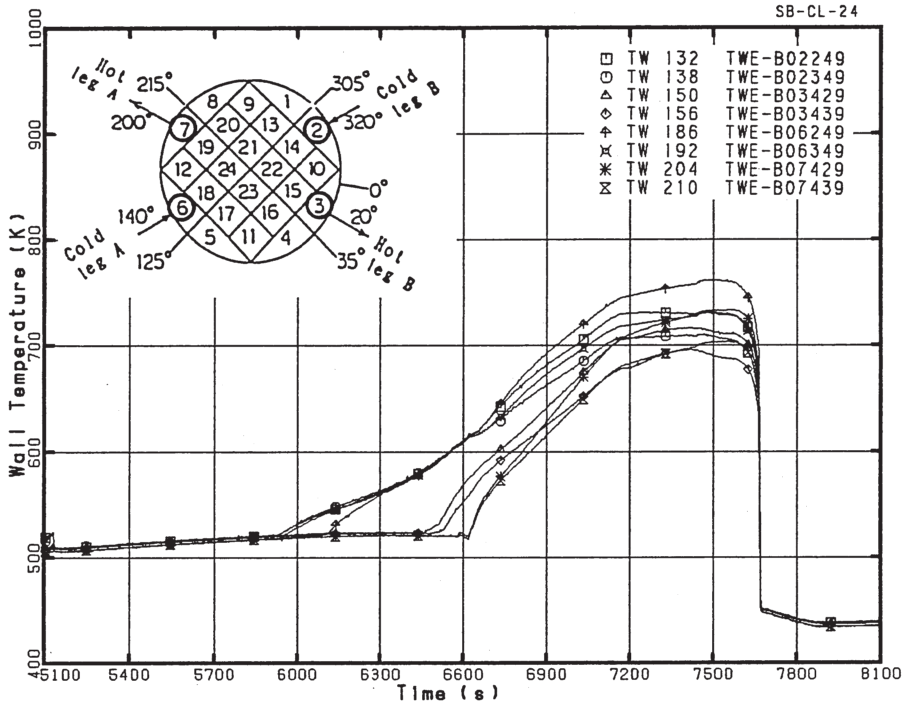

(1) Pos.9 in peripheral bundles

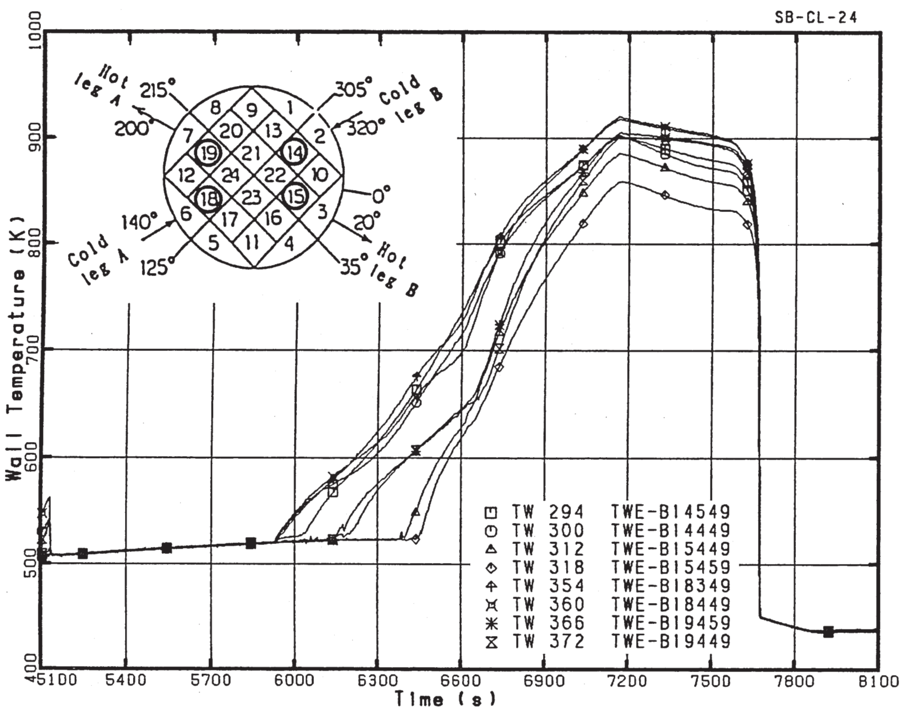

(2) Pos.9 in high-power bundles

Fig.4.6-12 Heater rod surface temperatures at Pos.9 in SB-CL-24 test

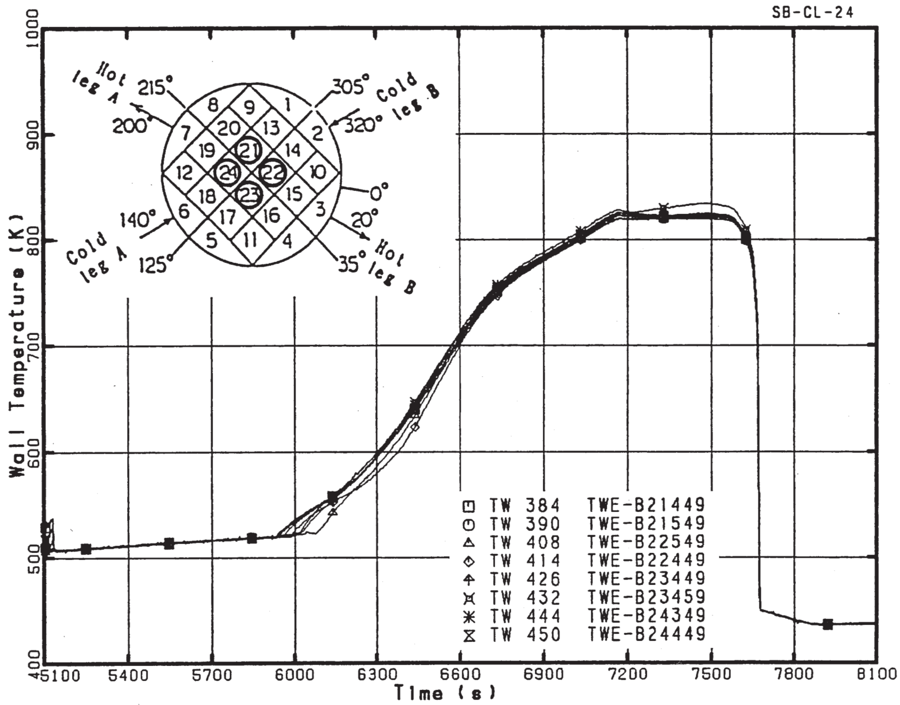

(3) Pos.9 in central bundles

Fig.4.6-12 Heater rod surface temperatures at Pos.9 in SB-CL-24 test

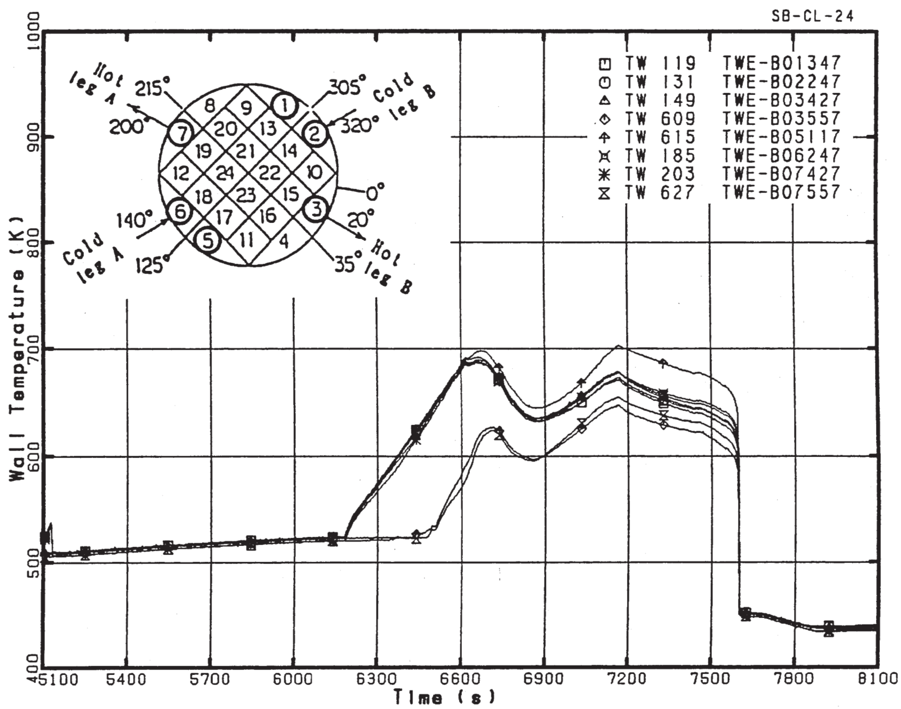

Fig.4.6-13 Heater rod surface temperatures at Pos.7 in peripheral bundles during SB-CL-24 test

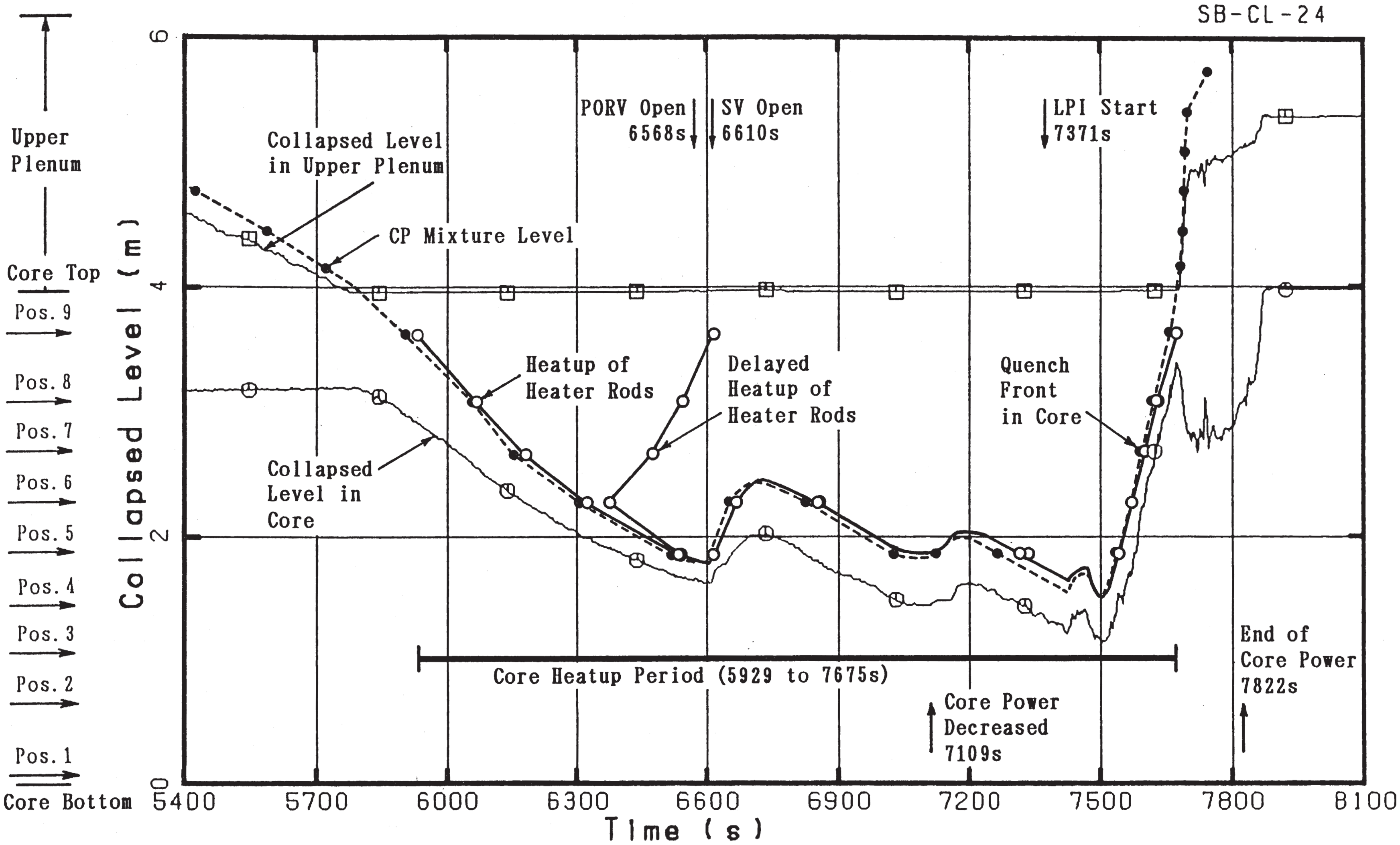

Fig.4.6-14 Core heat-up and quench behavior in SB-CL-24 test

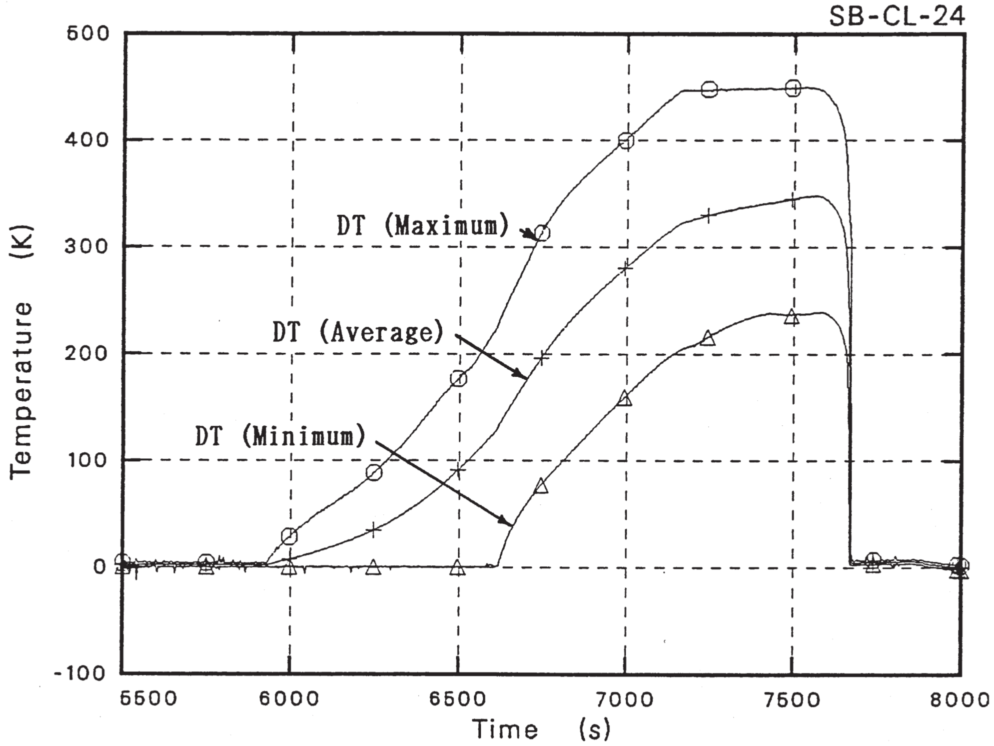

Fig.4.6-15 Distribution of heater rod temperature rises at Pos.9 in SB-CL-24 test

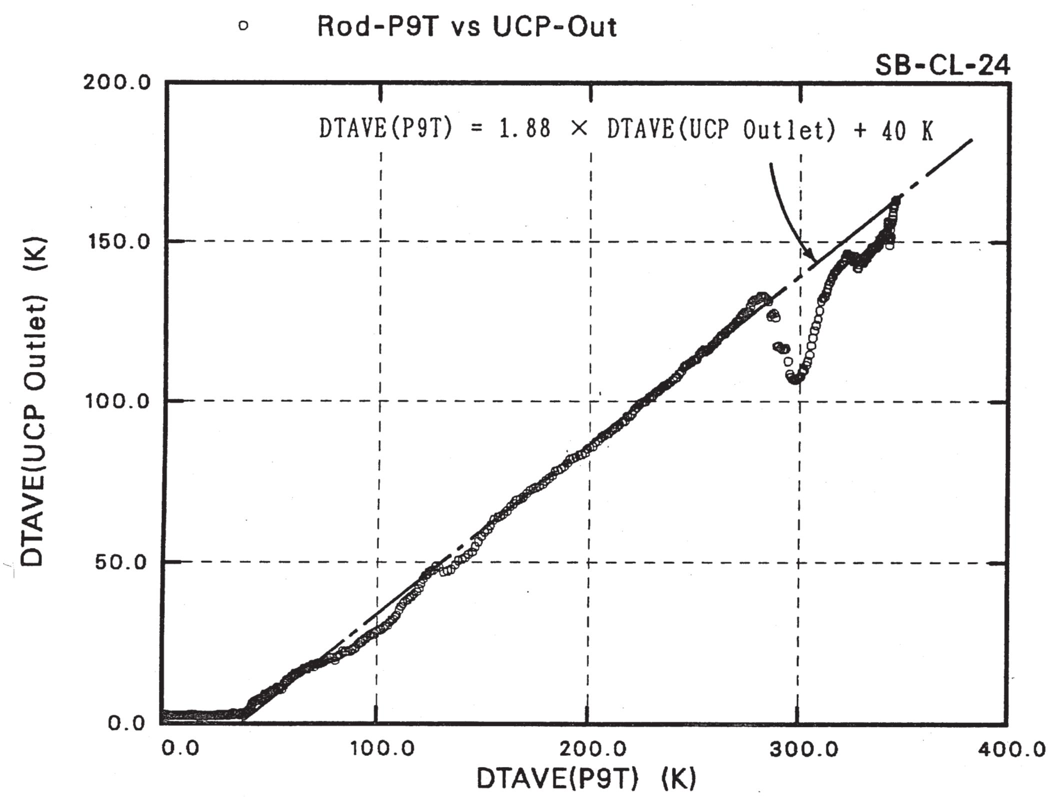

Fig.4.6-16 A relation of temperature rises at heater rod Pos.9, (Ave) and CET (Ave) in SB-CL-24 test (5900 - 7500 s)

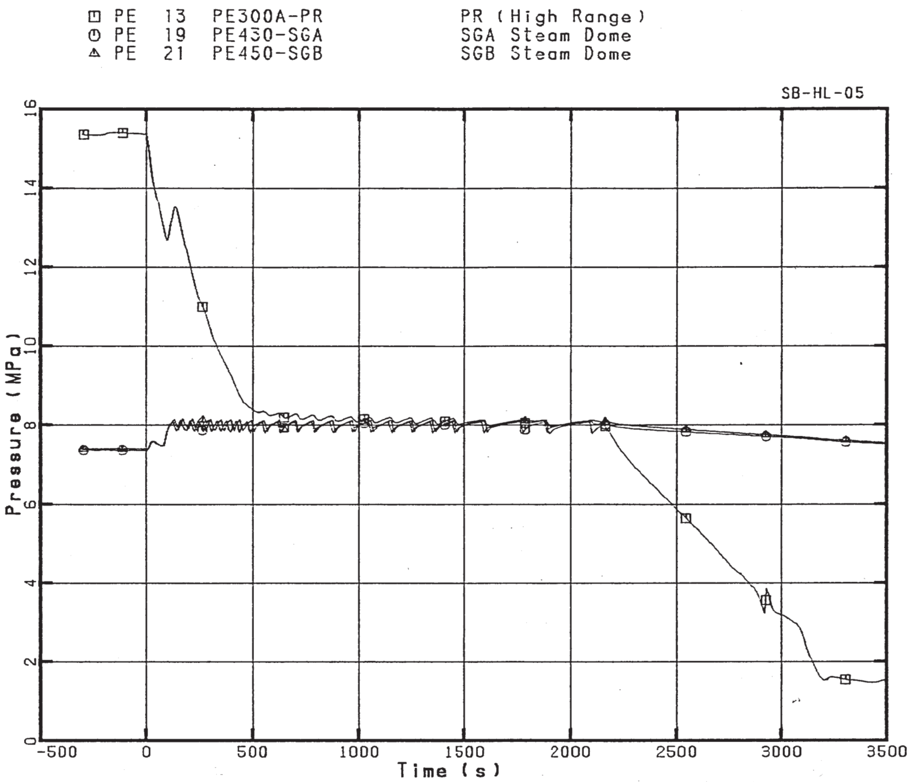

Fig.4.7-1 Primary and secondary pressures in LSTF 0.5% hot leg break test (SB-HL-05)

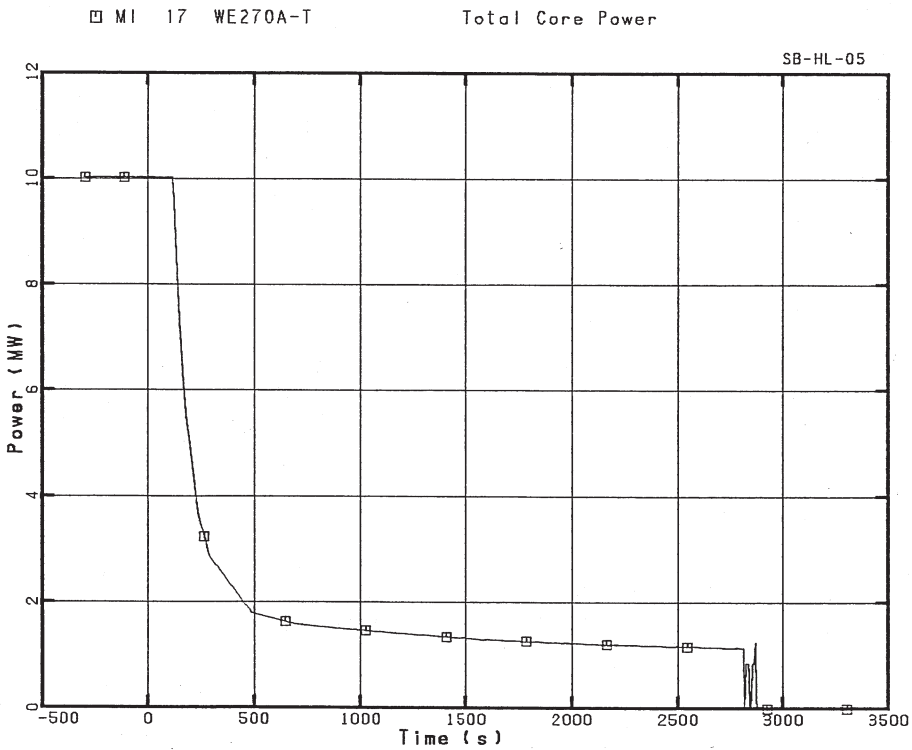

Fig.4.7-2 Core power decay curve in SB-HL-05 test

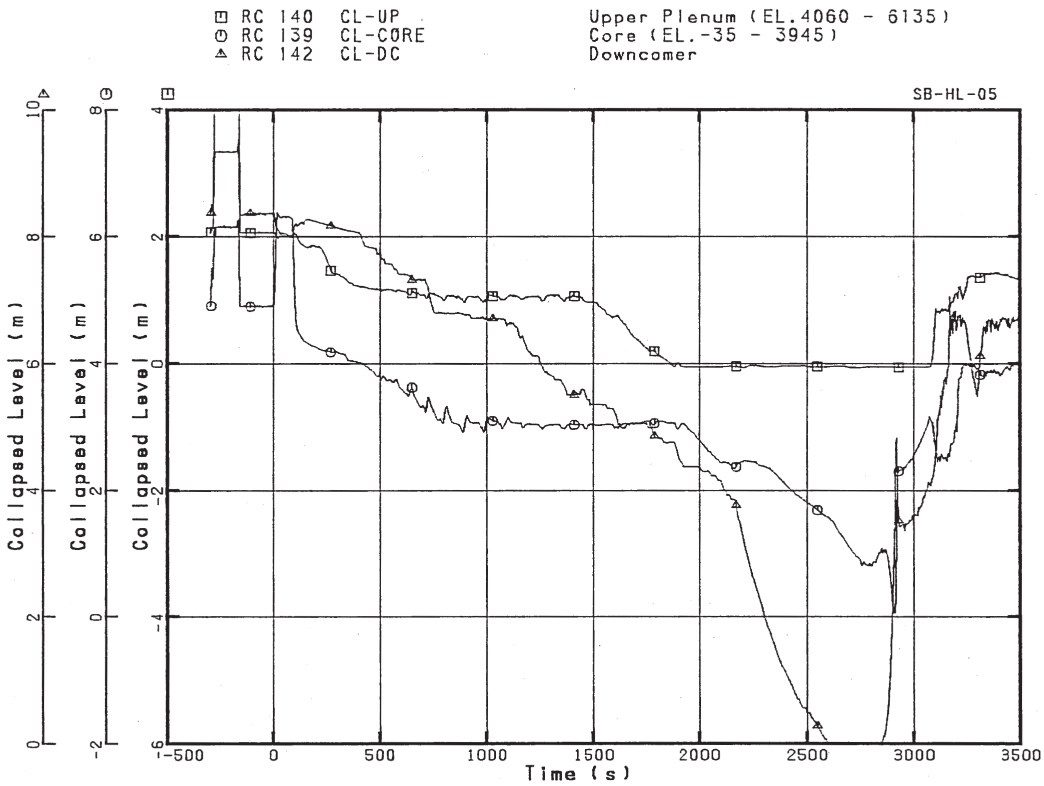

Fig.4.7-3 PV collapsed liquid levels in SB-HL-05 test

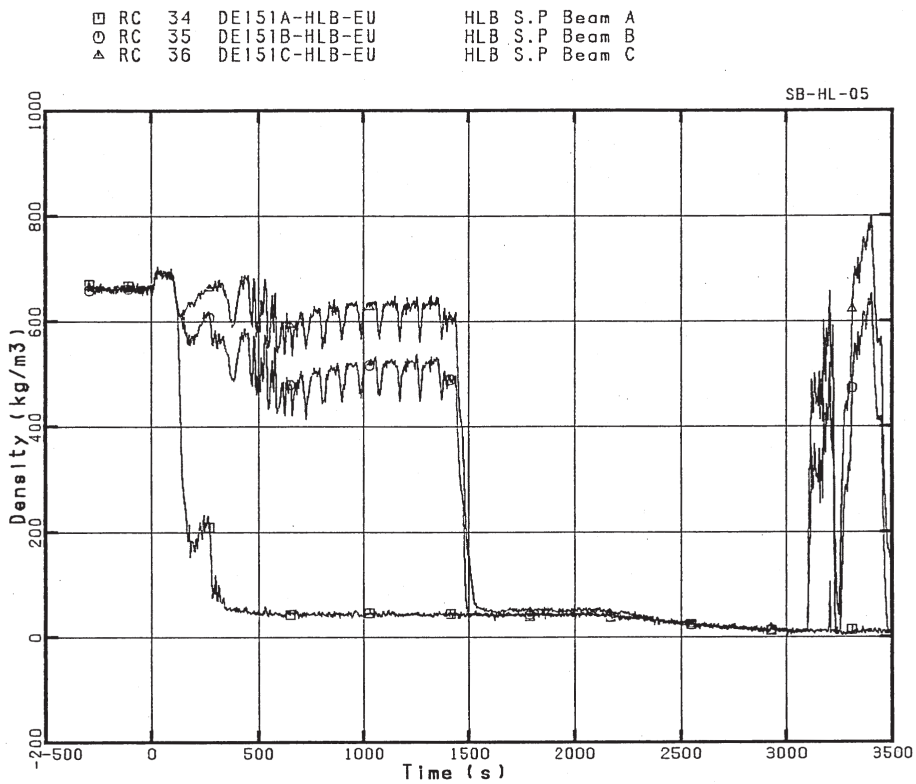

Fig.4.7-4 Fluid density data in broken loop hot leg (HL-B) in SB-HL-05 test

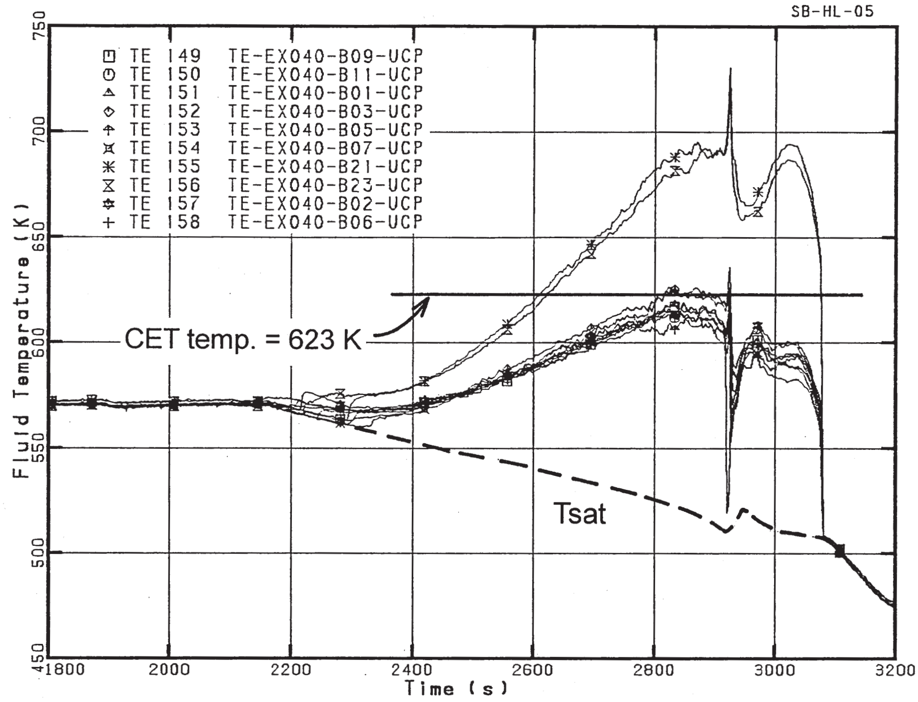

(1) CET temperatures above peripheral and central rod bundles

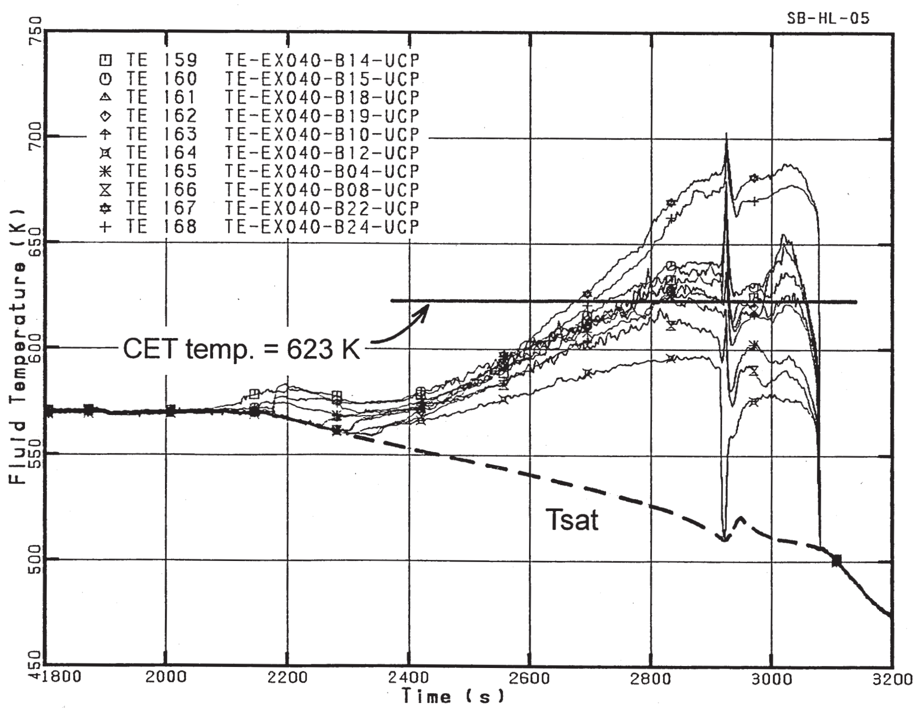

(2) CET temperatures above high-power and other rod bundles

Fig.4.7-5 CET temperatures during boil-off process in SB-HL-05 test

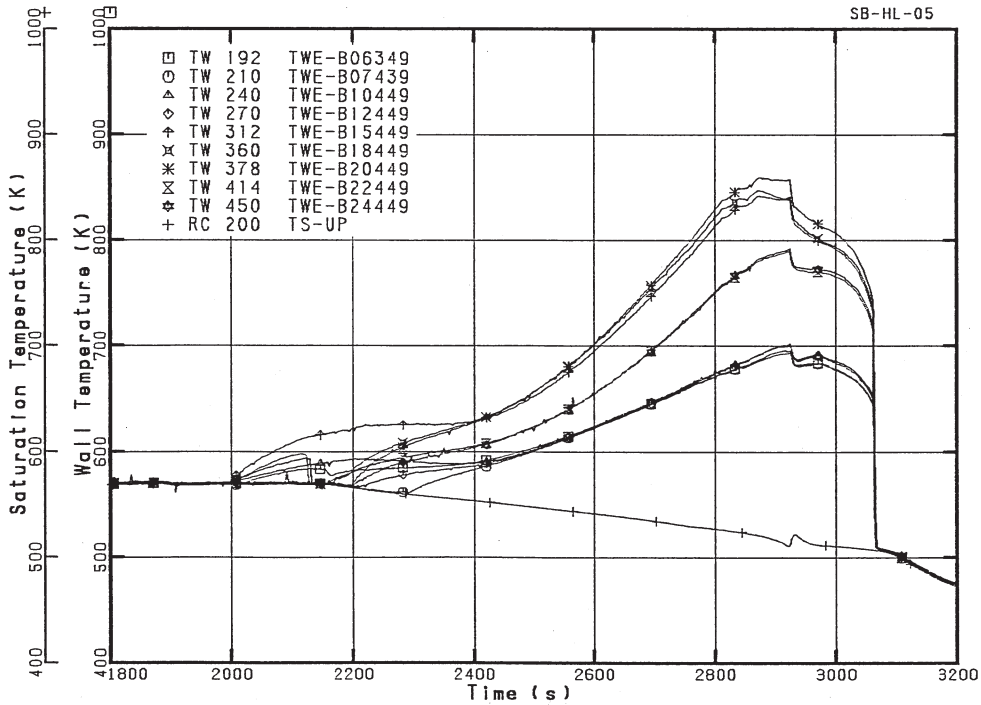

(1) Heater rod temperatures at Pos.9 (core top)

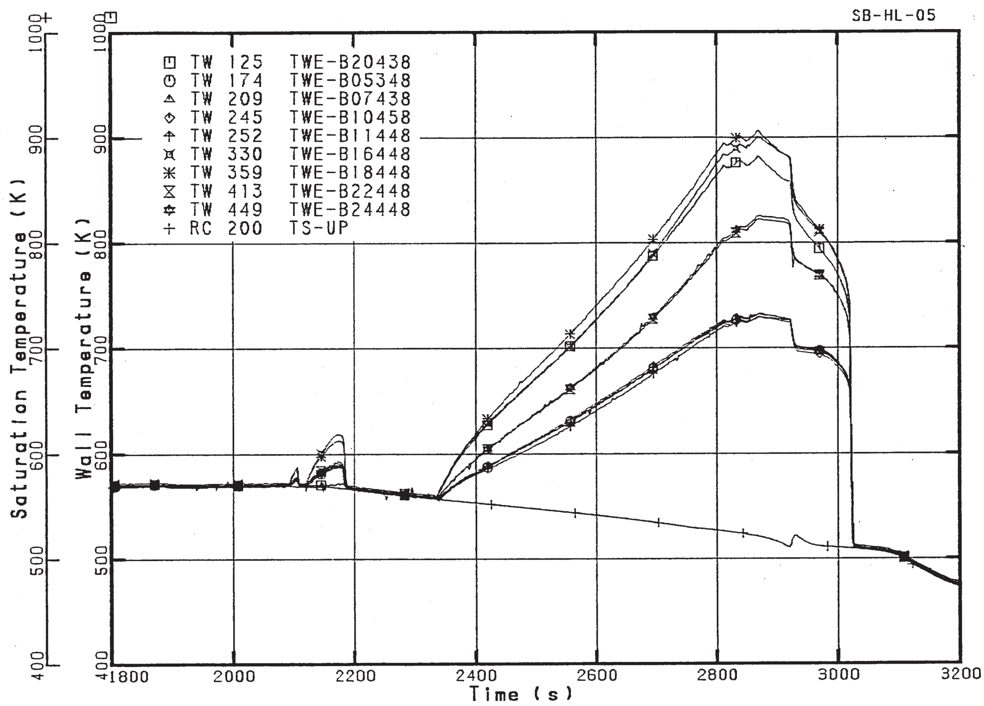

(2) Heater rod temperatures at Pos.8

Fig.4.7-6 Heater rod temperatures during boil-off process in SB-HL-05 test

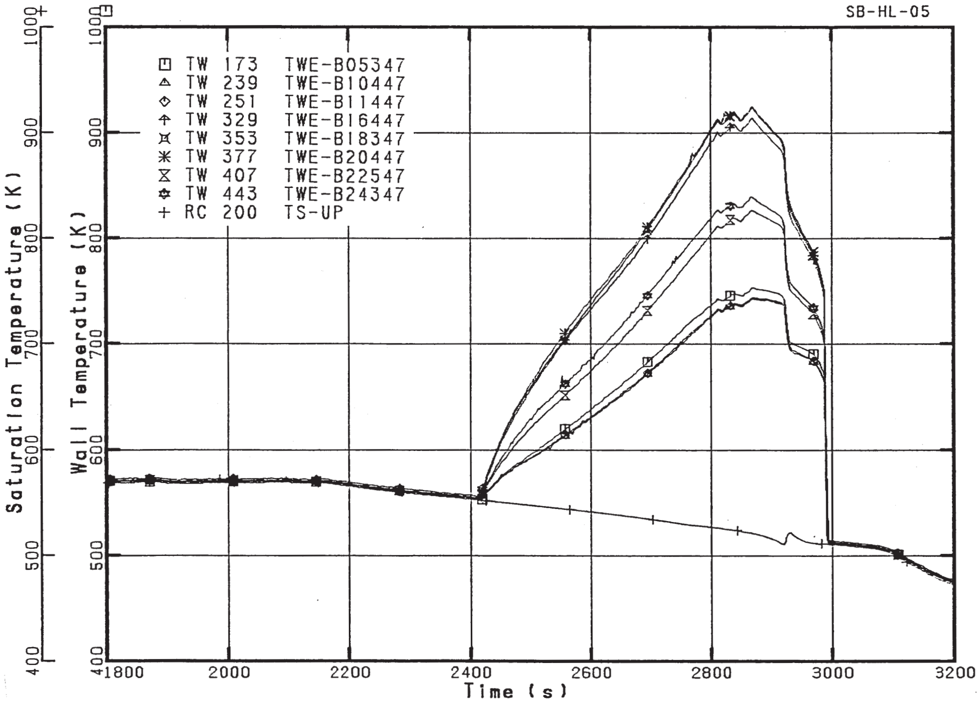

(3) Heater rod temperatures at Pos.7 with PCT measurement

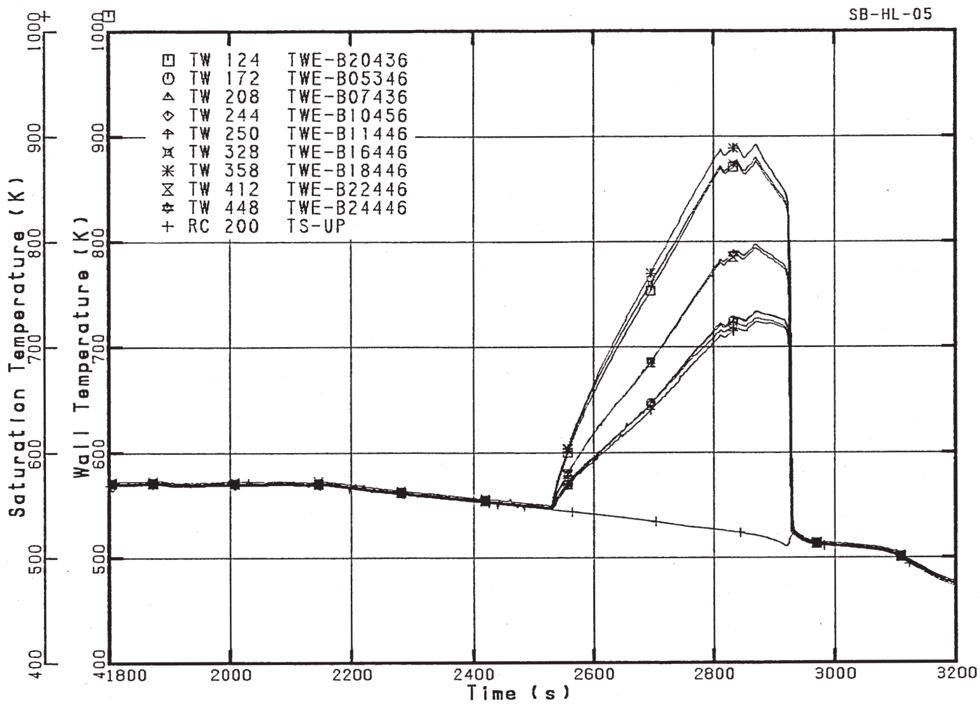

(4) Heater rod temperatures at Pos.6

Fig.4.7-6 Heater rod temperatures during boil-off process in SB-HL-05 test

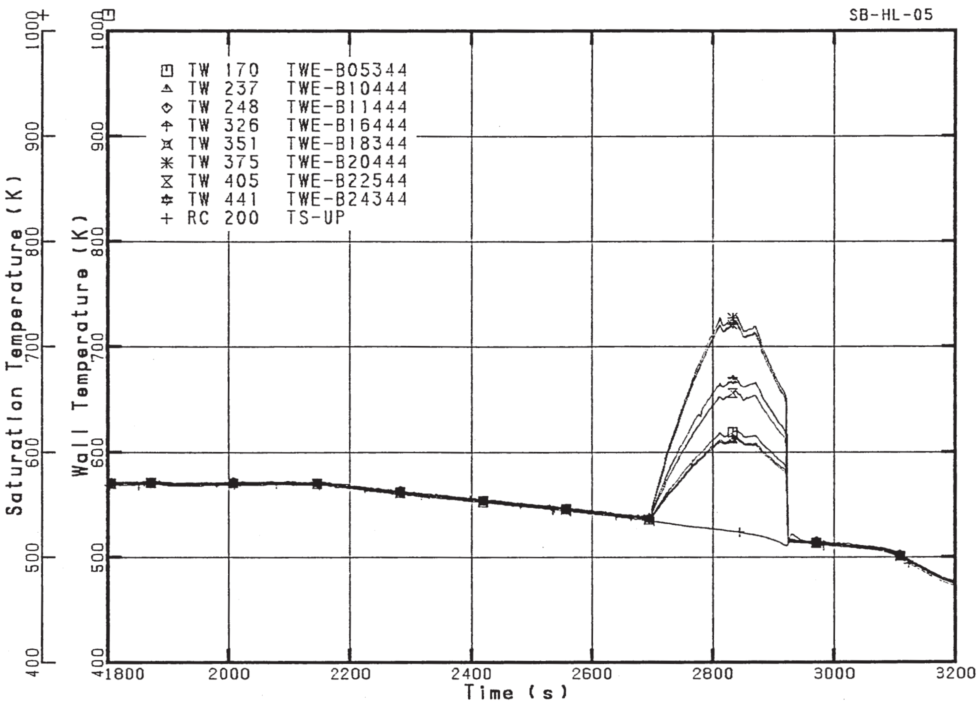

(5) Heater rod temperatures at Pos.4

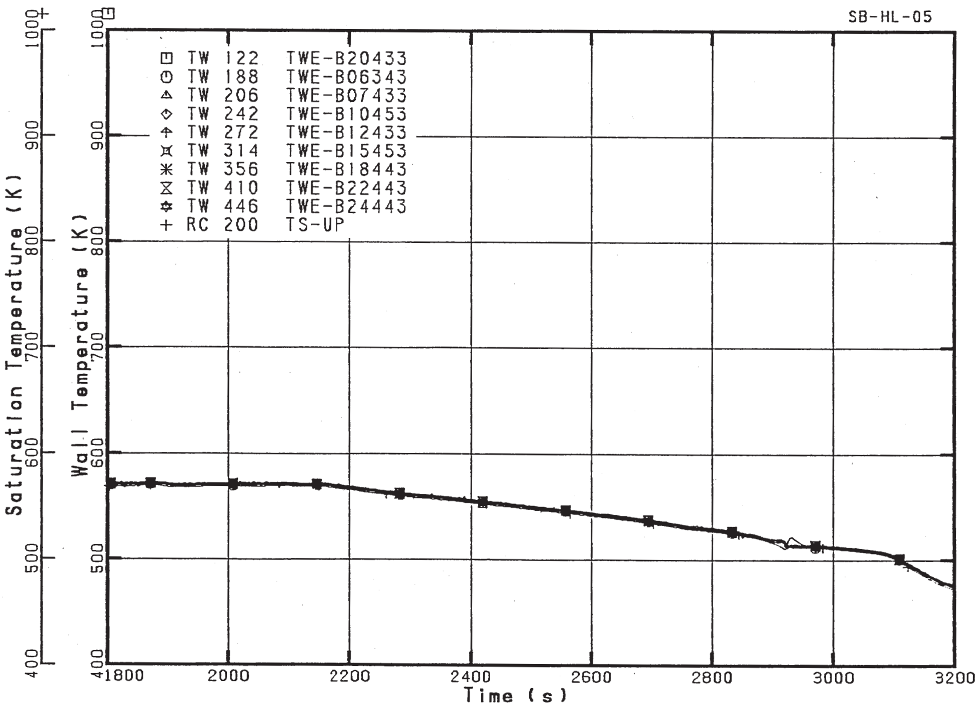

(6) Heater rod temperatures at Pos.3

Fig.4.7-6 Heater rod temperatures during boil-off process in SB-HL-05 test

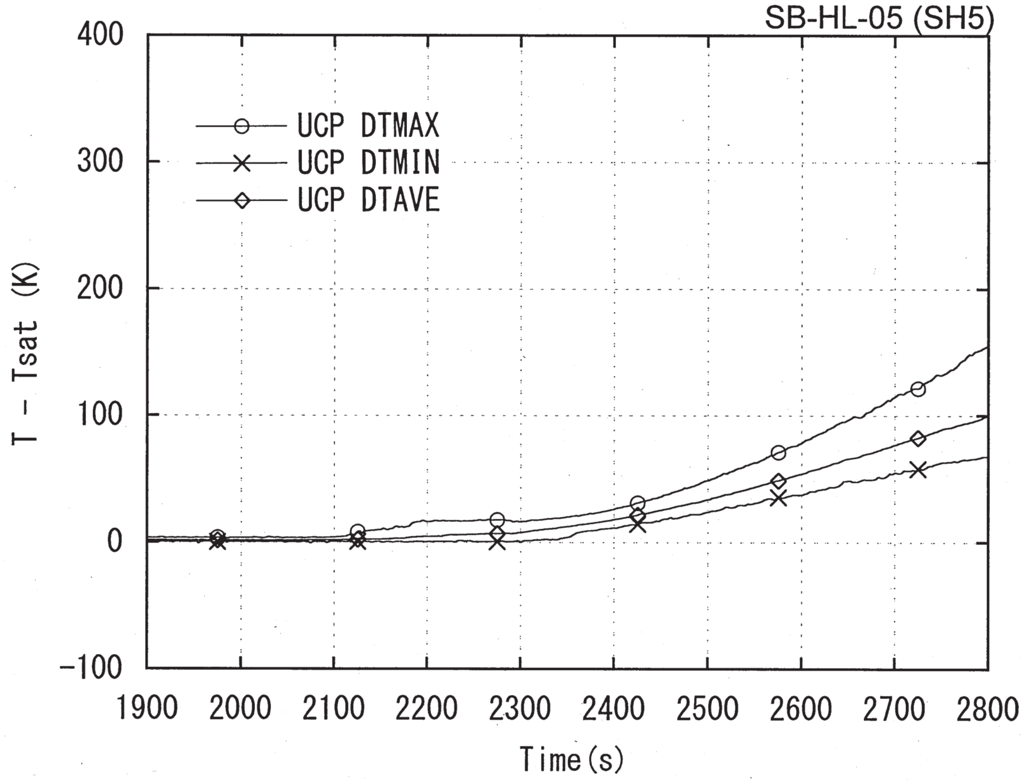

Fig.4.7-7 Distribution of all CET temperature rises above saturation temperature in SB-HL-05 test (DT_{MAX}, DT_{MIN}, DT_{AVE})

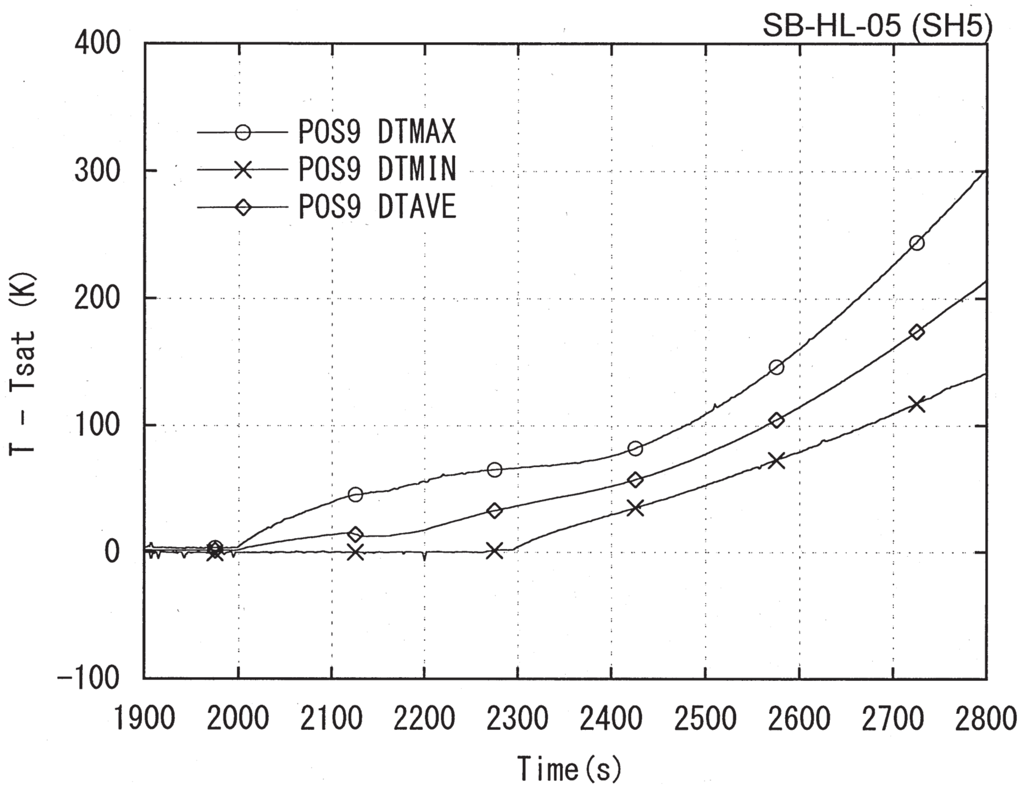

Fig.4.7-8 Distribution of heater rod temperature rises at Pos.9 in SB-HL-05 test (DT_{MAX}, DT_{MIN}, DT_{AVE})

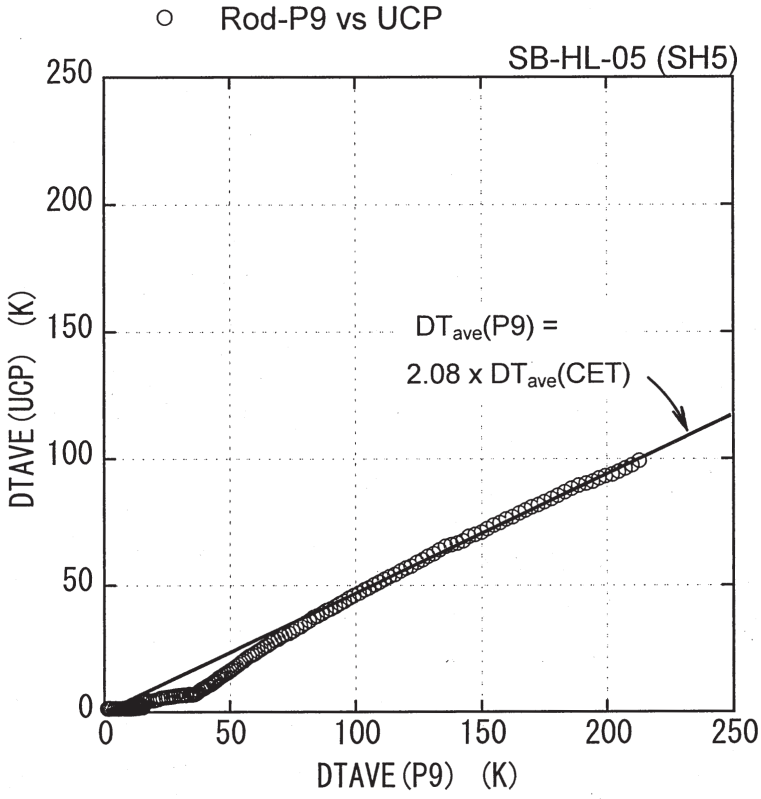

Fig.4.7-9 A relation of temperature rises at heater rod Pos.9, (Ave) and CET (Ave) in SB-HL-05 test (1900 - 2800 s)

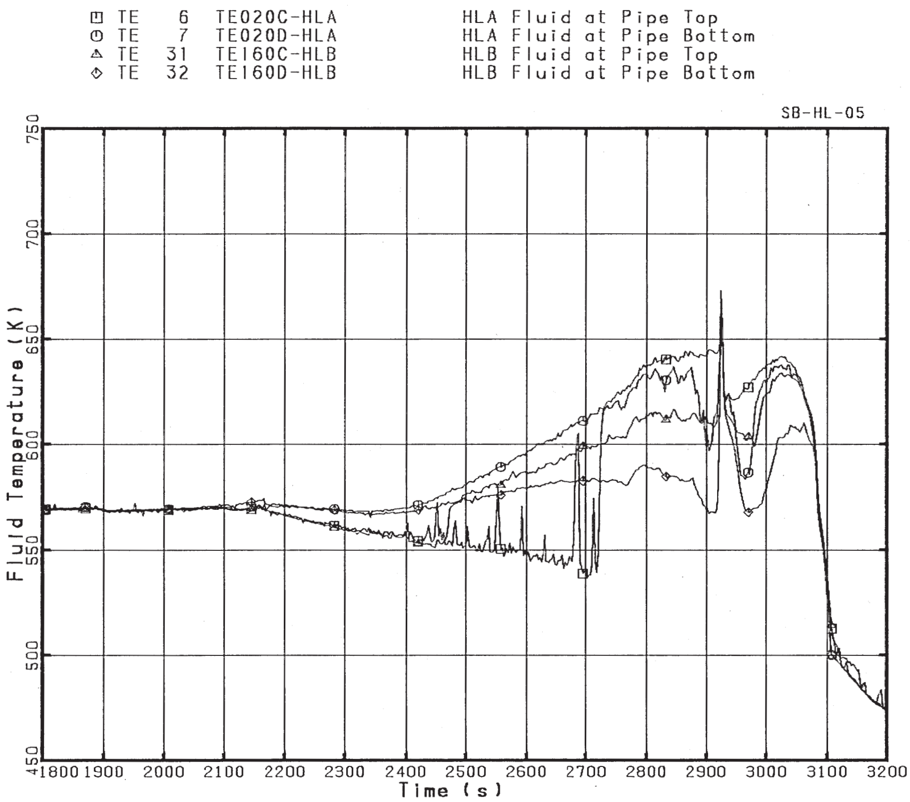

Fig.4.7-10 Fluid temperature data in hot legs during SB-HL-05 test

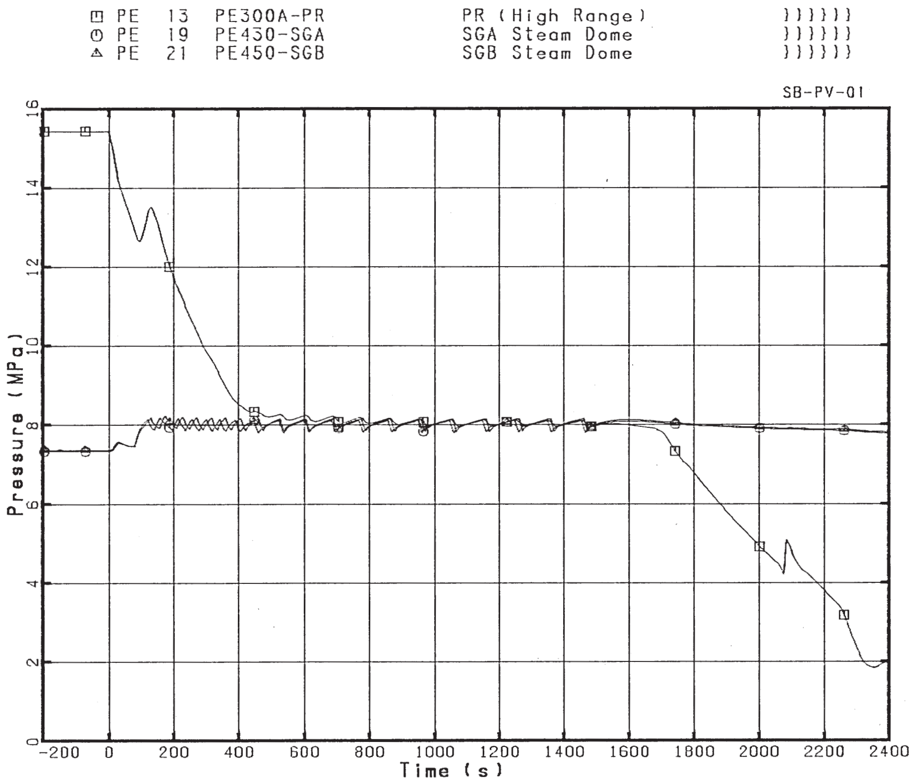

Fig.4.8-1 Primary and secondary pressures in LSTF 0.5% bottom break test (SB-PV-01)

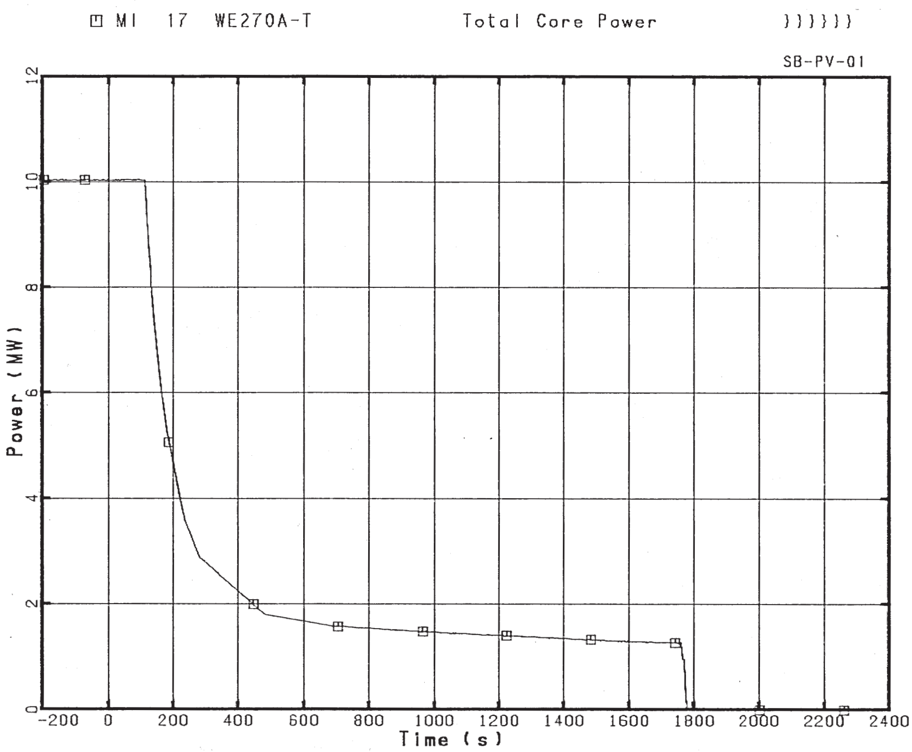

Fig.4.8-2 Core power decay curve in SB-PV-01 test

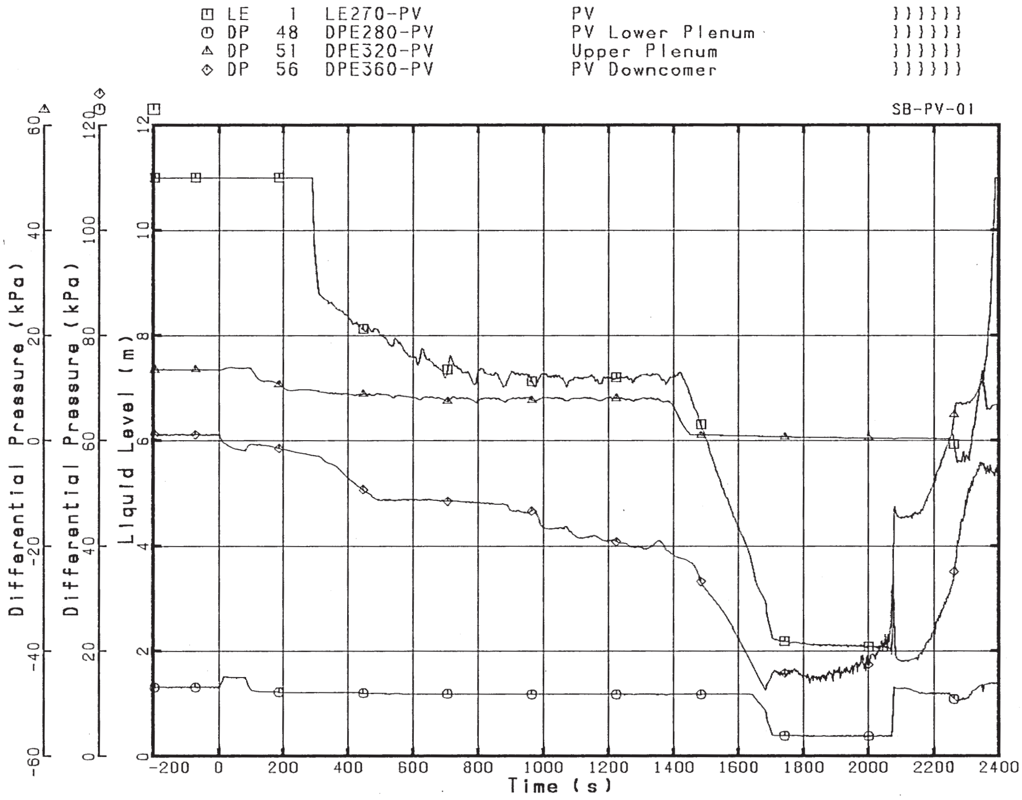

Fig.4.8-3 Liquid level in PV and DP data in UP, downcomer and LP in SB-PV-01 test

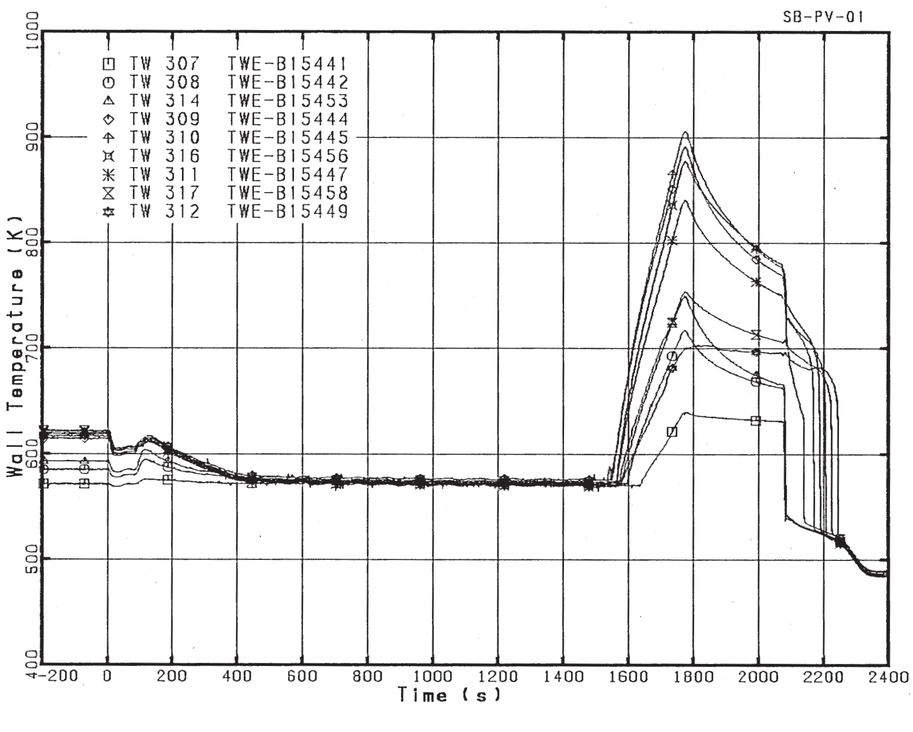

Fig.4.8-4 Representative heater rod surface temperatures in high-power bundle (B15) during SB-PV-01 test

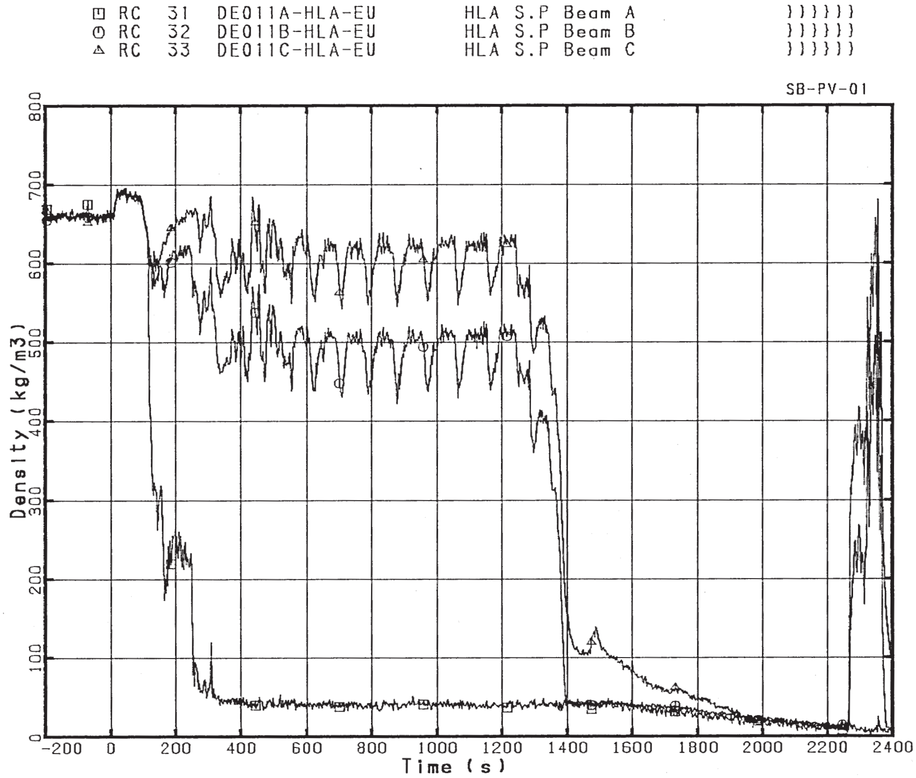

Fig.4.8-5 Fluid density data in intact loop hot leg (HL-A) in SB-PV-01 test

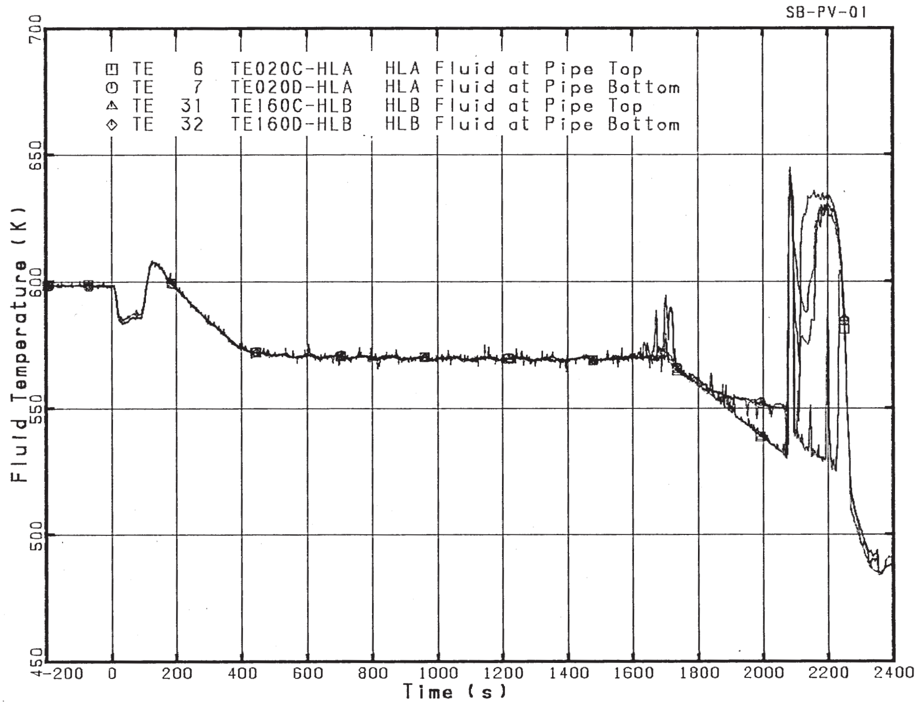

Fig.4.8-6 Fluid temperatures in two hot legs in SB-PV-01 test

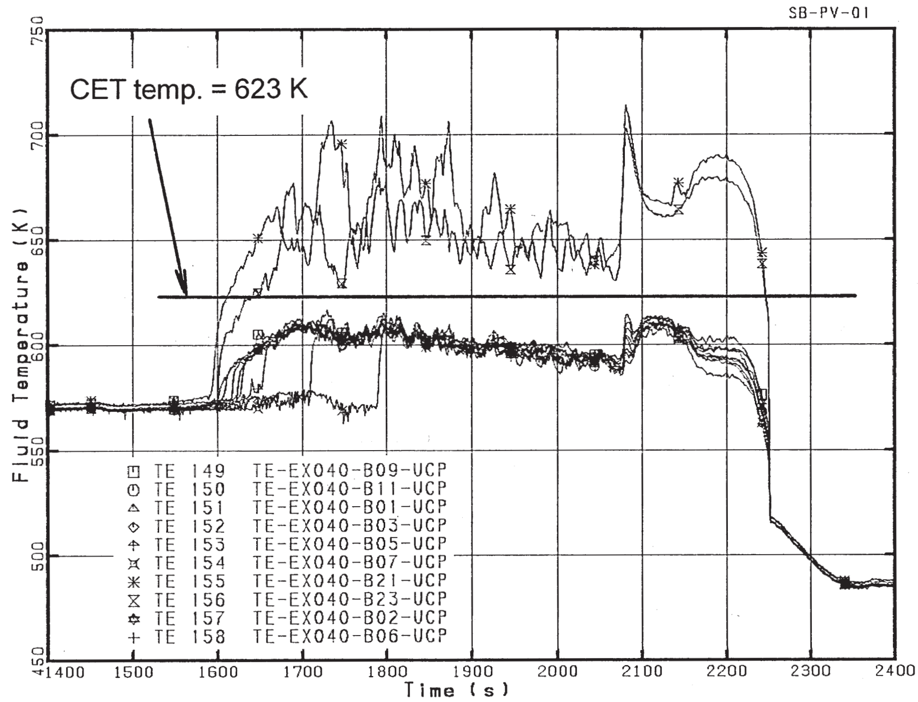

(1) CET temperatures above peripheral and central rod bundles

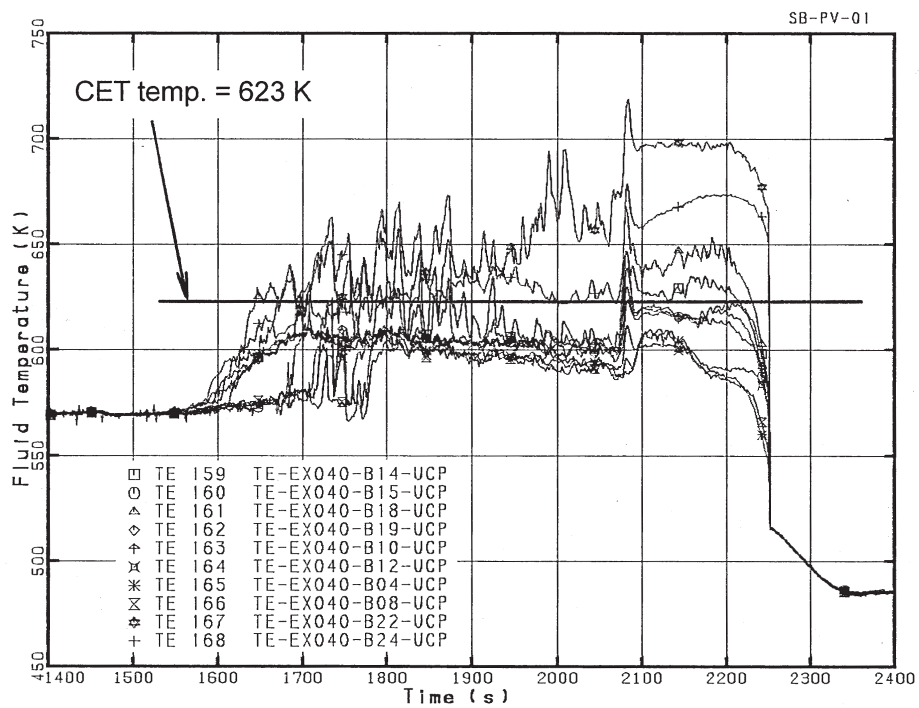

(2) CET temperatures above high-power and other rod bundles

Fig.4.8-7 CET temperatures during boil-off process in SB-PV-01 test

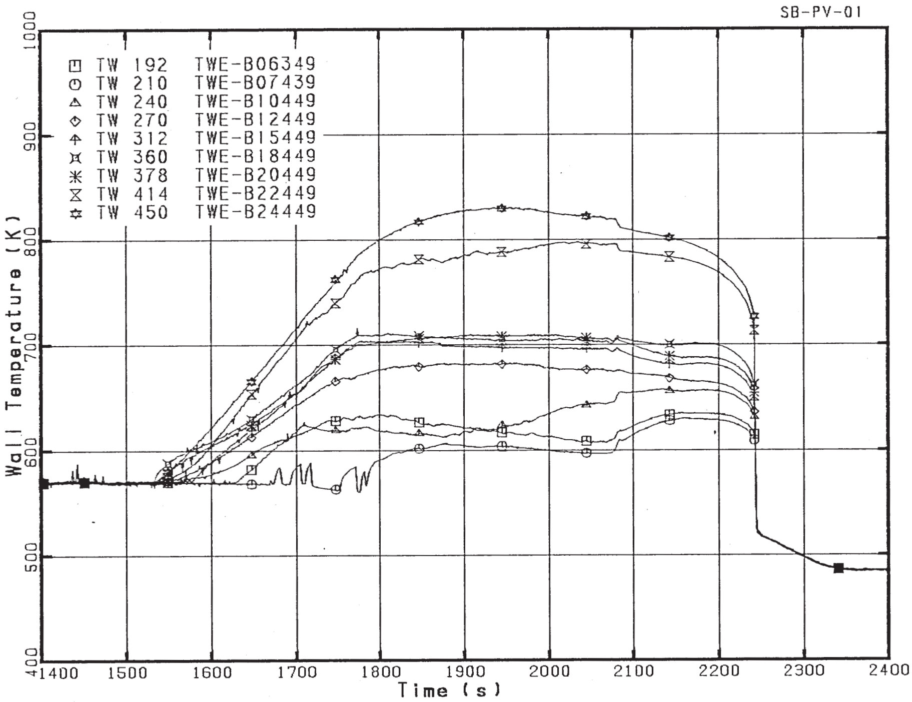

(1) Distribution of temperatures at heater rods at Pos.9 (core top)

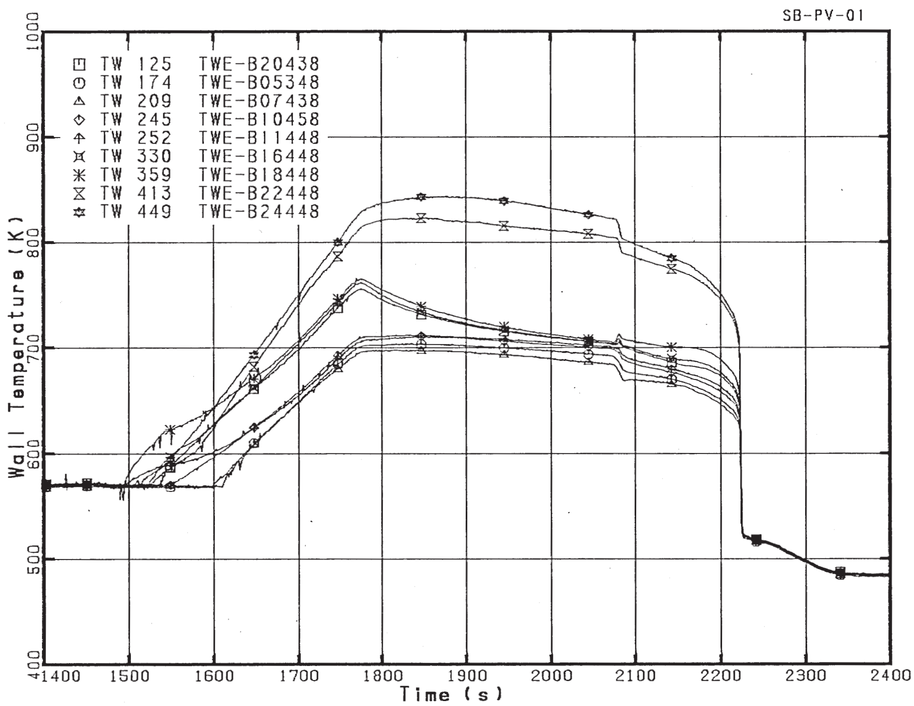

(2) Distribution of temperatures at heater rods at Pos.8

Fig.4.8-8 Heater rod surface temperatures during boil-off in SB-PV-01 test

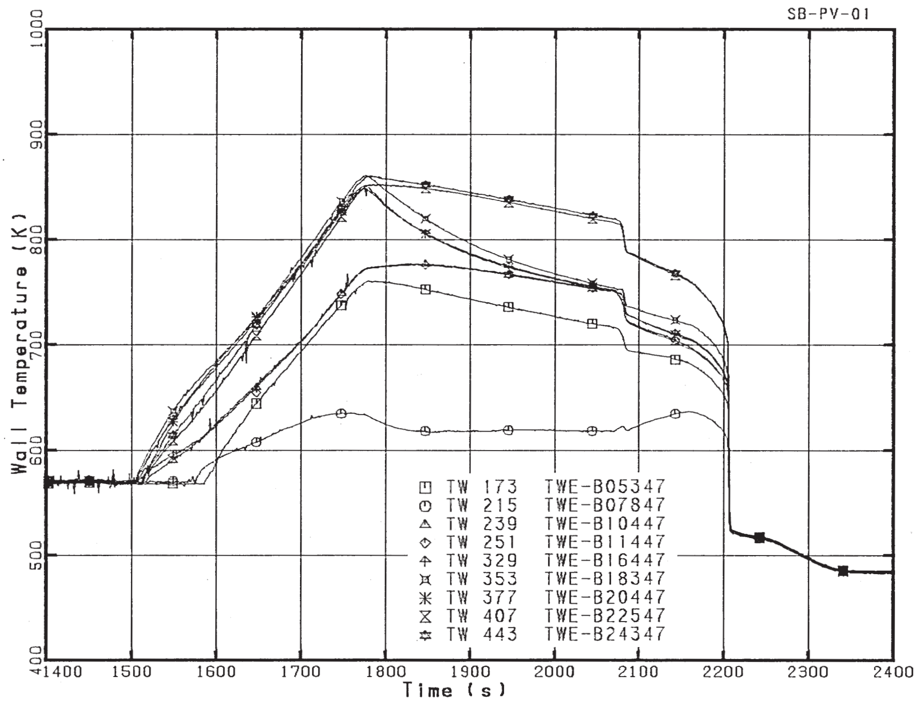

(3) Distribution of temperatures at heater rods at Pos.7

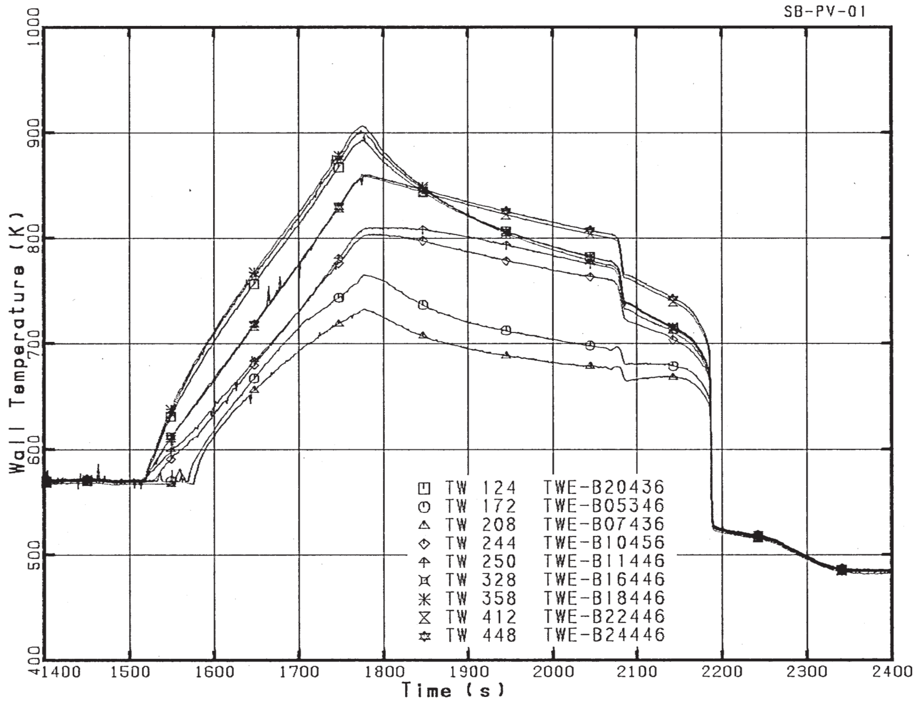

(4) Distribution of temperatures at heater rods at Pos.6

Fig.4.8-8 Heater rod surface temperatures during boil-off in SB-PV-01 test

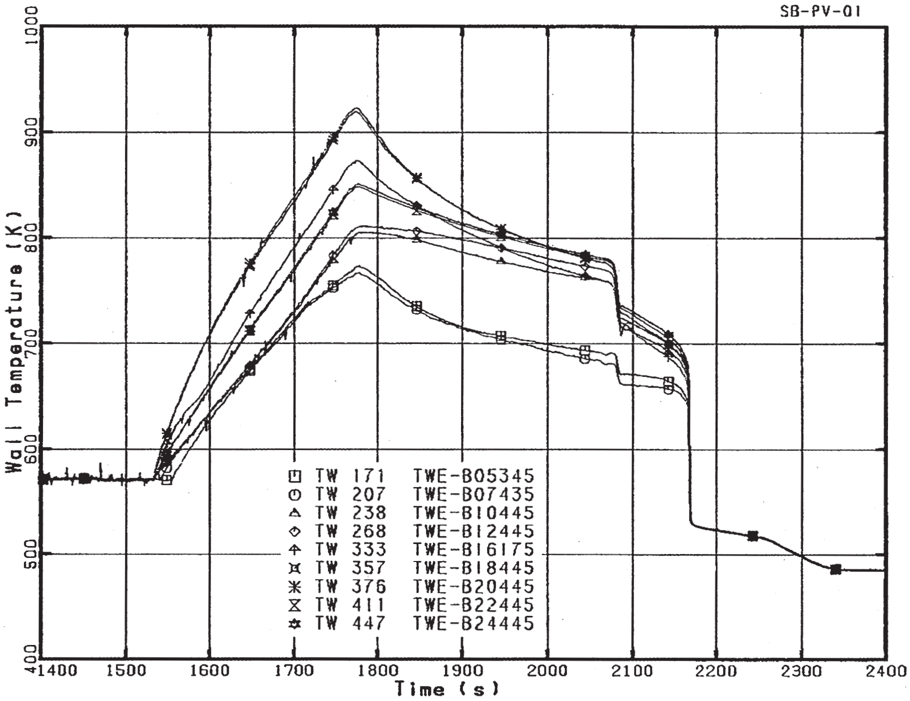

(5) Distribution of temperatures at heater rods at Pos.5 (core middle height)

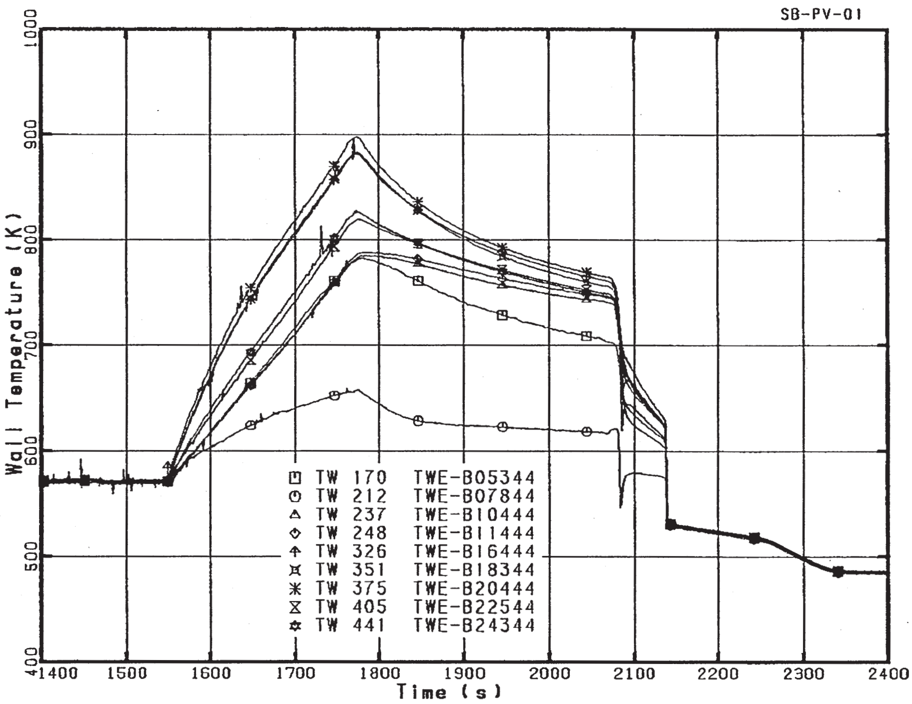

(6) Distribution of temperatures at heater rods at Pos.4

Fig.4.8-8 Heater rod surface temperatures during boil-off in SB-PV-01 test

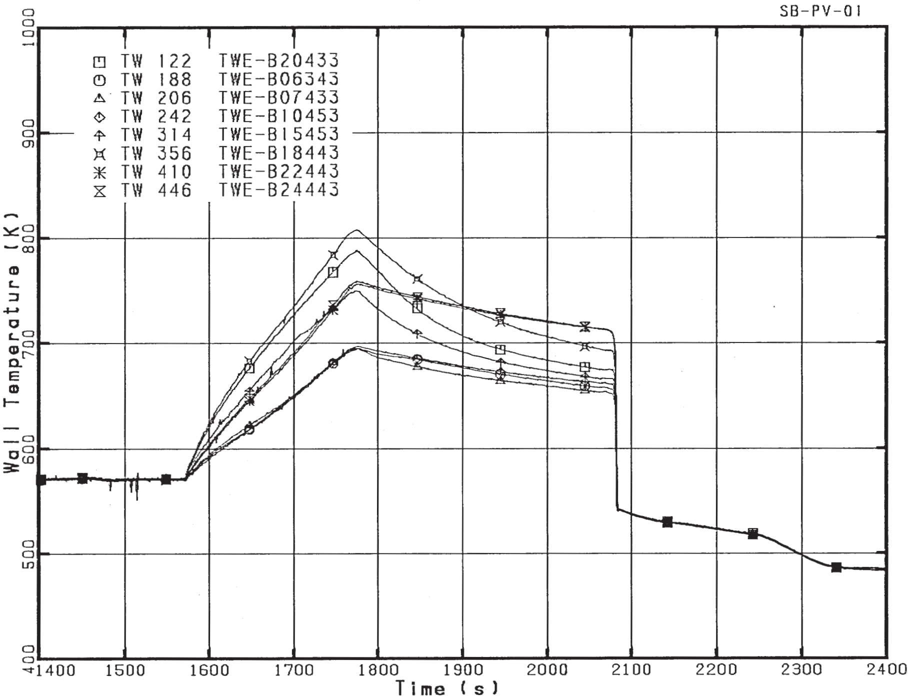

(7) Distribution of temperatures at heater rods at Pos.3

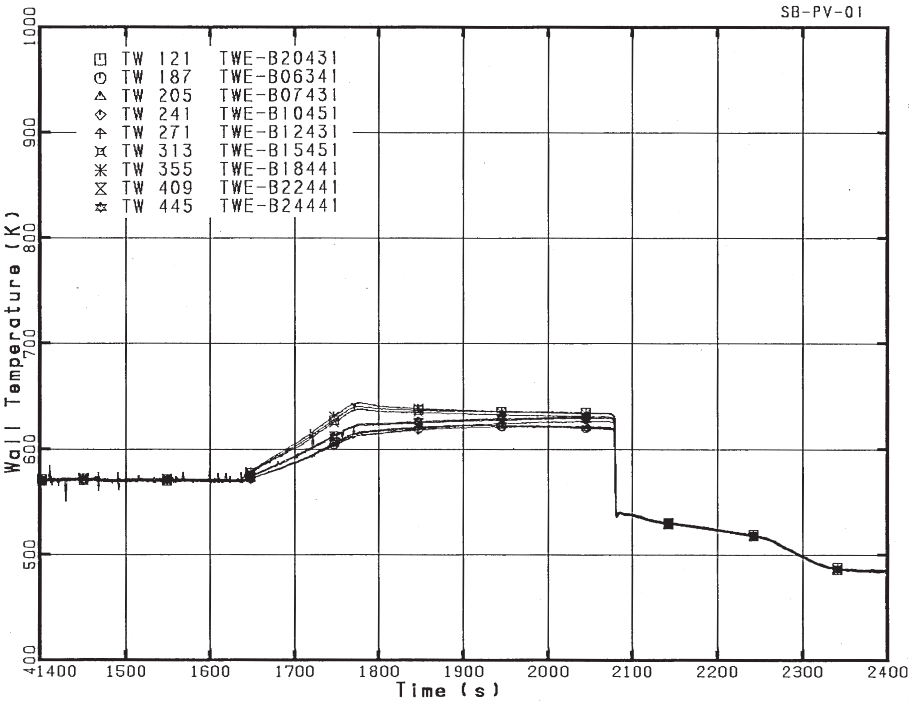

(8) Distribution of temperatures at heater rods at Pos.1 (core bottom)

Fig.4.8-8 Heater rod surface temperatures during boil-off in SB-PV-01 test

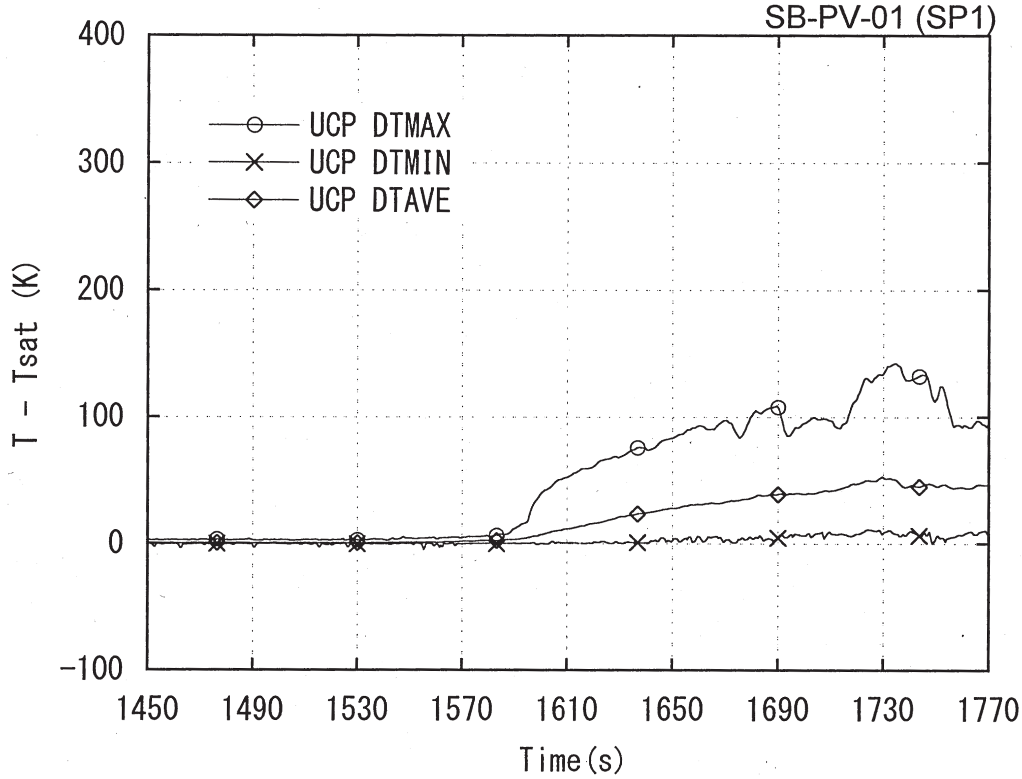

Fig.4.8-9 Distribution of all CET temperature rises above saturation temperature in SB-PV-01 test (DT_{MAX}, DT_{MIN}, DT_{AVE})

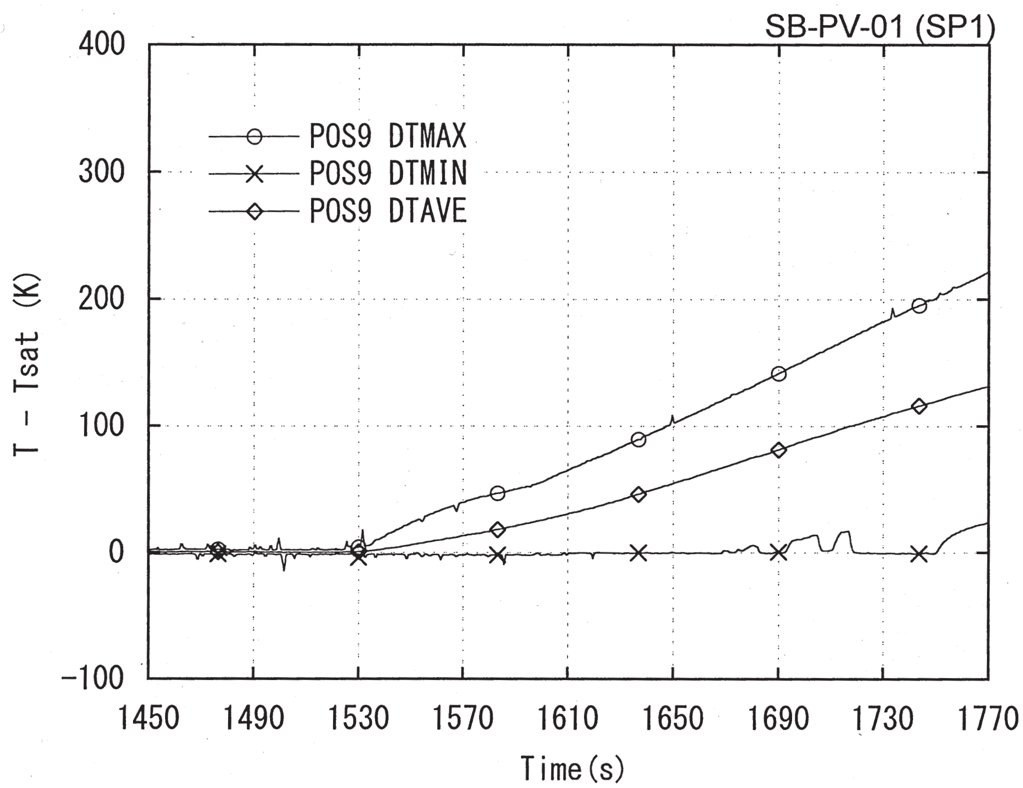

Fig.4.8-10 Distribution of heater rod temperature rises at Pos.9 in SB-PV-01 test (DT_{MAX}, DT_{MIN}, DT_{AVE})

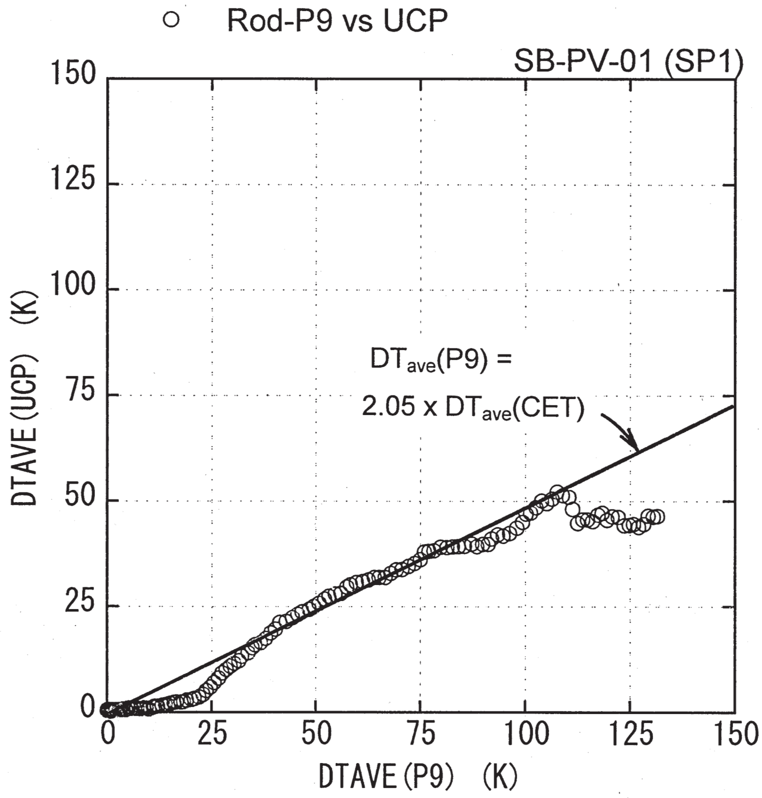

Fig.4.8-11 A relation of temperature rises at heater rod Pos.9, (Ave) and CET (Ave) in SB-PV-01 test (1450 - 1770 s)

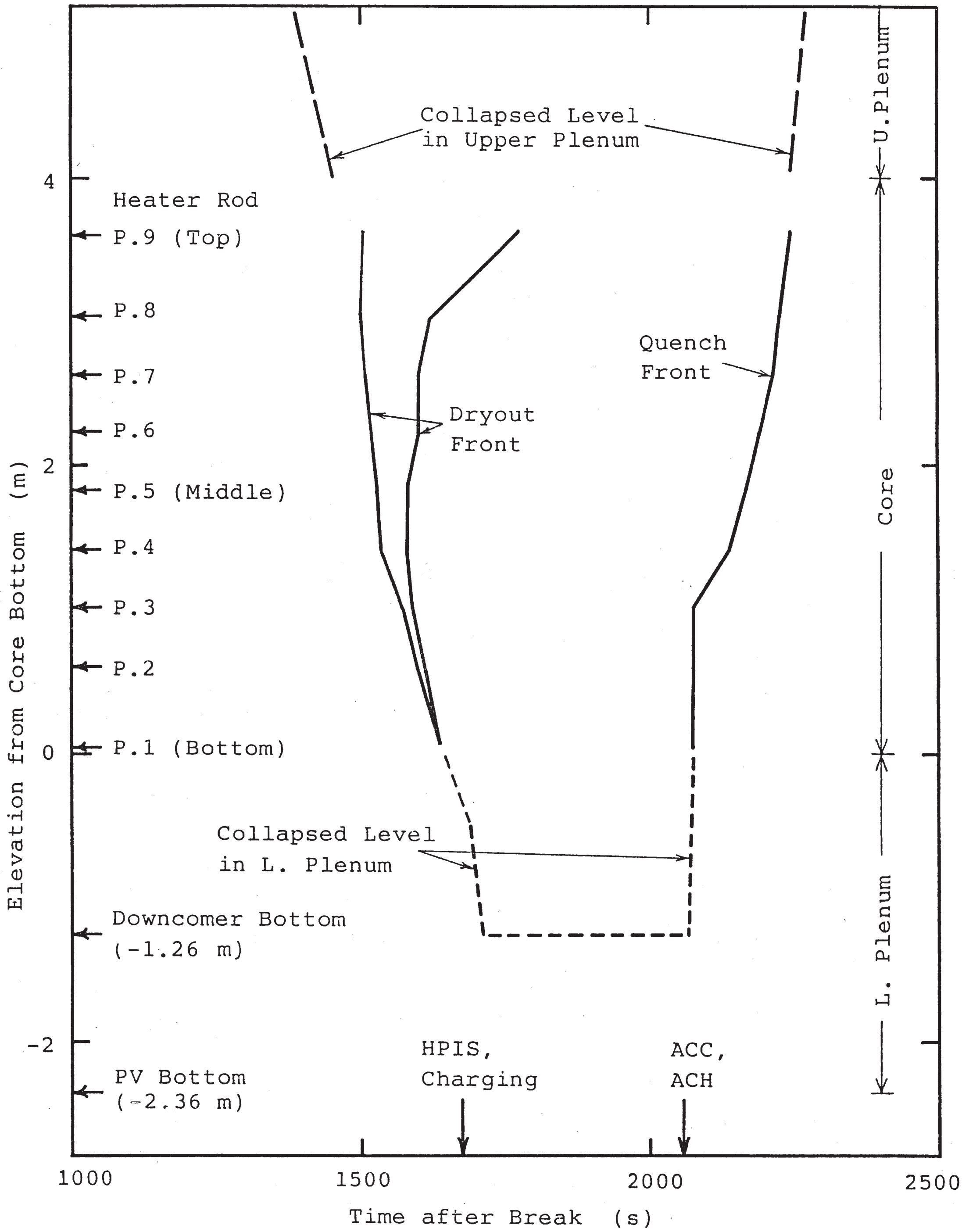

Fig.4.8-12 Core heat-up and quench behavior in SB-PV-01 test

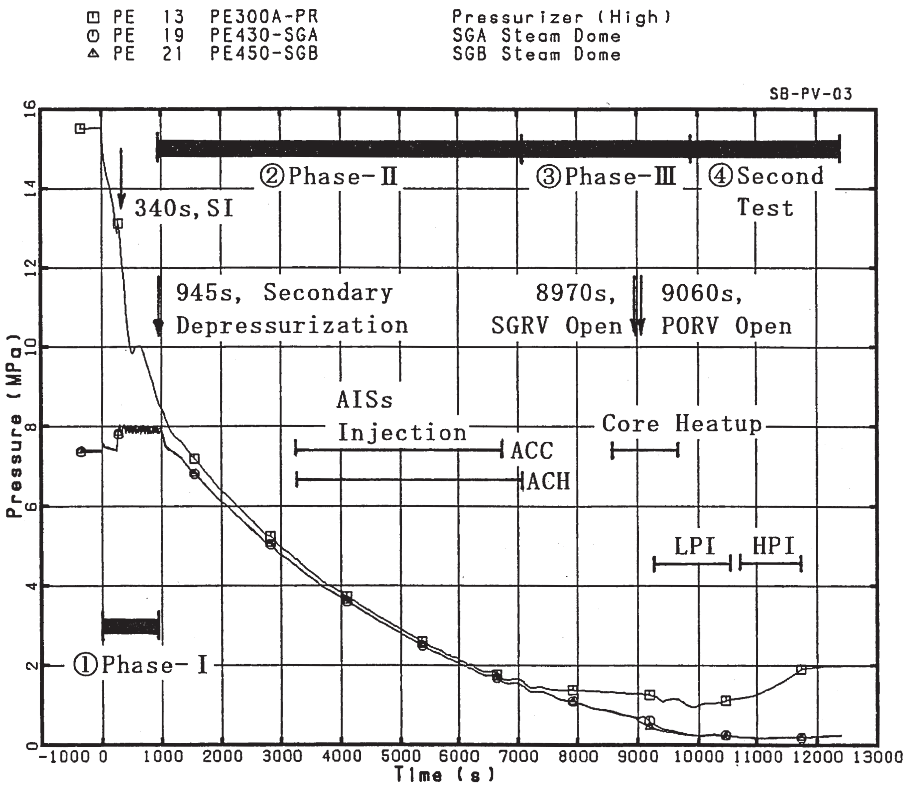

Fig.4.9-1 Primary and secondary pressures in LSTF 0.2% bottom break test (SB-PV-03)

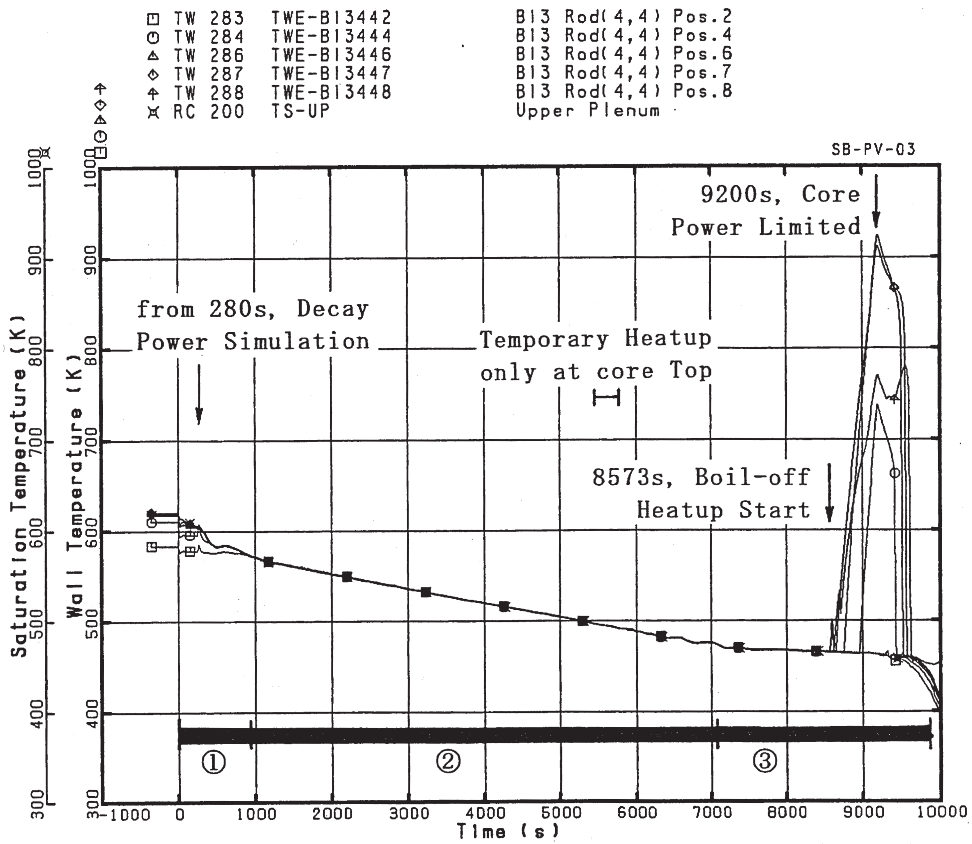

Fig.4.9-2 Representative heater rod surface temperatures in high-power bundle (B13) during SB-PV-03 test

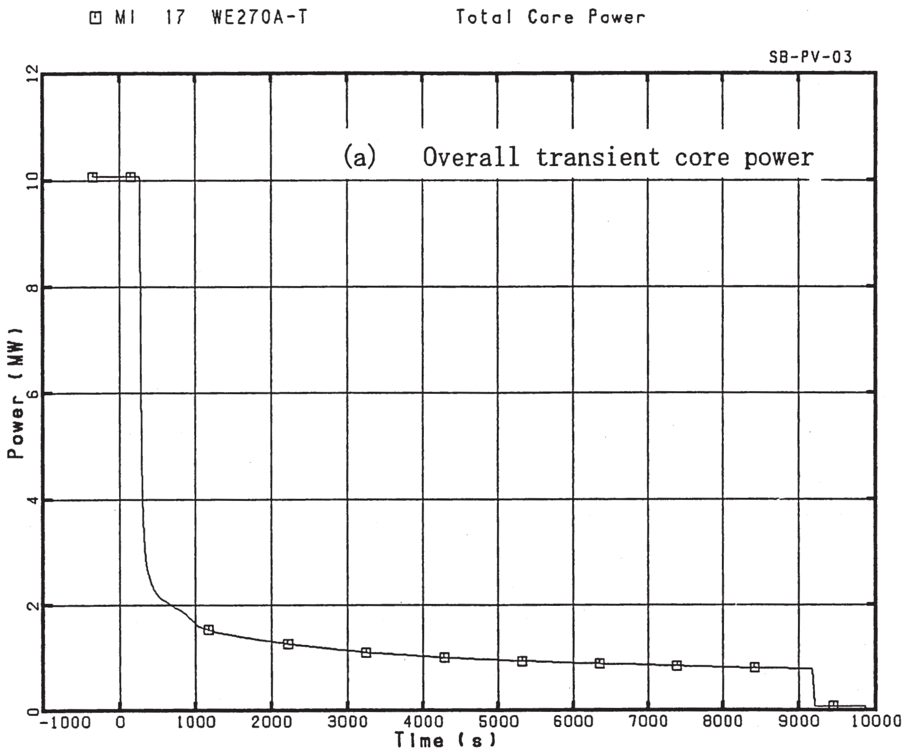

(1) Overall transient core power

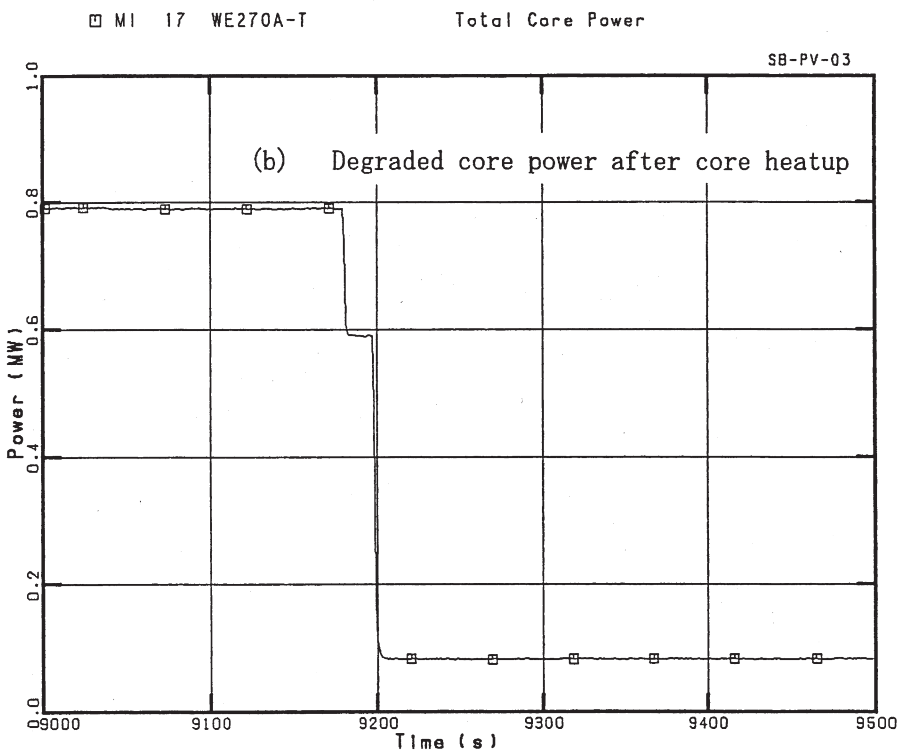

(2) Degraded core power after core heat-up

Fig.4.9-3 Core power decay curve in SB-PV-03 test

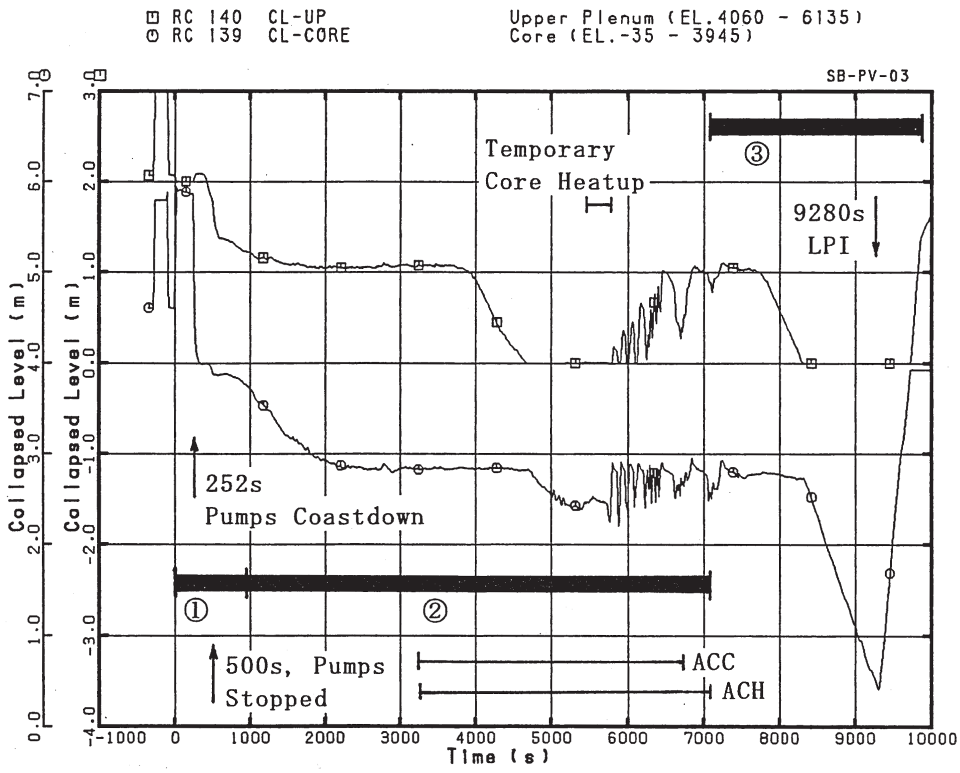

Fig.4.9-4 Collapsed liquid levels in core and UP during SB-PV-03 test

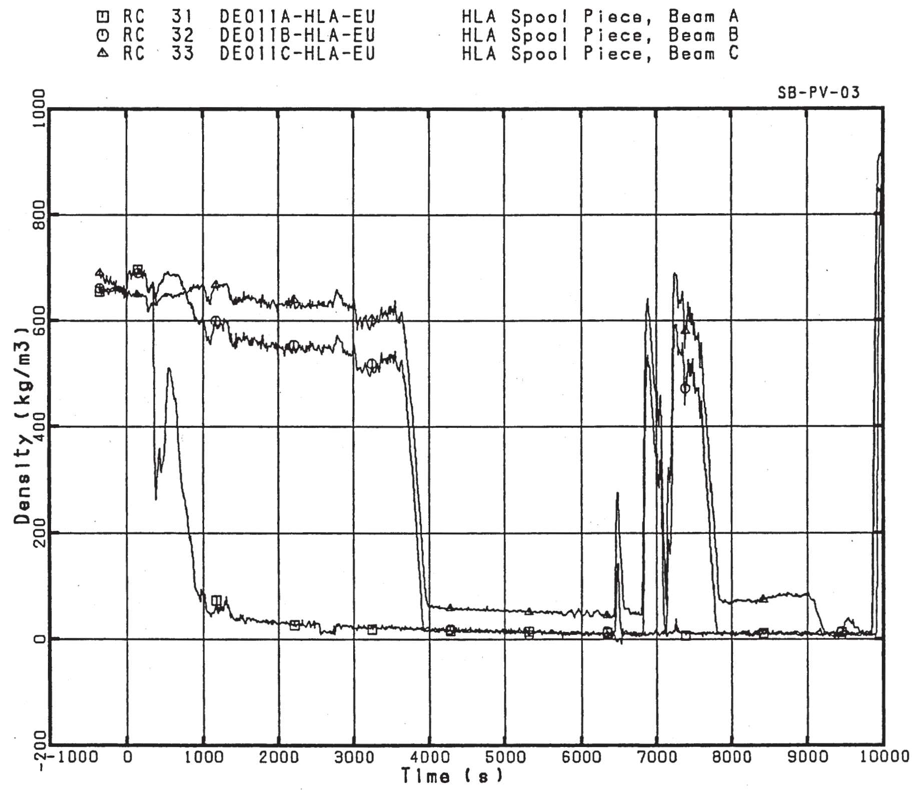

Fig.4.9-5 Fluid density data in intact loop hot leg (HL-A) in SB-PV-03 test

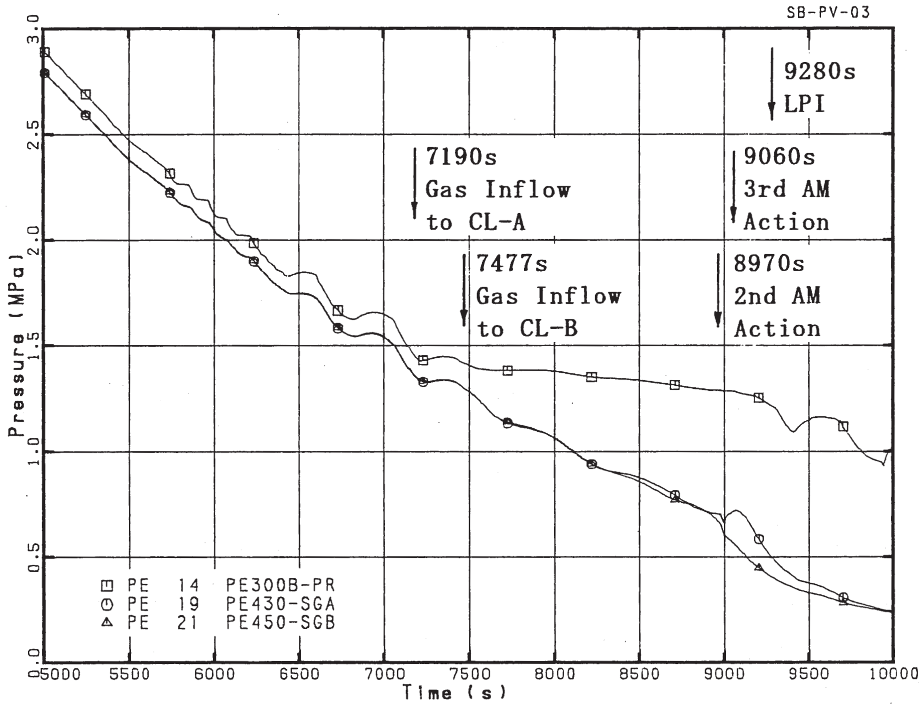

Fig.4.9-6 Degraded primary depressurization under gas inflow in SB-PV-03 test

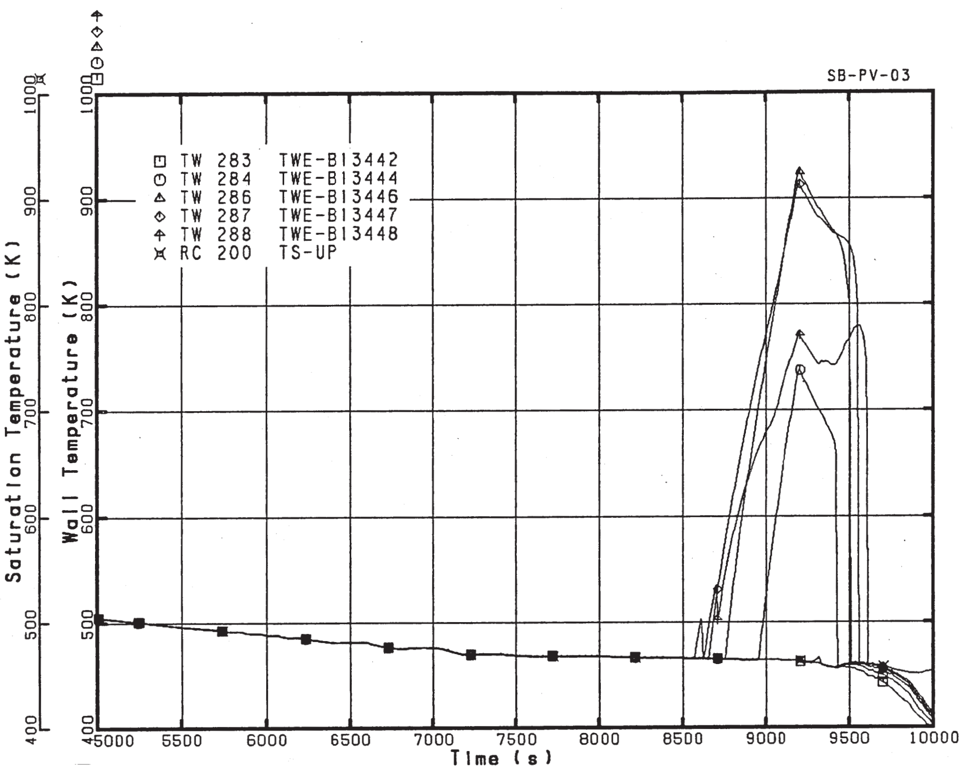

Fig.4.9-7 Representative heater rod surface temperatures with PCT of 925 K at Pos.6 in detail during SB-PV-03 test

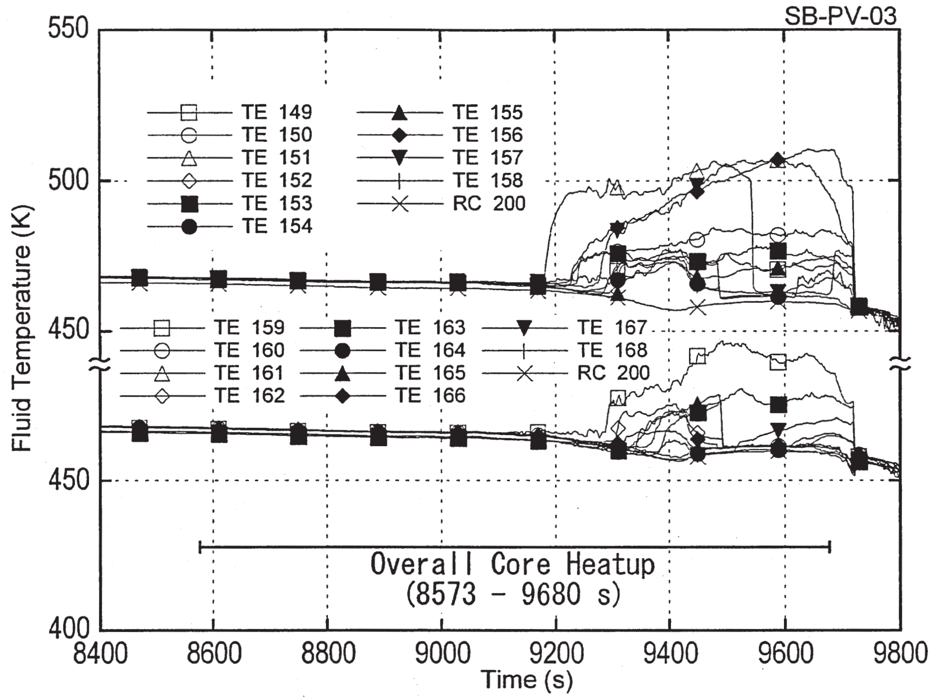

Fig.4.9-8 No CET temperature rises until PORV open (9060s) in SB-PV-03 test

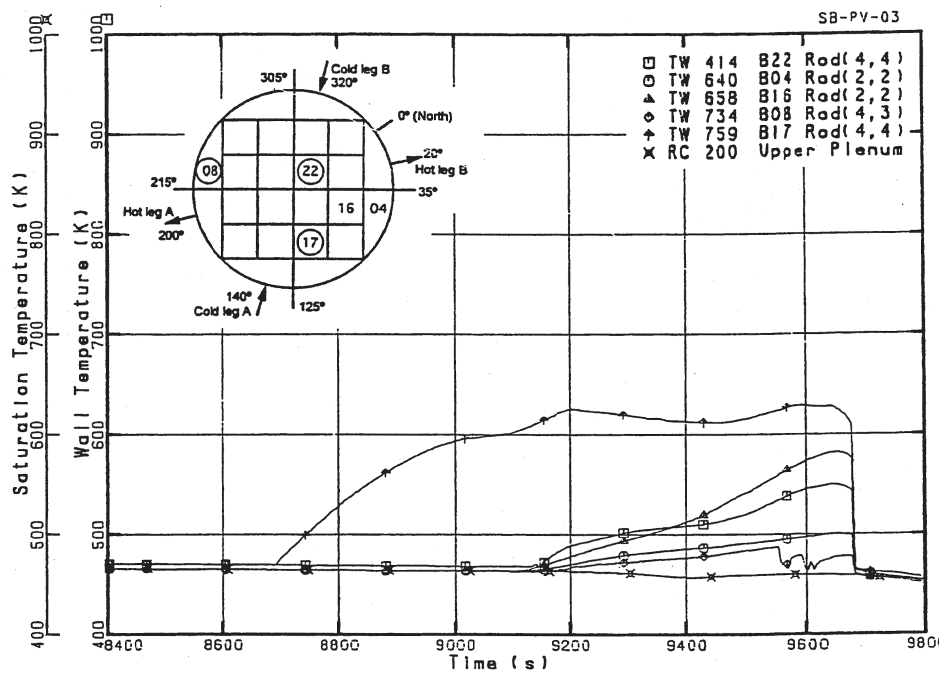

(1) Distribution of temperatures at heaters and tie rods at Pos.9 (core top)

Fig.4.9-9 Heater rod surface temperatures during boil-off in SB-PV-03 test

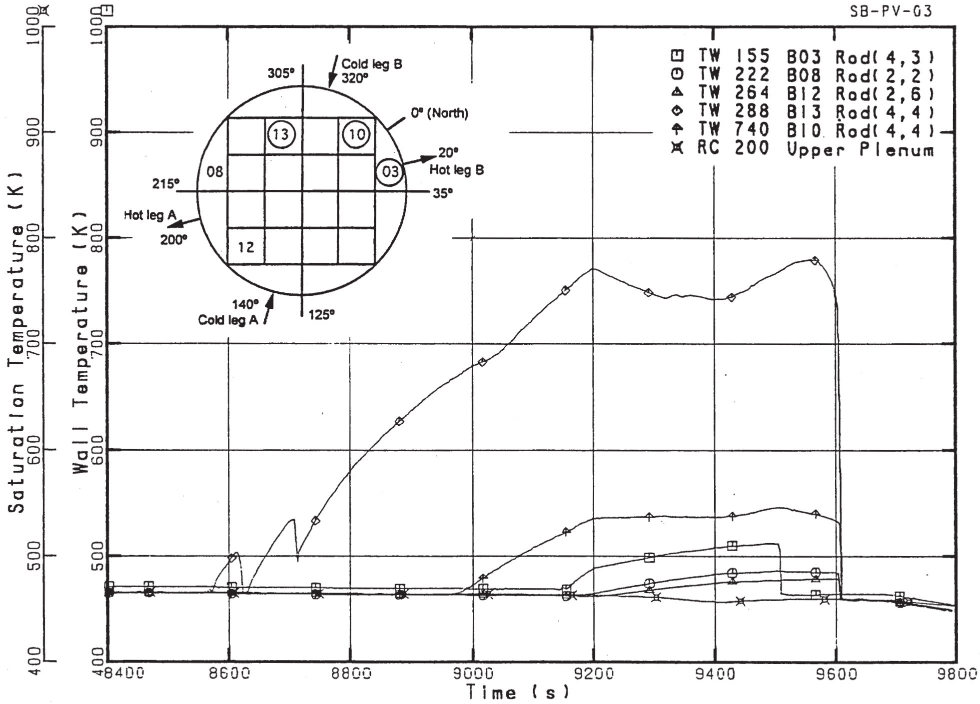

(2) Distribution of temperatures at heaters and tie rods at Pos.8

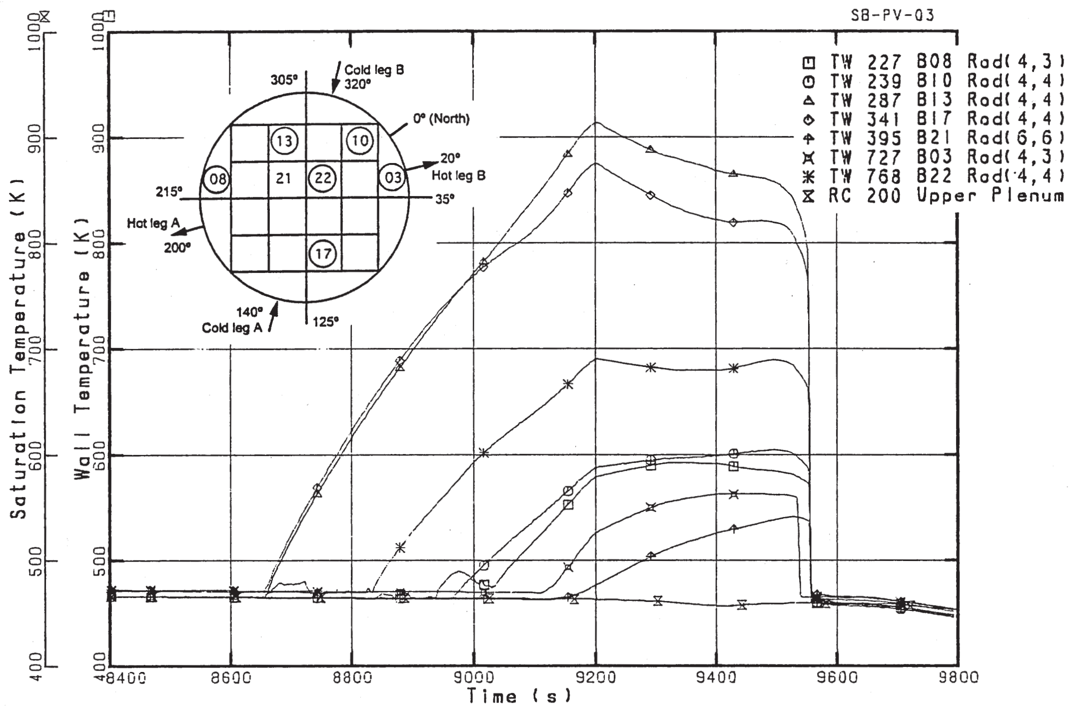

(3) Distribution of temperatures at heaters and tie rods at Pos.7

Fig.4.9-9 Heater rod surface temperatures during boil-off in SB-PV-03 test

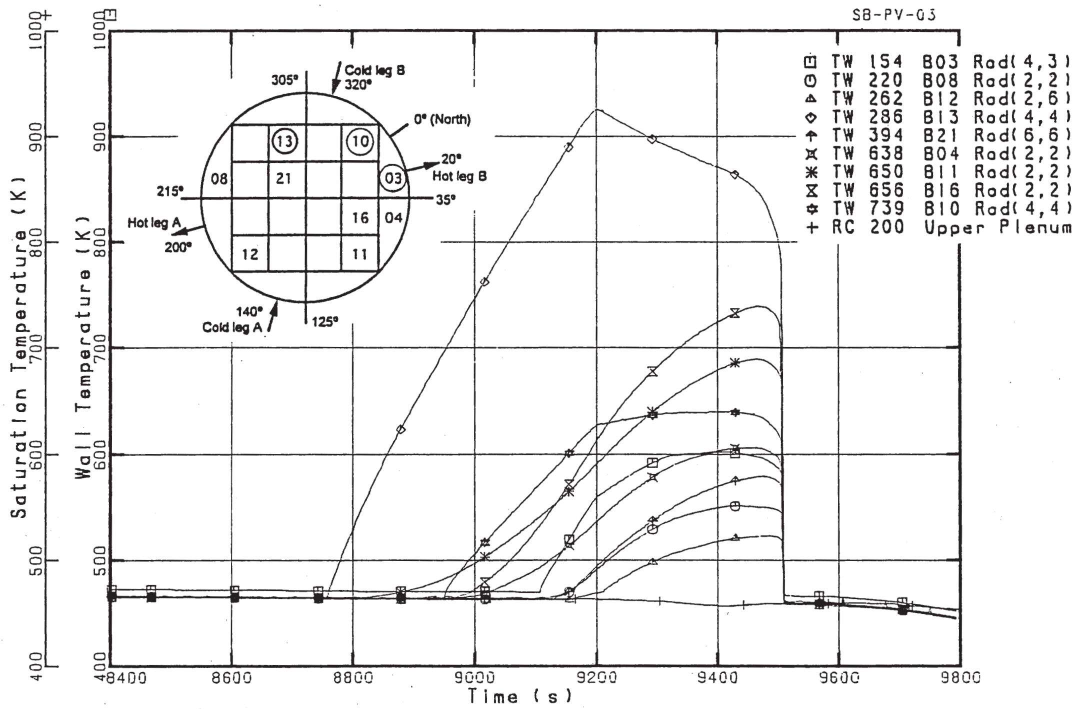

(4) Distribution of temperatures at heaters and tie rods at Pos.6

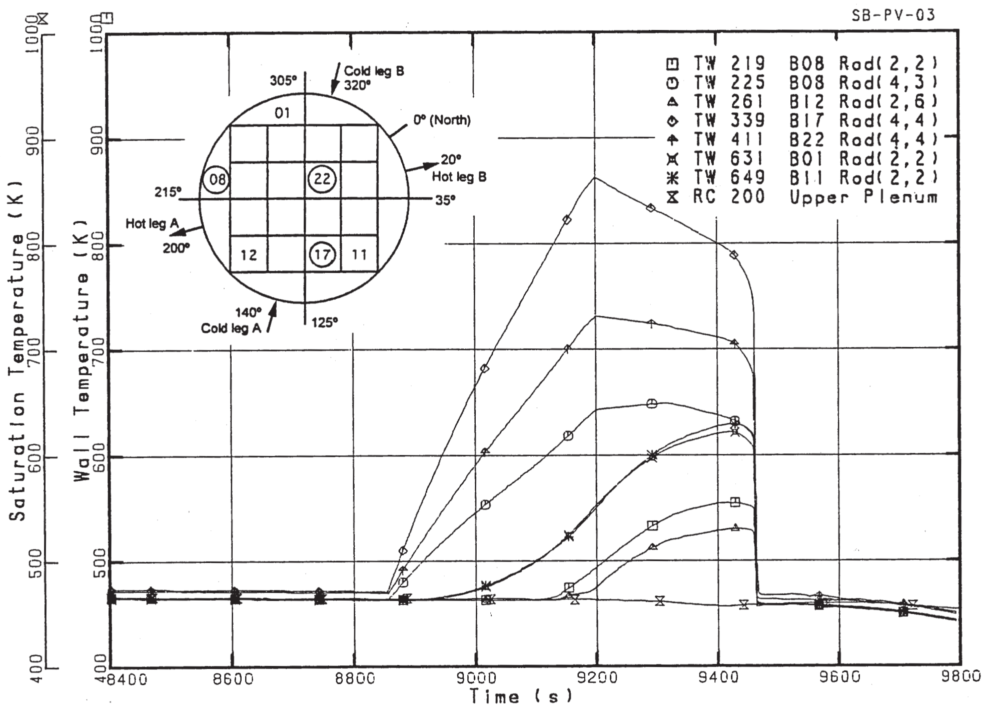

(5) Distribution of temperatures at heaters and tie rods at Pos.5 (Middle height)

Fig.4.9-9 Heater rod surface temperatures during boil-off in SB-PV-03 test

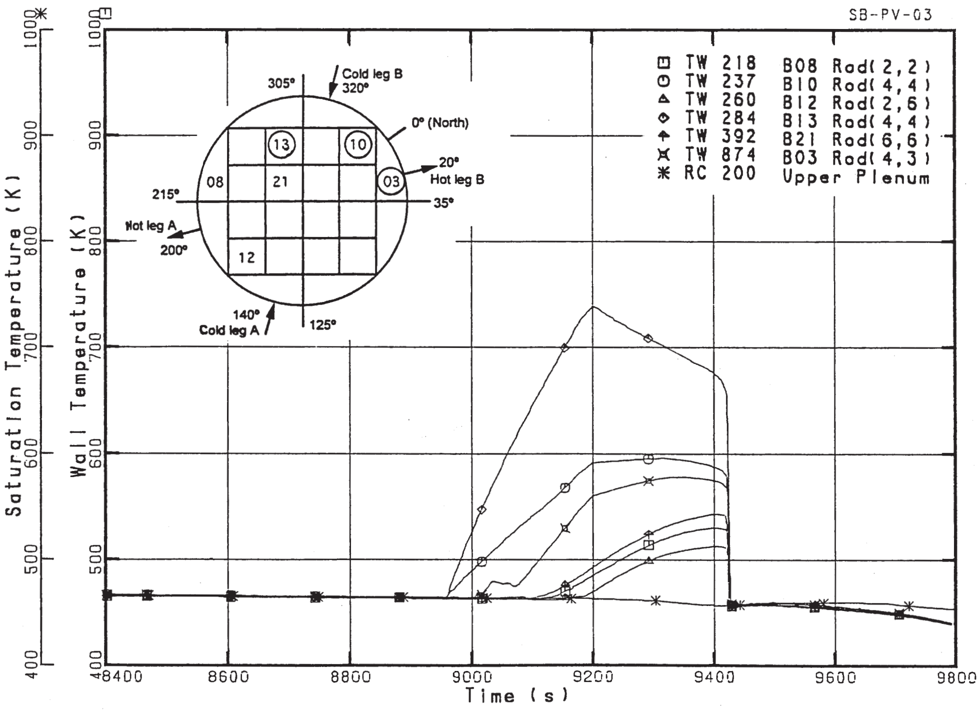

(6) Distribution of temperatures at heaters and tie rods at Pos.4

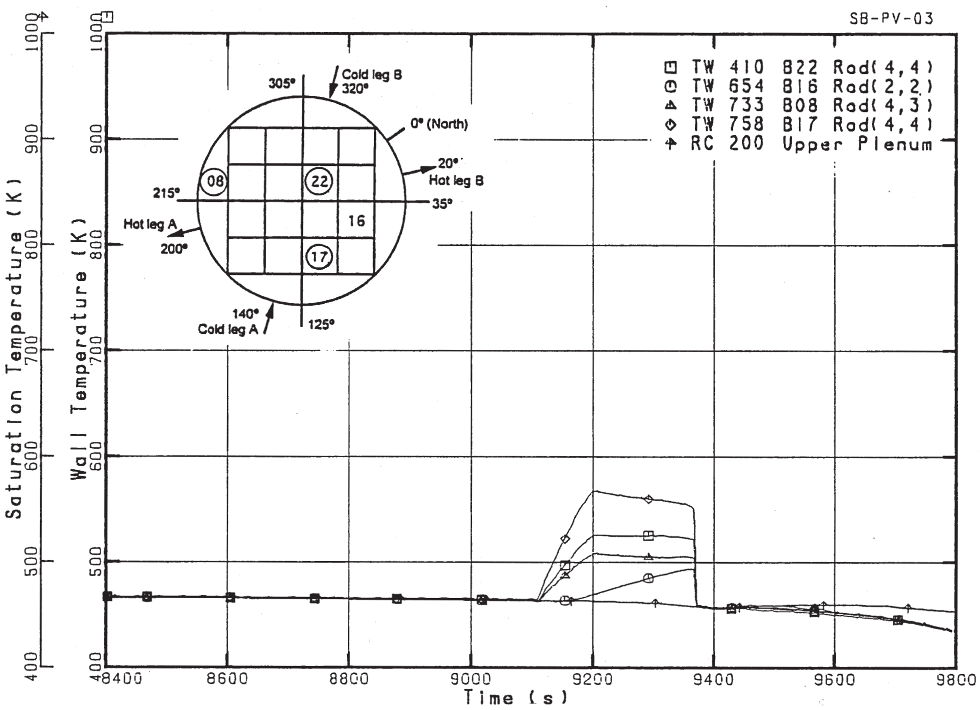

(7) Distribution of temperatures at heaters and tie rods at Pos.3

Fig.4.9-9 Heater rod surface temperatures during boil-off in SB-PV-03 test

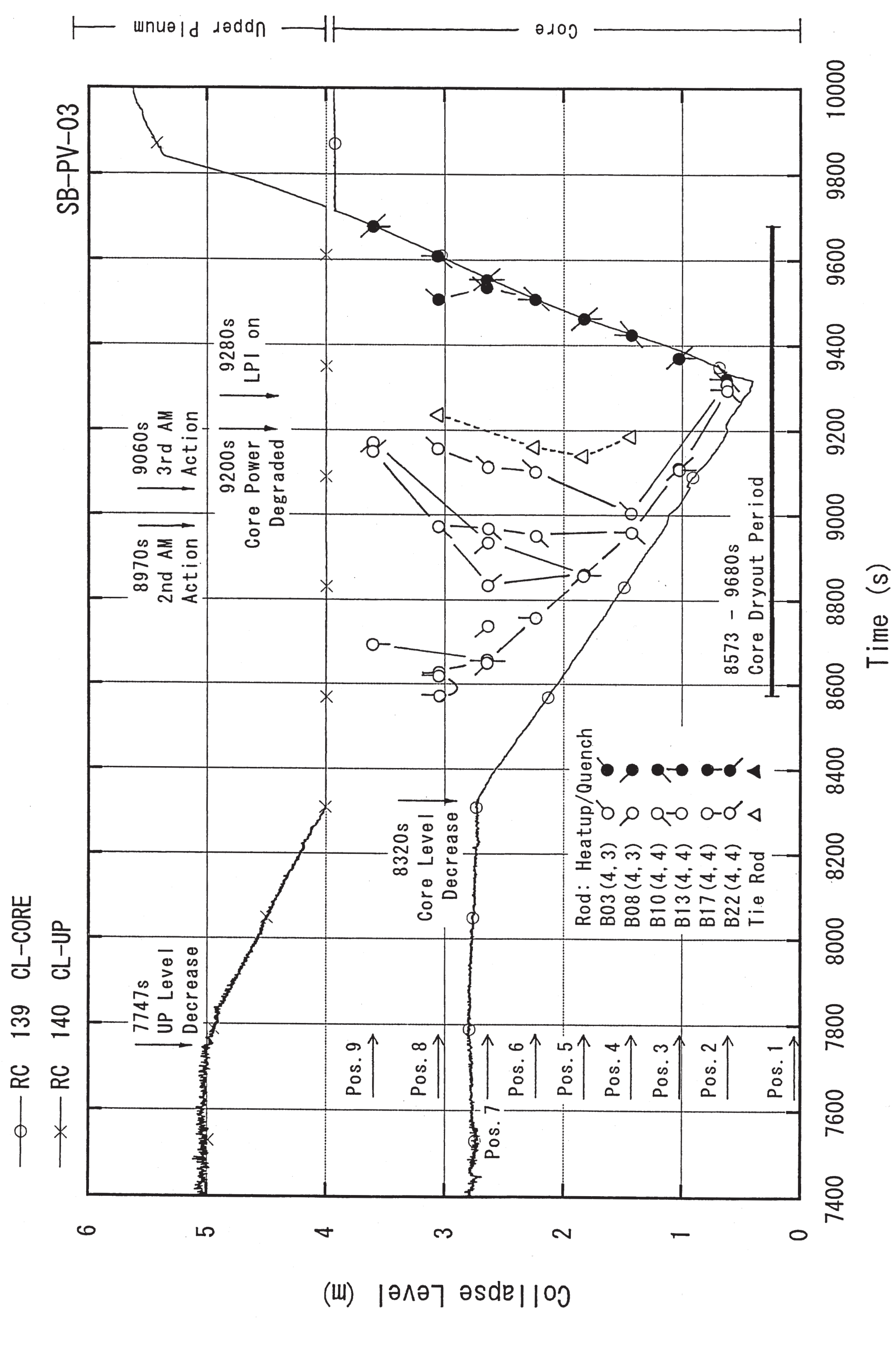

Fig.4.9-10 Core heat-up and quench behavior in SB-PV-03 test

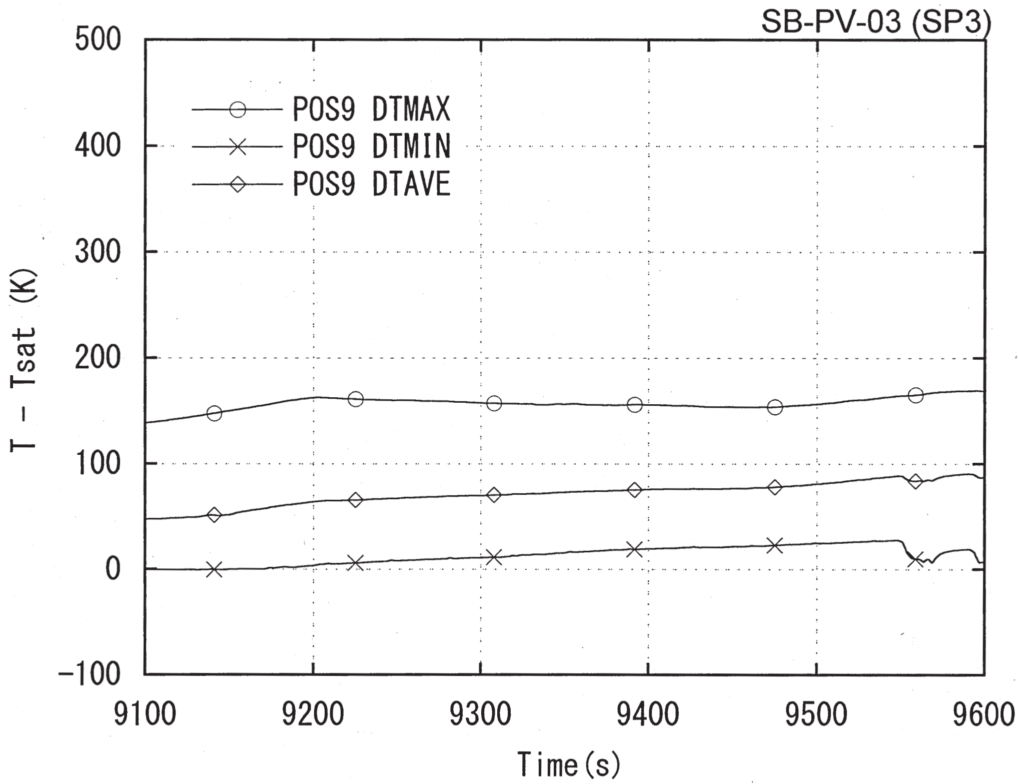

Fig.4.9-11 Distribution of heater rod temperature rises at Pos.9 after 9100s in SB-PV-03 test (DT_{MAX}, DT_{MIN}, DT_{AVE})

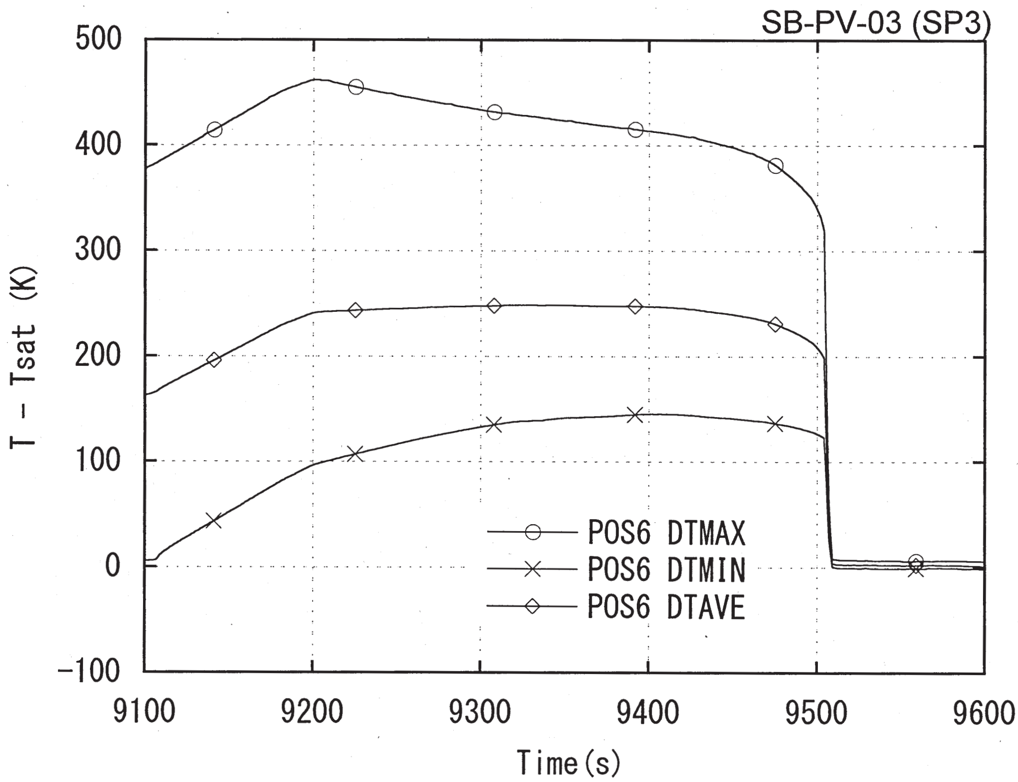

Fig.4.9-12 Distribution of heater rod temperature rises at Pos.6 after 9100s with maximum temperature rise in SB-PV-03 test (DT_{MAX}, DT_{MIN}, DT_{AVE})

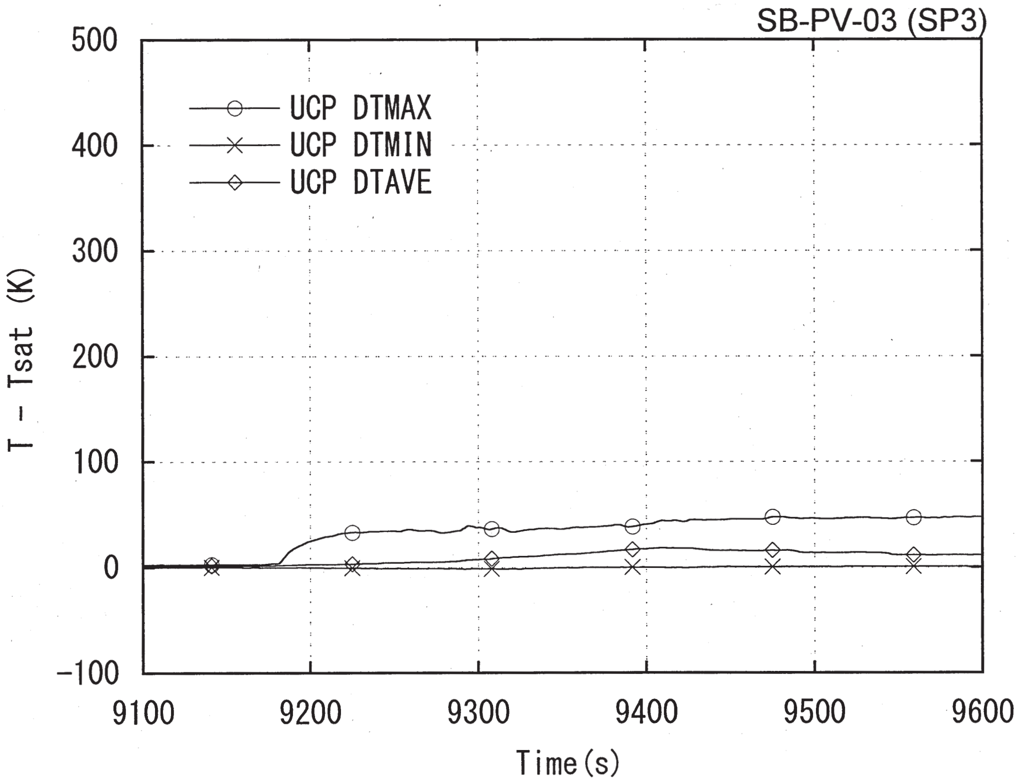

Fig.4.9-13 Distribution of all CET temperature rises above saturation temperature after 9100s in SB-PV-03 test (DT_{MAX}, DT_{MIN}, DT_{AVE})

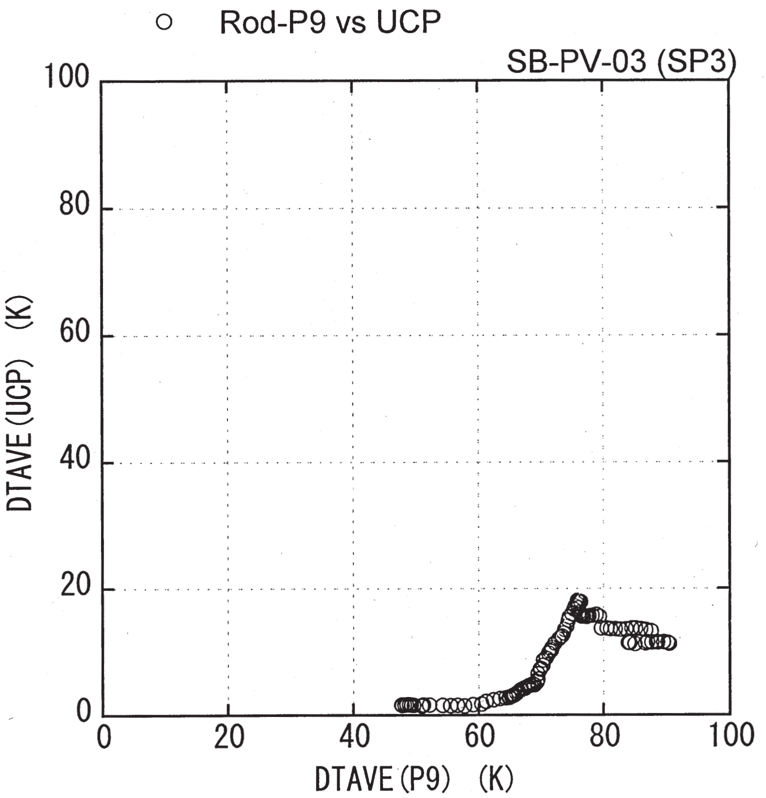

Fig.4.9-14 A relation of temperature rises at heater rod Pos.9, (Ave) and CET (Ave) after 9100s in SB-PV-03 test

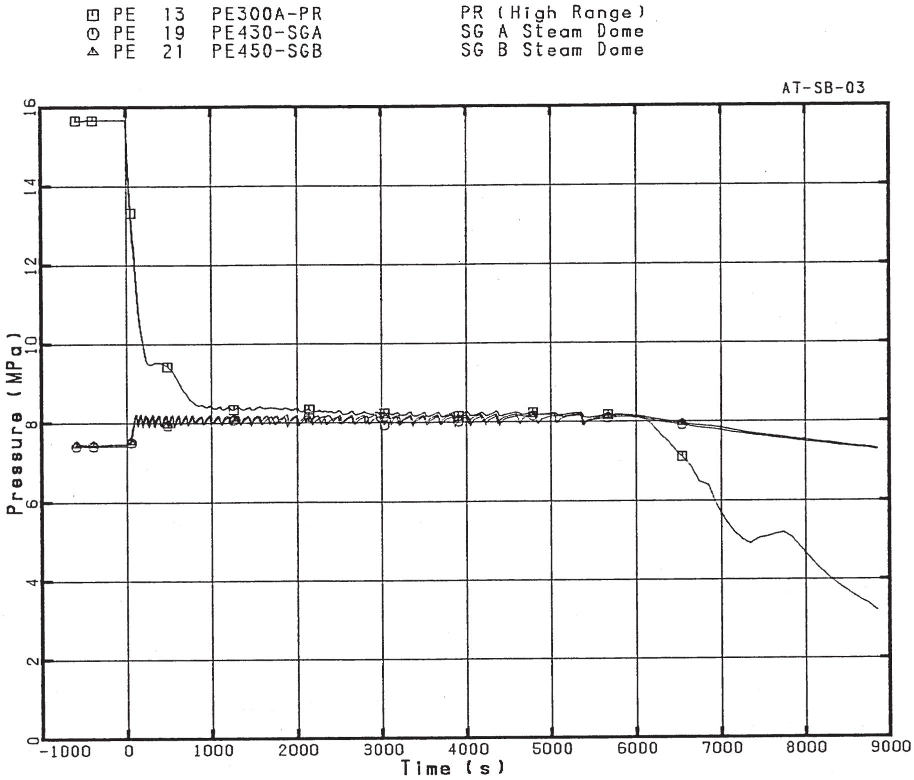

Fig.4.10-1 Primary and secondary pressures in LSTF TMI-type test (AT-SB-03)

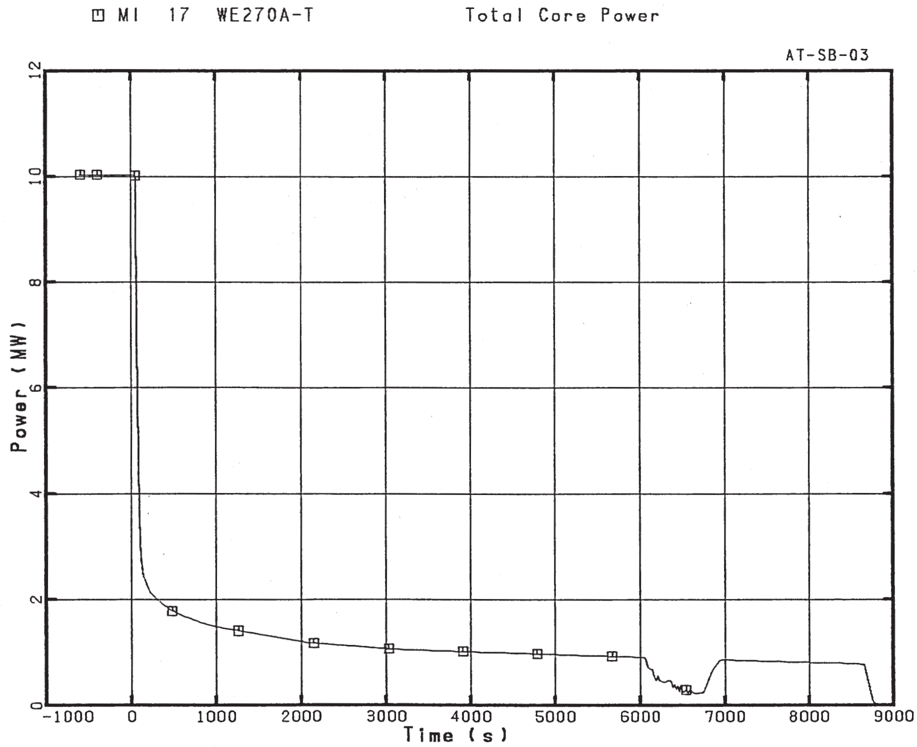

Fig.4.10-2 Core power decay curve in AT-SB-03 test

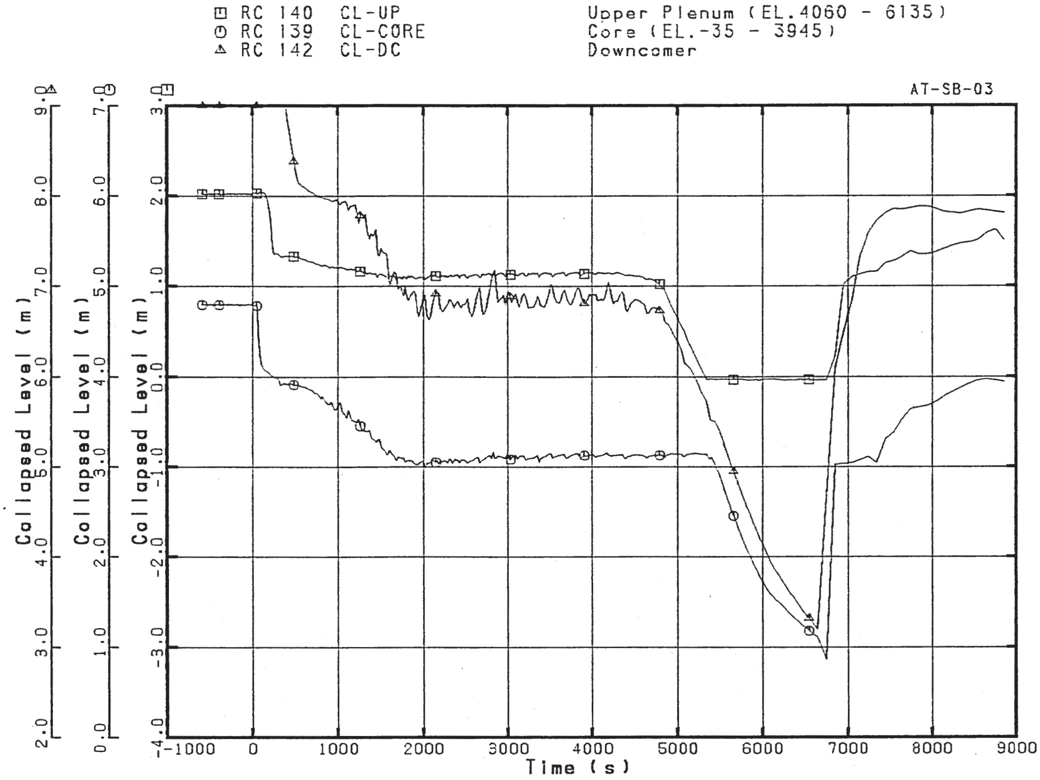

Fig.4.10-3 PV water levels in UP, core and downcomer in AT-SB-03 test

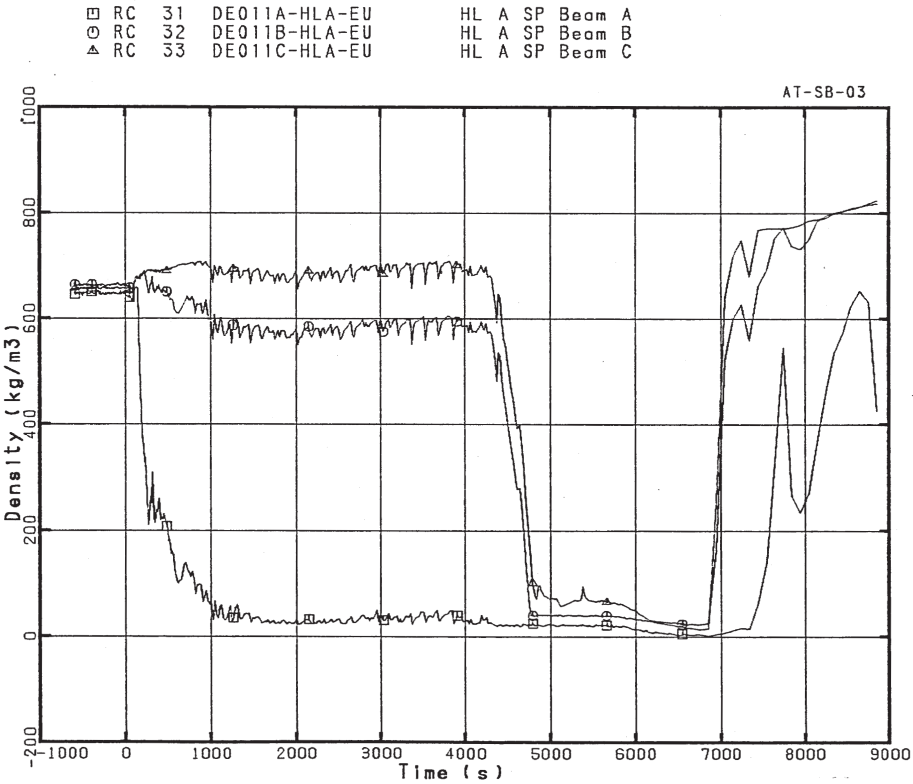

Fig.4.10-4 Fluid density data in intact loop hot leg (HL-A) in AT-SB-03test

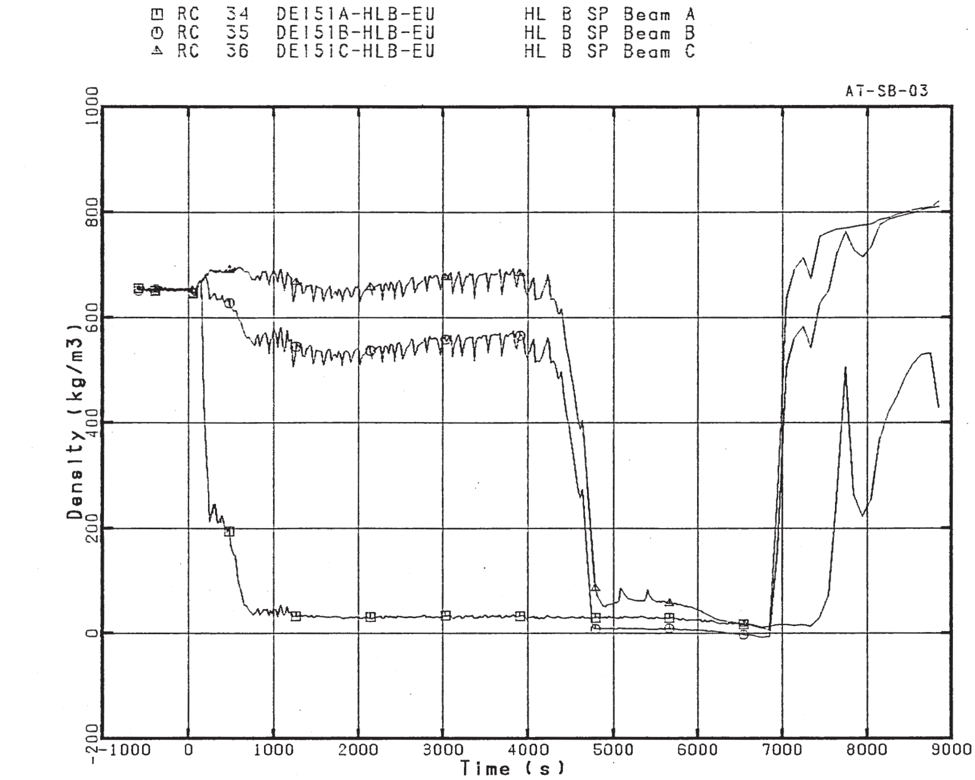

Fig.4.10-5 Fluid density data in broken loop hot leg (HL-B) in AT-SB-03test

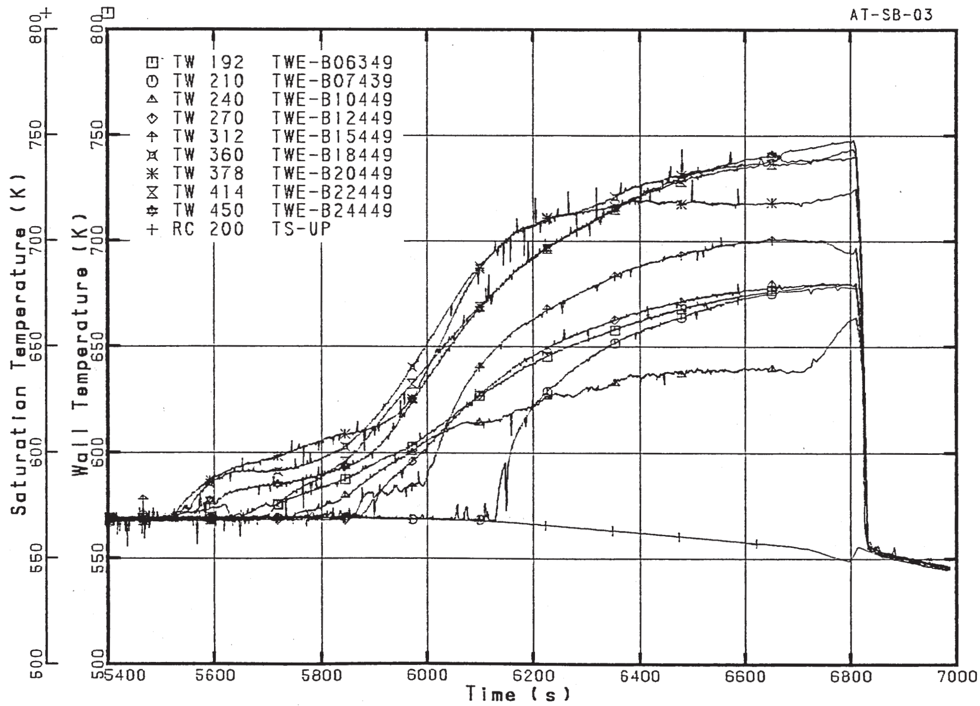

(1) Heater rod temperatures at Pos.9 (core top)

Fig.4.10-6 Heater rod surface temperatures during boil-off in AT-SB-03 test

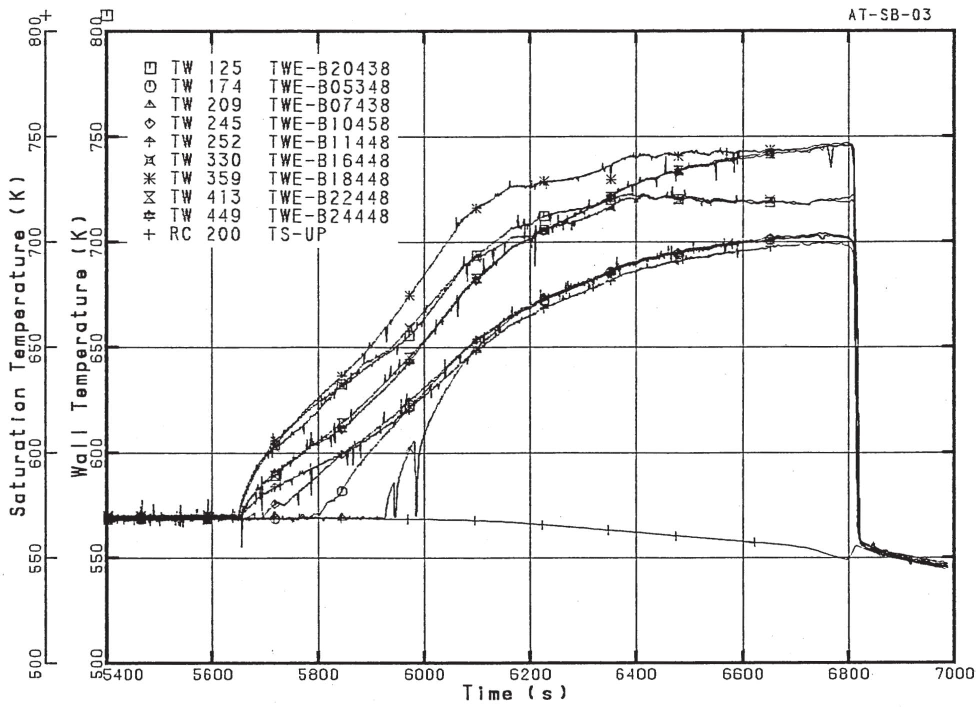

(2) Heater rod temperatures at Pos.8

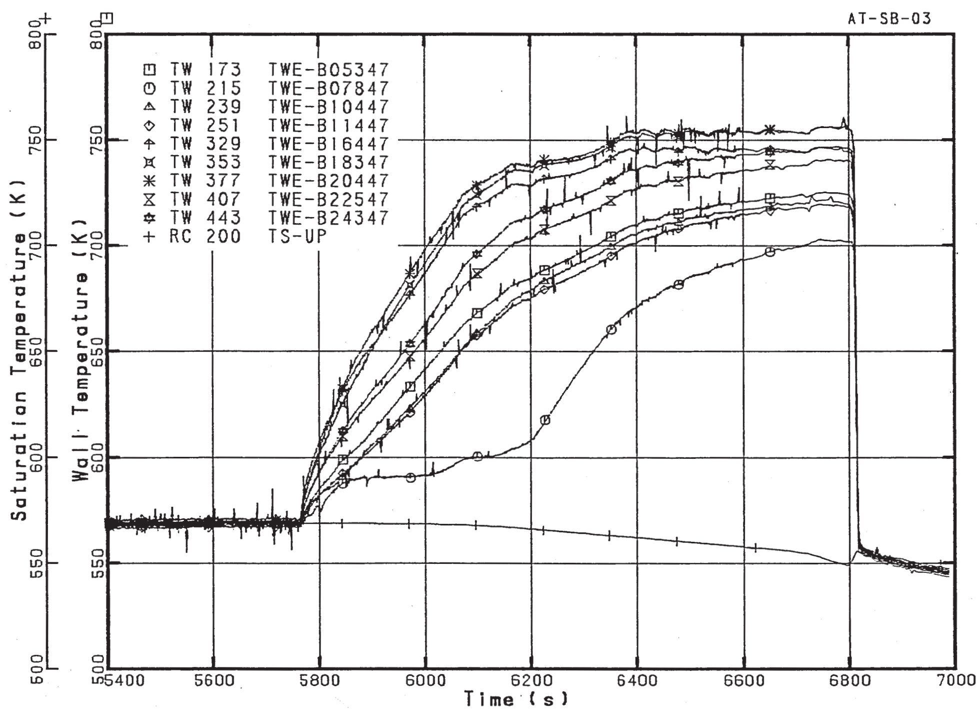

(3) Heater rod temperatures at Pos.7 with PCT measurement

Fig.4.10-6 Heater rod surface temperatures during boil-off in AT-SB-03 test

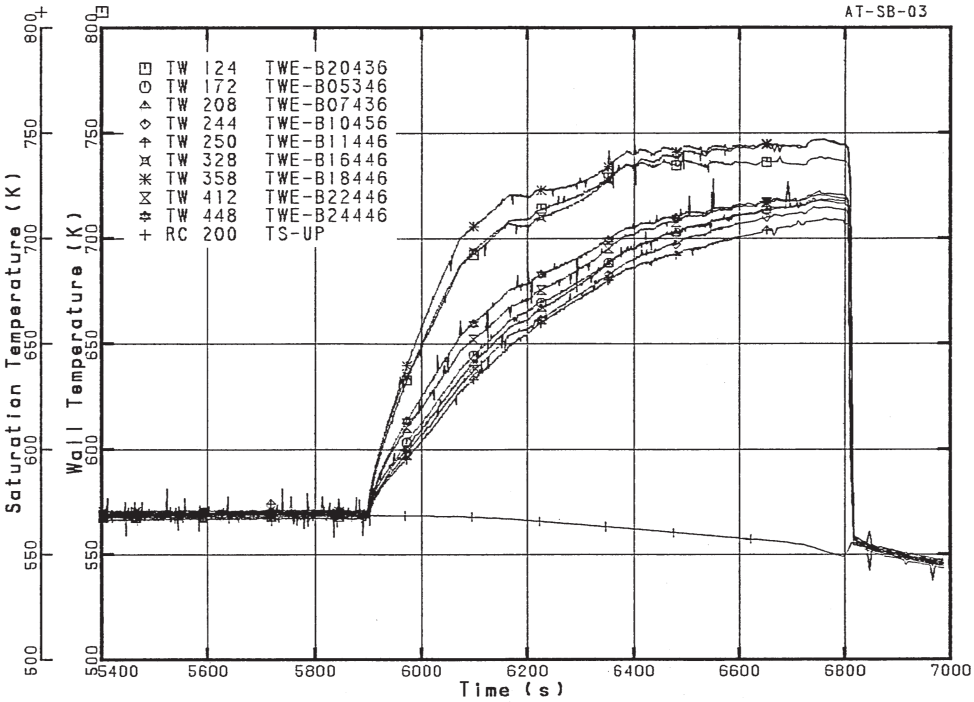

(4) Heater rod temperatures at Pos.6

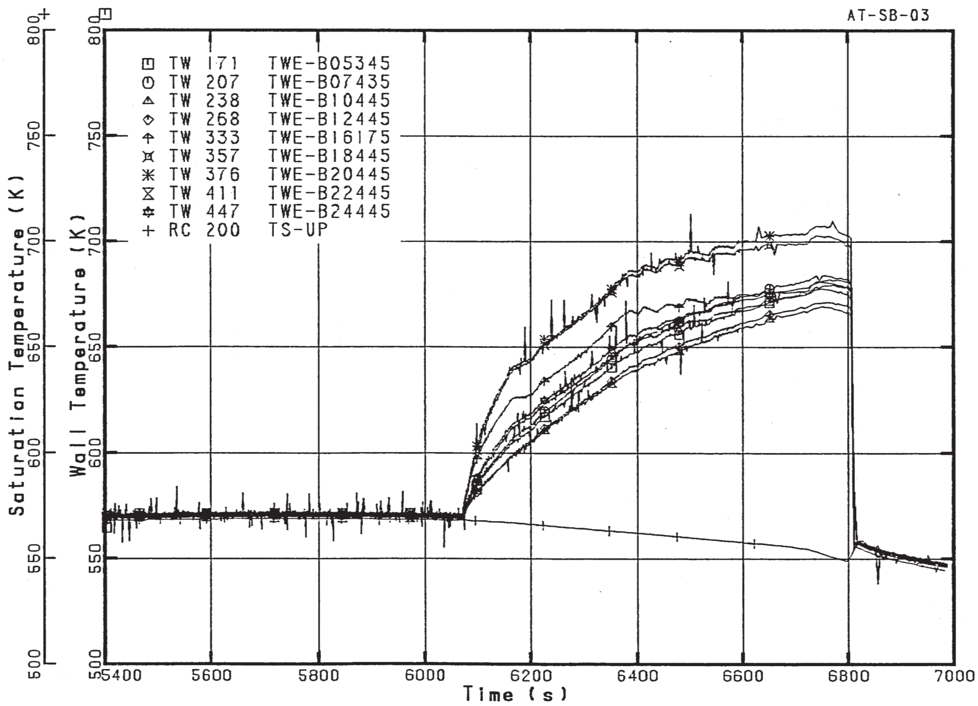

(5) Heater rod temperatures at Pos.5 (core middle height)

Fig.4.10-6 Heater rod surface temperatures during boil-off in AT-SB-03 test

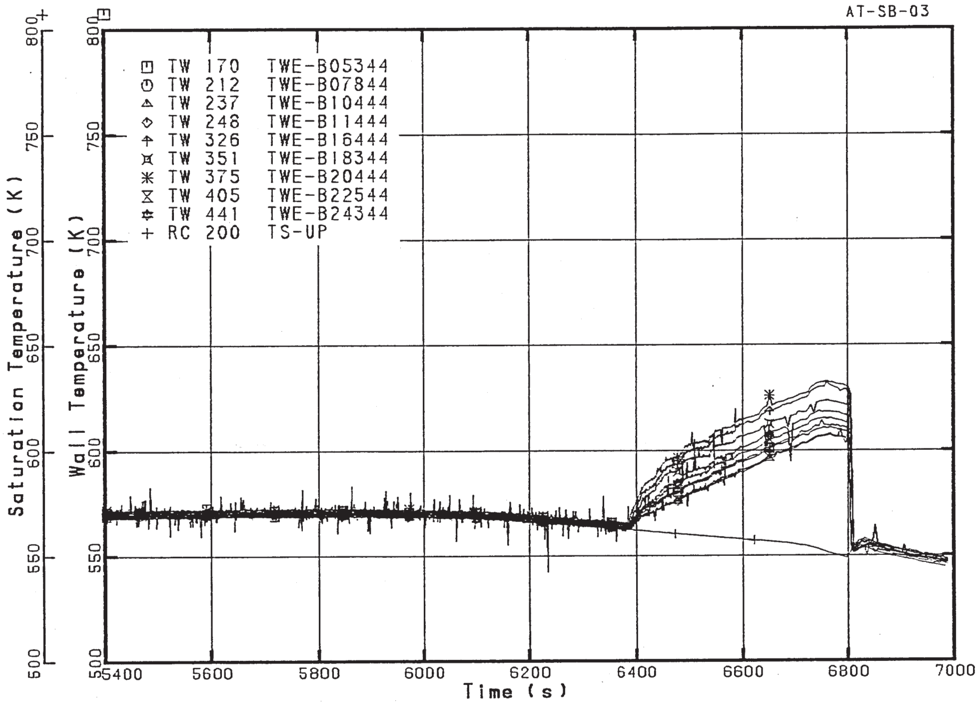

(6) Heater rod temperatures at Pos.4

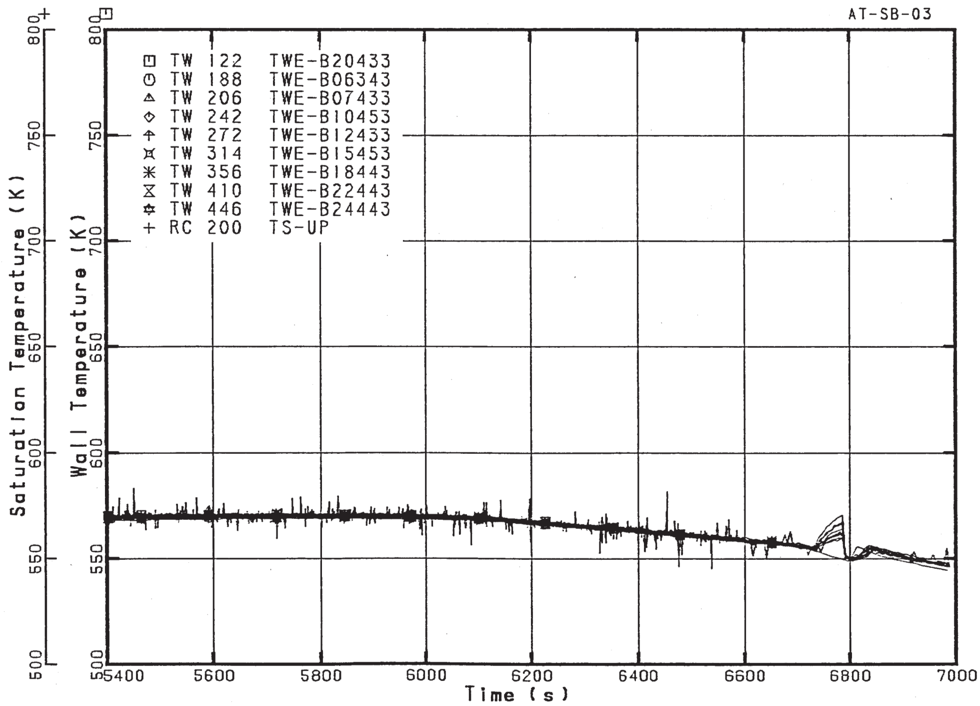

(7) Heater rod temperatures at Pos.3

Fig.4.10-6 Heater rod surface temperatures during boil-off in AT-SB-03 test

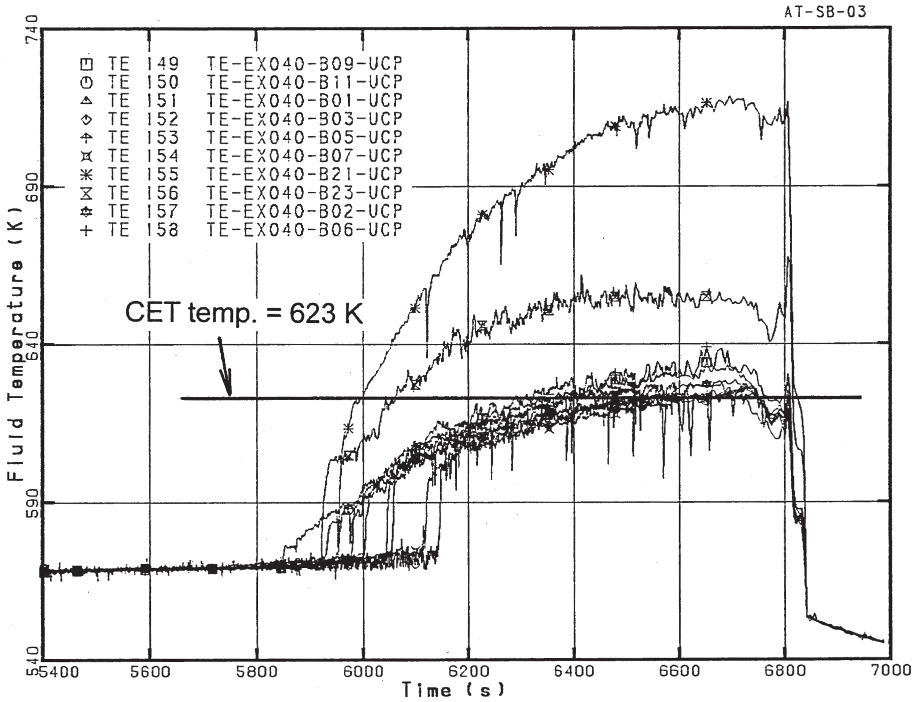

(1) CET temperatures above peripheral and central rod bundles

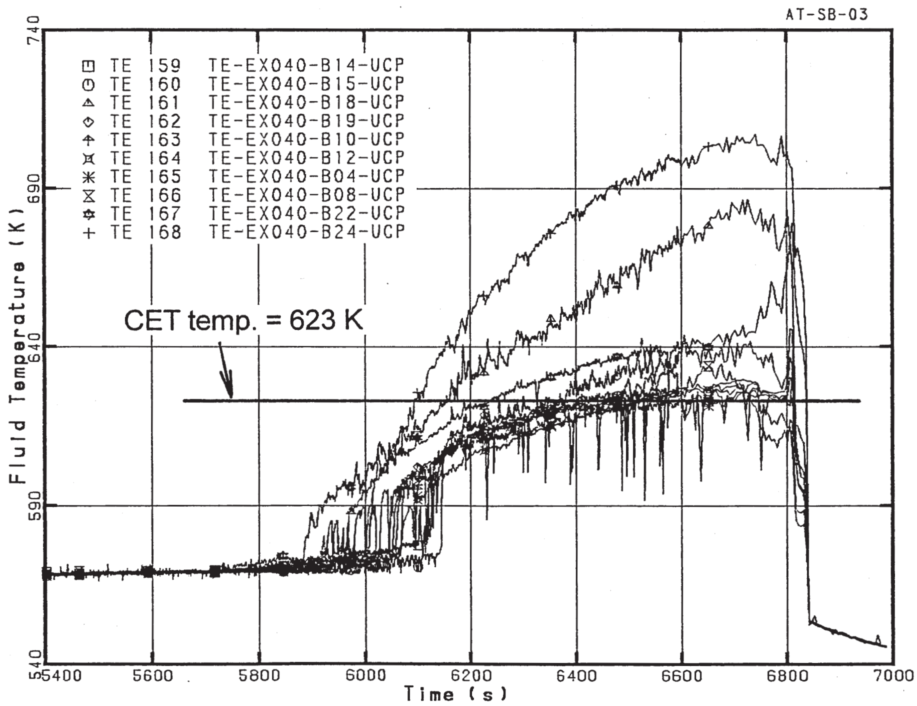

(2) CET temperatures above high-power and other rod bundles

Fig.4.10-7 CET temperatures during boil-off process in AT-SB-03 test

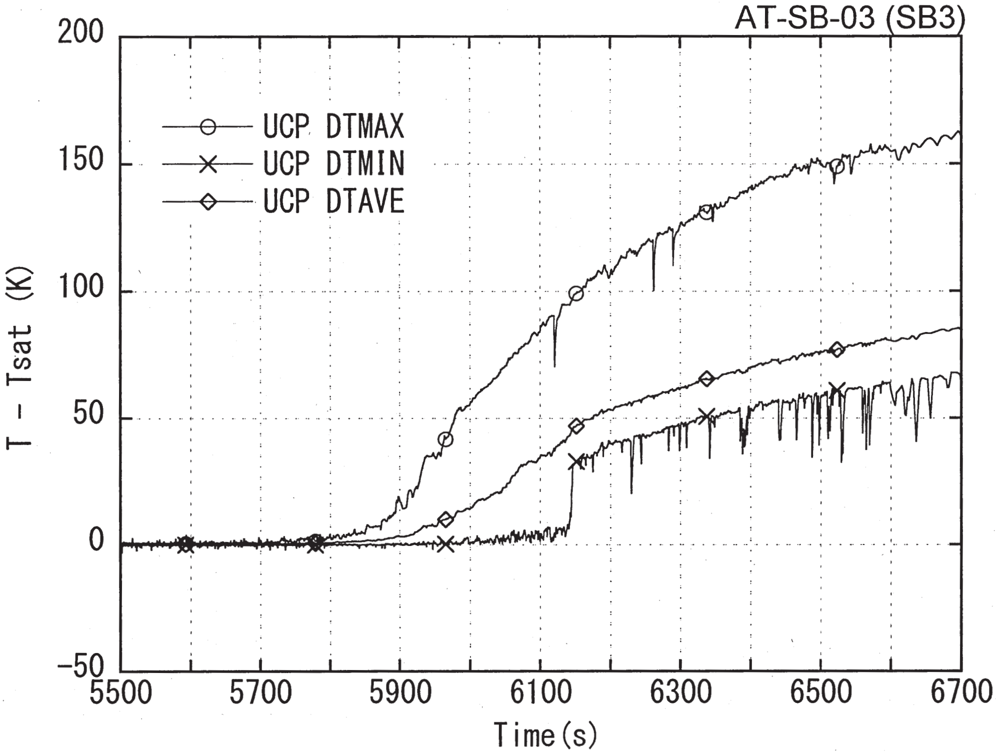

Fig.4.10-8 Distribution of all CET temperature rises above saturation temperature in AT-SB-03 test (DT_{MAX}, DT_{MIN}, DT_{AVE})

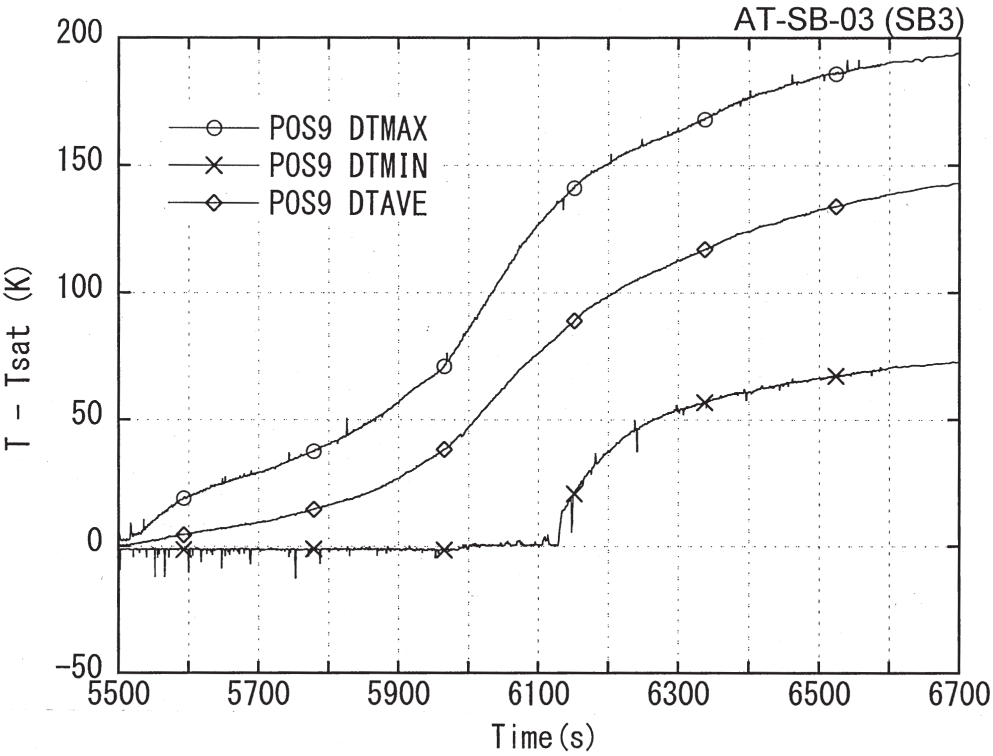

Fig.4.10-9 Distribution of heater rod temperature rises at Pos.9 in AT-SB-03 test (DT_{MAX}, DT_{MIN}, DT_{AVE})

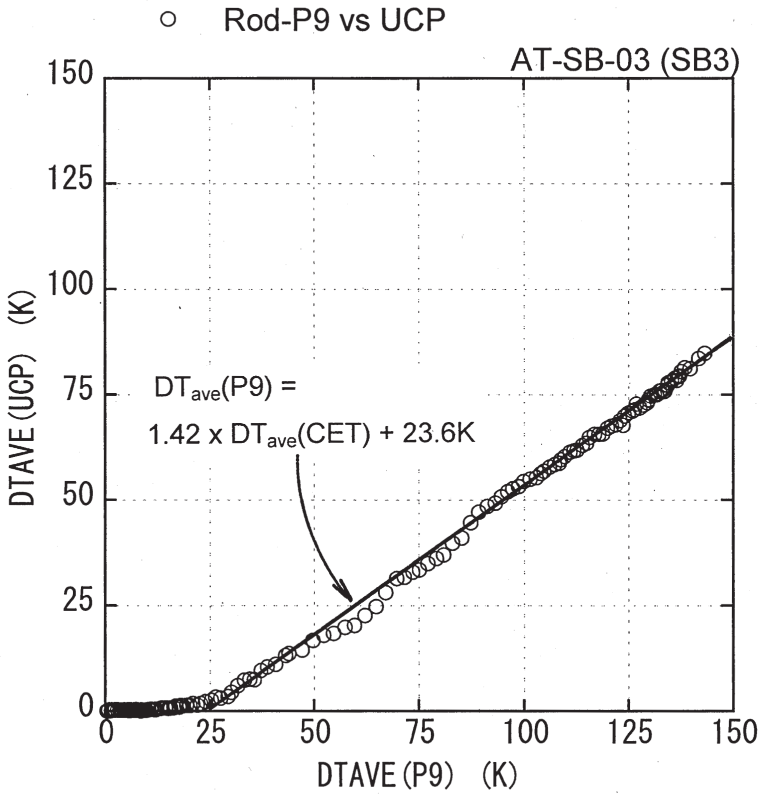

Fig.4.10-10 A relation of temperature rises at heater rod Pos.9, (Ave) and CET (Ave) in AT-SB-03 test (5500 - 6700 s)

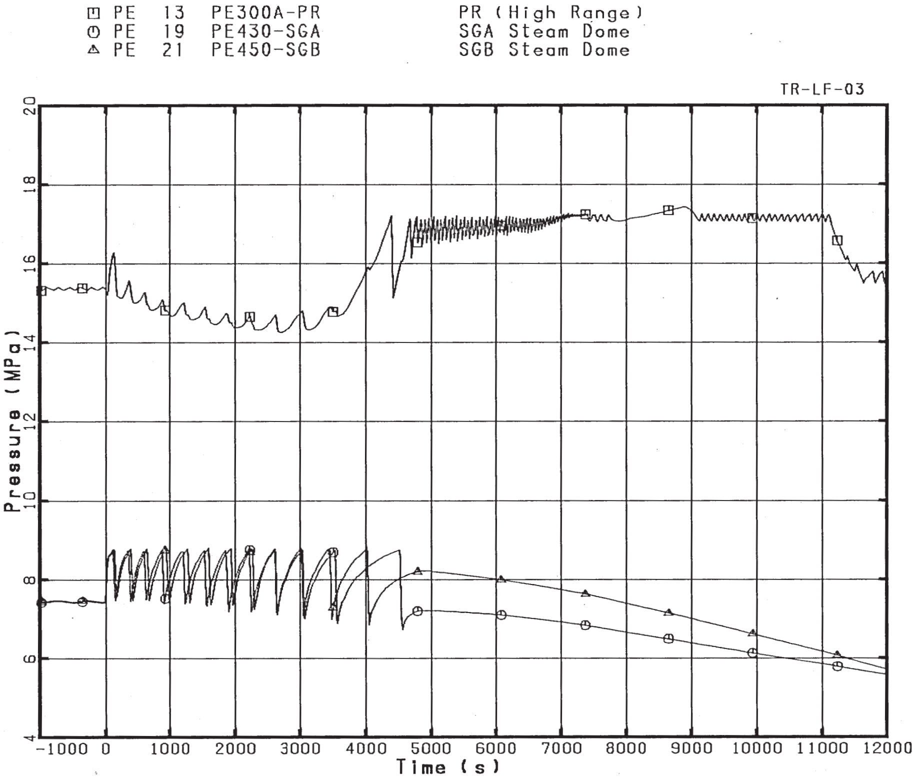

Fig.4.11-1 Primary and secondary pressures in LSTF TMLB' test (TR-LF-03)

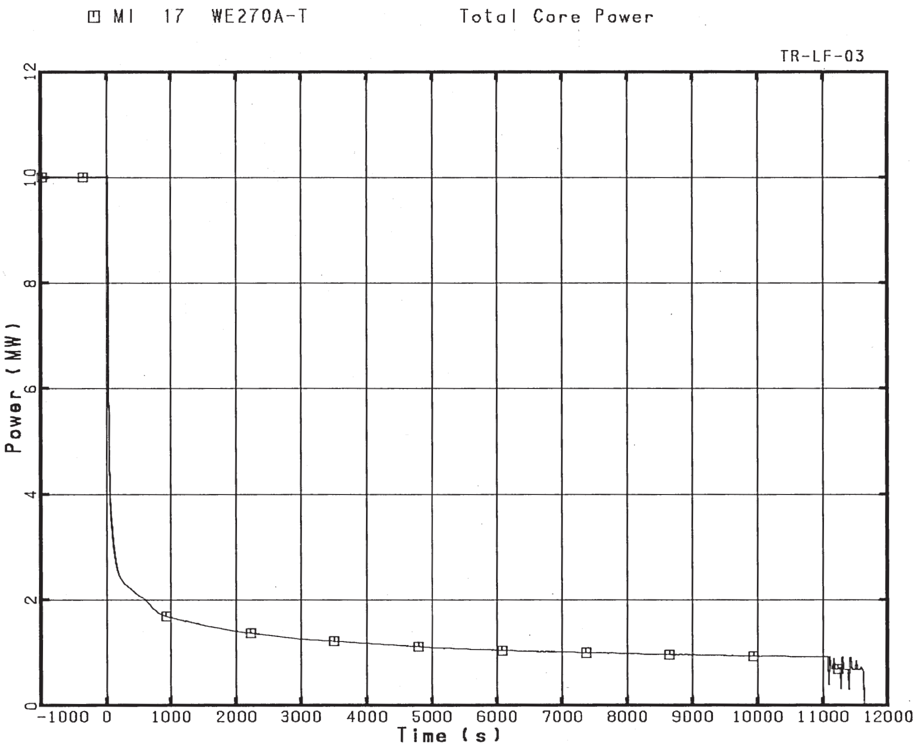

Fig.4.11-2 Core power decay curve in TR-LF-03 test

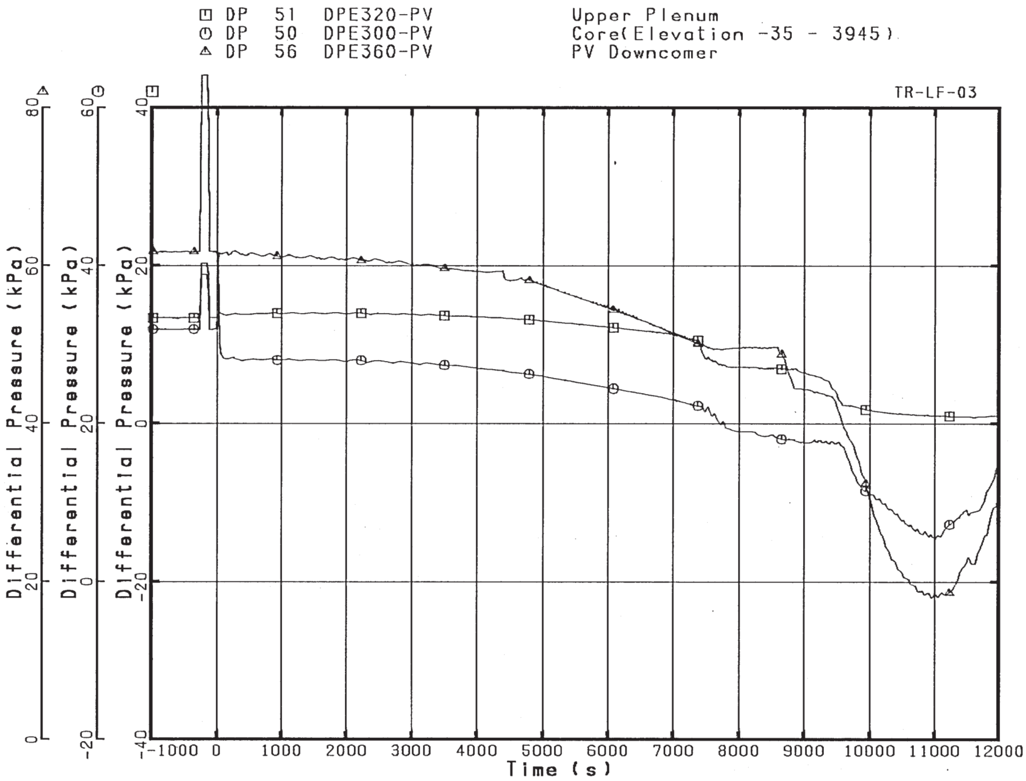

Fig.4.11-3 DP data in core, UP and downcomer in TR-LF-03 test

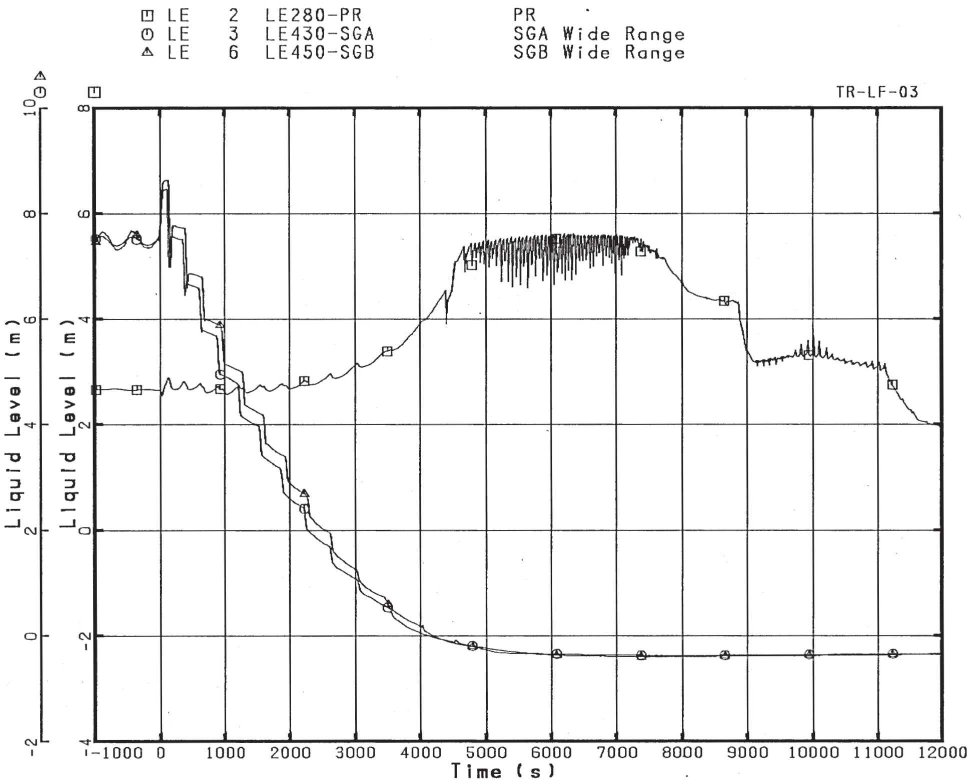

Fig.4.11-4 Water levels in pressurizer and two SG secondary sides

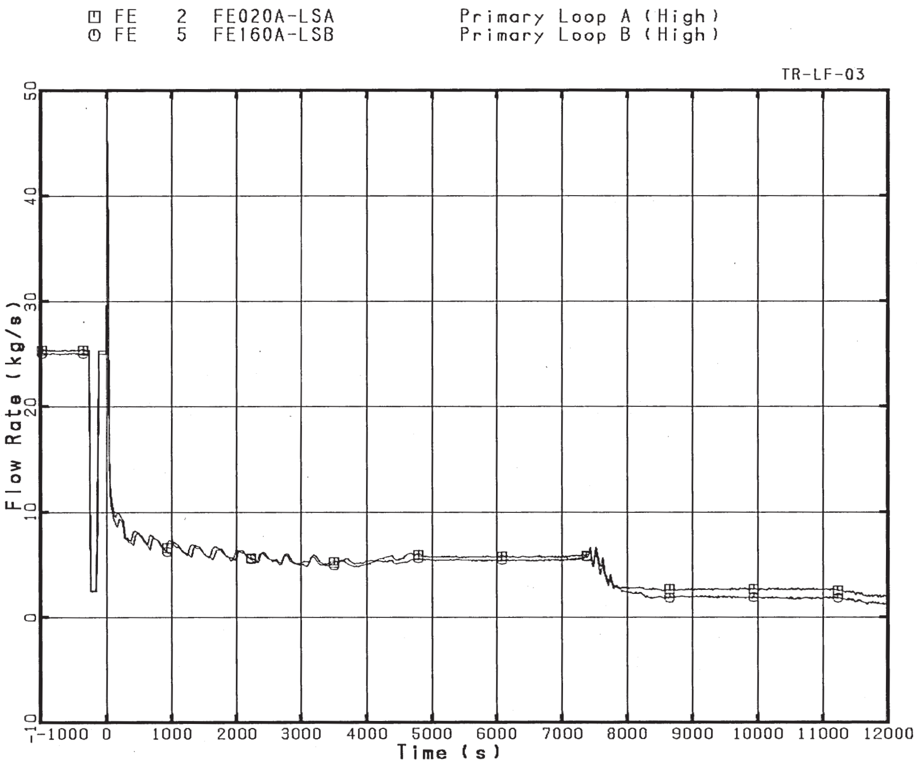

Fig.4.11-5 Primary loop flow rates in TR-LF-03 test

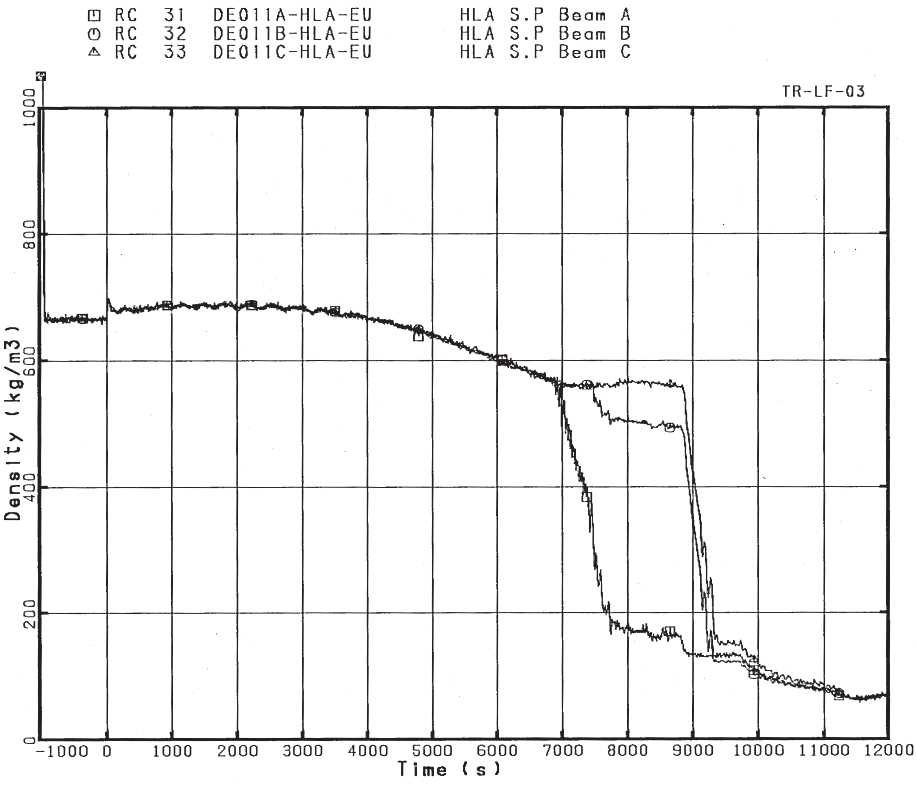

Fig.4.11-6 Fluid density data in intact loop hot leg (HL-A) in TR-LF-03 test

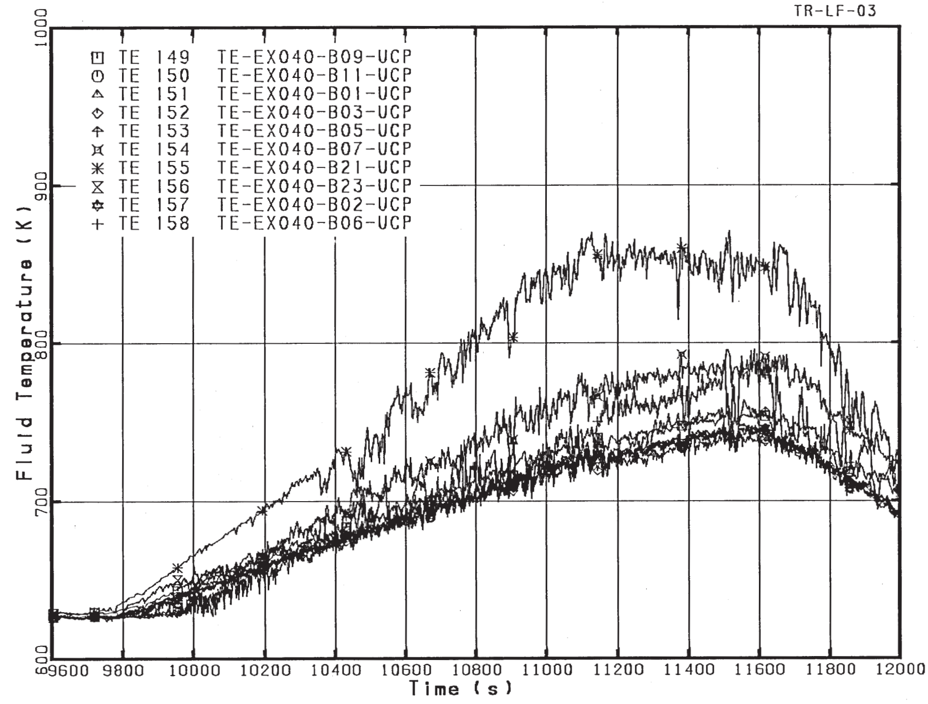

(1) CET temperatures above peripheral and central rod bundles

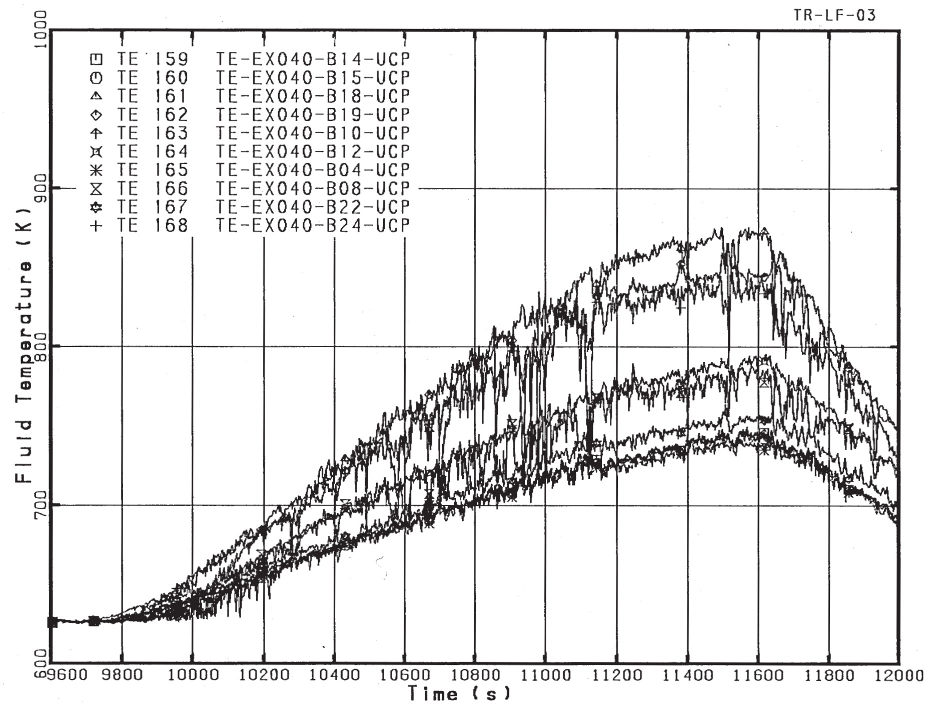

(2) CET temperatures above high-power and other rod bundles

Fig.4.11-7 CET temperatures during boil-off process in TR-LF-03 test

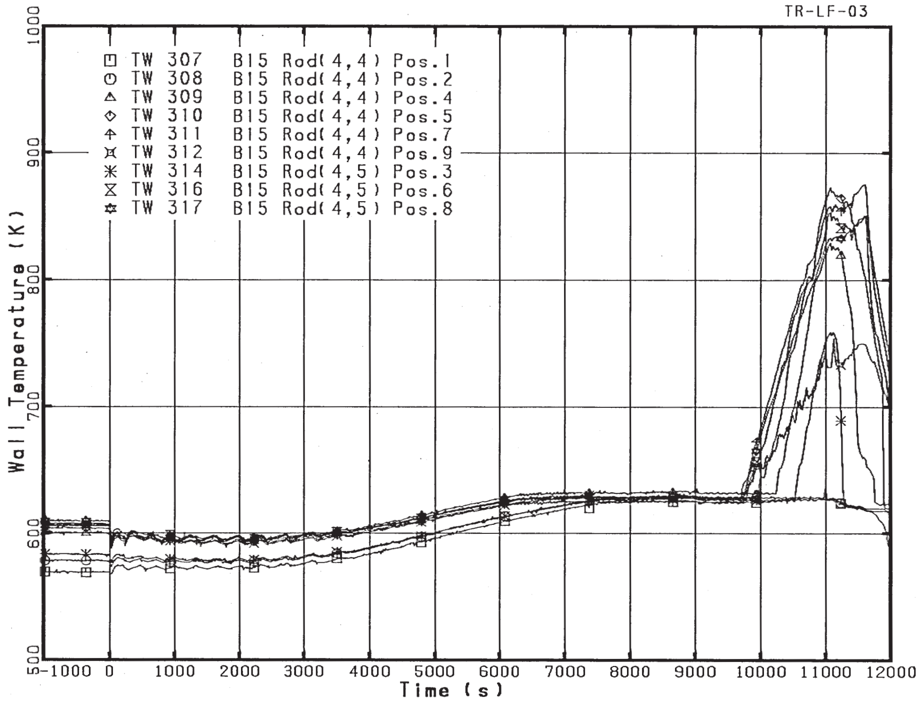

Fig.4.11-8 Representative core rod surface temperatures in TR-LF-03 test

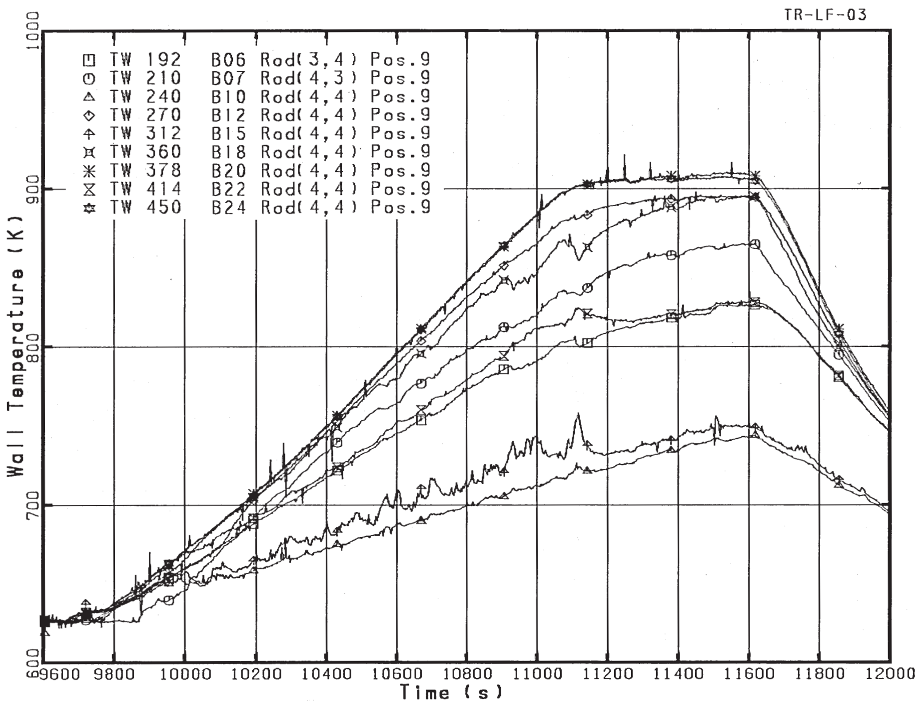

(1) Heater rod temperatures at Pos.9 (core top)

Fig.4.11-9 Heater rod temperatures during boil-off process in TR-LF-03 test

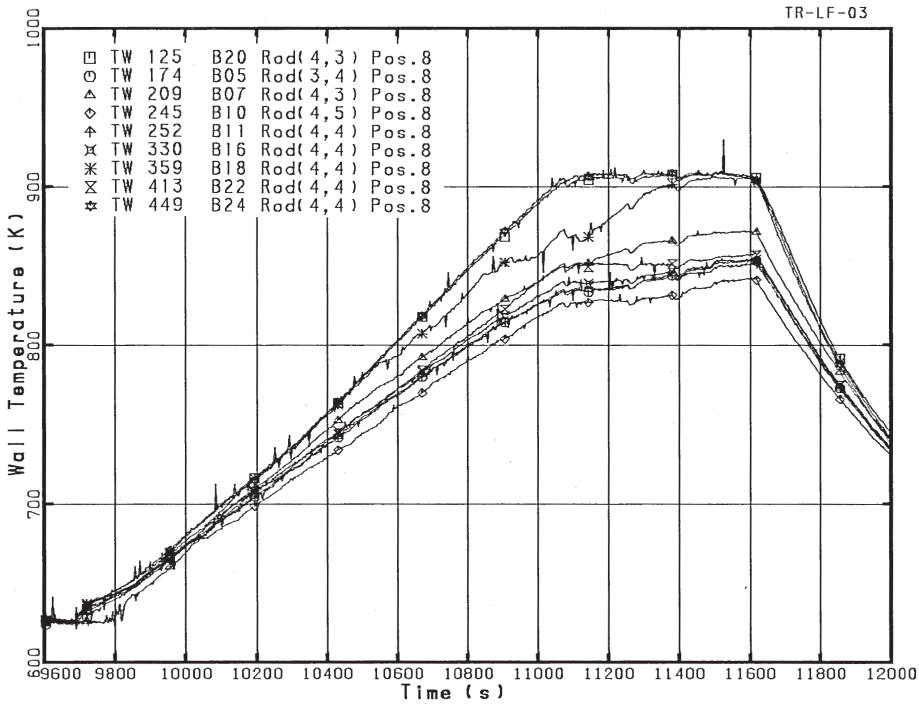

(2) Heater rod temperatures at Pos.8

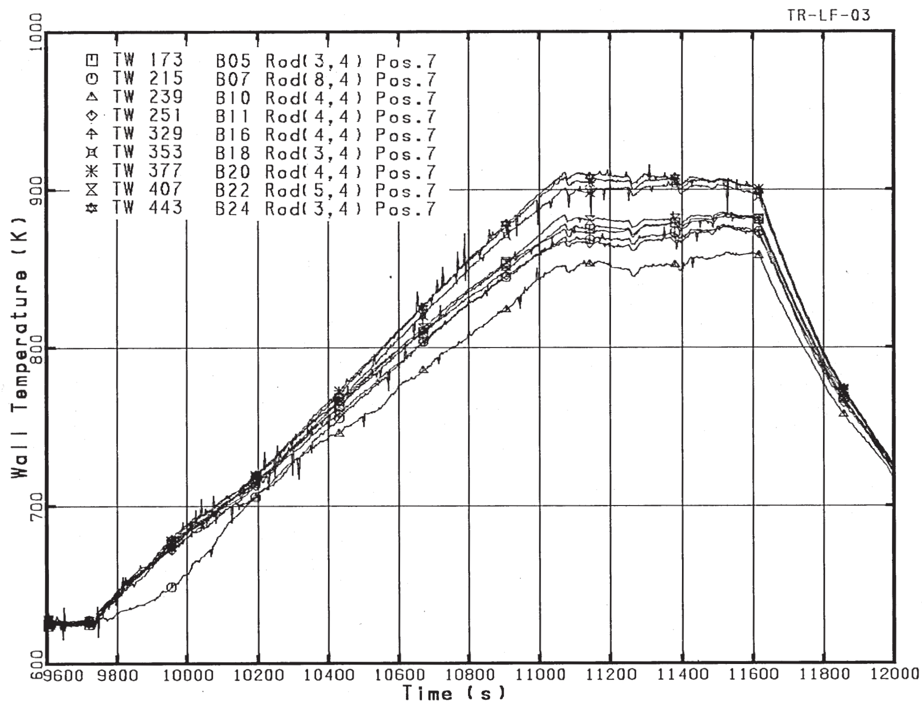

(3) Heater rod temperatures at Pos.7 with PCT measurement

Fig.4.11-9 Heater rod temperatures during boil-off process in TR-LF-03 test

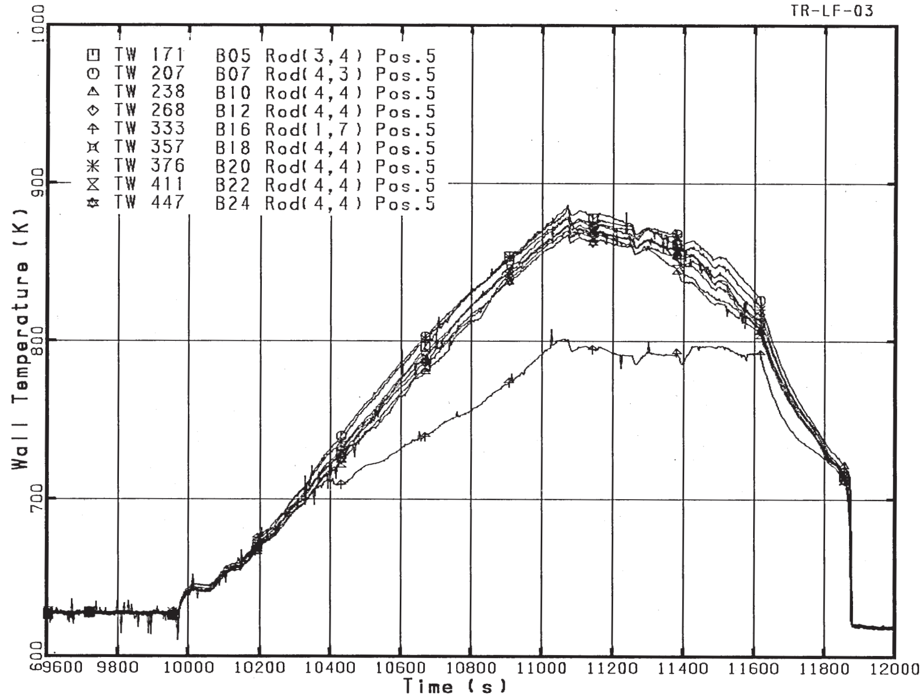

(4) Heater rod temperatures at Pos.5

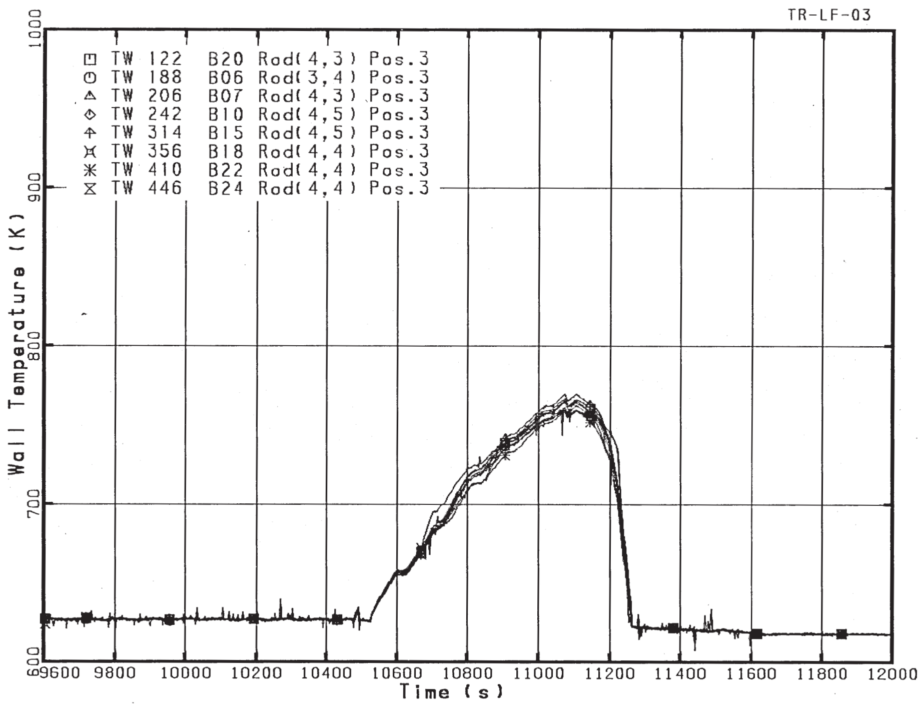

(5) Heater rod temperatures at Pos.3

Fig.4.11-9 Heater rod temperatures during boil-off process in TR-LF-03 test

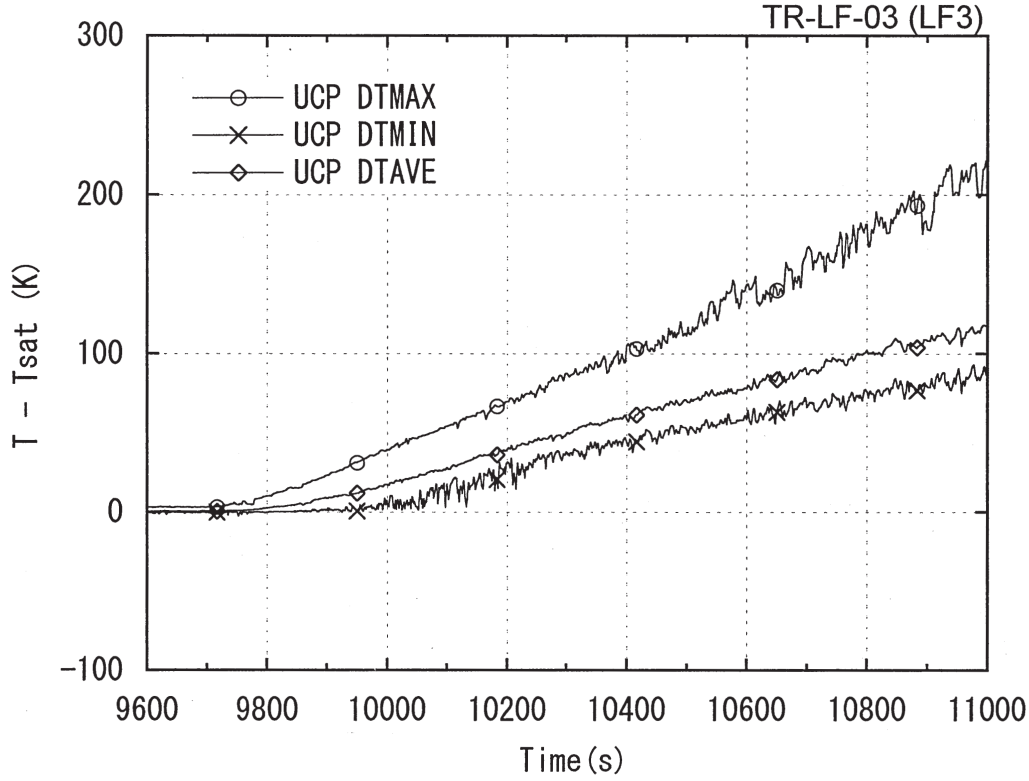

Fig.4.11-10 Distribution of all CET temperature rises above saturation temperature in TR-LF-03 test (DT_{MAX}, DT_{MIN}, DT_{AVE})

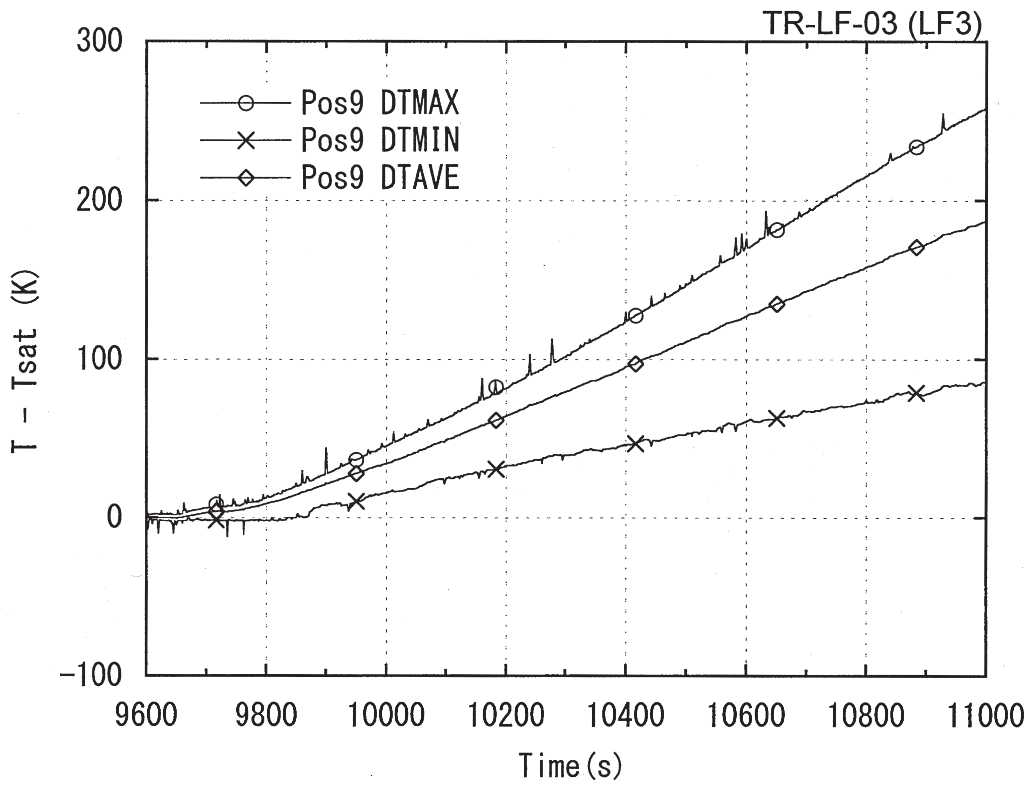

Fig.4.11-11 Distribution of heater rod temperature rises at Pos.9 in TR-LF-03 test (DT_{MAX}, DT_{MIN}, DT_{AVE})

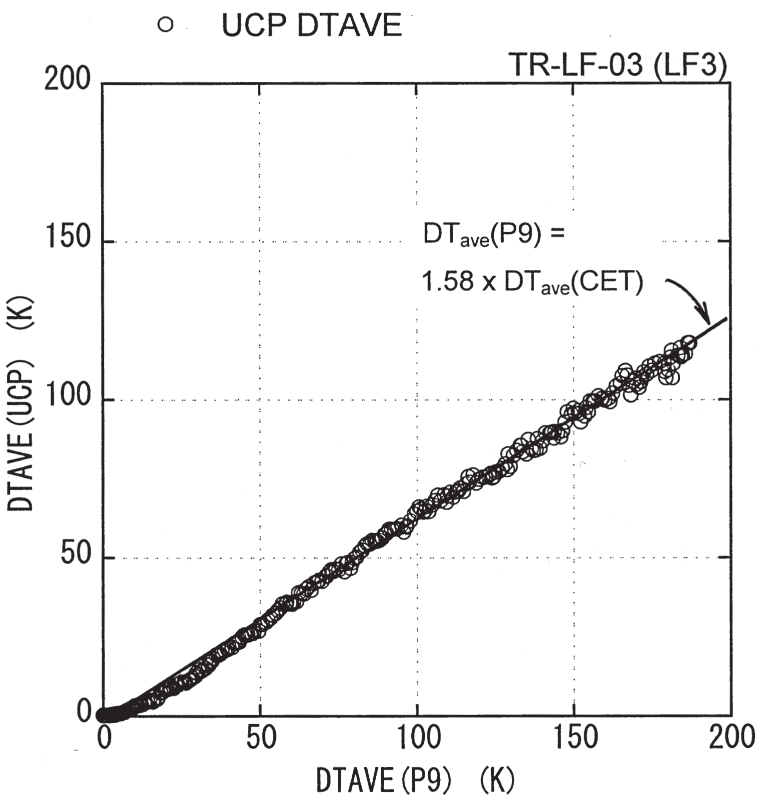

Fig.4.11-12 A relation of temperature rises at heater rod Pos.9, (Ave) and CET (Ave) in TR-LF-03 test (9600 - 11000 s)

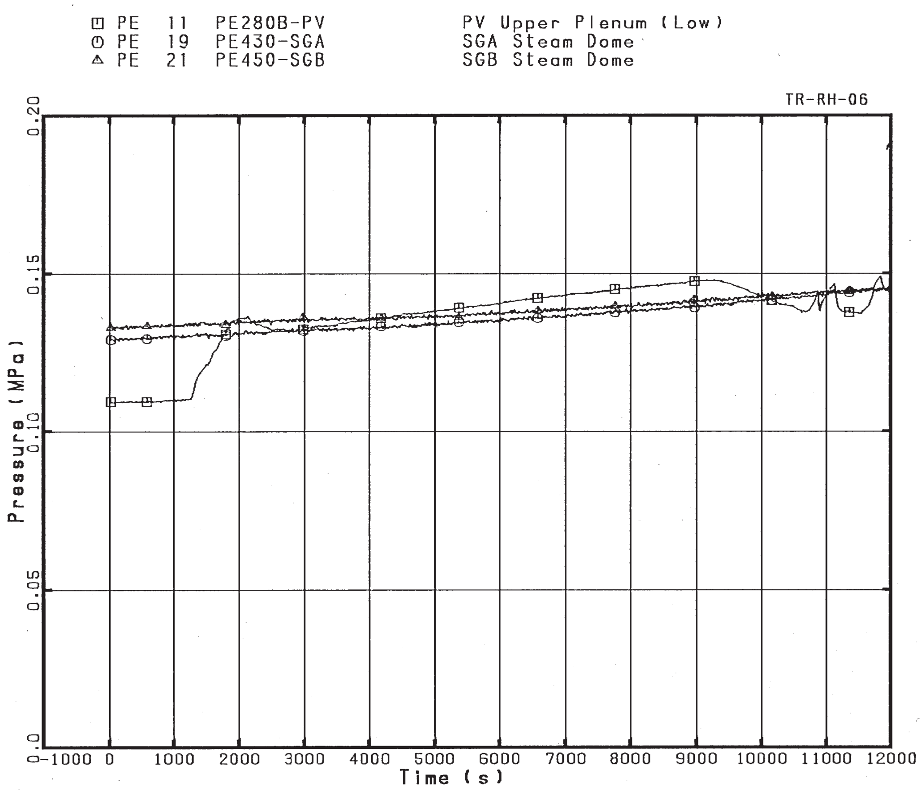

Fig.4.12-1 Primary and secondary pressures in LSTF loss-of-RHR test (TR-RH-06)

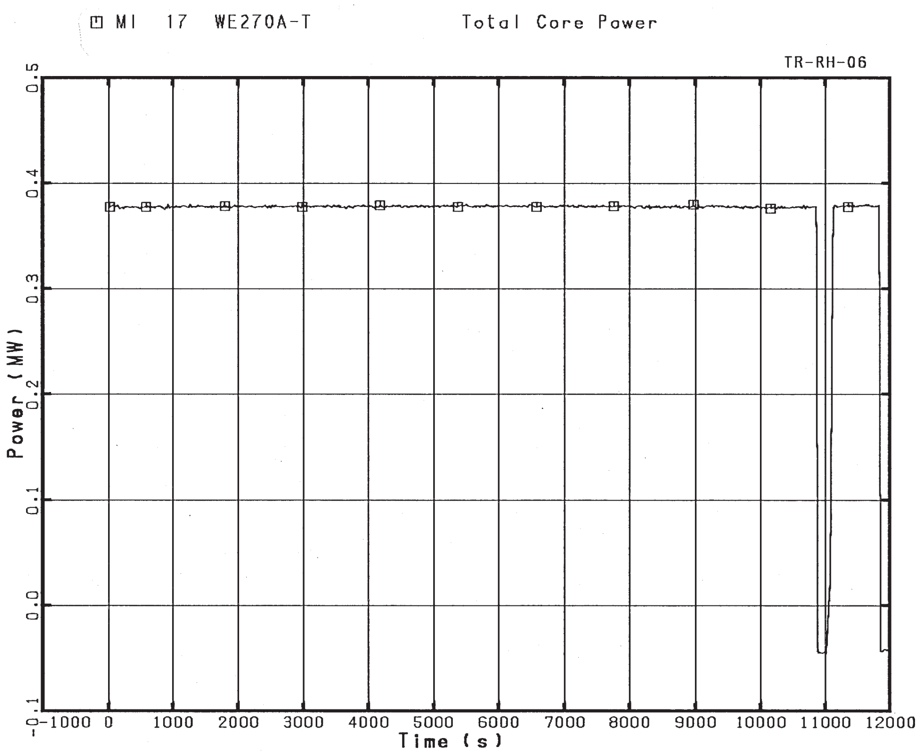

Fig.4.12-2 Core power decay curve in TR-RH-06 test

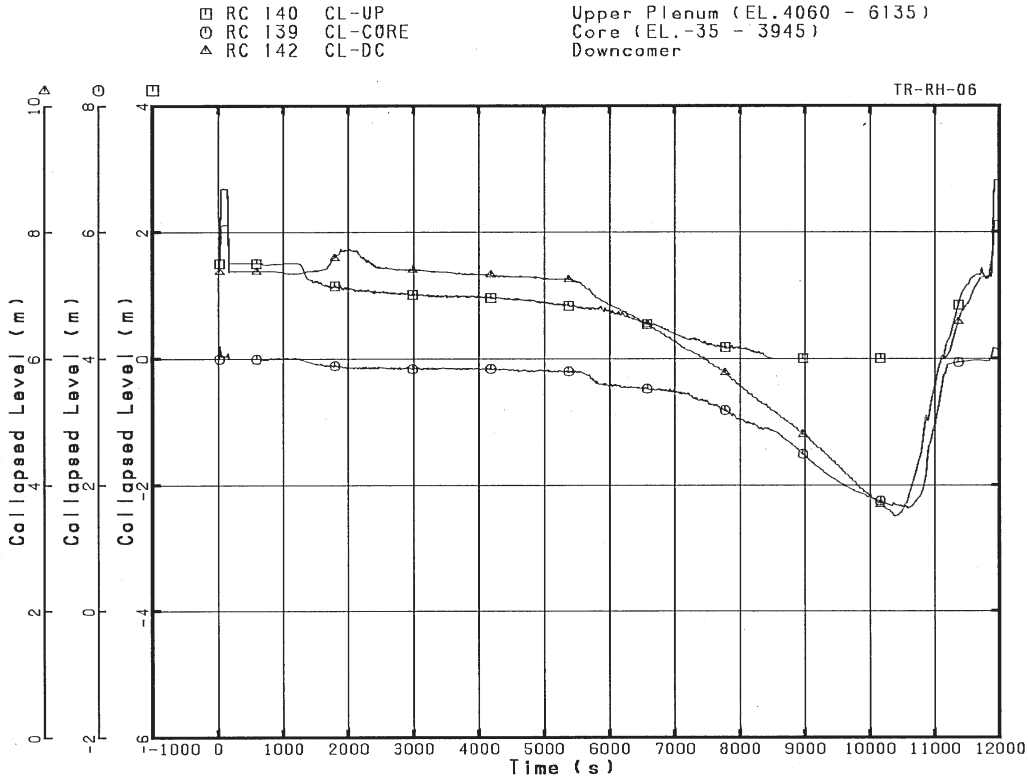

Fig.4.12-3 PV collapsed liquid levels in TR-RH-06 test

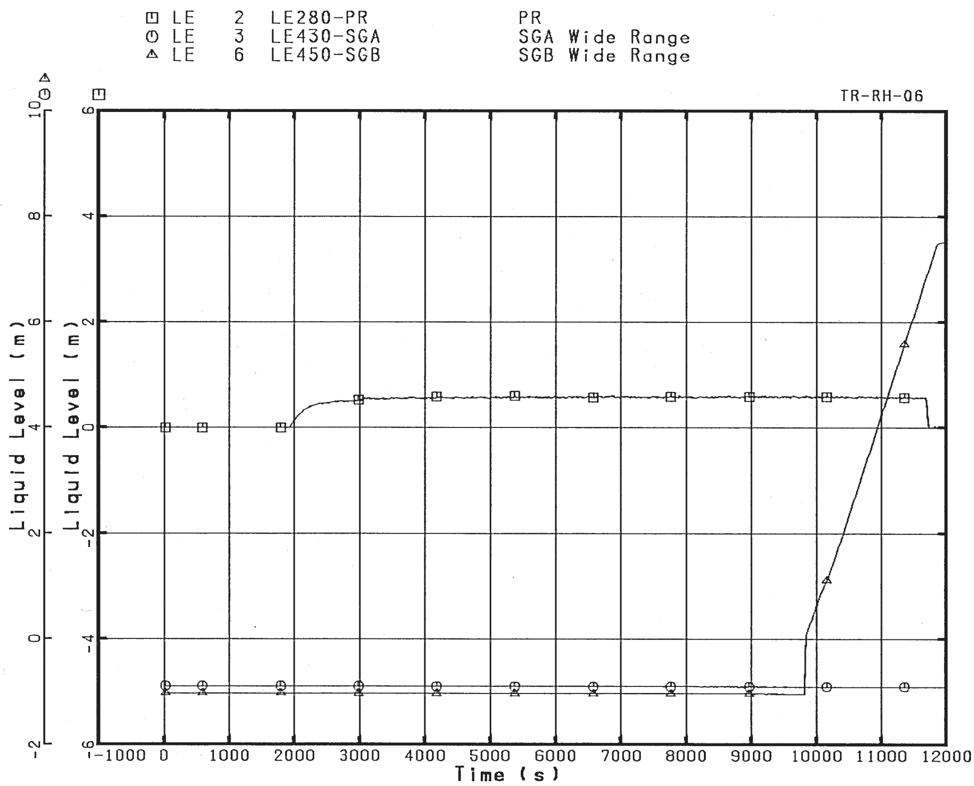

Fig.4.12-4 Water levels in pressurizer and two SG secondary sides

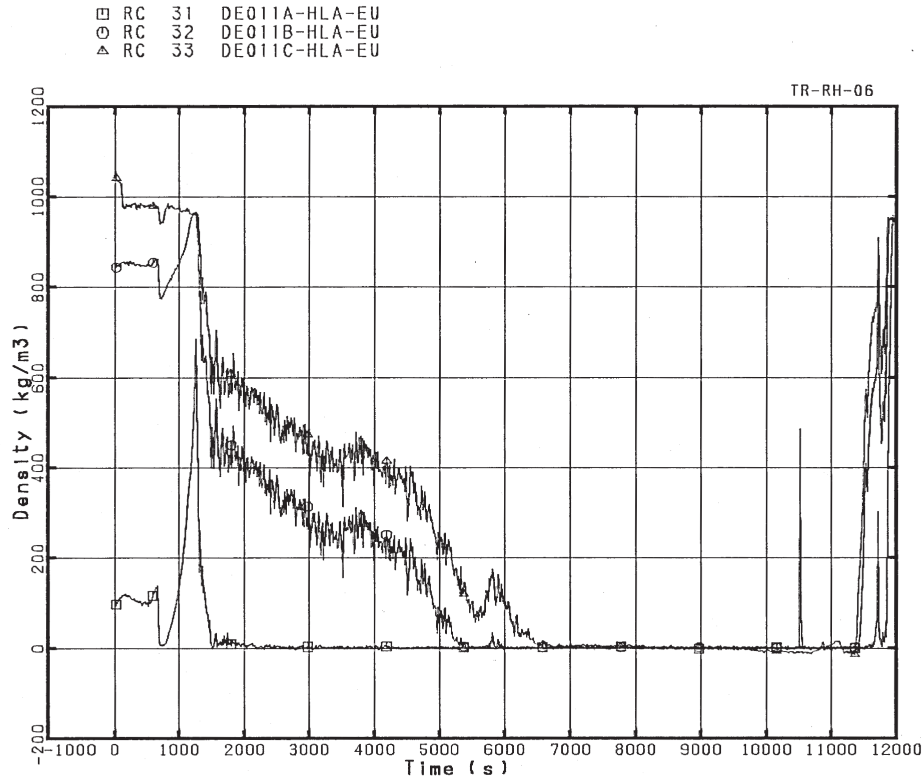

Fig.4.12-5 Fluid density data in intact loop hot leg (HL-A) in TR-RH-06 test

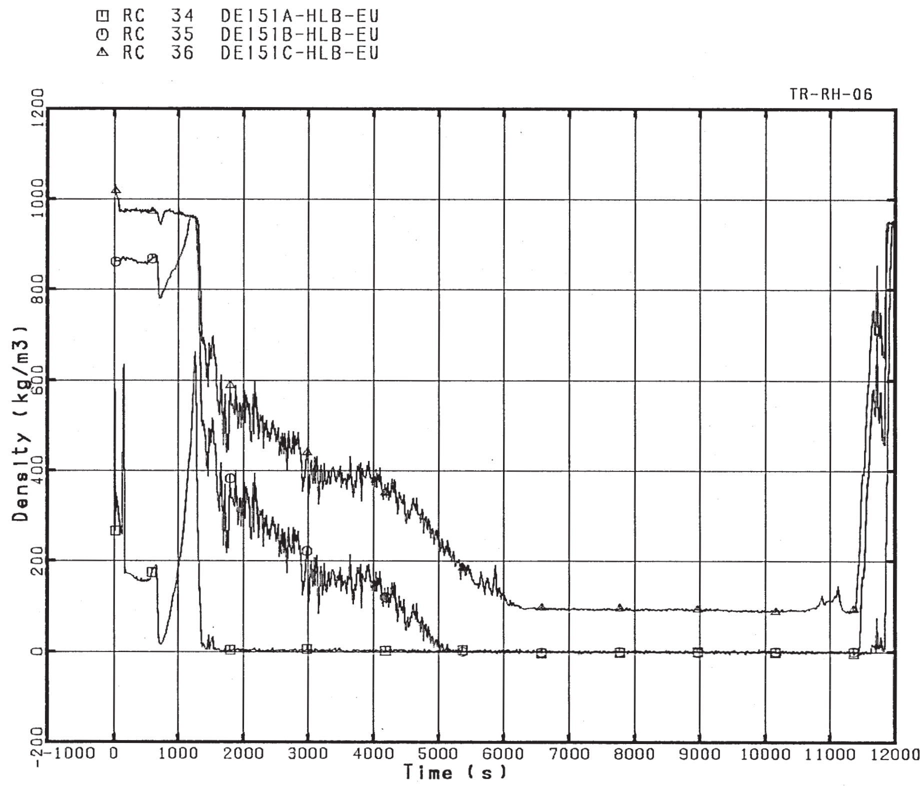

Fig.4.12-6 Fluid density data in broken loop hot leg (HL-B) in TR-RH-06 test

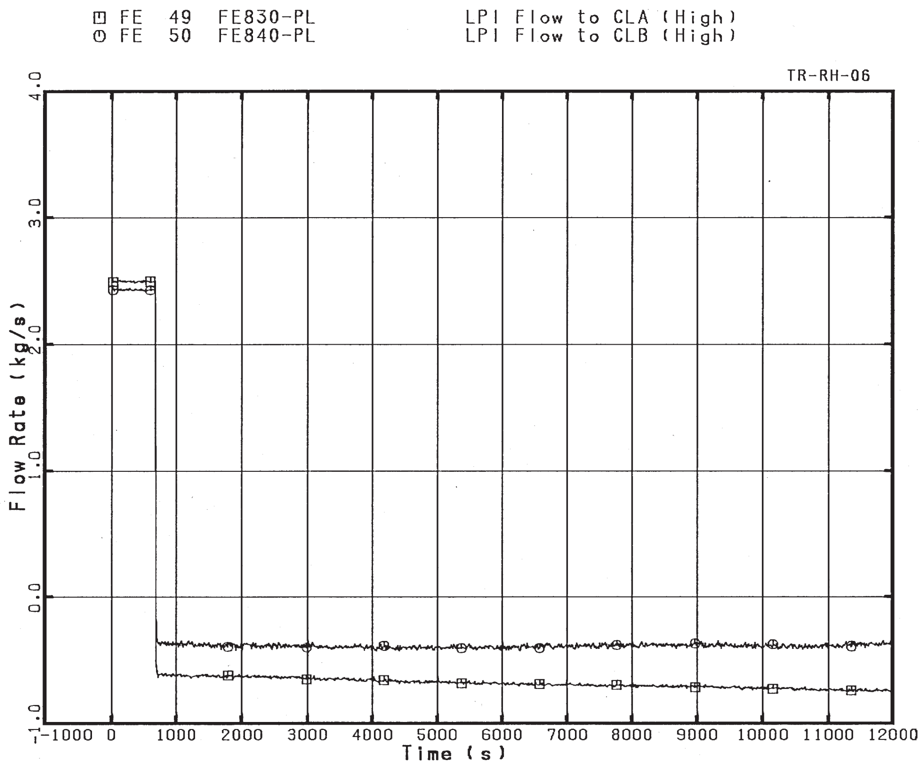

Fig.4.12-7 RHR flow rates to cold legs in TR-RH-06 test

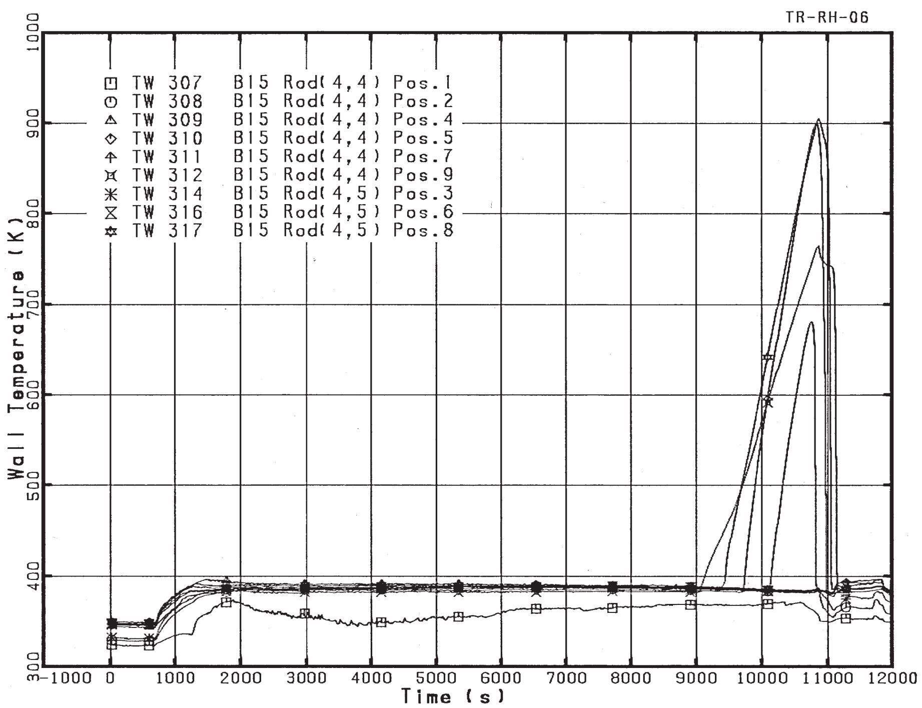

Fig.4.12-8 Representative core rod surface temperatures in TR-RH-06 test

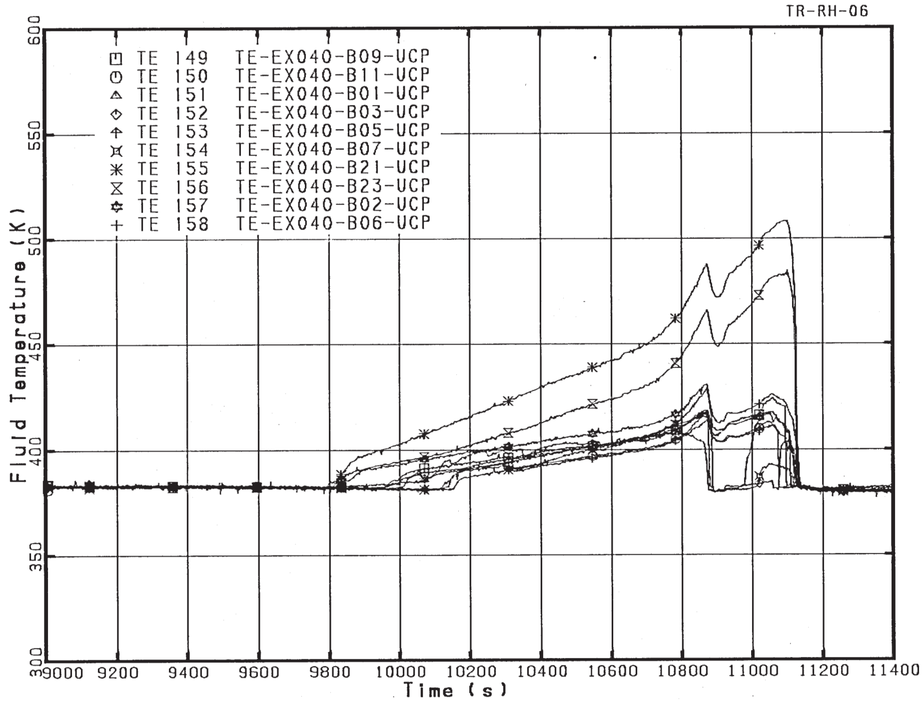

(1) CET temperatures above peripheral and central rod bundles

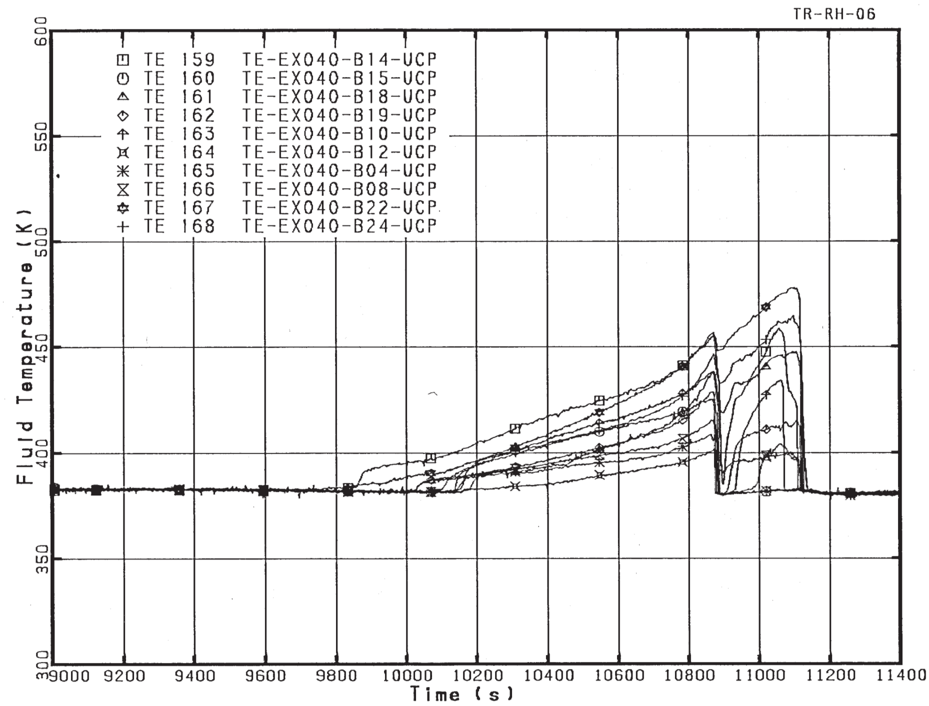

(2) CET temperatures above high-power and other rod bundles

Fig.4.12-9 CET temperatures during boil-off process in TR-RH-06 test

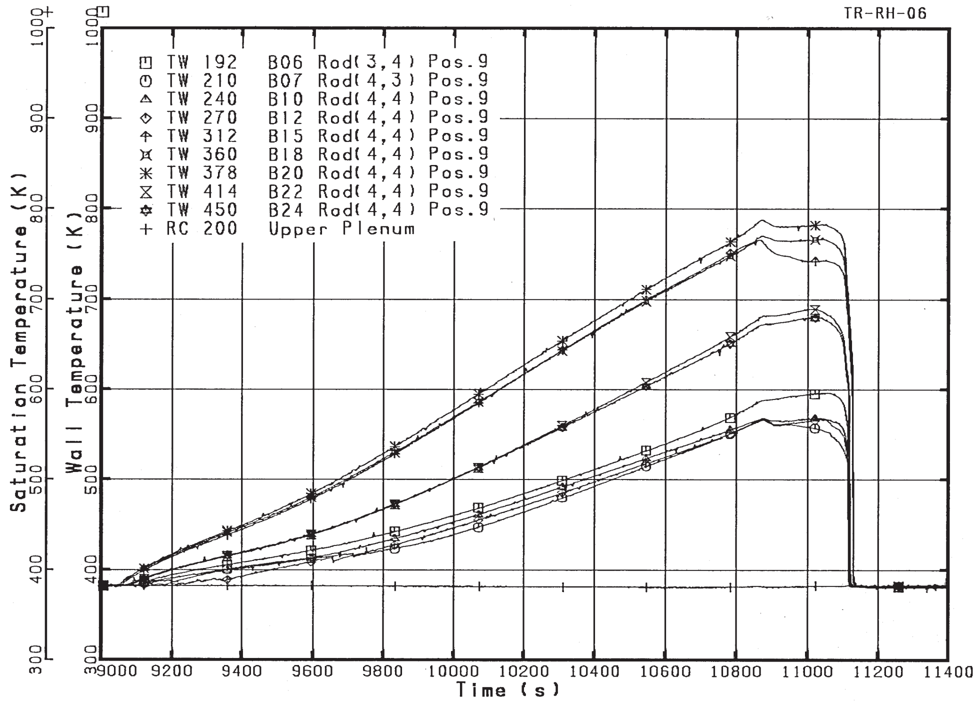

(1) Heater rod temperatures at Pos.9 (core top)

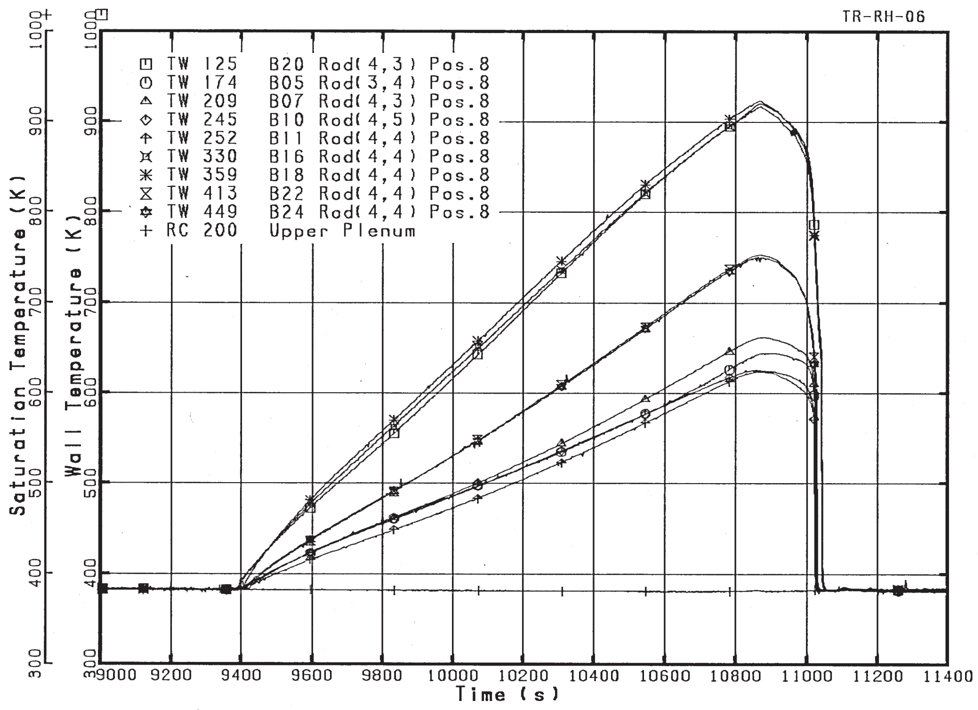

(2) Heater rod temperatures at Pos.8 with PCT measurement

Fig.4.12-10 Heater rod temperatures during boil-off process in TR-RH-06 test

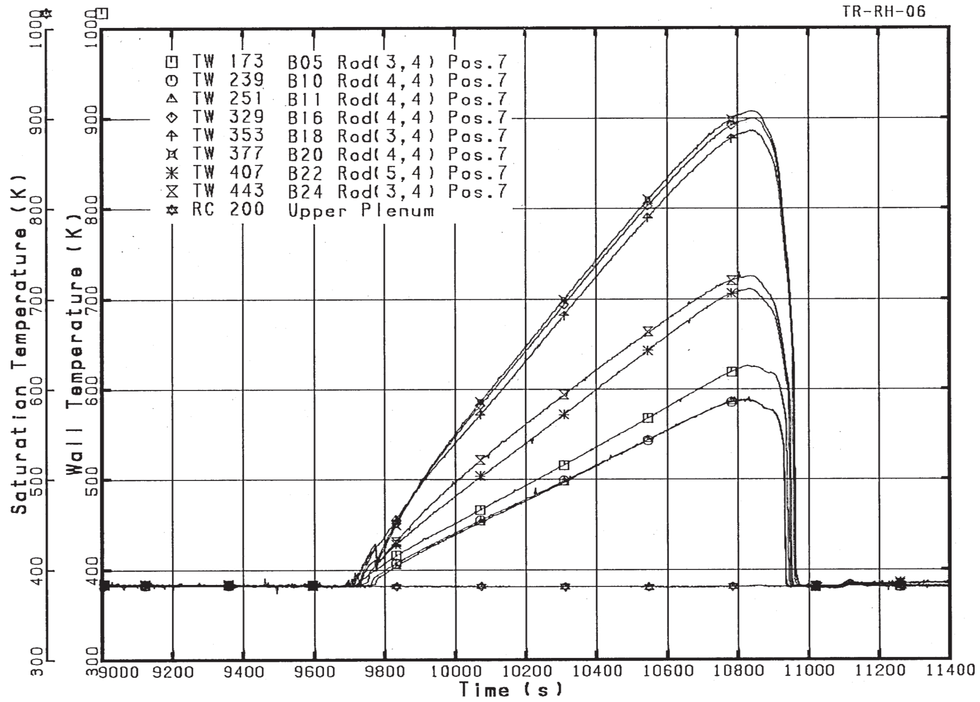

(3) Heater rod temperatures at Pos.7

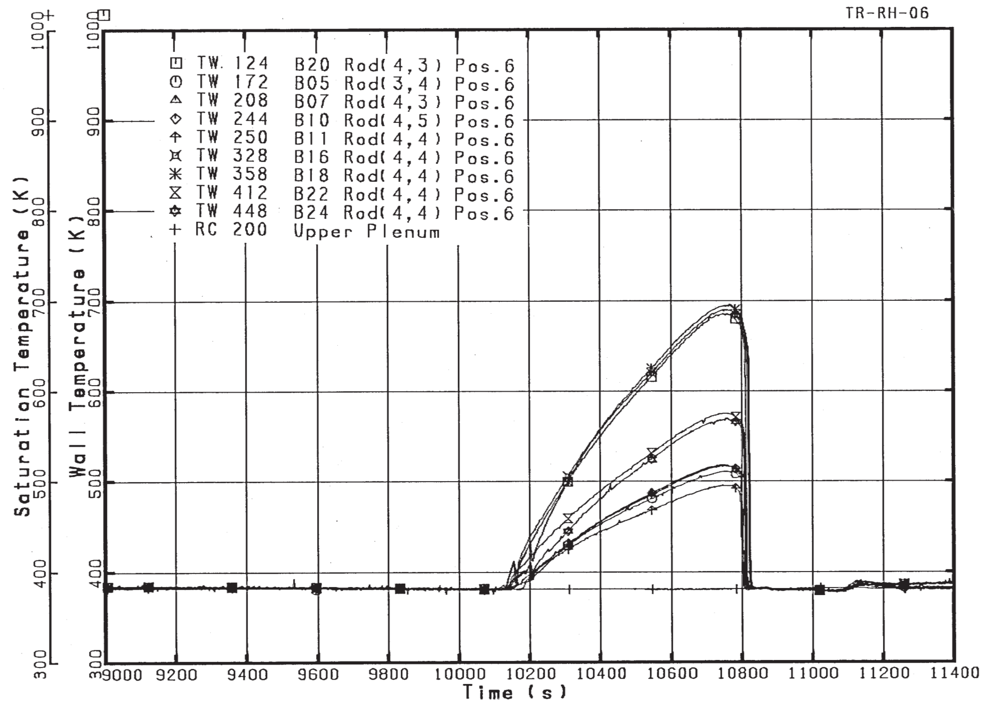

(4) Heater rod temperatures at Pos.6

Fig.4.12-10 Heater rod temperatures during boil-off process in TR-RH-06 test

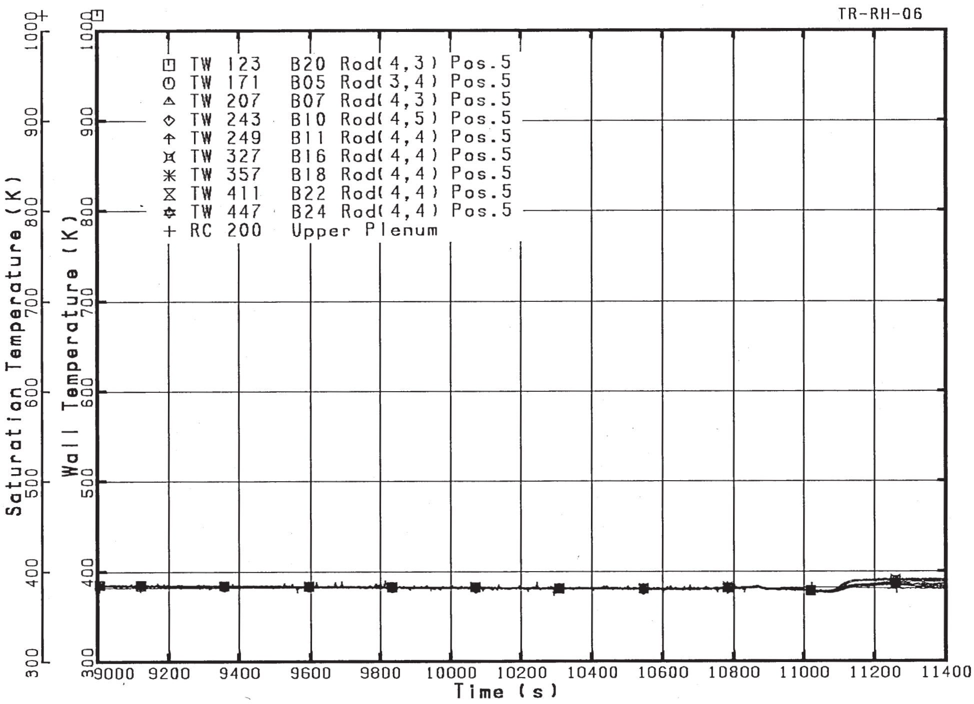

(5) Heater rod temperatures at Pos.5

Fig.4.12-10 Heater rod temperatures during boil-off process in TR-RH-06 test

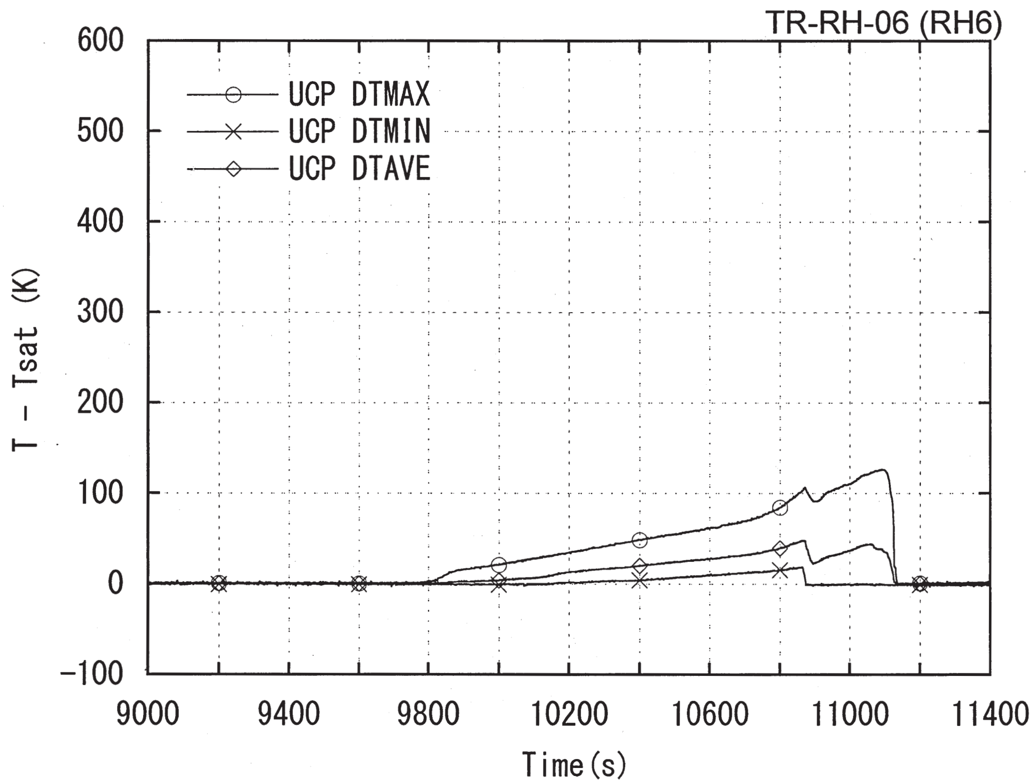

Fig.4.12-11 Distribution of all CET temperature rises above saturation temperature in TR-RH-06 test (DT_{MAX}, DT_{MIN}, DT_{AVE})

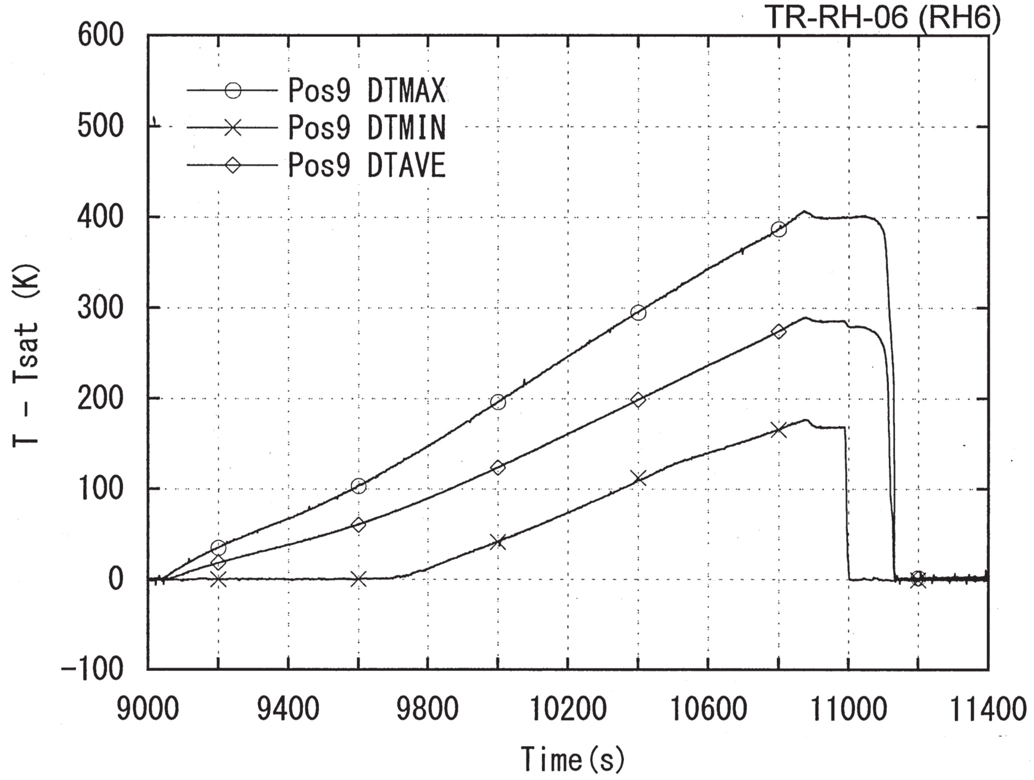

Fig.4.12-12 Distribution of heater rod temperature rises at Pos.9 in TR-RH-06 test (DT_{MAX}, DT_{MIN}, DT_{AVE})

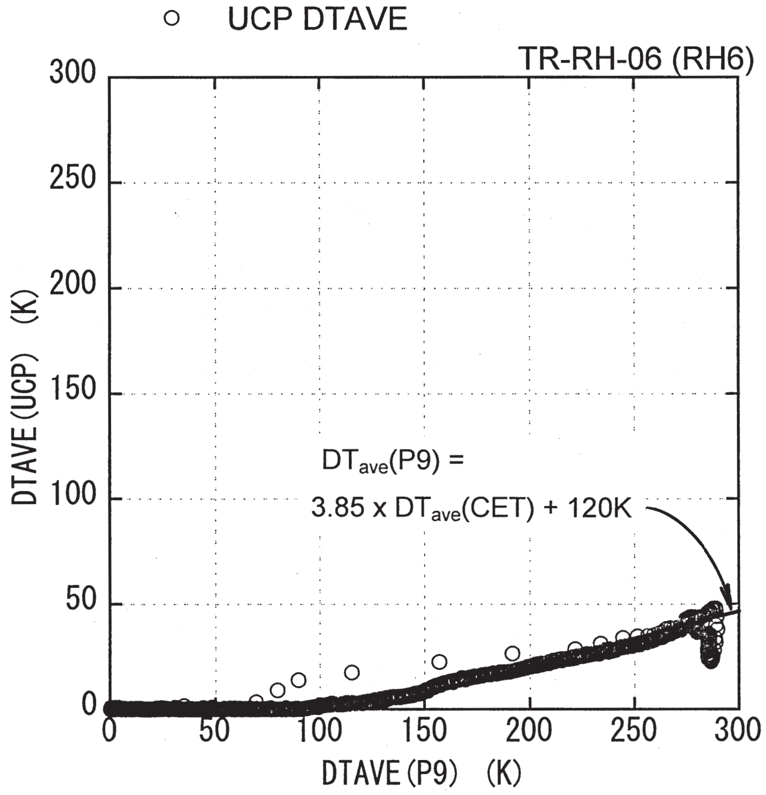

Fig.4.12-13 A relation of temperature rises at heater rod Pos.9, (Ave) and CET (Ave) in TR-RH-06 test (9000 - 11400 s)

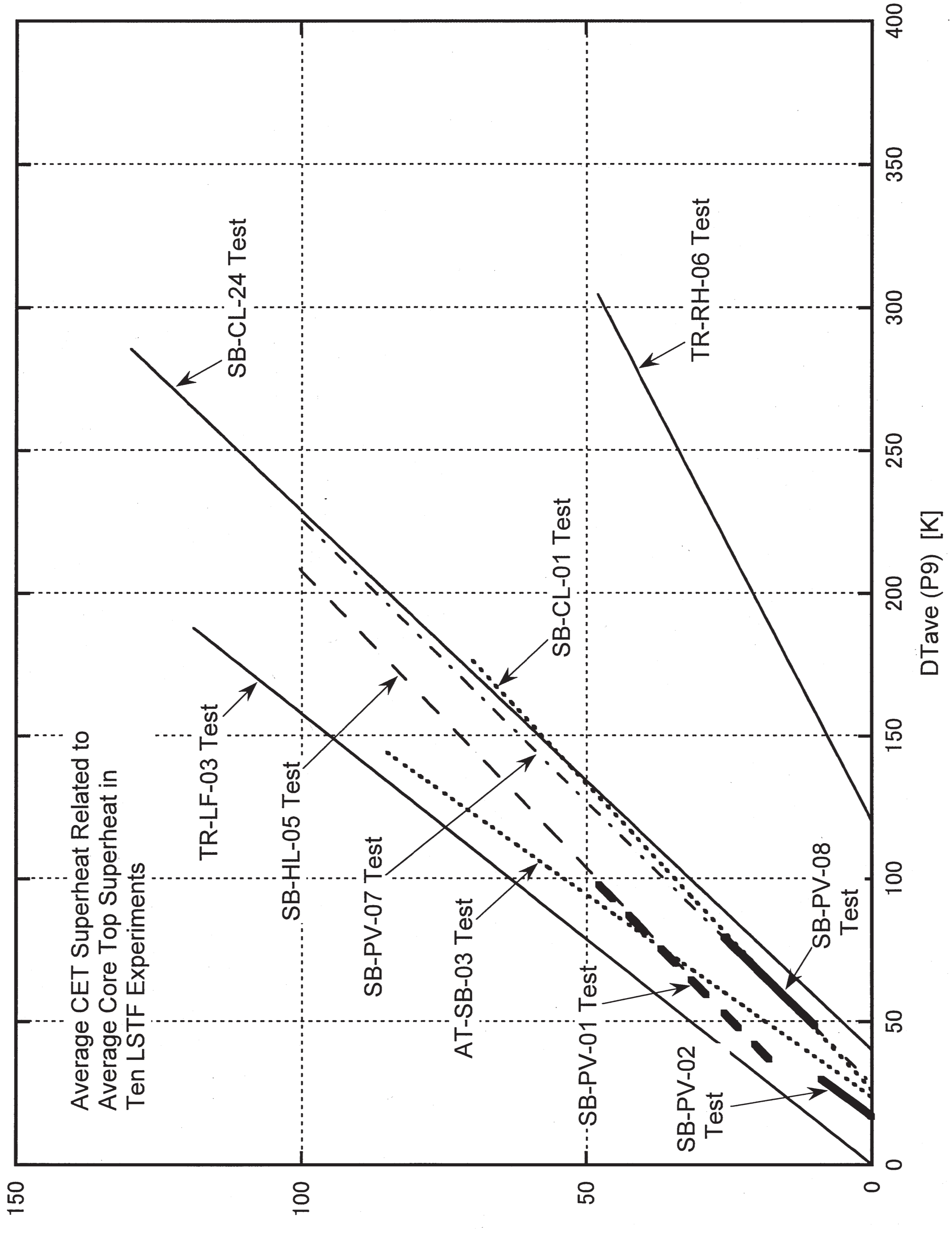

Fig.5-1 Relations of average heat-up behaviors between top core and CETs

国際単位系（SI）

表１．SI 基本単位

基本量	SI 基本単位	
	名称	記号
長さ	メートル	m
質量	キログラム	kg
時間	秒	s
電流	アンペア	A
熱力学温度	ケルビン	K
物質量	モル	mol
光度	カンデラ	cd

表２．基本単位を用いて表されるSI組立単位の例

組立量	SI 基本単位	
	名称	記号
面積	平方メートル	m^{2}
体積	立法メートル	m^{3}
速さ，速度	メートル毎秒	m/s
加速度	メートル毎秒毎秒	m/s^{2}
波数	毎メートル	m^{-1}
密度，質量密度	キログラム毎立方メートル	kg/m^{3}
面積密度	キログラム毎平方メートル	kg/m^{2}
比体積	立方メートル毎キログラム	m^{3}/kg
電流密度	アンペア毎平方メートル	A/m^{2}
磁界の強さ	アンペア毎メートル	A/m
量濃度[(a)]，濃度	モル毎立方メートル	mol/m^{3}
質量濃度	キログラム毎立法メートル	kg/m^{3}
輝度	カンデラ毎平方メートル	cd/m^{2}
屈折率[(b)]	（数字の） 1	1
比透磁率[(b)]	（数字の） 1	1

(a) 量濃度（amount concentration）は臨床化学の分野では物質濃度（substance concentration）ともよばれる。
(b) これらは無次元量あるいは次元１をもつ量であるが、そのことを表す単位記号である数字の１は通常は表記しない。

表３．固有の名称と記号で表されるSI組立単位

組立量	SI 組立単位			
	名称	記号	他のSI単位による表し方	SI基本単位による表し方
平面角	ラジアン[(b)]	rad	1 [(b)]	m/m
立体角	ステラジアン[(b)]	sr[(c)]	1 [(b)]	m$^{2/}$m^{2}
周波数	ヘルツ[(d)]	Hz		s^{-1}
力	ニュートン	N		m kg s^{-2}
圧力，応力	パスカル	Pa	N/m^{2}	m^{-1} kg s^{-2}
エネルギー，仕事，熱量	ジュール	J	N m	m^{2} kg s^{-2}
仕事率，工率，放射束	ワット	W	J/s	m^{2} kg s^{-3}
電荷，電気量	クーロン	C		s A
電位差（電圧），起電力	ボルト	V	W/A	m^{2} kg s^{-3} A^{-1}
静電容量	ファラド	F	C/V	m^{-2} kg^{-1} s^{4} A^{2}
電気抵抗	オーム	Ω	V/A	m^{2} kg s^{-3} A^{-2}
コンダクタンス	ジーメンス	S	A/V	m^{-2} kg^{-1} s^{3} A^{2}
磁束	ウエーバ	Wb	Vs	m^{2} kg s^{-2} A^{-1}
磁束密度	テスラ	T	Wb/m^{2}	kg s^{-2} A^{-1}
インダクタンス	ヘンリー	H	Wb/A	m^{2} kg s^{-2} A^{-2}
セルシウス温度	セルシウス度[(e)]	℃		K
光束	ルーメン	lm	cd sr[(c)]	cd
照度	ルクス	lx	lm/m^{2}	m^{-2} cd
放射性核種の放射能[(f)]	ベクレル[(d)]	Bq		s^{-1}
吸収線量, 比エネルギー分与, カーマ	グレイ	Gy	J/kg	m^{2} s^{-2}
線量当量, 周辺線量当量, 方向性線量当量, 個人線量当量	シーベルト[(g)]	Sv	J/kg	m^{2} s^{-2}
酸素活性	カタール	kat		s^{-1} mol

(a)SI接頭語は固有の名称と記号を持つ組立単位と組み合わせても使用できる。しかし接頭語を付した単位はもはやコヒーレントではない。
(b)ラジアンとステラジアンは数字の１に対する単位の特別な名称で、量についての情報をつたえるために使われる。実際には、使用する時には記号rad及びsrが用いられるが、習慣として組立単位としての記号である数字の１は明示されない。
(c)測光学ではステラジアンという名称と記号srを単位の表し方の中に、そのまま維持している。
(d)ヘルツは周期現象についてのみ、ベクレルは放射性核種の統計的過程についてのみ使用される。
(e)セルシウス度はケルビンの特別な名称で、セルシウス温度を表すために使用される。セルシウス度とケルビンの単位の大きさは同一である。したがって、温度差や温度間隔を表す数値はどちらの単位で表しても同じである。
(f)放射性核種の放射能（activity referred to a radionuclide）は、しばしば誤った用語で"radioactivity"と記される。
(g)単位シーベルト（PV,2002,70,205）についてはCIPM勧告2（CI-2002）を参照。

表４．単位の中に固有の名称と記号を含むSI組立単位の例

組立量	SI 組立単位		
	名称	記号	SI 基本単位による表し方
粘度	パスカル秒	Pa s	m^{-1} kg s^{-1}
力のモーメント	ニュートンメートル	N m	m^{2} kg s^{-2}
表面張力	ニュートン毎メートル	N/m	kg s^{-2}
角速度	ラジアン毎秒	rad/s	m m^{-1} s^{-1}=s^{-1}
角加速度	ラジアン毎秒毎秒	rad/s^{2}	m m^{-1} s^{-2}=s^{-2}
熱流密度，放射照度	ワット毎平方メートル	W/m^{2}	kg s^{-3}
熱容量，エントロピー	ジュール毎ケルビン	J/K	m^{2} kg s^{-2} K^{-1}
比熱容量，比エントロピー	ジュール毎キログラム毎ケルビン	J/(kg K)	m^{2} s^{-2} K^{-1}
比エネルギー	ジュール毎キログラム	J/kg	m^{2} s^{-2}
熱伝導率	ワット毎メートル毎ケルビン	W/(m K)	m kg s^{-3} K^{-1}
体積エネルギー	ジュール毎立方メートル	J/m^{3}	m^{-1} kg s^{-2}
電界の強さ	ボルト毎メートル	V/m	m kg s^{-3} A^{-1}
電荷密度	クーロン毎立方メートル	C/m^{3}	m^{-3} sA
表面電荷	クーロン毎平方メートル	C/m^{2}	m^{-2} sA
電束密度，電気変位	クーロン毎平方メートル	C/m^{2}	m^{-2} sA
誘電率	ファラド毎メートル	F/m	m^{-3} kg^{-1} s^{4} A^{2}
透磁率	ヘンリー毎メートル	H/m	m kg s^{-2} A^{-2}
モルエネルギー	ジュール毎モル	J/mol	m^{2} kg s^{-2} mol^{-1}
モルエントロピー, モル熱容量	ジュール毎モル毎ケルビン	J/(mol K)	m^{2} kg s^{-2} K^{-1} mol^{-1}
照射線量（Ｘ線及びγ線）	クーロン毎キログラム	C/kg	kg^{-1} sA
吸収線量率	グレイ毎秒	Gy/s	m^{2} s^{-3}
放射強度	ワット毎ステラジアン	W/sr	m^{4} m^{-2} kg s^{-3}=m^{2} kg s^{-3}
放射輝度	ワット毎平方メートル毎ステラジアン	W/(m^{2} sr)	m^{2} m^{-2} kg s^{-3}=kg s^{-3}
酵素活性濃度	カタール毎立方メートル	kat/m^{3}	m^{-3} s^{-1} mol

表５．SI 接頭語

乗数	接頭語	記号	乗数	接頭語	記号
10^{24}	ヨタ	Y	10^{-1}	デシ	d
10^{21}	ゼタ	Z	10^{-2}	センチ	c
10^{18}	エクサ	E	10^{-3}	ミリ	m
10^{15}	ペタ	P	10^{-6}	マイクロ	µ
10^{12}	テラ	T	10^{-9}	ナノ	n
10^{9}	ギガ	G	10^{-12}	ピコ	p
10^{6}	メガ	M	10^{-15}	フェムト	f
10^{3}	キロ	k	10^{-18}	アト	a
10^{2}	ヘクト	h	10^{-21}	ゼプト	z
10^{1}	デカ	da	10^{-24}	ヨクト	y

表６．SIに属さないが、SIと併用される単位

名称	記号	SI 単位による値
分	min	1 min=60s
時	h	1h =60 min=3600 s
日	d	1 d=24 h=86 400 s
度	°	1°=(π/180) rad
分	’	1’=(1/60)°=(π/10800) rad
秒	”	1”=(1/60)’=(π/648000) rad
ヘクタール	ha	1ha=1hm^{2}=10^{4}m^{2}
リットル	L，l	1L=11=1dm^{3}=10^{3}cm^{3}=10^{-3}m^{3}
トン	t	1t=10^{3} kg

表７．SIに属さないが、SIと併用される単位で、SI単位で表される数値が実験的に得られるもの

名称	記号	SI 単位で表される数値
電子ボルト	eV	1eV=1.602 176 53(14)×10^{-19}J
ダルトン	Da	1Da=1.660 538 86(28)×10^{-27}kg
統一原子質量単位	u	1u=1 Da
天文単位	ua	1ua=1.495 978 706 91(6)×10^{11}m

表８．SIに属さないが、SIと併用されるその他の単位

名称	記号	SI 単位で表される数値
バール	bar	1 bar=0.1MPa=100kPa=10^{5}Pa
水銀柱ミリメートル	mmHg	1mmHg=133.322Pa
オングストローム	Å	1 Å=0.1nm=100pm=10^{-10}m
海里	M	1 M=1852m
バーン	b	1 b=100fm^{2}=(10^{-12}cm)2=10^{-28}m^{2}
ノット	kn	1 kn=(1852/3600)m/s
ネーパ	Np	SI単位との数値的な関係は、対数量の定義に依存。
ベル	B	
デジベル	dB	

表９．固有の名称をもつCGS組立単位

名称	記号	SI 単位で表される数値
エルグ	erg	1 erg=10^{-7} J
ダイン	dyn	1 dyn=10^{-5}N
ポアズ	P	1 P=1 dyn s cm^{-2}=0.1Pa s
ストークス	St	1 St =1cm^{2} s^{-1}=10^{-4}m^{2} s^{-1}
スチルブ	sb	1 sb =1cd cm^{-2}=10^{4}cd m^{-2}
フォト	ph	1 ph=1cd sr cm^{-2} 10^{4}lx
ガル	Gal	1 Gal =1cm s^{-2}=10^{-2}ms^{-2}
マクスウェル	Mx	1 Mx = 1G cm^{2}=10^{-8}Wb
ガウス	G	1 G =1Mx cm^{-2} =10^{-4}T
エルステッド[(c)]	Oe	1 Oe ≙ (10^{3}/4π)A m^{-1}

(c) ３元系のCGS単位系とSIでは直接比較できないため、等号「 ≙ 」は対応関係を示すものである。

表10．SIに属さないその他の単位の例

名称	記号	SI 単位で表される数値
キュリー	Ci	1 Ci=3.7×10^{10}Bq
レントゲン	R	1 R = 2.58×10^{-4}C/kg
ラド	rad	1 rad=1cGy=10^{-2}Gy
レム	rem	1 rem=1 cSv=10^{-2}Sv
ガンマ	γ	1 γ =1 nT=10-9T
フェルミ		1フェルミ=1 fm=10-15m
メートル系カラット		1メートル系カラット = 200 mg = 2×10-4kg
トル	Torr	1 Torr = (101 325/760) Pa
標準大気圧	atm	1 atm = 101 325 Pa
カロリー	cal	1cal=4.1858J（「15℃」カロリー），4.1868J（「IT」カロリー）4.184J（「熱化学」カロリー）
ミクロン	µ	1 µ =1µm=10^{-6}m

（第8版，2006年改訂）